

***Synthesis, Characterization, and Performance
Evaluation of Single-step Silica Nanofluids for
Improved Flow Behaviour, Crude Mobilization,
and Carbon Utilization***



विद्यारत्नम् महद्भनम्

Thesis submitted in partial fulfilment

for the Award of Degree

Doctor of Philosophy

By

KRISHNA RAGHAV CHATURVEDI

RAJIV GANDHI INSTITUTE OF PETROLEUM TECHNOLOGY

JAIS, INDIA – 229304

PPE17002

2021

CERTIFICATE

It is certified that the work contained in the thesis titled "*Synthesis, Characterization, and Performance Evaluation of Single-step Silica Nanofluids for Improved Flow Behavior, Crude Mobilization, and Carbon Utilization*" by "*Krishna Raghav Chaturvedi*" has been carried out under our supervision and that this work has not been submitted elsewhere for a degree.

It is further certified that the student has fulfilled all the requirements of Comprehensive, Candidacy and SOTA/Open seminar.

Supervisor
(Dr. Tushar Sharma)

DECLARATION BY THE CANDIDATE

I, "*Krishna Raghav Chaturvedi*", certify that the work embodied in this thesis is my own bona fide work and carried out by me under the supervision of "*Dr. Tushar Sharma*" from "*August 2017*" to "*September 2021*" at the "*Petroleum Engineering & Geoengineering*", Rajiv Gandhi Institute of Petroleum Technology, Jais (India). The matter embodied in this thesis has not been submitted for the award of any other degree. I declare that I have faithfully acknowledged and given credits to the research workers wherever their works have been cited in my work in this thesis. I further declare that I have not willfully copied any other's work, paragraphs, text, data, results, etc., reported in journals, books, magazines, reports dissertations, theses, etc., or available at websites and have not included them in this thesis and have not cited as my own work.

Date:
Place:

Krishna Raghav Chaturvedi
Roll No: PPE17002

CERTIFICATE BY THE SUPERVISOR

It is certified that the above statement made by the student is correct to the best of our knowledge.

(Dr. Tushar Sharma)

(Supervisor)

(Dr. Satish Kumar Sinha)

Head of Department

(PE & GE)

CERTIFICATE

CERTIFIED that the work contained in the thesis titled “**Synthesis, Characterization, and Performance Evaluation of Single-step Silica Nanofluids for Improved Flow Behavior, Crude Mobilization, and Carbon Utilization**” by Mr. **Krishna Raghav Chaturvedi** has been carried out under my supervision. It is also certified that he fulfilled the mandatory requirement of TWO quality publications arose out of his thesis work.

It is further certified that the two publications (copies enclosed) of the aforesaid Mr. **Krishna Raghav Chaturvedi** have been published in the Journals indexed by –

- (a) SCI
- (b) SCI Extended
- (c) SCOPUS

Supervisor & Convener, DPGC

(Dr. Tushar Sharma)

COPYRIGHT TRANSFER CERTIFICATE

Title of the Thesis: Synthesis, Characterization, and Performance Evaluation of Single-step Silica Nanofluids for Improved Flow Behavior, Crude Mobilization, and Carbon Utilization

Name of the Student: Krishna Raghav Chaturvedi

Copyright Transfer

The undersigned hereby assigns to the Rajiv Gandhi Institute of Petroleum Technology Jais all rights under copyright that may exist in and for the above thesis submitted for the award of the "Doctor of Philosophy".

Date:

Krishna Raghav Chaturvedi

Place:

Roll No: PPE17002

Note: However, the author may reproduce or authorize others to reproduce material extracted verbatim from the thesis or derivative of the thesis for author's personal use provided that the source and the Institute's copyright notice are indicated.

Dedicated To

My Beloved Parents

For their endless love, support, and encouragement

Acknowledgements

First and foremost, I would want to express my heartfelt gratitude to Dr Tushar Sharma, my Doctoral Supervisor, for his patient direction and support, as well as his continuing encouragement, patience, and great confidence in me throughout my research journey. As I go through my studies and daily life, his vast knowledge and experience serve as a source of inspiration. I am very grateful for the many helpful discussions and suggestions that I have received during the thesis preparation process. Every discussion has improved the quality of my work and helped me become a more effective researcher overall. His guidance also taught me the fundamentals of the workplace. This, I think, will allow me to be a better person in the future, both professionally and personally.

My parents and relatives also deserve the most gratitude from my side as this journey would have been very tough had they not provided emotional support for me throughout it. My parents, Mr Prasanna Raghav and Mrs Reeta Raghav were my rock of Gibraltar, my constant source of strength and faith in myself which propelled me to overcome all hurdles in a short period. A big thanks in my thesis is owed to my sister, Garima whose efforts and sacrifices on various personal and professional fronts helped me focus on my research work with utmost and ultimate dedication. I thank Shalini for all her efforts and hard work in being my constant companion through the various highs and the few lows of my PhD journey. I would also like to dedicate this thesis to my beloved friend, Sharmistha, who unfortunately left this world early and who I wish is in a much better place than us all.

I would also like to take this opportunity to extend my deepest gratitude to the external collaborators in my work. The support and constructive criticism of Prof. A. S. K Sinha (Director, Rajiv Gandhi Institute of Petroleum Technology, Jais), Prof. Japan Trivedi (Alberta University, Canada), Prof. Stefan Iglauer (Edith Cowan University, Australia), and Dr Mahmood Amani (Texas A&M University at Qatar, Qatar) in making my work more elegant and structured is highly appreciated. Thank you all for your time, faith and support.

I would like to express my gratitude to the faculty members of the Department of Petroleum Engineering and Geo-engineering for their help and support during my research work. I would also like to acknowledge the role of RGIPT, Jais for providing me with financial help, laboratory support, and the facilities I need to perform my research successfully. A special note of thanks is also owed to the various research and administrative staff members who ensured that I was never deprived of my peace during my stay at RGIPT.

Finally, I consider myself very lucky to be a member of the Enhanced Oil Recovery Laboratory (EOR) research group and the memories, experiences and knowledge I have acquired from this place will stay with me lifelong. I would want to express my gratitude to all members of the EOR laboratory for creating and maintaining a nice environment. For this, my labmates, Dr Ramesh, Dr Ravi Shankar, Alpana, Anjanay, Rishiraj and Ashim are acknowledged for making this workspace lively and productive. I'd like to also express my gratitude to my colleagues Dr R. R. Ujjwal, Dr Saurabh, Dr Bilal, Dr Alok, Dr Bijoy, Dr Mukarram, Himanshu, Abhishek Anand, Abhishek Kumar, Rakesh Verma, Girish Joshi, Saurabh Tiwary, Nehil Shreyash Sidharth, and many more whose constant support made my PhD journey,

an unforgettable one. I am grateful to them for their support. You are fully deserving of all of my accolades for support.

....Krishna Raghav Chaturvedi

Table of Contents

Acknowledgements.....	i
Table of Contents.....	v
List of Figures.....	ixi
List of Tables.....	xvii
List of Abbreviations.....	xixi
Preface.....	xxii
Thesis Organization.....	xxvii
Chapter 1: Introduction and Literature Survey.....	1
1.1 Background.....	1
1.2 Challenges with CO ₂ injection.....	3
1.3 Issues related to current additives used for mobility control.....	4
1.4 Motivation- nanofluids for mobility control of CO ₂	6
1.5 Objective.....	9
1.6 Scope.....	9
1.7 Novelty.....	9
Chapter 2: Single-Step Silica Nanofluid for Improved Carbon Dioxide Flow and Reduced Formation Damage in Porous Media for Carbon Utilization.....	13
Abstract.....	13
2.1. Introduction.....	14
2.2 Materials and Methods.....	17
2.2.1 <i>Synthesis of silica nanofluids</i>	18
2.2.2 <i>Characterization of silica nanofluids</i>	18
2.2.3 <i>Carbon dioxide flow and nanoparticle retention experiments</i>	20
2.3 Results and Discussion.....	21
2.3.1 <i>Synthesis of silica nanofluids</i>	21
2.3.2 <i>Characterization of silica nanofluids</i>	23
2.3.4 <i>Morphological details of silica nanofluids</i>	27
2.3.5 <i>FTIR analysis</i>	29
2.3.6 <i>UV-vis analysis</i>	30
2.3.7 <i>Carbon dioxide flow behavior in porous media</i>	31
2.3.8 <i>NP retention in porous media</i>	39

2.3.9 <i>Techno-economic analysis of silica nanofluids</i>	41
2.4 Conclusion.....	42
Chapter 3: Rheological Analysis and EOR Potential of Surfactant Treated Single-Step Silica at High Temperature and Salinity	45
Abstract	45
3.1 Introduction	46
3.2 Materials & Methods.....	48
3.2.1 <i>Materials</i>	48
3.2.2 <i>Critical Micellar Concentration (CMC) determination of Nanofluid-Surfactant formulation</i>	49
3.2.3 <i>Additive adsorption in porous media</i>	49
3.2.4 <i>Oil recovery experiments using single-step silica nanofluids</i>	50
3.3 Results and Discussion.....	51
3.3.1 <i>Silica nanofluid degradation</i>	51
3.3.2 <i>Single-step silica nanofluid degradation as a function of salinity</i>	56
3.3.3 <i>Silica nanofluid stabilization by surfactant</i>	59
3.3.4 <i>Flow behavior study of surfactant treated nanofluids</i>	64
3.3.5 <i>Oil recovery runs</i>	70
3.4 Conclusion.....	74
Chapter 4: CO₂ Capturing Evaluation of Single-Step Silica Nanofluid through Rheological Investigation for Nanofluid Use in Carbon Utilization Applications ...	77
Abstract	77
4.1 Introduction	78
4.2 Materials and Methods	81
4.2.1 <i>Materials</i>	81
4.2.2 <i>Preparation and characterization of nanofluid</i>	82
4.2.3 <i>Preparation of CO₂ laden silica nanofluids</i>	82
4.2.4 <i>Rheological investigation of CO₂-loaded silica nanofluids</i>	83
4.3 Results and Discussion.....	84
4.3.1 <i>Shear rheological behavior of nanofluids</i>	84
4.3.2 <i>Effect of temperature on rheological properties</i>	88
4.3.3 <i>Dynamic rheological behavior</i>	91
4.3.4 <i>Effect of CO₂ capturing on shear rheology of nanofluids</i>	97
4.3.5 <i>Effect of CO₂ capturing on the viscoelasticity of silica nanofluids</i>	100

4.4 Conclusion	103
Chapter 5: In-Situ Formulation of Pickering CO₂ Foam for Enhanced Oil Recovery and Improved Carbon Storage in Sandstone Formation	105
5.1 Introduction	106
5.2 Materials & Methods.....	109
5.2.1 <i>Materials</i>	109
5.2.2 <i>Preparation of injection solutions</i>	110
5.2.3 <i>Porous media investigations</i>	111
5.3 Results and discussion	112
5.3.1 <i>Sand pack flooding results</i>	112
5.3.2 <i>Evaluation of surfactant-treated solutions for carbon storage</i>	119
5.4 Conclusion	124
Chapter 6: Experimental Investigations to Evaluate Surfactant Role on Absorption Capacity of Nanofluid for CO₂ Utilization in Sustainable Crude Mobilization	127
Abstract	127
6.1 Introduction	128
6.2 Experimental work.....	133
6.2.1 <i>Materials</i>	133
6.2.2 <i>Experimental set-up for CO₂ absorption</i>	133
6.2.3 <i>Microscopic characterization of nanofluid samples</i>	133
6.2.4 <i>Fabrication of sand-pack for displacement studies</i>	134
6.3 Results and discussion	135
6.3.1 <i>IFT studies with nanofluid and crude oil</i>	135
6.3.2 <i>Microscopic characterization of nanofluids</i>	136
6.3.3 <i>Surfactant role on CO₂ absorption of nanofluids</i>	138
6.3.4 <i>Effect of absorption on IFT of crude oil</i>	141
6.3.5 <i>Fluid displacement studies</i>	143
6.4 Conclusion	146
Chapter 7: Effect of Single-Step Silica Nanoparticle on Rheological Characterization of Surfactant Based CO₂ Foam for Effective Carbon Utilization in Subsurface Applications	149
Abstract	149
7.1 Introduction	150
7.2 Materials and Methods.....	155

7.2.1 Materials.....	155
7.2.2 Preparation and characterization of nanofluids	155
7.2.3 Methodology for foam formulation.....	155
7.2.4 Visual and microscopic characterization of nanofluids	157
7.2.5 Measurement of IFT of CO ₂ -nanofluid system	157
7.2.6 Rheological investigation of Pickering foam.....	158
7.3 Results & Discussion	158
7.3.1 Stability analysis of Pickering CO ₂ foams.....	159
7.3.2 Microscopic characterization of Pickering CO ₂ foams.....	162
7.3.3 Thermal stability of Pickering foams.....	164
7.3.4 Interfacial tension between silica nanofluid and CO ₂	166
7.3.5 Shear rheological behavior of Pickering foams	168
7.3.6 Dynamic rheological behavior of Pickering foams	170
7.3.7 Hysteresis analysis of Pickering foams	173
7.4 Conclusion.....	175
Chapter 8: Conclusion and Future Directions	177
8.1 Conclusion.....	177
8.2 Proposed industrial applications.....	179
8.3 Future research direction	179
References	181

List of Figures

Figure 1.1: Plot of CO ₂ emissions and atmospheric accumulation of CO ₂ as a function of time. It can be observed that there is a direct correlation between these two.	2
Figure 1.2: Sequence of carbon capture, utilization and storage (CCUS). This work has majorly focused on geological storage and utilization (enhanced oil recovery) of CO ₂	3
Figure 1.3: Existing challenges with CO ₂ injection in porous media. Adapted from Chaturvedi and Sharma [21].	4
Figure 1.4: Role of nanofluids as mobility control agents in CO ₂ injection. Adapted from Chaturvedi and Sharma [21].	8
Figure 1.5: Schematic showing enhanced CO ₂ absorption and retention by a complex created from the adsorption of PAM on the surface of NP. Adapted from Chaturvedi et al. [10].	11
Figure 2.1: In-situ CO ₂ flow behaviour with and without nanofluids for CO ₂ -EOR applications.	16
Figure 2.2: Visual appearance of silica nanofluids prepared by varying concentration of NH ₄ OH and TEOS in the aqueous phase of PAM (1000 ppm). Sample S1, S2 and S3 have similar concentrations (0.044M TEOS) but varying size (34, 82, and 142 nm respectively). Samples S4 and S5 have almost similar sizes (36 and 39 nm) but different concentration (0.18 and 0.27 M) of TEOS.....	22
Figure 2.3: Effect of storage time (15, 30, 45, and 60 days) on the average particle size distribution of different nanofluids viz., S1, S2, S3, S4, and S5 at ambient conditions.....	25
Figure 2.4: Effect of high PAM concentration (2000 ppm) on synthesis of silica NPs. With 2000 ppm PAM, interaction between TEOS and NH ₃ led to white globules (instead milky appearance) those eventually settled at the bottom.	25
Figure 2.5: DLS based zeta-potential measurements of different nanofluids as a function of the storage period (15, 30, 45, and 60 days).	27
Figure 2.6: SEM (a, b) and TEM (c, d) images of S1 and S2 nanofluids at ambient conditions. The morphological structure of S1 and S2 is non-agglomerated and the	

presence of small spots (SEM images) is the result of gold coating, performed to illuminate the top surface of nanofluid layer.	28
Figure 2.7: FTIR spectra (absorbance vs. wavenumbers) of S1 nanofluid prepared by 0.044 M TEOS and 0.28 M NH ₄ OH in presence of 1000 ppm PAM.....	29
Figure 2.8: Time-dependent (a: 0 and b: 60 days) UV-vis analysis of different nanofluids at ambient conditions where changes in peak absorbance are result of agglomeration between suspended NPs.....	31
Figure 2.9: Different instances (in min) of CO ₂ breakthrough from porous sand-packs for water, PAM, and most stable nanofluids (S1, S4, and S5) at ambient conditions. At breakthrough, colour of UI changes from green to red.....	35
Figure 2.10: Pressure profiles of CO ₂ flow in sand-packs 100% saturated by water, PAM, and nanofluids (S1, S4, and S5).	37
Figure 2.11: The amounts of liquid recovered as displacement efficiency per unit of CO ₂ injected in sand-packs 100% saturated by water, PAM, and nanofluids (S1, S4, and S5).	38
Figure 2.12: Schematic showing how NP is trapped under different mechanisms during NP transport in porous and permeable pore throats.	40
Figure 3.1: Average particle size observed for silica nanofluids as a function of storage uration at (a) 30 °C, (b) 60 °C and (c) 90 °C.....	53
Figure 3.2: Thermogravimetric analysis of synthesized single step silica nanofluid samples.....	55
Figure 3.3: Average particle size observed for silica nanofluids as a function of salinity for (a) S1 (0.1 wt%), (b) S2 (0.5 wt%) and (c) S3 (1 wt%).	58
Figure 3.4: Aggregates formed in nanofluid S1 in the presence of 8 wt% NaCl. ..	59
Figure 3.5: The electrical conductivity of silica nanofluid S1 as a function of surfactant treatment (wt%).....	61
Figure 3.6: Average particle size observed for silica nanofluids with added surfactant (0.216 wt%) as a function of salinity for (a) S1 (0.1 wt%), (b) S2 (0.5 wt%) and (c) S3 (1 wt%).	61
Figure 3.7: The effect of surfactant concentration on (left) average particle size and (right) zeta-potential values for silica nanofluid S1 in saline conditions.....	63
Figure 3.8: Schematic showing trapping/retention of injected fluids under different mechanisms during fluid injection in porous and permeable pore throats.	64

Figure 3.9: Viscosity versus shear rate profiles of polymer and sole silica nanofluids at 30 °C. (b) Viscosity versus shear rate profiles of polymer-surfactant and surfactant treated silica nanofluids at 30 °C. The pressure during measurement was 0.1 MPa.	66
Figure 3.10: (a) Viscosity versus shear rate profiles of polymer & sole silica nanofluids and (b) polymer-surfactant & surfactant treated silica nanofluids obtained as effluent after centrifugation at 30 °C.	66
Figure 3.11: (a) Viscosity versus shear rate profiles of polymer & sole silica nanofluids and (b) polymer-surfactant & surfactant treated silica nanofluids obtained as effluent after centrifugation at 90 °C.	67
Figure 3.12: (a) Viscosity versus shear rate profiles of polymer & sole silica nanofluids and (b) polymer-surfactant & surfactant treated silica nanofluids obtained as effluent after centrifugation at 30 °C with 4 wt% NaCl solution saturated sand-packs.	67
Figure 3.13: Cumulative oil recovery in varying temperature and salinity conditions by sole and surfactant treated single step silica nanofluids.	72
Figure. 4.1: Stability of single-step and two-step synthesized silica nanofluids as a function of storage period.	81
Figure. 4.2: Plots of viscosity (closed symbols: ●) and shear stress (open symbols:○) vs. shear rate experiments of silica nanofluids as a function of particle size at 303 K and 0.1 MPa.	85
Figure. 4.3: Effect of increasing shear rate on viscosity (closed symbols:●) and shear stress (open symbols:○) vs. shear rate profiles of silica nanofluids as a function of particle concentration at 303 K and 0.1 MPa.	87
Figure 4.4: Effect of increasing temperature (303, 323, and 353 K) on viscosity (closed symbols:●) and shear stress (open symbols:○) data of nanofluid S1 and compared with the ones of water.	90
Figure 4.5: Strain-sweep analysis (at angular frequency of 10 rad.s ⁻¹) showing effect of different particle (a-c) size and (d-e) concentration on viscoelastic properties (G' and G'') of nanofluids [a: S1 (34 nm, 0.1 wt%); b: S2 (82 nm, 0.1wt%); c: S3 (142 nm, 0.1 wt%); d: S4 (36 nm, 0.5 wt%); e: S5 (39 nm, 1 wt%)] at 303 K.	92
Figure 4.6: Temperature dependence (a: 323 and b: 353 K) strain-sweep measurements (G' and G'') of nanofluid S1, exhibiting NP size of 34 nm and concentration 0.1 wt%.	94

Figure 4.7: Frequency based viscoelastic response (G' and G'' vs. frequency), at constant strain amplitude (2%), of different silica nanofluids (a: S1; b: S2; c: S3; d: S4; e: S5) as a function of different particle (a-c) size and (d-e) concentration. Different flow regimes showing dominance of viscous (G'') /elastic (G') nature in nanofluid are also evident from Figure.95

Figure 4.8: Effect of high temperature (a: 323 and b: 353 K) on frequency based viscoelastic properties (G' and G'') of nanofluid S1.....96

Figure 4.9: Visual appearance of nanofluid S1 (a) before and (b) after CO₂ capturing experiment at 300 rpm. The presence of CO₂ bubbles in the aqueous phase of S1 is shown by microscopic image.....97

Figure 4.10: Effect of CO₂ inclusion, at different stirring rates (300 and 600 rpm), on shear rheological properties e.g. viscosity (solid symbols) and shear stress (open symbols) measurements of nanofluid S1 at ambient conditions (303 K and 0.1 MPa).98

Figure 4.11. Strain-sweep measurements (G' and G'' vs. strain) to determine the impact of high temperature 353 K (c,d) on CO₂ capturing potential of nanofluid S1 at different stirring rates (a: 300 rpm and b: 600 rpm). G' (solid symbols) and G'' (open symbols)..... 101

Figure 4.12: Frequency-sweep analysis (G' and G'' vs. frequency) to measure effect of high temperature 353 K (c,d) on CO₂ capturing potential of nanofluid S1 at different stirring rates (a: 300 rpm and b: 600 rpm). G' (solid symbol) and G'' (open symbols)..... 102

Figure 5.1: Pressure drop as a function of fluid injected (PV) in sand-packs for various runs at temperature 333 K. 115

Figure 5.2: Resultant oil recovery (% OOIP) as a function of fluid injected (PV) in sand-packs for different flooding experiments at the test temperature of 333 K.... 116

Figure 5.3: Schematic showing dependence of bubble gas strength on NP presence. At higher NP concentrations, NPs participate less in increasing bubble strength due to higher agglomeration. 118

Figure 5.4: Comparative front formation while (top) sole gas injection and (bottom) nanofluid injection followed by gas injection..... 120

Figure 5.5: Pressure drop as a function of fluid injected (PV) in oil depleted sand-packs for flow behaviour runs at varying flow rates. The test temperature was 333 K.	121
Figure 5.6: The amounts of gas injected and liquid recovered at varying flow rates in oil depleted sand-packs saturated with 0.5 PV SNF-1.0.	122
Figure 5.7: Pressure drop as a function of fluid injected (PV) in oil depleted sand-packs for flow behaviour runs after injection of varying slug-sizes of SNF-1.0. The test temperature was 333 K.....	123
Figure 5.8: The amounts of gas injected and liquid recovered after injection of slug sizes in oil depleted sand-packs saturated with SNF-1.0. The flow rate was 30 ml/hr.....	124
Figure 6.1: Competitive surfactant-NP adsorption on CO ₂ surface in surfactant treated silica nanofluid.....	131
Figure 6.2: Selection of CMC value of SDS through IFT measurements between crude oil and different nanofluids (S1: 0.1 wt%; S2: 0.5 wt%; S3: 1.0 wt%). Increasing nanofluid concentration (0.1 to 1 wt%) showed reduction in CMC requirement of SDS.	136
Figure 6.3: Microscopic images of surfactant-treated PAM fluid and nanofluids (0.1-1 wt%) after CO ₂ absorption experiments at 323 K and 12 bar.	137
Figure 6.4: CO ₂ molality results for DI water, PAM fluid, and different nanofluids with and without surfactant at (a): 323 K and (b): 353 K. Unit of values in plot is mol. of absorbed CO ₂ /kg of solvent.....	139
Figure 6.5: IFT measurements between crude oil and surfactant-treated nanofluids before and after CO ₂ absorption experiments in equilibrium cell at 323 K and 4 bar.	142
Figure 6.6: Water cut and resultant oil recovery (% OOIP) results for (a): water; (b): carbonated polymer (CP), and (c): carbonated surfactant-polymer (CSP) fluids as a function of fluid injected (PV) in sand-pack at test temperature of 323 K. EOR slug S (0.5 PV) was injected after a primary water flooding (W) of 2 PV. Displacement experiment is ended with chase water flooding (C) of 2.5 PV.	144
Figure 6.7: Water cut and resultant oil recovery (% OOIP) results for carbonated nanofluids (CN) of varying NP concentration (a: 0.1; b: 0.5; and c: 1.0 wt%) as a function of fluid injected (PV) in sand-pack at test temperature of 323 K.....	145

Figure 7.1: Schematic showing anticipated effect of increasing shear on the bubble shape in Pickering foams.	154
Figure 7.2: Experimental schematic showing equipment assembly utilized for foam generation.....	156
Figure 7.3: Representative image showing distinct foam and liquid phases in the glass cylinder (left). Normalized height of foam generated from various silica nanofluids as a function of time (right).....	160
Figure 7.4: Visual appearance images of foams in graduated glass vials as a function of time.	161
Figure 7.5: Microscopic image and bubble size distribution of Pickering foam prepared using silica nanofluid S1 as a function of time.	163
Figure 7.6: Microscopic image and bubble size distribution of Pickering foam prepared using silica nanofluid S2-S5, immediately after preparation. The observations were performed at ambient pressure and temperature.	164
Figure 7.7: Thermal stability of Pickering foam prepared using silica nanofluid S1, immediately after preparation. The bubble size increased on increasing temperature and after evaporation, a solid layer of deposition was found on the location of the foam lamella.....	165
Figure 7.8: Actual images of the nanofluid droplets in CO ₂ environment.	166
Figure 7.9: Representative image showing the droplet shape of nanofluids in an atmosphere of CO ₂ . These images were used to obtain the IFT of the CO ₂ -fluid system.	167
Figure 7.10: The effect of increasing NP size (a), concentration (b), and temperature (c) on viscosity data of Pickering foams prepared using nanofluid S1-S5.	169
Figure 7.11: Plots of strain-sweep analysis (at angular frequency of 10 rad.s ⁻¹) illustrating effect on viscoelastic properties (G' and G'') of nanofluids of different particle (a–c) size and (d–e) concentration [a: S1 (36 nm, 0.1 wt%); b: S2 (82 nm, 0.1 wt%); c: S3 (147 nm, 0.1 wt%); d: S4 (35 nm, 0.5 wt%); e: S5 (37 nm, 1 wt%)]. The effect of temperature 60 °C (f) and 90 °C (g) on the Pickering foam of silica nanofluid S1 has also been reported.....	171
Figure 7.12: Plots of the frequency based response (at angular strain amplitude of 2%) illustrating effect on viscoelastic properties (G' and G'') of nanofluids of different particle (a–c) size and (d–e) concentration. The effect of temperature 60 °C (f) and 90 °C (g) on the Pickering foam of silica nanofluid S1 is also reported.....	172

Figure 7.13: Schematic showing various stages of foam destabilization in porous media due to constrained pore throats. 173

Figure 7.14: Plot of values of viscosity obtained during loading (increasing shear rate) and unloading (reducing shear rate) in Pickering foam prepared using silica nanofluid S1 (36 nm, 0.1 wt%). (Temperature= 30 °C). 174

List of Tables

Table 1.1: Use of chemical additives in past studies for CO ₂ mobility control applications.....	5
Table 3.1: Properties of crude oil used in this study.....	53
Table 3.2: Nomenclature, concentration, average particle size, and particle frequency of synthesized nanofluids.....	54
Table 4.1: Nomenclature, concentration, average particle size and pH of synthesized silica nanofluids	82
Table 5.1: Petro physical properties and oil recovery obtained during flooding runs.....	162
Table 7.1: Nomenclature and foam volume of the Pickering foams stabilized using single-step silica nanofluids.....	162
Table 7.2: Interfacial tension measurements of CO ₂ -water/nanofluid system at ambient temperature and pressure= 12 bar. The values provided are the average of 5 measurements.....	167

List of Abbreviations

CCS	Carbon capture and storage
CCUS	Carbon capture utilization and storage
DLS	Dynamic Light Scattering
FE-SEM	Field Emission Scanning Electron Microscopy
IFT	Interfacial tension
NPs	Nanoparticles
PAM	Polyacrylamide
SDS	Sodium dodecyl sulfate
TGA	Thermogravimetric analysis
UV-vis	Ultraviolet-Visible
XRD	X-Ray diffraction
DI water	Deionized water
PV	Pore volume
EOR	Enhanced oil recovery
CO ₂	Carbon dioxide
CMC	Critical micellar concentration
EDS	Energy dispersive spectroscopy
TEM	Transmission electron microscopy
TEOS	Tetra-ethyl orthosilicate

Preface

The incessant rise in carbon emissions along with an increase in energy demand has created a unique conundrum for the developing world. Not only is there a need to improve the recovery of hydrocarbons from existing oilfields but it is also essential that the carbon footprint of the produced oil be reduced, to ensure a sustainable economic and ecological balance in the coming decades. For this, CO₂-based enhanced oil recovery (EOR) methods hold immense potential as not only do they improve oil recovery via causing it to swell and reducing its viscosity but also sequester a significant amount of CO₂ in the subsurface. While the versatility of CO₂-based EOR methods has been established in several studies, its wider application is constrained by the unique flow behavior of CO₂ in porous media, namely, its tendency to channel, bypass oil pockets and yield insufficient areal coverage in the reservoir. While several studies have proposed the use of mobility control agents like polymers, surfactants or conventional nanomaterials, their application itself is hindered by their tendency to degrade under temperature, adsorb on the rock surface, agglomerate and plug the narrow pore throats in the porous media. Thus, this work reports the synthesis of novel silica nanofluids (colloidal suspensions of particles in the nanometer range) in a base solution of 1000 ppm polyacrylamide (PAM). The fabricated nanofluids were investigated to establish their size, dispersion stability, rheological characteristics, flow behavior and oil mobilization potential was suitably compared with conventional methods in the presence of conventional oilfield additives like surfactant and conventional oilfield conditions. Additionally, the synthesized silica nanofluids were evaluated to establish their CO₂ absorption and retention potential under varying pressure and temperature conditions. Finally, the silica nanofluids were

evaluated for CO₂ foam formulation wherein their positive effect on foam stability and rheology was established. The basic layout of the work is as follows.

Initially, the essentiality and fundamental advantages of CO₂-EOR will be elaborated along with a listing of the challenges most likely encountered while conventional CO₂ injection. This includes gas bypass, liquid channeling and gas-induced formation damage which will be discussed in this chapter. This will be followed by a discussion on the current mobility control agents like polymers and surfactants which are used to increase the retention duration of CO₂ in the reservoir and the need for a newer, more efficient mobility control agent derived from existing nanomaterials and oilfield chemicals will be established. Furthermore, the basics of colloidal stability along with a brief discussion on how conventional nanomaterials are prepared and why they are unsuitable for this task will also be provided. The effect of temperature, salinity and other external oilfield agents on stability of nanofluids has also been discussed followed by the proposed mechanisms of superior stability in single-step silica nanofluids.

This has been followed by the synthesis of novel silica nanofluids in a base fluid of 1000 ppm PAM using the sol-gel method will be reported. The nanofluids were characterized using particle size analysis along with advanced imaging techniques like SEM and TEM to establish their spherical shape and un-agglomerated nature. The synthesized nanofluids of varying size (30-150 nm) and concentration (0.1-1 wt%) did not exhibit any agglomeration for 60 days. The nanofluids were then analyzed for mobility control of CO₂ in a synthesized porous media (sand-packs) wherein they exhibited excellent improvement in performance. Finally, the nanofluids were analyzed for retention inside a porous media where negligible sedimentation and retention inside sand-packs was observed. The factors investigated

were length of sand-pack, injection rate, temperature, and colloidal concentration in the sand-pack. Thus, in this chapter, the synthesis of a stable colloidal nanofluid solution was reported along with its flow applications.

Following this the stability of the synthesized nanofluids was investigated in the presence of temperature (30-90 °C) and salinity (0-8 wt% NaCl). The inclusion of salt did promote agglomeration (formation of clusters greater than the size of individual nanoparticles, NPs) in the nanofluids, the addition of an anionic surfactant, sodium dodecyl sulfate (SDS) improved the stability of their stability and improved cumulative oil recovery from sand-packs, even in the presence of moderate salinity (4 wt% NaCl). The efficacy of anionic surfactant for stabilizing nanofluids in a saline environment was also discussed along with the mechanism involved. Thus, in this chapter, the synergy between oilfield additives like surfactants, polymers and silica nanofluids was established for conventional EOR applications.

Next, the viscosity and viscoelastic property of the synthesized nanofluids was ascertained using a modular compact rheometer. The nanofluids displayed improved viscosity and viscoelastic nature, which was attributed to the presence of colloidal NPs in the suspension. The inclusion of CO₂ was found to alter the rheological behavior of the nanofluid, though no escape of CO₂ from the nanofluid was observed even when high shear values were applied. Therefore, from this chapter, it can be concluded synthesized nanofluids have excellent flow properties even in conjunction with CO₂ and their use in CO₂-based EOR and geo-storage is proposed for field applications.

Furthermore, the role of surfactant-alternating gas (SAG) injection was investigated for sand-packs wherein in-situ CO₂ Pickering foam formulation was

established inside the sand-packs. The role of slug size, gas injection speed and surfactant concentration were investigated and understood via pressure drop and fluid recovery observations. The foam movement in the sand-pack was validated by the recovery of fluids at the outlet and the pressure drop profile. Lowering the CO₂ injection rates increased their areal coverage inside the sand-pack and thus, the formulated nanofluid system was proposed for carbon geo-storage.

Next, the synthesized nanofluids were used for CO₂ absorption and retention, with and without the addition of SDS. The inclusion of SDS yielded the formation of CO₂ Pickering foam which was stable and showed high CO₂ absorption than conventional nanofluids. Mechanisms influencing CO₂ absorption and then, retention inside the body of the nanofluid in presence of the surfactant were also understood and discussed. This was followed by the application of CO₂-laden surfactant-treated silica nanofluids for oil recovery from sand-packs. From this work, the applicability of surfactant-treated nanofluids was established for enhanced oil recovery in conjunction with CO₂ for carbon sequestration.

This is then followed by the investigation of the effect of silica nanofluids on CO₂-foams wherein their foaming ability, stability, and microscopic bubble size distribution were observed as a function of time and temperature. This was followed by the observation of shear and dynamic rheological behavior of CO₂ Pickering foams where foams exhibited shear-thinning nature. This was followed by the investigation of rheological hysteresis in foams wherein shear rate was increased, then held and finally reduced to establish shear thinning nature of silica stabilized Pickering foams. This work established the stability of Pickering foams in oilfield conditions.

Finally, a comprehensive list of conclusions from the various investigations performed in this study would be reported. The highlight of the study were superior performance obtained in enhanced oil recovery applications from sand based media along with a significant increase in carbon storage in the subsurface. A suggested line of future works to further explore the field application of formulated silica nanofluids is also proposed for applications other than energy and carbon sequestration. The observations presented in this study underscore the significant performance enhancement of novel silica nanofluids and thus, their use is proposed for improved flow behavior and carbon utilization in subsurface oilfield applications.

Thesis Organization

Chapter 1: The first chapter summarizes the basic introduction of nanofluids and their need for enhanced oil recovery and carbon utilization applications. The various challenges related to nanofluid use will also be discussed in this chapter followed by the comparative analysis of the two methods of nanofluid synthesis.

Chapter 2. In this chapter, the synthesis of silica nanofluids is reported via the *Stober* sol-gel method in a medium of 1000 ppm PAM solution. The synthesized nanofluids were then evaluated using advanced imaging methods like SEM/TEM, DLS and zeta-potential to establish their stability. Next, the CO₂ flow behavior in porous media in presence of nanofluids was evaluated followed by NP retention investigation in porous media.

Chapter 3. Conventionally, saline medium has been found to destabilize silica nanofluids. Thus, in this chapter, the stability of silica nanofluids was investigated in the presence of saline medium and the role of salt was then negated using an anionic surfactant, SDS. Next, the role of nanofluids (with and without surfactant treatment) was explored for oil recovery from sand-packs with saline formation water.

Chapter 4. The rheological behavior of the silica nanofluids was then explored under relevant thermal conditions to establish their visco-elastic behavior. The effect of CO₂ absorption on nanofluids was also understood via rheological characterization of the nanofluids which was not found to have any detrimental effect on them.

Chapter 5. To establish better CO₂ utilization in brownfield and carbon storage applications, the behavior of surfactant-alternating gas was understood in context of varying pore volume injection, flow rate of gas injected and amount of

surfactant added to the nanofluid. The areal sweep of the injected gas established by the pressure drop profile observed during the study.

Chapter 6. The CO₂ absorption potential of the silica nanofluids, with and without surfactant, was explored using the pressure decay method. The role of CO₂ on IFT between crude oil and nanofluids solutions was also explored followed by the duration of CO₂ retention within the nanofluid solution. Finally, these nanofluids were used for oil recovery from sand-packs to establish their efficacy in oil mobilization applications.

Chapter 7. The surfactant-treated nanofluid solutions were then used for foam formation and their rheological behavior was understood under varying shear and thermal conditions. The formulated foam was found to remain stable even under adverse conditions, indicating the longevity of Pickering foams. This nature was also understood via the rheological hysteresis investigation of the Pickering foams.

Chapter 8. In this section, the conclusion of this thesis has been presented in a coherent manner. This work aims to promote nanotechnology applications for effective carbon utilization and the conclusion is organized to put forth this aspect before the readers of this work. Furthermore, a suggested course of future work is also proposed in this book section.

Chapter 1

Introduction and Literature Survey

1.1 Background

Globally, scientists have come to a consensus that increasingly higher emissions of CO₂ as the byproduct of anthropogenic activities are responsible for the wide fluctuation in the prevailing climatic conditions [1,2]. CO₂, as a greenhouse gas, is becoming a global threat for human health and environment as its atmospheric concentration has already crossed the permissible limit of 350 ppm [3]. Empirical data has suggested that burning of fossil fuels is directly responsible for the increasing CO₂ in the atmosphere (see Figure 1.1). This increase in CO₂ emissions has directly led to an increase in erratic weather patterns worldwide which continue to pose a challenge for human living and sustenance worldwide [4,5]. The efforts seeking its atmospheric reduction are receiving widespread attention in recent times.

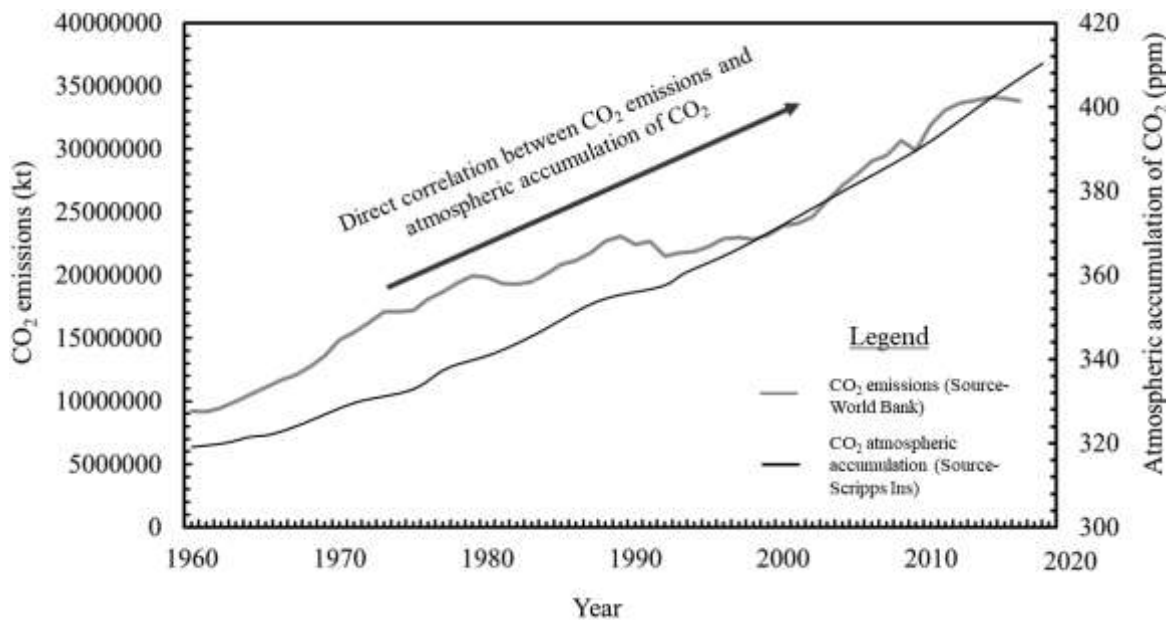


Figure 1.1: Plot of CO₂ emissions and atmospheric accumulation of CO₂ as a function of time. It can be observed that there is a direct correlation between these two.

Simultaneously, it has also been estimated that the global energy demand will increase due to increasing standards of living in the developing countries (particularly India, China and Nigeria) and most of this surplus demand is likely to be fulfilled majorly using fossil fuels [6,7]. Thus, it is of extreme importance that newer technologies and processes be developed and applied which manage to achieve both, i.e., the reduction of some amount of CO₂ from the air and improving hydrocarbon recovery from existing oilfields. Several research developments on different scales have been proposed and many are still in the development stage to capture and sequester CO₂ [8,9]. A few such approaches involve the use of Amines, Ionic Liquids, Porous materials like Polymers or Graphene, Nanoparticles (NPs) etc. One of the methods is to utilize CO₂ on large scale for underground storage and the oil recovery optimization (Figure 1.2), where CO₂ is expected to create enough miscibility with trapped oil and mobilize its lighter hydrocarbon components towards surface [10–13].

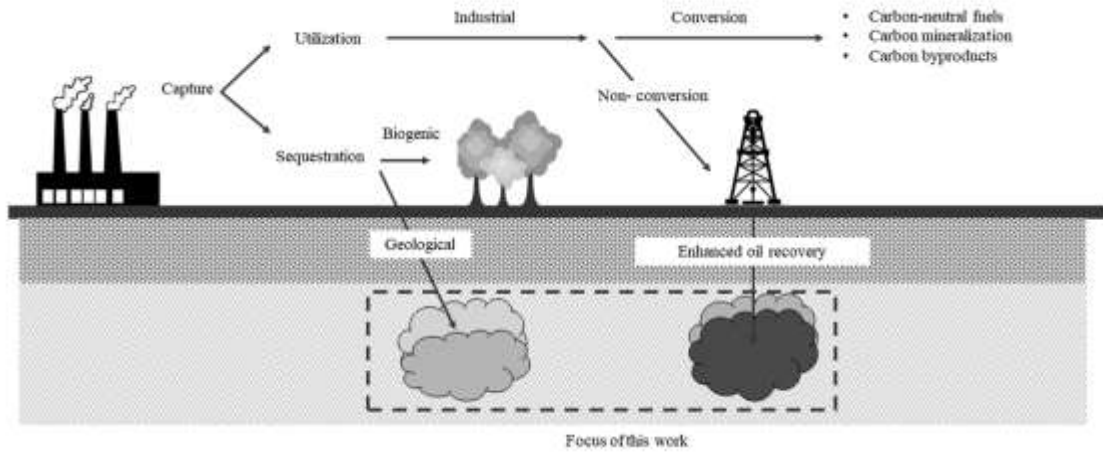


Figure 1.2: Sequence of carbon capture, utilization and storage (CCUS). This work has majorly focused on geological storage and utilization (enhanced oil recovery) of CO₂.

1.2 Challenges with CO₂ injection

However, the injection of CO₂ as a gas is plagued with several challenges of its own as CO₂ has the tendency to finger through the residual liquid layers [14,15]. CO₂ being the lighter gas than the crude oil, results in its early breakthrough due to bypassing and the viscous fingering effects. This significantly reduces efficiency of CO₂-geological storage, and volumetric sweep efficiency [16–18]. Not only does it reduce the volumetric storage of the injected gas but also wastes expensive and ecological degrading CO₂ gas [19]. Furthermore, the large CO₂ bubbles (see Figure 1.3), formed due to gas mobility in porous media, are unable to access the smaller pores as the small pore throats in the reservoir deter the flow of large bubbles of CO₂, creating blockages and causing bypassing of pockets of oil [18]. CO₂ also undergoes gravitational segregation (where the lighter gas is displaced upward by the heavier formation fluids) which complicates gas storage integrity and may cause premature leakage [15,20].

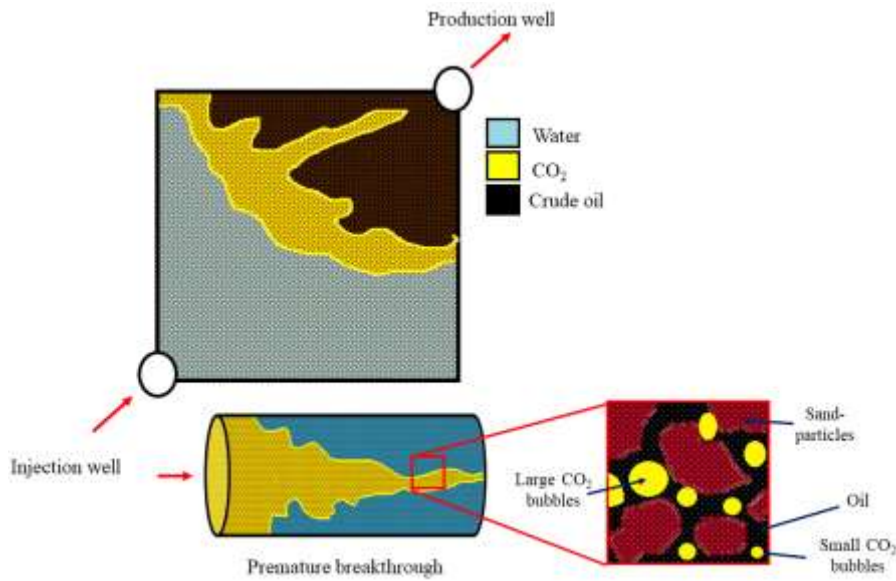


Figure 1.3: Existing challenges with CO₂ injection in porous media. Adapted from Chaturvedi and Sharma [21].

Thus, there is a need to formulate new additives to either viscosify the CO₂ or inject an additional fluid before gas injection to hold back the CO₂ during its injection, akin to how polymers are used to solve the water-channeling issues [22,23].

1.3 Issues related to current additives used for mobility control

For mobility control of injected CO₂ gas, commonly used additives can be polymers and surfactants which are already in use for EOR operations [24–26]. Surfactants are usually added to injected fluids because of natural tendency to reduce interfacial tension (IFT) between injected fluid and crude oil, enabling its easier mobilization [27–29]. However, surfactants are susceptible to adsorption on rock surface which reduces its overall efficacy in field applications [30,31]. Alternatively, polymers can be added to injection fluid to increase its viscosity and displace oil by the macroscopic process. However, polymers exhibit degradation at elevated temperatures which possess a challenge from an operational and ecological standpoint [32]. Additionally, polymers display an inferior tendency to mobilize oil from low permeability cores [33]. Furthermore, extended injection

of polymer solutions in subsurface formations is not desired as they tend to clog the pore-throats [34]. A list of chemical additives used for mobility control of CO₂ has been provided as Table 1.1.

Table 1.1: Use of chemical additives in past studies for CO₂ mobility control applications.

S.No.	Authors	Study	Chemical additive used	Remarks
1	Chaturvedi and Sharma (2019)	[11]	Polyacrylamide (PAM)	PAM (1000 ppm concentration) increases the CO ₂ capturing ability of water which ensures increased mobility control for use in carbonated water flooding.
2	Zhao et al. (2015)	[35]	Ethylenediamine	CO ₂ when injected along with ethylenediamine reacts to form ammonium carbamate which decreases CO ₂ mobility by blocking high permeability.
3	Zhang et al. (2012)	[22]	Poly (Vinyl Ethyl Ether) (PVEE), Poly (1-decane) (P-1-D)	PVEE and P-1-D were proposed to viscosify pure CO ₂ in order to ensure enhanced mobility control.
4	Rahmani (2018)	[36]	Silica Nanoparticles (SiNPs)	Methyl coated SiNPs (size = 12nm) was injected along with CO ₂ to form stable foams which reduces gas mobility in limestones.
5	Elhag et al. (2014)	[37]	Switchable diamine surfactant	C ₁₆₋₁₈ N(EO)C ₃ N(EO) ₂ generated stable viscous CO ₂ foam at 120°C for application in mobility control of CO ₂ EOR.

6	Haghtalab et al. (2015)	[38]	SiO ₂ and ZnO NPs	A comparative study was performed for water-based nanofluids among which water based ZnO nanofluids showing better absorption and solubility measurement for CO ₂ .
7	Rousseau et al. (2012)	[39]	Polydimethylsiloxane (PDMS)	CO ₂ dissolved polymer PDMS was used as a mobility control agent.
8	Sagir et al. (2016)	[40]	Nonyl phenol ethoxylate sulphonate (NPES)	Feasibility of synthesized CO ₂ -philic surfactant NPES was studied for mobility control applications.
9	Føyen et al. (2012)	[41]	Brij L23, Igepal CO-720, Tergitol NP-10, Tergitol TMN10, Tergitol 15-S-9 and Alpha olefin sulfonate (AOS)	Five CO ₂ soluble and one water soluble surfactant were characterized for foaming ability formulation of which aid in mobility control applications.

Hence, a suitable chemical additive must be identified to increase retention of injected CO₂ in formations where the application of conventional chemical additives is hindered by adverse conditions.

1.4 Motivation- nanofluids for mobility control of CO₂

Nanofluids are a relatively modern technological advancement in the field of material science which has the potential to improve the efficacy of processes in various industrial applications [42]. Nanofluids, comprise solid nanoparticles (NPs, of nanometer range) suspended in a solution, usually water. Compared to the base fluid and comparative particles of the same material in the micro-meter size range, nanofluids have been found to exhibit superior heat and mass transfer, electrical conductivity, rheological behavior, and

flow control [43–45]. This improved performance of nanofluids can be attributed to their smaller size which enables the presence of more atoms on its surface, directly improving their participation in chemical and physical interactions and established superior surface area/ volume [46,47]. These unique properties of the nanofluid have led to researchers exploring their use to improve the flow properties of fluids [48–50], as refrigerant and heat transfer fluids [51,52], in solar water heating [53], for CO₂ capture and transport [10,38,54,55] and as injection fluids in enhanced oil recovery (EOR) operations [56–58]. Silica nanofluids (SiO₂/water) have found great application in several industrial applications on account of their ease of fabrication, low cost of synthesis, and higher suitability for surface modification [54,59]. NPs improve the efficiency of the process through reduction in CO₂-water surface forces (to form CO₂ foam) [60,61], increase in water viscosity (called polymer effect), and the inclusion of active surface sites of small nanoparticles (NPs) in solution for better absorption of CO₂ molecules [10,38]. The trait that makes NP-based formulation suitable for CO₂ absorption is also associated with large surface area per unit volume, and improved rheological properties [62]. Some other advantages associated with the use of NPs are a superior reduction in surface tension of gas-water system to create CO₂ bubbles resulting increased *in-situ* absorption. Furthermore, the presence of nanofluids enables the breakdown of large CO₂ bubbles into smaller CO₂ size, enabling them to access a wider region of the reservoir (see Figure 1.4). Nanofluid can be used as a potential solvent to achieve higher values of CO₂ absorption with respect to their base fluid and also enable a control of unfavorable CO₂ mobility in the reservoir. However, the synthesis of a nanofluid is critical for any industrial application due to shortcomings such as agglomeration of NPs, reduced dispersion stability, and premature sedimentation under the effect of gravitational forces [63,64]. NPs are solid particulates and in a nanofluid, their agglomeration leads to the formation of NP clusters of large size

and relatively denser than the sole NPs. These clusters may settle faster due to gravitational action resulting reduced dispersion stability in a nanofluid and as a result, nanofluid will be ascertained as an unstable colloidal suspension for CO₂ absorption.

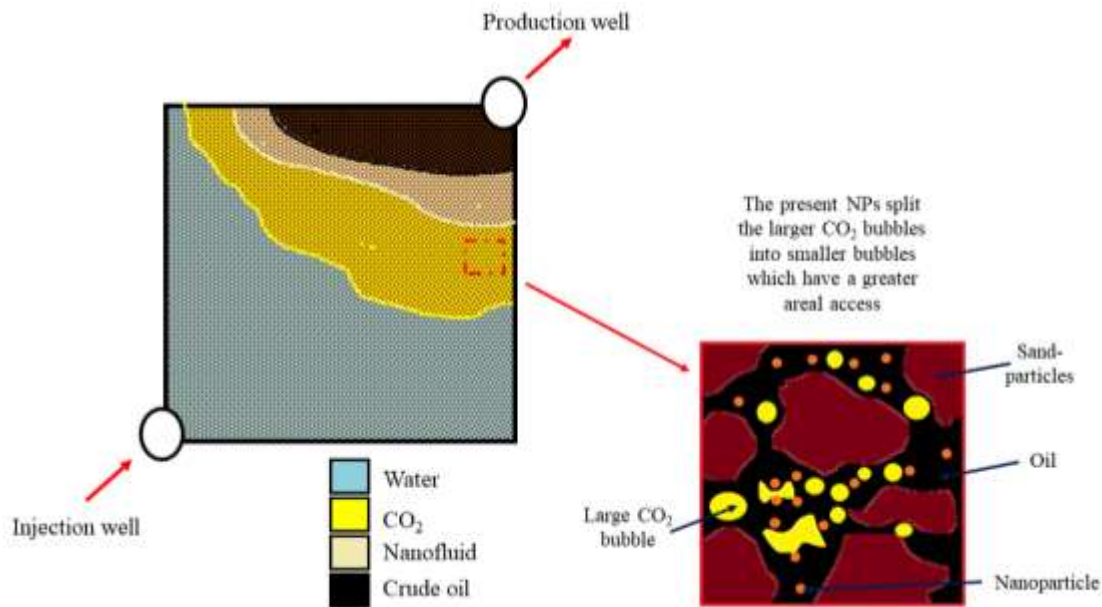


Figure 1.4: Role of nanofluids as mobility control agents in CO₂ injection. Adapted from Chaturvedi and Sharma [21].

Thus, nanofluid synthesis in a base fluid of less viscosity (such as water) is susceptible to show higher settlement and the water nanofluid will be rendered as unstable [65]. However, their wider application in flow and heat transfer applications is constrained by their tendency to agglomerate (which reduces the surface area but conserves the mass) in the base fluid [66]. This increases suspended particle size (due to the formation of homo-aggregates) which are more prone to stuck up and aggregation [67]. It is thus highly desirable to prepare stable nanofluid which exhibits superior stability so as most of the NPs participate in CO₂ absorption phenomenon, which is the main focus of this work.

1.5 Objective

Synthesis and performance evaluation of novel polymer based single-step silica nanofluids for enhanced oil recovery and carbon utilization applications.

1.6 Scope

The scope of the study is divided into several subsections that are noteworthy to achieve the proposed objective of the work in real field applications.

The scope involves:-

1. Synthesis and characterization of novel single-step silica nanofluids using oilfield polymer and evaluate their dispersion stability.
2. Investigate the dispersion stability and rheological properties of formulated silica nanofluids under desired conditions.
3. Quantify CO₂ absorption, retention and foaming ability of silica nanofluids for injection in porous media.
4. Determine compatibility of formulated silica nanofluid with conventional oilfield additives like surfactants for chemical and CO₂-based EOR.
5. Investigate nanofluid role in various application of CO₂ in oilfield applications like CWI, foam flooding and report on their synergy observed in lab scale testing.

1.7 Novelty

While earlier methods to synthesize silica nanofluids have ranged from using any chemical additive (like polymer, surfactant, or other colloidal solid like TiO₂/Ag NPs) or by pH-controlled synthesis, for this work, the synthesis of a stable silica nanofluid was attempted via the single-step method [68]. Unlike the two-step method where commercially obtained nanopowder is added to a base fluid to prepare a nanofluid, in the single-step method, the nanoparticles are synthesized inside the base fluid [69]. Compared to

nanofluids formulated by the method of two-step, single-step nanofluids have higher stability and resist agglomeration for a longer duration which allows for more individual NPs to participate in improving the efficacy of industrial application [70]. Furthermore, newer, easier methods utilizing only the conventional laboratory equipment have been developed for fabricating silica nanofluids of single-step origin which has further increased the likelihood of their widespread adoption. To further impart the stability to the single-step silica nanofluids, the base solution used was PAM, instead of water. One of the solutions to improve the stability of water based nanofluids is to use additives such as high molecular weight polymer such as polyacrylamide (PAM) that provides higher viscosity to water during dissolution. NPs mixed together with PAM is expected to form a complex macromolecular cross-linking structure resulting from the adsorption of PAM chains on the surface of dispersed NPs as proposed by the scheme in Figure 1.5. However, despite the vital importance of PAM in the formulation of nanosuspensions globally, the study showing PAM based silica nanofluid for CO₂ absorption for oilfield applications is fairly limited in the literature.

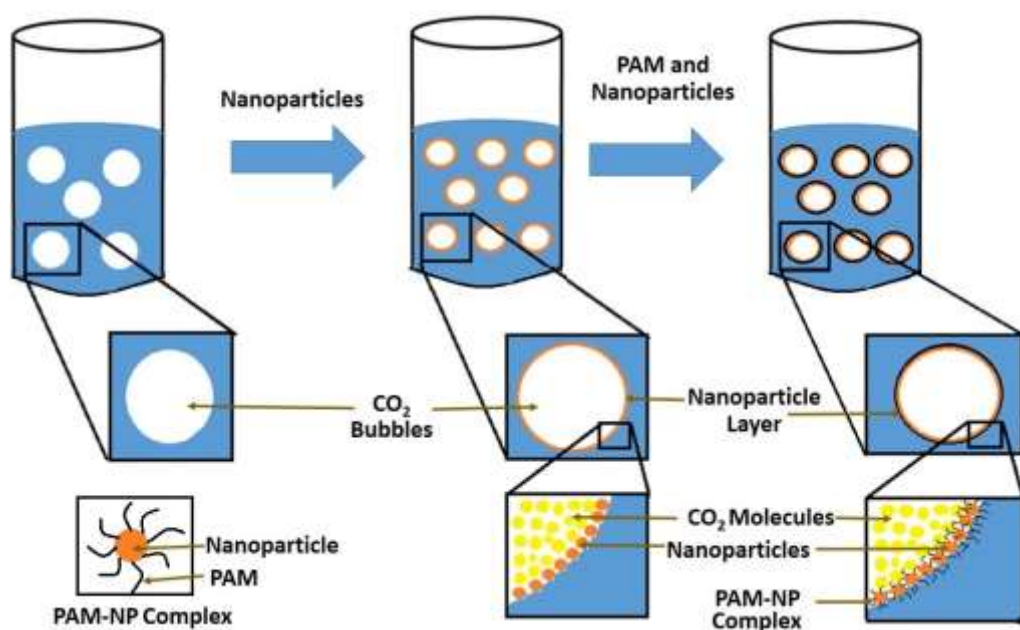


Figure 1.5: Schematic showing enhanced CO₂ absorption and retention by a complex created from the adsorption of PAM on the surface of NP. Adapted from Chaturvedi et al. [10].

Furthermore, since PAM solution is also commonly used in the polymer flooding method of EOR and CO₂ in viscous polymer phase is expected to remain trapped for longer period than water, the novelty of the work lies in the use of silica NPs (as nanofluid) to improve the CO₂ absorption capacity of polymer methods of CO₂ sequestration and EOR projects. Also, since low viscosity and non-wetting nature of CO₂ is responsible for an early breakthrough of the injected gas at the surface during an EOR process, nanofluid with enhanced CO₂ absorption may solve these issues. CO₂ laden nanofluids will carry more CO₂ than carbonated water injection allowing engineers to sequester comparatively more CO₂ easily and securely in the sub-surface.

Single-Step Silica Nanofluid for Improved Carbon Dioxide Flow and Reduced Formation Damage in Porous Media for Carbon Utilization

Abstract

Water-alternating gas (WAG) is affected by viscous fingering and trapping of reservoir oil that can be addressed by advanced methods such as nanofluids, those not only increase CO₂ capturing but also provide significant control on its viscous fingering. Therefore, this study reports the use of single-step silica nanofluids, of controllable nanoparticle (NP) size (below 100 nm), for improved CO₂ flow and reduced formation damage in porous and permeable media. Polyacrylamide (PAM, 1000 ppm) was used as viscosifier and found favorable for enhanced dispersion stability (more than 2 months) in nanofluids. The parameters, such as amount of precursor (Tetraethylorthosilicate-TEOS) and catalyst (ammonium hydroxide-NH₄OH), stirring speed, ultra-sonication time, and the amount of PAM were varied. Silica NPs were highly stable against agglomeration as reported by DLS, FTIR, TEM, SEM, and UV methods. With silica nanofluid, CO₂ breakthrough significantly delayed and CO₂ remained in sand-pack for longer duration than water/PAM. CO₂ in presence of NPs made stable foam that was viscous and least mobile (than CO₂) as confirmed by progressive increase in pressure while CO₂ flow with water/PAM was unstable as pressure varied non-uniformly. This is of key importance for CO₂ sequestration studies in porous reservoirs. Since NPs are solid substances, they can

retain in sand-pack during nanofluid use for CO₂ utilization strategies. NP retention was determined using an experimental investigation for different (1) sand-pack length, (2) flow rate, (3) NP concentration, and (4) test temperature. NP retention of only 8-12% of total injected amount was reported. Sand-pack length was found to be the most influential variable.

2.1 Introduction

Miscible CO₂ flooding, immiscible CO₂ flooding, and geo-storage are important gas-based oilfield applications where CO₂ is viewed as a possible solution to (1) meet energy demands by increasing hydrocarbon recovery and (2) reduce the amount of anthropogenic CO₂ emissions in air [71–75]. Since pressure requirements for CO₂ injection are lower than other gases (N₂ and hydrocarbon gas), CO₂ exhibits better adaptability for a range of hydrocarbon reservoirs [76]. Theoretically, the injected CO₂ should dissolve in the crude body, causing oil to swell which will lower its viscosity and increase its mobilization towards production well [77–79]. This is only possible if CO₂ after injection comes in contact with the residual or trapped oil which typically dwells in low size pore channels of porous media. However, it has been observed that CO₂ flooding results in lower than expected oil recovery due to poor sweep efficiency as CO₂ channels through the oil pockets (called CO₂ channeling problem - CCP) [80,81]. The poor sweep can be attributed to the high mobility contrast between CO₂ and the reservoir crude oil [82,83]. Conventionally, the viscosity of CO₂ (μ_{CO_2}) has been found to be in the range of ~0.05 to 1 cP which is markedly lower than oil viscosity (μ_{oil}) which causes CO₂ channeling a major concern as it results in premature CO₂ breakthrough [84]. Hence, it is of key importance that CO₂ breakthrough should be delayed by controlling its mobility; a controlled CO₂ movement is expected to create blockage to subsequent injection of CO₂ as a result, injected CO₂ will be

forced to enter in most of the pore channels in reservoir. This will increase the areal sweep efficiency of injected CO₂ which is vital for CO₂ storage in porous media and oil recovery.

The injection of alternating slugs of water and CO₂ (also referred as water alternating gas, WAG) is one of the effective techniques to reduce CO₂ channeling problem [80,85,86]. However, a balance between amounts of injected water and CO₂ is required to achieve as too much gas leads to viscous fingering whereas too much water provides trapping of oil by water. As a result, methods showing enhancement in water viscosity are explored to reduce viscous fingering of gas. Conventionally, high molecular weight water-soluble polymers (e.g. polyacrylamide-PAM and hydrolyzed polyacrylamide-HPAM) were used [87]. But, these methods also exhibited challenges such as instability at high temperature and sensitivity to salt conditions [88]. An interdisciplinary nanomaterial called nanofluid has shown better performance than conventional fluid due to its large surface area per unit volume [89], better structure [90], and distinct optical properties [91], selectivity and stability for electroreduction of CO₂ [92] and rheological properties [62,67]. The role of nanofluids in CO₂ foam and CO₂-enhanced oil recovery (EOR) methods has been discussed in literature studies. Nanofluids can stabilize CO₂ foam flood by reducing the rate of thin film collapse at foam's gas-liquid interface which makes CO₂ less mobile and thus, it is more likely to displace the residual oil from the reservoir [93]. NPs provide significant increase in the resistance factor of CO₂ foam (4-16 times) which is beneficial for obtaining higher oil recovery from the reservoir. Foam resistance factor is the ratio of pressure drop (ΔP_{CO_2-NP}) observed across the porous media during CO₂/silica NP injection and pressure drop ($\Delta P_{CO_2-brine}$) observed during CO₂/ brine injection [94]. An excellent stability of CO₂ foam was achieved with the use of silica NPs and the use of nanoparticle stabilized CO₂ foam for oil recovery applications from quasi 2D porous media was reported by [95,96]. In another study that was carried out in sand-packs (prepared using sand of size

250-355 μm), the use of silica NPs was found to improve CO_2 foam stability which as a result increases the oil recovery by 11% original oil in place (OOIP) [97]. Separately, Risal et al. [98] investigated the use of surface modified silica nanofluids on the stability and pore plugging properties of CO_2 foam flowing through a glass-bead pack of 34% porosity. As a result, incremental oil recovery is increased by 18% OOIP after water flooding. In addition, Alzobaidi et al. [99] also found NPs could be used to improve sweep efficiency during CO_2 injection in a brine filled sandstone core for CO_2 sequestration. Significant delay in CO_2 breakthrough is possible with NP stabilized foam as proposed by schematic in Figure 2.1, where foam front uniformly sweeps the reservoir pores than water.

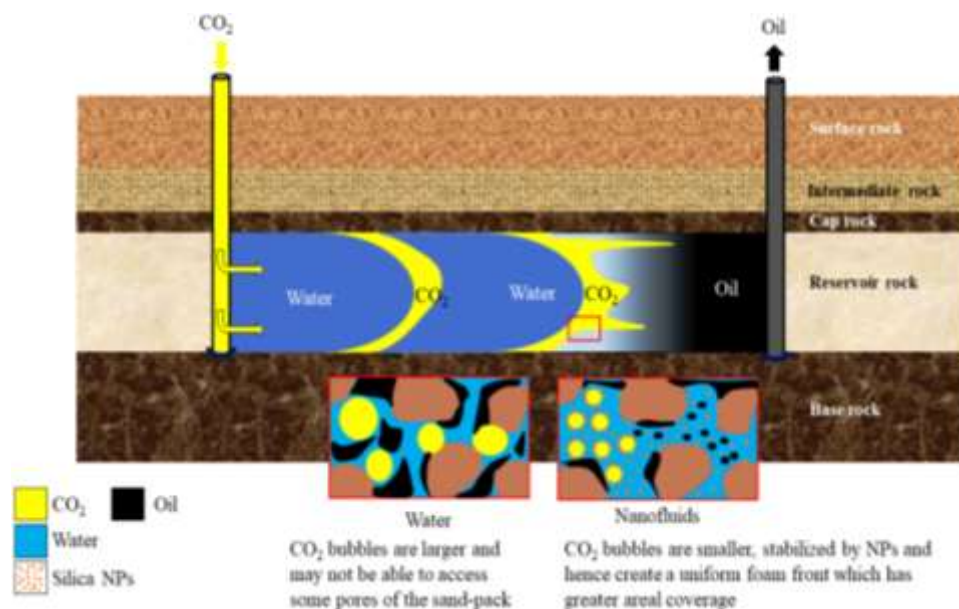


Figure 2.1: In-situ CO_2 flow behaviour with and without nanofluids for CO_2 -EOR applications.

Additionally, nanofluids have the tendency to increase oil production on their own by pore channel plugging [100], favorable mobility contrast [101], and wettability alteration [102]. The preparation of a nanofluid is the most crucial stage in the use of nanofluid. There are two main methods to synthesize nanofluids: two-step and single-step method. However, nanofluids prepared by the two-step method have found to exhibit poor

stability with time. The other method of nanofluid synthesis is single-step method; here NPs, instead of adding externally, are synthesized in-situ from base chemical constituents to final NP in solution itself. Compared to nanofluid of two-step, single-step nanofluids are more stable and less prone to NP agglomeration in base fluid [103]. Another advantage of single-step nanofluid lies in NP synthesis of controlled size that meets the requirements of nanofluid usage in reservoirs of narrow pore size. The novel aspect of the current work lies in the synthesis of surfactant-free reservoir compatible silica nanofluid of oilfield polymer PAM for effective utilization of CO₂ in porous media. Silica NPs have been prepared only by varying the concentration of TEOS, PAM dissolved in H₂O, NH₄OH, and ethanol without the use of any surfactant. A set of displacement experiments were conducted to establish NP retention (resulting from the flow of nanofluid) in sand-packs of varying lengths, and an experimental approach to ascertain NP retention accurately at varying flow rates and different temperature was reported.

2.2 Materials and Methods

Chemical, Tetraethylorthosilicate (TEOS, assay > 99%), Ammonium hydroxide (sp. gr. 0.91 and 25% NH₃ content), Ethanol (EtOH, assay>99.9%) and water-soluble polymer polyacrylamide (PAM) (molecular weight = 10 million Dalton) were obtained from commercial vendors. A Millipore[®] Elix-10 purification apparatus (electrical conductivity of water = 0.0054 mS.cm⁻¹) was used to deionize (DI) the water. A magnetic stirrer (IKA-C-MAG-HS7) was used to disperse and dissolve PAM in DI water at stirring speed of 600 rpm for 1 h. All chemicals were weighed using an accurate digital weighing balance (Mettler Toledo[®], ME204/A04) with a repeatability of 0.1 mg. An ultrasonic cleaner (Rivotek[®], Mumbai) at frequency 25 Hz was used to sonicate the aqueous suspensions.

2.2.1 Synthesis of silica nanofluids

In this study, silica nanofluids were prepared using a well-established method called sol-gel [104–106]. The sol-gel method typically uses a solvent to create an environment for the action of precursor in system. In this work, 1000 ppm PAM solution is used as solvent where TEOS is chosen as precursor. TEOS supplies the basic constituents (Si and O) for the synthesis of SiO₂ NPs. Since TEOS is a non-polar chemical hence its miscibility in water is ensured by ethanol that helps to dissolve TEOS in PAM solution. TEOS was further activated by the addition ammonium hydroxide to initiate controlled aggregation that leads to the formation of SiO₂ NPs in suspension, henceforth referred as silica nanofluids. The role of ammonium hydroxide is essential as it controls the growth size due to the presence of NH₂ group [107]. First, PAM solution of 1000 ppm is prepared by dissolving 1 gm powder in 1000 ml DI water at a stirring speed of 600 rpm for 8 h [108]. Next, Ethanol (500 ml) was added in PAM solution while stirring at 600 rpm was kept on for 15 min. It was followed by sonication at 25 kHz in a sonication bath for 15 min. During the entire process, the flask was sealed using a rubber stopper to ensure that no contamination took place. TEOS of required volume (0.045-0.18 mol) was added and the mixture is sonicated to ensure complete mixing. Ammonium hydroxide (0.28-0.56 mol) was added after 0.5 h to promote condensation reaction and the solution was finally sonicated for next 2 h. This results into a milky appearance in solution, assuring the presence of silica NPs.

2.2.2 Characterization of silica nanofluids

To determine the size of NPs, dynamic light scattering (DLS) measurements were performed for silica nanofluids using a particle size analyzer (Nano ZS, Malvern® UK). DLS uses a 173° detector scattering angle for the measurements and all measurements were conducted at 298 K. Zeta potential (ζ) was measured using zeta sizer unit of Nano ZS

(Malvern® UK). To ensure any aggregation or sedimentation in nanofluids, initial DLS measurements were performed within 1 week of nanofluid preparation and repeated regularly until 60 days.

SEM analysis (Nova NanoSEM 450, ThermoFisher® USA) was performed to visualize the morphology of synthesized silica NPs. A drop from the synthesized samples was taken using a micro-pipette and dropped on a glass slide. The glass slides were then dried in an oven at 423 K to evaporate aqueous phase resulting only NPs left on the surface of slide. The dried layer of NPs was then gold-coated and analyzed in SEM instrument to record the images. To ascertain the morphological details of NPs, 2-3 micrographs were taken from different locations on the slide. The synthesis of silica NPs were also characterized by frequently used high-resolution transmission electron microscopy (HRTEM) technique using JEM-200CX (JEOL® Japan) instrument.

Fourier transform infrared (FTIR) spectrometer (Perkin Elmer® USA) was used to record the FTIR spectra of TEOS (precursor) and synthesized NPs. To obtain FTIR spectra, the mode attenuated total reflectance (ATR) was used as it enables the nanofluids samples to be examined directly in a liquid state without further preparation. The IR spectra were collected at 4 cm² spectral resolution utilizing a 1 min data collection time.

The synthesized silica NPs were also analyzed using UV-vis spectroscopy experiments. These experiments were conducted using UV-vis 3200 equipment (Lab® India) to determine the absorption of NPs. The nanofluids were examined for these experiments at room temperature (303 K) with a 1 nm/s scan rate over the wavelength ranges 190 to 1100 nm. For each UV experiments, fresh cuvette was used to prevent contamination and minimize errors in the measurements.

2.2.3 Carbon dioxide flow and nanoparticle retention experiments

For CO₂ flow and NP retention experiments, synthetic sand-packs, those resemble as porous and permeable sandstone formations were prepared using sand of average size ranges from 200-380 μm [11,109]. The properties and characterization of the sand-particles have been also reported in detail in our previous work [109]. However, for the sake of brevity, some details are provided. The sand was carefully washed using toluene and dried at a high temperature in an oven to remove any moisture. A mineralogical characterization of the sand-particles was performed using an XRD machine (X-Ray Diffractometer D8 Advance, Bruker, India) and was found to contain primarily quartz (88 wt%) along with traces of kaolinite (6 wt%), feldspar (2 wt%) and chlorite (1 wt%) [109]. The sand-packs were prepared in sand-pack holders of varying lengths (2-24 inch). These holders were manufactured using stainless steel and supplied by D-CAM Engineering works, Ahmedabad, India. The sand-pack was prepared by manual ramming of sand down the sand-pack holder using a custom-built rod along with a saturating fluid (water, PAM solution and nanofluids of varying concentration). A predetermined amount (300 ml) of saturating fluid had been kept in a wash bottle and was subsequently added with sand in sand-pack holder. This process of ramming and adding constituents (sand and saturating medium) was continued till the sand-pack becomes 100% saturated and covered the top of holder. The remaining fluid (i.e. saturating medium) kept in the wash bottle was carefully measured using a graduated cylinder and the difference between the initial and final amount was used to establish the porosity in pore space of the synthesized sand-packs [11]. To further ascertain that all pore spaces were occupied by the saturating medium, a syringe pump (Make 100DX, Teledyne ISCO[®], USA) was used to pump the saturating medium across the sand-pack till the inlet and outlet flow rates become same[11]. For CO₂ flow behavior, CO₂ from a high pressure cylinder (capacity 47 L at 98 bar) was pumped in sand-

pack using syringe pump operated at constant flow rate mode of 1 ml/min. The back-pressure exerted by the fluid flow was measured using a pressure transducer attached at the outlet end of sand-pack holder.

2.3 Results and Discussion

The synthesis of silica nanofluids using different chemicals *e.g.* PAM, TEOS, and NH_4OH are discussed first followed by the discussion on various characterization details of silica NPs. Next, application of silica nanofluids for CO_2 flow behavior (breakthrough time, pressure profile, and displacement efficiency) and NP retention under different conditions (length, flow rate, concentration, and temperature) is discussed.

2.3.1 Synthesis of silica nanofluids

The synthesis of silica nanofluids is performed using a procedure similar to the one adopted by Kim et al. [106]. This method used water as solvent to prepare silica nanofluid however, the current study used 1000 ppm PAM solution as it is a typical concentration of oilfield polymer methods. It has been reported that acid-catalyzed hydrolysis is very slow process as compared to basic hydrolysis process resulting base-catalyzed process is preferred to synthesize ultra-fine monodispersed SiO_2 NPs [110]. Hence, NH_3 was used as catalyst to promote the hydrolysis of TEOS in ethanol and PAM solution. High NH_3 content is tended to increase the rate of hydrolysis in reaction and produce bigger size particles [104] therefore, dropwise addition for longer period is recommended to control the growth and size of NPs [111]. For nanofluids (S1-S3), the composition of TEOS was kept constant (0.045M) and the concentration of ammonia was increased between 0.28-0.56 M. With NH_4OH addition, the solution exhibited different changes in appearance. Nanofluid S1 appeared to be clear suspension, almost similar to pure PAM solution (Figure 2.2).

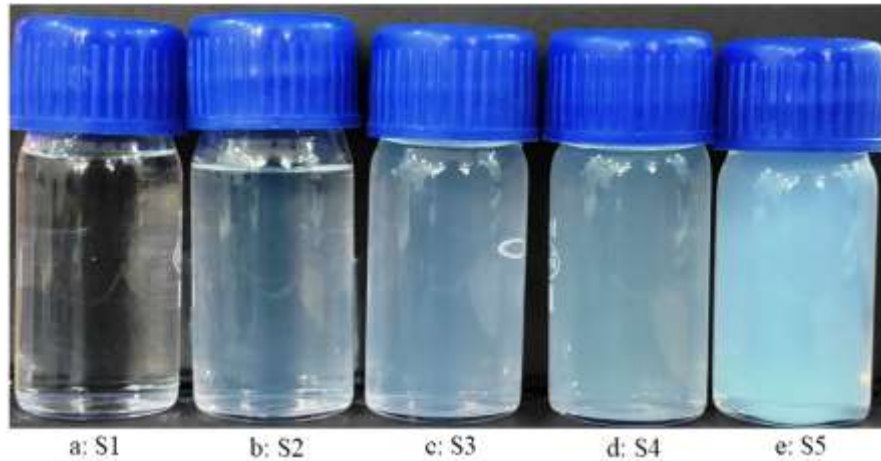


Figure 2.2: Visual appearance of silica nanofluids prepared by varying concentration of NH_4OH and TEOS in the aqueous phase of PAM (1000 ppm). Sample S1, S2 and S3 have similar concentrations (0.044M TEOS) but varying size (34, 82, and 142 nm respectively). Samples S4 and S5 have almost similar sizes (36 and 39 nm) but different concentration (0.18 and 0.27 M) of TEOS.

The colloidal appearance of S2 is diluted milky while S3 exhibited milky appearance where maximum amount of ammonia was 0.56 M (Figure 2). In nanofluid S4 and S5, the concentration of TEOS was varied such as 0.09 and 0.18 M, respectively while the concentration of ammonia remained constant (0.28 M). These nanofluids are relatively dense in color and exhibited greater amount of white appearance. Thus, compared to ammonia, the increase in TEOS amount had greater effect on the colloidal appearance of nanofluid.

These nanofluids were visually analyzed for the change in their appearance with time [45,112]. For that, a certain volume of nanofluids is placed in a transparent glass vial and images were taken at regular intervals using a camera [113]. The images were compared to observe any change in the appearance of nanofluid. In addition, the bottom of the glass vials was regularly checked for any NP sedimentation. It was observed that the

nanofluid did not exhibit any change in appearance over a period of 15 days followed by 45 and 60 days as no NP deposited at the base of glass vial due to sedimentation. Timofeeva et al. [114] prepared a silica nanofluid solution using two-step synthesis which was stable for a day in the presence of surfactant (Benzalkonium chloride and cetrimonium bromide). The single-step synthesis of silica nanofluids using Stober process was attempted by Weichold et al. [115] who reported a stability of 3 days for nanofluids. The two-step synthesis of silica nanofluids using surfactant, TX-100, was attempted by Zhao et al. [116] where nanofluids exhibited stability of 21 days. In our previous study [10], PAM as dispersing agent was used for the synthesis of two-step silica nanofluids those exhibited a dispersion stability of 24-30 days. Thus, in this study, size controlled nanofluids of extended stability (60 days) are synthesized using single-step method and moreover, these nanofluids were stable without the use of any other chemicals.

2.3.2 Characterization of silica nanofluids

The nanofluids were characterized by DLS measurements for size and zeta-potential of synthesized silica NPs. The largest particle size observed in this investigation was 142 nm for sample S3 while a particle size of 34 nm was obtained for sample S1. Thus, when NH_3 is increased from 0.28 M to 0.56 M, the particle size increased from 34 (S1) to 142 nm (S3). The reason for increased NP size may be attributed to high amount of NH_3 content that increases the rate of hydrolysis of TEOS and form $[\text{Si}(\text{OC}_2\text{H}_5)_{4-x}(\text{OH})_x]$ compound. This compound subsequently condenses to produce a large number of oligomers those led to the formation of large-size particles [104]. These results are in accordance with the findings of Kim's work [106] who reported the formation of silica NPs of size 30, 70, and 120 nm when the concentration of ammonium hydroxide was 0.28, 0.42, and 0.56 mol, respectively, and the corresponding NP size observed in this study was 34 nm, 82 nm and 142 nm for S1, S2, and S3, respectively. The particle size for S4 and S5

was found to be 36 nm (TEOS: 0.09 M) and 39 nm (TEOS: 0.180 M), respectively. With increasing TEOS concentration (0.044–0.27 M), a small increase in size of NPs was obtained when concentration of other chemical constituents kept constant, which is consistent with the findings of Kim et al. [106]. TEOS, being the primary source of monomer, will primarily determine the concentration of nuclei/primary particles present in the system. Hence, the increase in particle size is attributed to the increase in concentration of primary particles at the induction period, i.e. primary particles mainly [TEOS]. The induction period is the time period when generation of nuclei takes place from the supersaturated solution and induces formation of primary particles.

Time-dependent (15, 45, and 60 days) DLS based size distribution in nanofluids is presented in Figure 2.3. From Figure 2.3, it can be inferred that no significant change in size of nanofluid S1 was observed over the period of time and its average particle size remained 34 ± 10 nm for the entire 60 days. For S2-S5, a higher variation in size was observed for nanofluid S3; the average particle size in S3 was 142 nm (0 day) which changed to 268 nm (15 days), 522 nm (45 days), and 612 nm (60 days) (see Figure 2.3). For S4 and S5, the variation in size was much less (between 12-20 nm). From these results, it can be inferred that nanofluids (S1, S4, and S5) of smaller NP size exhibited less variation than nanofluids (S2 and S3) of higher NP size. The physical stability of NPs in nanofluid has been majorly improved by the inclusion of PAM which sterically stabilized the NPs from agglomeration resulting shelf life of nanofluids improved.

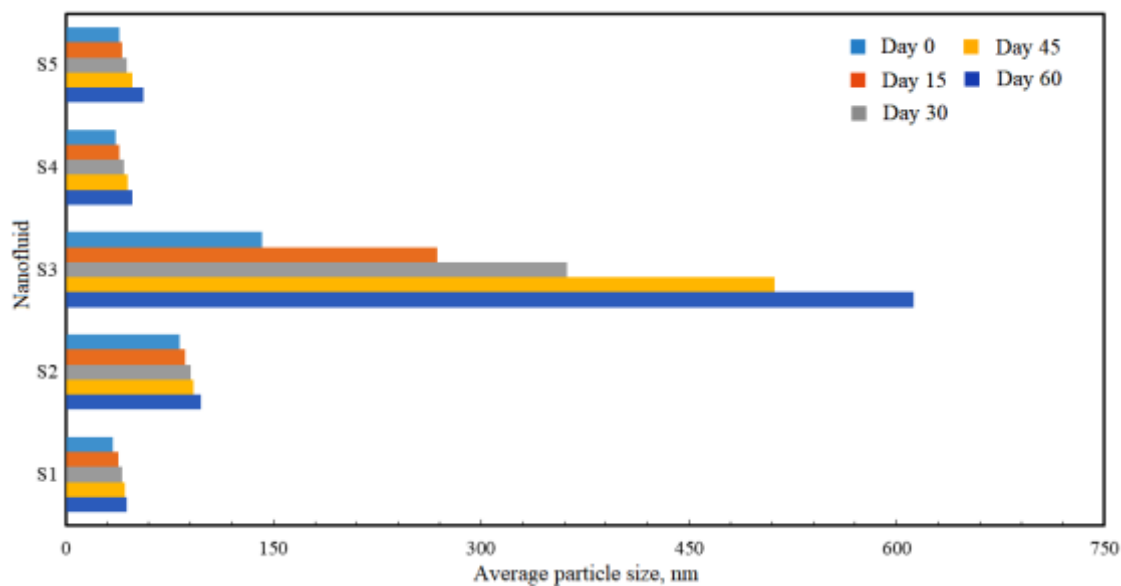


Figure 2.3: Effect of storage time (15, 30, 45, and 60 days) on the average particle size distribution of different nanofluids viz., S1, S2, S3, S4, and S5 at ambient conditions.



Figure 2.4: Effect of high PAM concentration (2000 ppm) on synthesis of silica NPs. With 2000 ppm PAM, interaction between TEOS and NH_3 led to white globules (instead milky appearance) those eventually settled at the bottom.

The effect of high PAM concentration (2000 ppm) on particle size was also explored. It was observed that a high concentration of PAM did not yield any silica NPs. TEOS and NH_3 formed small white globules which settled in the bottom of solvent as shown in Figure 2.4. This may be attributed to the fact that 2000 ppm PAM solution is

highly viscous and consequently, it did not allow the desired interaction between reaction constituents. Thus, for the synthesis of single-step silica nanofluids, the use of 1000 ppm PAM was favorable as stable nanofluids of desired NP size (100-300 nm) is developed by varying the concentration of promoter (NH_3) and precursor (TEOS).

Zeta potential analysis evaluates the stability of suspended NPs (in colloidal suspension) through electrophoretic behavior of the fluid [117]. This is because the free charges in the base fluid get attracted to the opposite charges on the dispersed particles resulting in the development of a layer of charged ions. Zeta potential measure the potential difference between the PAM solution and the stationary layer of silica NPs. For colloidal suspensions, zeta potential value lies in between ± 30 mV is regarded as stable regime [64]. At the time of preparation, all nanofluids were stable colloidal suspensions as zeta-potential value remained higher than -30 mV. With time, the stability of nanofluids did not change much as zeta-potential value of nanofluids remained in stable regime until 45 days of storage period (Figure 2.5). The stability of S2 and S3 nanofluids slightly reduced (unstable zone) after 60 days as their zeta potential value decreases to -29.1 mV and -26.9 mV, respectively. S1, S4, and S5 were stable even after 60 days and their zeta-potential value was higher than -30 mV as shown in Figure 2.5. It is to be noted here that change in zeta potential depends on particle size that has been significantly varied in S2 and S3 (Figure 2.3) while size variation in S1, S4, and S5 was minimal due to no agglomeration. Thus, this involves several possibilities for nanofluid application in oilfield projects where their use gets limited due to tendency to agglomerate and settle.

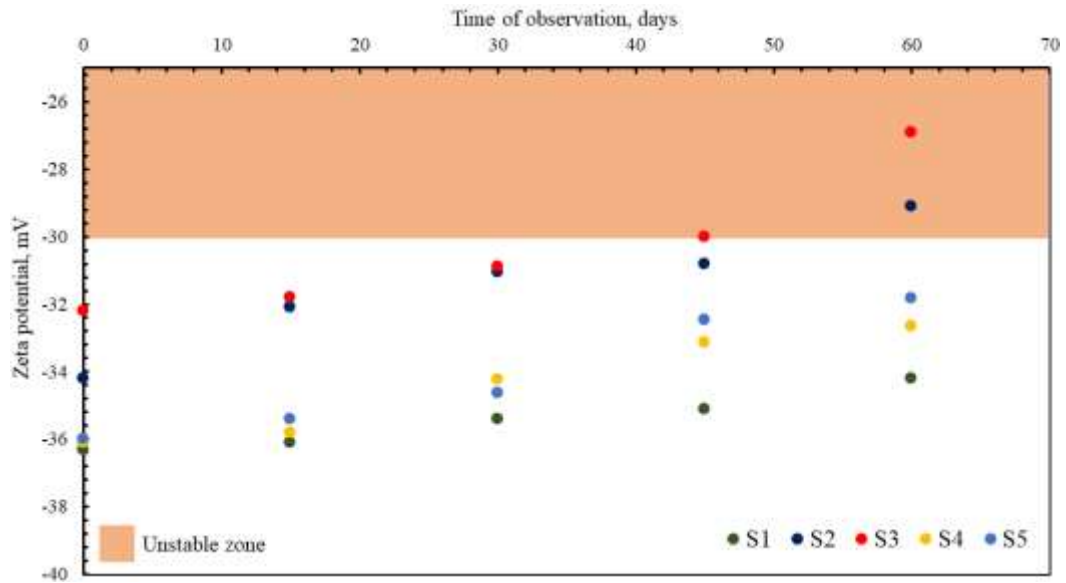


Figure 2.5: DLS based zeta-potential measurements of different nanofluids as a function of the storage period (15, 30, 45, and 60 days).

Non-agglomerated NPs would be able to access narrower pore throats and thus, these NPs will be able to mobilize a greater amount of oil from the reservoir [118]. They are also less prone to mechanical trapping and gravitational settling which reduces the likelihood of formation damage. Smaller and non-agglomerated NPs would be able to travel long distance from the injector due to their smaller size [119]. In addition, non-agglomerated NPs have a greater surface area than agglomerated NPs which increases their participation in chemical reactions [120]. In comparison to other nanomaterials, spherical NPs display an optimized ratio between the surface area and volume which is desirable for maximum cargo loading [121].

2.3.4 Morphological details of silica nanofluids

To understand the morphology of silica NPs, SEM and TEM analysis was performed on S1 and S2 nanofluids and the results are shown in Figure 2.6. SEM images were obtained from dried layer of S1 and S2 nanofluids while NP images in the aqueous phase are presented by TEM images. From SEM and TEM results, it is evident that the

synthesized NPs were of uniform spherical shape and did not show any event of agglomeration even after the lengthy process of sample preparation for SEM (drying) and TEM.

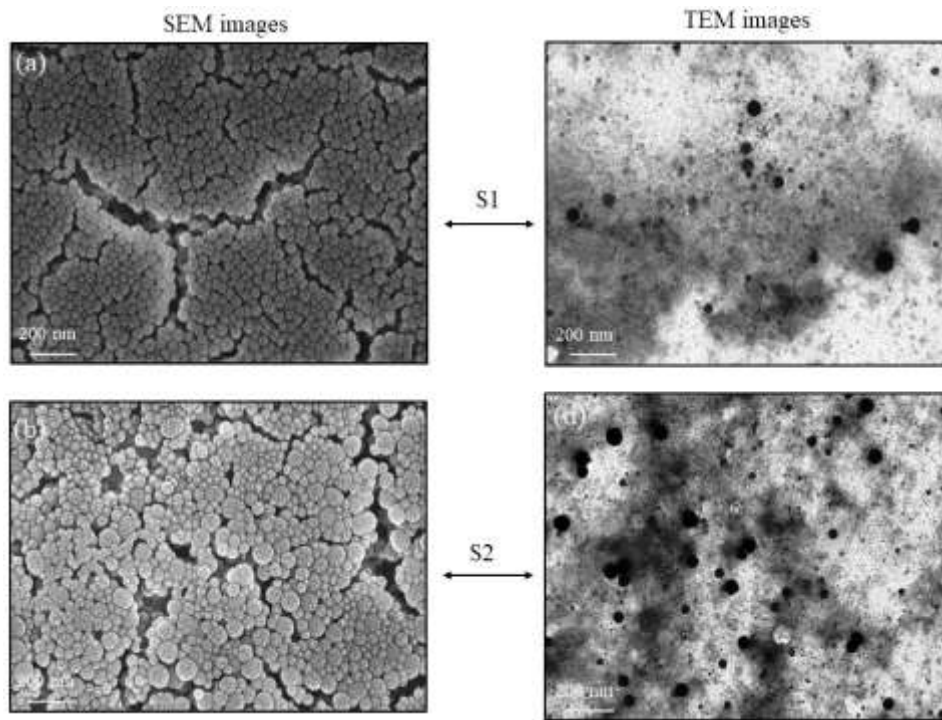


Figure 2.6: SEM (a, b) and TEM (c, d) images of S1 and S2 nanofluids at ambient conditions. The morphological structure of S1 and S2 is non-agglomerated and the presence of small spots (SEM images) is the result of gold coating, performed to illuminate the top surface of nanofluid layer.

SEM images also confirm that NP size in S2 is greater than the one in S1, which is consistent with DLS measurements. However, synthesized nanofluids have excellent potential to flow through pore channels of even low size where conventional nanofluids typically plug the pores and show challenges for industrial applications. Smaller NPs will be able to pass through these pores while larger agglomerated particles would be unable to perform in such an environment. The morphology of silica NPs resembles to consist of small spots on the surface of NPs. These spots were generated during gold coating process

which was performed to illuminate the top surface of NPs. TEM images of S1 and S2 nanofluids show non-agglomerated NP distribution in Figure 2.6, respectively. The spherical shape and difference in size of NPs are also evident from TEM images, consistent with SEM analysis. A spherical NP is also more likely to remain at the centre of a fluid flow which would reduce the likelihood of NP retention due to mechanical trapping and surface adsorption [122]. Thus, the uniform size of synthesized nanofluids makes them suitable candidates for EOR applications in porous media with constricted pore throats.

2.3.5 FTIR analysis

To confirm the chemical structure related to the functional groups and purity of nanofluids, FTIR analysis was performed. FTIR spectra of silica NPs for S1 nanofluid is shown in Figure 2.7.

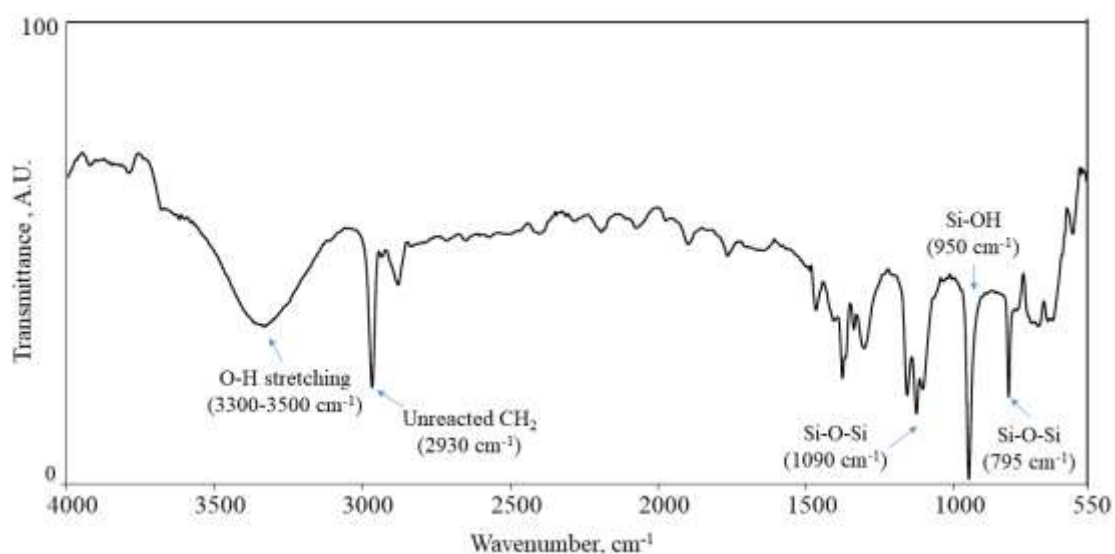


Figure 2.7: FTIR spectra (absorbance vs. wavenumbers) of S1 nanofluid prepared by 0.044 M TEOS and 0.28 M NH₄OH in presence of 1000 ppm PAM.

FTIR spectra of the colloidal particles typically show absorption bands arising from asymmetric vibration of Si–O (1090 cm⁻¹), asymmetric vibration of Si–OH (950 cm⁻¹), and symmetric vibration of Si–O (795 cm⁻¹). The absorption bands between 800 and 1260 cm⁻¹

¹ can be attributed to the superimposition of various Si–O–Si peaks, Si–OH bonding, and residual peaks which are due to the remnants of unreacted organic groups. Water shows an intense characteristic absorption band between 3300 cm⁻¹ and 3500 cm⁻¹ which was assigned to O–H stretching in H–bonded water [123]. The absorption band at 2930 cm⁻¹ (CH₂) denotes the presence of unreacted TEOS in silica NPs [124]. A similar FTIR profile for silica NPs and their synthesis using TEOS has been reported in previous studies [125,126]. From FTIR data, it can be conclusively stated that the use of PAM did not alter any chemical structure or purity of silica NPs.

2.3.6 UV-vis analysis

UV-vis analysis is one of the effective techniques to establish the stability of suspended particles in colloidal solutions. Typically, a non-agglomerated distribution of particles will show higher absorption as minimum rays will pass through the solution and vice-versa. In addition, the peak absorbance is directly related to the concentration of particles in the system; a high peak corresponds to more particles in nanofluid and low peak corresponds to only a few particles [127]. UV data of nanofluids (S1-S5) was plotted in Figure 2.8. When UV readings were taken immediately after the preparation of nanofluid, the peak was observed at 2.8 (at 230 nm) for nanofluid S1. The corresponding value of absorption peak for S2 and S3 was found to be 3.45 and 3.92, respectively. For S4 and S5, where particle concentration was relatively higher, the peak absorbance value increased to 4.82 and 5.40, respectively. To correlate agglomeration (leading to sedimentation) in nanofluids, UV experiments were repeated after a period of 60 days. The peak absorbance value of S1, S4, and S5 did not show any major change and the values were found to be at 2.76, 4.68, and 5.22, respectively (Figure 2.8b). However, S2 and S3 nanofluids exhibited a change in UV after 60 days resulting peak absorbance reduced to 3.11 and 3.02, respectively.

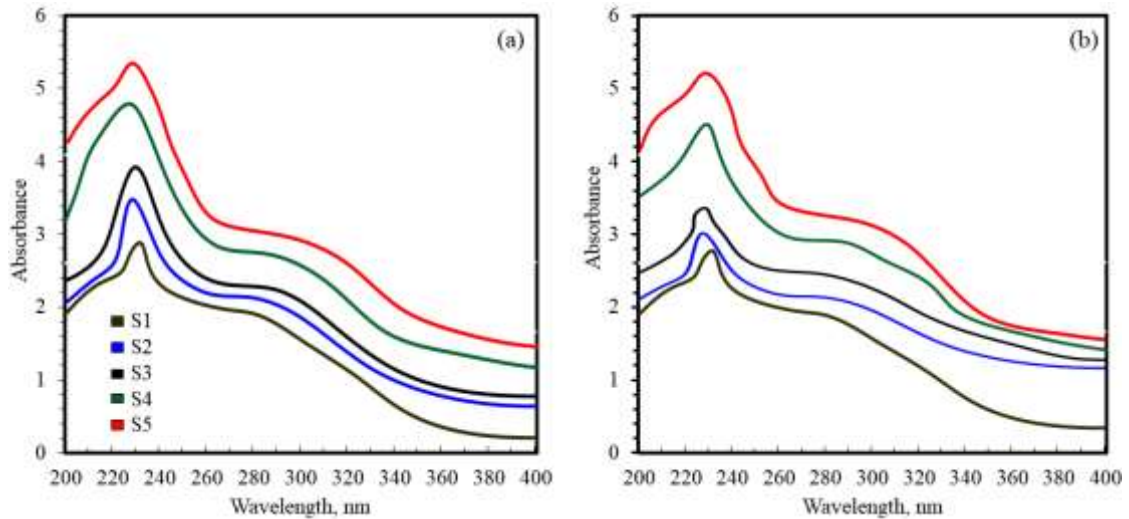


Figure 2.8: Time-dependent (a: 0 and b: 60 days) UV-vis analysis of different nanofluids at ambient conditions where changes in peak absorbance are result of agglomeration between suspended NPs.

The reason for reduced absorbance in S2 and S3 can be attributed to agglomeration as a result, more rays percolated (without absorption) through the nanofluid phase [127]. Therefore, particle size was higher for S2 and S3 nanofluids than S1, S4, and S5 nanofluids, consistent with DLS measurements. S1 exhibited smallest particles (~34 nm) and least precursor (TEOS) concentration and it showed insignificant fall in absorbance peak even after 60 days, indicating high colloidal stability. From UV-results, it can be established that the nanofluid showing insignificant dependency on UV analysis are promising candidates for pore penetration and least formation damage during injection in hydrocarbon formations.

2.3.7 Carbon dioxide flow behavior in porous media

The underground injection of CO₂ is associated with various challenges such as viscous fingering (mobility contrast between CO₂ and residual fluid) and gravity override (density difference between CO₂ and residual fluid) [82,128], which makes the entire CO₂ flow unstable leading to premature breakthrough and insignificant areal coverage. To

address these challenges, proposed improvements include mobility control, conformance modifications, and use of CO₂ thickeners, where chemical enhanced CO₂ flooding have been shown as one of the most promising techniques. Currently, CO₂ foam generation is achieved by adding a foaming agent (surfactant) to improve CO₂ mobility in reservoir pores [129]. However, surfactants have significant limitations at elevated temperature [130]. The thermal stability of NPs makes them promising for CO₂ flow in harsh conditions viz., high temperature and pressure, varying shear rates, and extreme salinity [131]. NPs adsorption to stabilize liquid/liquid and liquid/gas interfaces has been well described in the literature [132] and their small size (in the range of 1–300 nm) allows them to flow through the small pore throats in sedimentary rock [133]. The knowledge of the interaction between the reservoir oil and injected CO₂ is essential for the success of any nanofluid assisted CO₂ flooding. Key variables that must be studied before a CO₂-EOR project are CO₂-injected associated gas percentage, CO₂ in oil solubility, oil density, oil viscosity, and oil composition. With an increase in CO₂ injected gas percentage, the oil density tends to reduce due to higher CO₂ dissolution in oil. This increases the ability of CO₂ to extract more hydrocarbon constituents from crude oil due to lower oil viscosity, a key to plan CO₂-EOR projects in light to intermediate crude oil reservoirs [77]. The formation pressure has been found to exhibit a net positive impact on CO₂-EOR as high pressure increases CO₂ foam stability and thus, it improves foam potential to displace oil from the reservoir [134,135]. Conversely, an increase in reservoir temperature reduces the efficacy of CO₂-EOR as high temperature tends to deform foam and its flow properties [60,136], which is of key importance to screen EOR parameters causing CO₂ foam flood to fail at high temperature conditions. Also, before the application of foam-EOR in oil reservoirs, a major concern is the foam stability when it comes in contact with oil [137,138]. A thin liquid film, known as pseudo-emulsion film, is responsible for the stability of foam in presence of oil.

Because, in absence of pseudo-emulsion film, the oil droplets enter into gas-water interface and cause the foam to breakdown due to oil spreading which eventually destabilize the foam [139]. Thus, mechanisms which are linked to the instability of foam in presence of oil are (1) thinning of aqueous film due to entry of oil drop [140,141], (2) oil spreading on gas foam [142], and (3) the presence of a pseudo-emulsion film [143].

Typically, crude oil comprises of several constituents ranging from C_2 to C_{36} with increasing carbon number denoting an increase in heaviness. Crude oil, comprised of intermediate components, tends to have more effect on CO_2 stability as lighter oil (which consists of short chain alkanes) shows higher miscibility with CO_2 [144,145]. Wang [146] investigated the application of multi-contact miscible CO_2 injection in three natural crude oils (specific gravity 0.8-0.9) to ascertain the effect of oil composition on CO_2 miscibility. Using high pressure glass cell, it was established that CO_2 -crude oil interactions can be subdivided into three stages: CO_2 condensation, extraction-condensation, and extraction. In crude oils comprised majorly of lighter components (C_5 - C_{20}), CO_2 is more miscible and extracts these components by forming a stable miscible front which is less prone to breakdown. This also allows for the production of some amount of heavier components up to C_{36} . However, in heavy crude oils which contain lesser percentage of lighter components (C_5 - C_{20}), a high quality miscible front is unable to be formed. CO_2 is unable to extract most of the components and hence, it is not viable for oil recovery from heavy oil reservoirs.

In a separate study, it was found that the presence of multi-ring aromatic compounds is detrimental for CO_2 -miscibility with oil and thus, it has resulted into lower oil recovery [147]. For EOR applications, CO_2 solubility in crude oil is directly influenced by specific gravity i.e. heaviness of the crude oil and the effect of CO_2 -solubility on oil density is more pronounced in lighter oil than heavier oil [77]. Mechanistically, the process of CO_2 -related oil displacement acts as a differentiator amongst the various components of crude oil as

CO₂ injection results in varying flow rates in crude oils with different composition [148]. Lighter oil compositions are quickly displaced by CO₂ (produced faster) whereas heavier compositions move at a slower pace which eventually leads to change in crude oil composition along with an increase in displacement time. Using component analysis and microscopic modelling, there are three main stages in the process of CO₂-based oil recovery from a homogenous reservoir [35,149]. The oil produced in the initial stage of injection has the same composition as the original oil composition (as it has not come in contact with CO₂). The oil produced during the middle stage of injection generally comprises of lighter compositions (due to CO₂-oil dissolution). Most of the oil produced during the later stage of CO₂ injection are comprised of heavy compositions which were initially left behind during the start of CO₂ injection. CO₂-EOR laboratory study utilizing slim tubes have shown that the carbon number (C_n) of maximum concentration component increases with an increase in CO₂ injection volume [150]. For CO₂ flow studies, the prepared sand-pack (length = 24 inches and diameter = 1.5 inches) was entirely (100%) saturated using water, 1000 ppm PAM solution, and nanofluids (S1, S4, and S5) at constant flow rate of 20 cc/sec and then CO₂ was injected to flow through the saturated sand-packs at constant flow rate (1 ml/min) using a syringe pump. The obtained results and their discussions have been provided in following sub-sections.

Breakthrough time is the total time CO₂ takes to permeate completely through the porous media. Early breakthrough indicates that CO₂ finds the pore of least resistance and reach the outlet end soon without entering into un-swept pore throats. Therefore, a delayed breakthrough is recommended as more CO₂ can be injected to come in contact with oil-bearing zones that can help to improve sweep efficiency from the reservoirs. To measure breakthrough time, the outlet end of sand-pack holder was submerged in universal indicator (UI) fluid that was monitored for color change in presence of CO₂. Since the color of UI

fluid was initially green (neutral pH), the introduction of CO₂ turned the solution color red due to the formation of carbonic acid (acidic pH) as depicted in Figure 2.9.

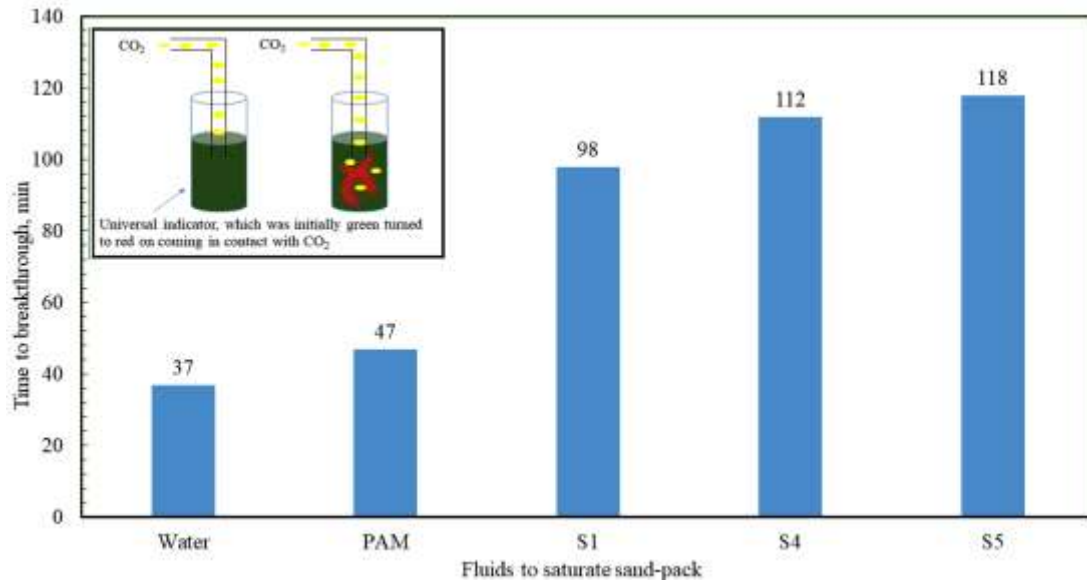


Figure 2.9: Different instances (in min) of CO₂ breakthrough from porous sand-packs for water, PAM, and most stable nanofluids (S1, S4, and S5) at ambient conditions. At breakthrough, colour of UI changes from green to red.

This was defined the instance of CO₂ breakthrough from porous sand-pack and the details of breakthrough time for each fluid are provided in Figure 2.9. It was observed that the breakthrough time of CO₂ in water-saturated sand-pack was 37 min. For PAM solution, the breakthrough time increased to 47 min, this indicates CO₂ residence in sand-pack was longer in presence of PAM solution therefore, PAM delayed CO₂ breakthrough by 10 min than water. A substantial increase in breakthrough time was measured during CO₂ flow in sand-packs saturated with nanofluids. From these results, it is evident that silica nanofluids increased CO₂ retention in sand-pack for longer duration than water/PAM. Silica NPs probably made Pickering foam that is more viscous than injected CO₂ as a result, it delayed CO₂ breakthrough by increasing its retention in sand-pack [10].

During CO₂ flow through sand-pack saturated by various fluids (water, PAM solution, and nanofluids), the back-pressure was recorded at regular intervals and the pressure profiles have been presented in Figure 2.10. Pressure in sand-pack generated due to the resistance offered by present fluid in pore throats. Water, being less dense, offered minimal resistance to CO₂ flow while PAM and nanofluids are viscous therefore, these fluids offered significant resistance to CO₂ flow. Consequently, pressure profiles of CO₂ flow through sand-packs were significantly different (Figure 2.10). There is limited volume inside the sand-pack and injected CO₂ can either (a) displace some fluid and make space for itself or (b) be compressed. For water-saturated sand-pack, some amount of CO₂ is compressed and most of the remaining CO₂ displaces existing water from the sand-pack. Therefore, the pressure variation of CO₂ flow in water-saturated sand-pack is not significant and after CO₂ breakthrough (at 37 min), no further variation in pressure was observed as the injected CO₂ has established a flow between the inlet and outlet. After this point, no further injection of CO₂ was carried out. In addition, it is to be noted here that the increasing pressure is the indication of restricted CO₂ flow resulting further CO₂ injection will be transferred sideways in other pore throats. This probably did not happen with water as pressure remained plateau. In case of PAM, the pressure exhibited a sharp increase during CO₂ flow in sand-pack due to the good mobility ration of polymer and its value kept rising till a peak of 62 psi was recorded after 45 min of injection. This was followed by a sharp drop in pressure as CO₂ breakthroughs from outlet end (47 min). In addition, it is also to be noted here that a steep increase in pressure is the sign of highly restricted entry of CO₂ in pore throats of sand-pack. Therefore, pressure shoots to maximum value and returns to minimum when CO₂ made entry into the pore. This suggests use of PAM can control mobility and breakthrough but it cannot increase areal contact of CO₂ in porous media.

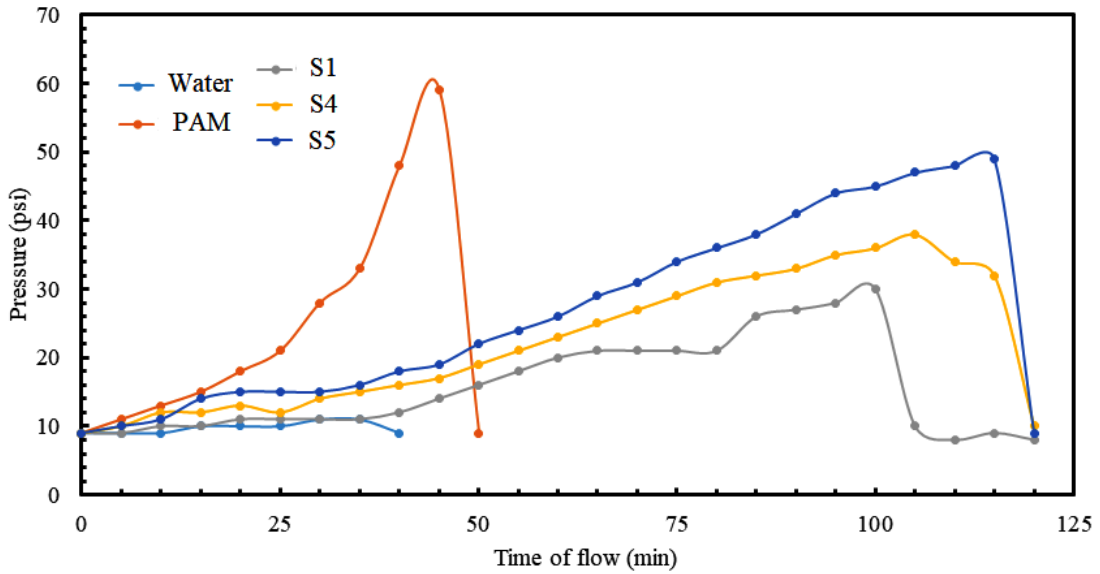


Figure 2.10: Pressure profiles of CO₂ flow in sand-packs 100% saturated by water, PAM, and nanofluids (S1, S4, and S5).

An unrestricted entry with high areal sweep can be achieved if the size of CO₂ bubbles is reduced; CO₂ disintegration into smaller bubbles will increase the surface area of CO₂ to contact more oil-bearing zones through increased access to pore throats. NPs can help to produce smaller CO₂ bubbles by reducing interfacial tension of injected CO₂. In silica nanofluid, silica NPs (due to less size) may easily migrate through pore throats in sand-pack and these NPs can help to reduce interfacial tension of CO₂ when it flows through these pores. Thus, the entry of smaller bubbles will be relatively less restricted than bubble of higher size consequently, pressure will not increase much as observed for CO₂ flow in nanofluid (S1, S4, and S5) saturated sand-packs in Figure 2.10. It is evident from progressive increase in pressure that CO₂ disintegrates into smaller bubbles and formed viscous foam in presence of silica NPs. The structure of this foam is governed by mixed entanglements of PAM-NP in which CO₂ bubbles remained trapped and provided significant mobility control on subsequent injection of CO₂. As a result, CO₂ could not finger through viscous foam instead it pushes foam uniformly (like piston displacement) in sand-pack before final breakthrough at outlet. A progressive increase in pressure also hints

that CO₂ foam did not decay with time otherwise pressure would have varied differently, this might be due to steric stabilization of CO₂ bubbles in foam structure [10]. Therefore, breakthrough time significantly increased to 98, 112 and 118 minutes for S1, S4, and S5 nanofluids. The delay in breakthrough indicates that CO₂ residence in pore throats was longer that made more injection of CO₂ possible, a key advantage for CO₂ sequestration and CO₂-foam flooding using silica nanofluids in porous reservoirs. The purpose was to control CO₂ mobility in porous media by nanofluid and compare with water/PAM fluid, and to determine how much CO₂ can be injected before it finally breakthroughs from the outlet which is of key importance for effective CO₂ utilization in porous media. The amount of fluid received from outlet has been provided in Figure 2.11.

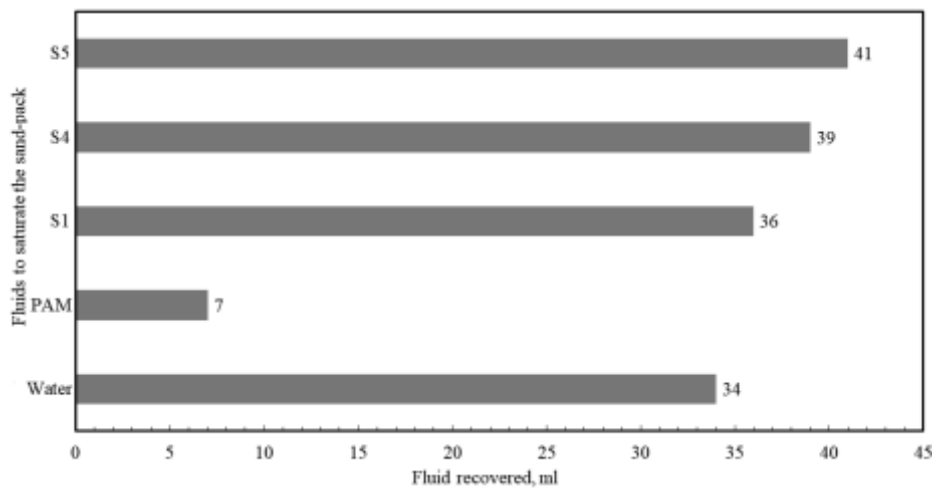


Figure 2.11: The amounts of liquid recovered as displacement efficiency per unit of CO₂ injected in sand-packs 100% saturated by water, PAM, and nanofluids (S1, S4, and S5).

From Figure 2.11, it can be observed that 37 ml (time to breakthrough = 37 min, injection = 1 ml/min, Figure 2.9) CO₂ injection in a water-saturated sand-pack yielded 34 ml of water. The fluid displacement efficiency per unit of CO₂ injected was 0.91. This means that some amount of CO₂ (the difference = 3 ml) was compressed into the body of water as CO₂ is a compressible fluid and has the tendency to be dissolved in water [151].

This is not desirable in cases where area of the storage reservoir is finite and displaced fluids may not have sufficient space to be moved. This will increase back-pressure on the pumping units as more pressure will be required to dissolve the water with CO₂ [152]. For PAM, the amount of fluid recovered was only 7 ml even after CO₂ resides in sand-pack for 47 min before breakthrough (see Figure 2.9 and 2.11). The fluid displacement efficiency per unit of CO₂ injected for PAM was only 0.14 which is very low. The low fluid displacement efficiency can be explained by the variation in mobility between displacing fluid and displaced fluid which leads to viscous fingering [18]. On the other hand, the amount of fluid recovered during CO₂ injection in silica nanofluids was 36 ml (for 98 ml CO₂ in S1), 39 ml (for 112 ml CO₂ in S4), and 41 ml (for 118 ml CO₂ in S5). Nanofluids were almost similar to PAM solution in viscosity, the only difference between their effect on CO₂ flow behavior was inclusion of NP that not only increased fluid displacement efficiency per unit of CO₂ but also increased CO₂ coverage in sand-pack by delaying its breakthrough. The displacement efficiency per unit of CO₂ injected for nanofluids ranged in between 34-38%.

2.3.8 NP retention in porous media

A porous media can be defined as a complex material in which pore throats of different sizes exist where NP may retain during the injection. NP retention may adversely affect rock properties such as porosity, permeability, and wettability where enhanced retention is a form of formation damage [62]. However, NPs also have proven as wettability modifiers in hydrocarbon formations [153]. NP retention is the result of its adsorption on pore walls instead of migrating to CO₂/fluid interface; this undesired adsorption adversely affects the properties of rock such as permeability. Conventionally, the retention of NPs in porous formation can be of various forms: (i) particle adsorption; particles adhere to the pore walls due to electrostatic interactions, (ii) mechanical trapping; particle size is greater

than pore throats, and (iii) gravitational settling: density difference between NPs and aqueous phase (see Figure 2.12 for scheme on trapping mechanisms).

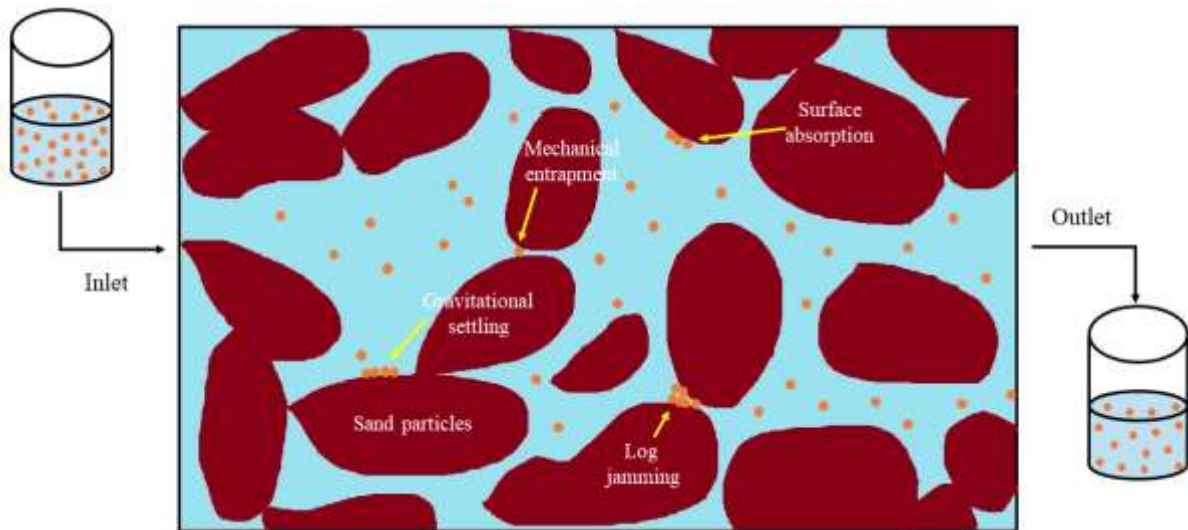


Figure 2.12: Schematic showing how NP is trapped under different mechanisms during NP transport in porous and permeable pore throats.

Therefore, knowledge of NP retention in the porous media is essential during nanofluid use for CO₂ flow strategies.

From our investigations, it was observed that NP retention is not very severe and only 8-12% (average of five injections) of total injected amount retained in sand-pack for all experiments. From results, it can be inferred that the length of sand-pack was the most influential variable; the data showed that increasing length of sand-pack exhibited an exponential increase on NP retention. This can be used to establish that NP retention will increase for longer porous media and for higher mass concentration of NPs used. However, between 14 and 24-inch sand-pack lengths, NP retention reached to minimal and this indicates that maximum amount of NP retention occurs near the entrance of sand-pack as shown by sharp decrease in NP recovery during 0-14 inch region. NP retention conditions for silica nanofluids are consistent with previous findings [154]. A similar trend was

observed for flow rates, where high flow rate of 2 ml/min showed that NPs spent smaller amount of time in sand-pack and consequently, lower NP retention was observed. Interestingly, the temperature had marginal effect on NP retention in sand-pack; an approximate 2% increase in retention was observed at 363 K compared to 333 K. Thus, the obtained results had some interesting observations such as (1) the concentration of silica NPs did play a significant role in NP retention and (2) more silica NPs would retain if NPs are already present in reservoir. The experimental investigation on NP retention would allow for future researchers to ascertain the impact of NP retention on environment before using for commercial enterprises [155,156]. Apart from oilfield, single-step nanofluid can find application in other applications such as nanofluid use as thermo-physical fluid for heat and mass transfer due to extended shelf life [157].

2.3.9 Techno-economic analysis of silica nanofluids

Nanofluids have received significant attention in industrial applications due to their superior properties. However, in oilfield, nanofluid application is hindered by the need to have specialized facilities for their synthesis onsite. Conventional nanofluids have a limited shelf-life and this complicates the attempt to synthesize them in a lab and then transport them to well-head. Single-step silica nanofluids of extended stability are reservoir compatible colloidal suspensions, to be utilized for field projects. In addition, the method (sol-gel) is widely acceptable and thus, it presents technically no challenge in nanofluid synthesis. For the proposed field application, scalability of the process to synthesize nanofluids in bulk quantities would remain a challenge. It is also important to consider all limitations related to the utilities and infrastructure before the usage of these nanofluids. This seems to be less challenging for single-step silica nanofluid as its synthesis relies on the use of similar utilities and infrastructure (blenders, homogenizers) used for conventional surfactant flooding.

A major challenge for single-step nanofluid is to be financially competitive when compared to two-step silica nanofluid. To perform a rudimentary cost comparison, 2 separate single-step and two-step silica nanofluids of equal concentration (0.1 wt%) and volume (100 ml) were prepared. To prepare two-step silica nanofluids, commercially available silica NPs (size ~ 15 nm, Sisco Research Lab Pvt. Ltd., India) were used. To further simplify the calculations, the expenses on utilities (water and electricity) and labour costs were assumed to be equal for both methods, and only the cost of chemicals has been considered in this study. It has also been assumed that 5% of all chemicals will be wasted in the synthesis. The cost to synthesize two step nanofluids was found to be 0.25 USD per 100 ml of solution. Similarly, the cost to synthesize single-step nanofluids was found to be 0.27 USD per 100 ml of solution. Hence, it is possible to manufacture single-step silica nanofluids of superior stability on a similar budget. The study also could not account for the massive economies of scale that a commercial vendor has in manufacturing silica NPs, enabling him to sell his NPs at a cheaper rate. When manufactured on a larger scale, the cost to manufacture single-step silica NPs would further reduce, increasing its financial appeal for potential users.

2.4 Conclusion

In this study, single-step silica nanofluids of varying size (34-142 nm) were synthesized for oilfield applications *viz.*, improved the CO₂ flow behavior and reduced NP retention in porous and permeable sand-packs of mesh size 40. Polymer PAM (1000 ppm), which is a common oilfield viscosifier, was found to increase the dispersion stability (more than 2 month) of synthesized nanofluids, where concentration of silica NPs was controlled by the addition of TEOS (as precursor) and the size was controlled by the addition of NH₄OH (as base catalyst). Synthesized nanofluids of low size (34-39 nm) were extremely stable against agglomeration as confirmed by insignificant change in zeta-potential

measurements up to 2 months therefore, these nanofluids did not exhibit any increase in NP size and sedimentation. The synthesized nanofluids (S1, S4, and S5) were then used as saturating fluids in porous sand-packs to ascertain their viability in reducing CCP. Nanofluids greatly increased the retention of CO₂ in sand-pack by 2-2.5 fold than water/PAM, where nanofluid (S5) exhibited maximum CO₂ retention of 2 h in sand-pack by delaying the final breakthrough from outlet. CO₂ mobility is controlled by foam that was stable (to decay) and more viscous than pure CO₂, while CO₂ in presence of water and PAM did not form any foam resulting it breakthroughs within 37 and 47 min, respectively. Nanofluids also did not show an adverse pressure profile (during CO₂ flow) like the one observed with PAM fluid, hence their use in oilfield applications for increasing the duration of carbon retention in reservoirs can be recommended. Finally, to analyze NP retention in a sandstone formation, NP retention was determined by displacement tests in sand-packs. The parameters investigated for NP retention were (1) length of sand-pack, (2) rate of nanofluid injection, (3) temperature of sand-pack, and (4) concentration. For five subsequent injections, NP retention was found to remain in between 8-12% which is better than the use of conventional two-step silica nanofluids in a reservoir. Thus, single-step silica nanofluid, due to its nanometer size, can be a promising method for oilfield applications where minimal NP retention and improved CO₂ flow in porous media is required.

Rheological Analysis and EOR Potential of Surfactant Treated Single-Step Silica at High Temperature and Salinity

Abstract

Single-step nanofluids have shown better stability and size control properties than conventional two-step nanofluids under similar conditions. However, for wide-spread oilfield acceptance, there is a need to investigate the role of oilfield conditions viz., temperature, salt on stability of single-step nanofluids. Thus, in this study, single-step silica nanofluids were synthesized in base fluid (1000 ppm polyacrylamide, PAM) and their stability was investigated using methods such as dynamic light scattering (DLS) and rheological analysis to establish their viability as suitable enhanced oil recovery (EOR) agents. PAM is a widely used oilfield practically applicable polymer. Primarily, the single-step silica nanofluids were found to destabilize at higher temperatures (≥ 90 °C) due to thermal stability issues of PAM at high temperatures. This was also understood by PAM rheology. The inclusion of salt reduced the stability of nanofluids due to the suppression of inter-particle repulsive forces. The addition of an anionic surfactant (SDS) improved nanofluid stability by reducing salt-induced NP agglomeration; increasing surfactant concentration initially improved nanofluid resistance to salt induced agglomeration and at high surfactant concentrations, the nanofluids exhibited greater NP agglomeration even in the absence of salt. The oil recovery results also showed that surfactant use in the synthesis

of silica nanofluid for oil recovery applications may provide better results than sole silica nanofluid. Based on the observations, surfactant treated single-step silica nanofluid use was found favorable for oilfield practices where conventional nanofluids may show challenges.

3.1 Introduction

Nanofluids are novel colloidal suspensions of nanoparticles (NPs, size ≤ 100 nm) dispersed in a base fluid which have superior rheological mass transfer properties [157], CO₂ absorption capacity, due to their better structuring [90], and exceptionally high surface area to volume ratio [158]. In recent years, silica nanofluids have gained widespread use in the oil industry due to their superlative properties, low cost of fabrication and the ease of their surface modification [159–162]. It is also stated that the superior surface area to volume ratio makes nanoparticles more reactive than corresponding micron-sized peers due to possessing proportionally more atoms available on the surface for chemical interactions [47]. However, the dispersed NPs are prone to agglomeration when dispersed in a solution which leads to the formation of aggregates, several magnitudes larger than the size of individual NPs [127]. Particle agglomeration is a process which reduces the surface free energy by amplifying the size of NP aggregates and correspondingly, reducing NP surface area [47]. It can also be categorized as a mass-conserving but population-reducing exercise [66]. Agglomeration may take place due to the need of the NPs to reduce surface free energy, due to random motion leading to particles colliding and sticking together (Brownian agglomeration), the capture of smaller particles (which are slowly settling) by the larger particles that tend to settle faster (Gravitational agglomeration) or the rapid change in particle trajectories which lead to higher NP collisions and cohesions (Turbulent agglomeration) [66]. An external factor influencing NP agglomeration is salinity [163–165]. In saline environments, salt electrolytes reduce the inter-particle (between individual

NPs) repulsive forces corresponding to higher collisions among NPs and consequently, particle coagulation which causes separation of phases [166].

Regardless of its cause of the occurrence, NP agglomeration reduces the particle surface area available for participation in chemical interactions and shifts the particle size distribution to the higher side. Larger particle agglomerates are unable to match the performance of their smaller-sized counterparts. When used for CO₂ absorption by pressure decay in an equilibrium cell, larger silica NP agglomerates were formed when NP concentration was increased from 0.1 wt% to 1 wt% and the increasing concentration reduced the CO₂ loading capacity of the nanofluids by 8-14%. Separately, larger NP agglomerates are unable to access the narrower pore throats in a hydrocarbon reservoir and are unable to mobilize the trapped oil in them [118]. Larger NP aggregates are highly prone to mechanical trapping and gravitational settling and thus, will be able to travel a shorter distance from the injector well [119]. Hence, it becomes essential to synthesize stable nanofluids that would be able to resist agglomeration for wide-scale industrial adoption, especially in the oilfield applications. At present, nanofluids stabilization is attempted by including polymers [167], surfactants [168], other NPs like TiO₂ [127] or a combination of surfactant-polymer additives [169] though the effectiveness of such methods is constrained by operating temperature, duration of storage and formation salinity. These methods can stabilize silica nanofluids until a duration of 24-42 days, though their efficacy is further reduced in adverse saline conditions.

A separate approach to synthesize stable nanofluids for industrial applications is to alter the method of silica nanofluid preparation. Conventionally, nanofluids are formulated by dispersing commercially obtained nanopowder in a base fluid using a particle homogenizer. This process is referred to as two-step nanofluid fabrication and the nanofluids formulated using this method are highly prone to agglomeration. In single-step

synthesis of nanofluids, the nanoparticles are grown *in-situ* in a base fluid using a precursor [106]. For oilfield applications, several nanofluids have been explored however silica nanofluids have gained widespread use due to their low cost, ease of fabrication, high modification adaptability, and reservoir compatibility [96,168,170]. In addition, unlike two-step silica nanofluids, single-step silica nanofluids are less prone to agglomeration and are stable for a longer period [103].

However, comprehensive studies extolling the use of single-step silica nanofluids for oil field application are yet to be performed as the potential oilfield application of single-step silica nanofluid dispersions as foam stabilization agents, drilling fluid additives or tracer elements is constrained by the lack of knowledge of single-step NP dispersion and agglomeration properties, especially in conditions of adverse salinity and temperature and in the presence of other widely used oilfield chemicals like surfactants. Thus, in this study, we have investigated the stability of single-step silica nanofluids of varying concentration (0.1-1 wt%) for oilfield applications, especially for reservoirs at high temperature and of adverse salinity. The particle size and zeta potential as a function of temperature (30-90 °C) and formation salinity (0-8 wt% NaCl) were measured. A surfactant, sodium dodecyl sulfate (SDS) was used to stabilize the nanofluids. The work aims to establish the suitable conditions for single-step silica nanofluid use in high temperature/ saline reservoirs and investigate the synergistic role a surfactant may play in stabilizing silica nanofluids in such adverse conditions.

3.2 Materials & Methods

3.2.1 Materials

Anionic surfactant, sodium dodecyl sulphate (SDS) (purity ~ 85%; alkalinity = 5 Meq/mL; sodium chloride and sodium sulfate: 8%; unsulfated alcohols: 4%; SDS CAS No: 151-21-3) was obtained from Sisco Research Lab Pvt. Ltd. India. The other chemicals used

in this work have been reported in Chapter 2. The method to synthesize the nanofluid has also been reported in Chapter 2.

3.2.2 Critical Micellar Concentration (CMC) determination of Nanofluid-Surfactant formulation

Surface tension measurements were conducted, using a laboratory stalagmometer, to determine the CMC value of the surfactant (SDS) [171]. The stalagmometer is a circular glass tube which has a large diameter bulb located in its middle section. The bottom end of the glass tube is designed narrow. This forces the liquid to fall in the form of a drop when its droplet weight becomes greater than the surface tension. The surface tension of formulations was determined by allowing the droplets to fall and the number of droplets was counted. The CMC of a solution is reached when the surface tension value insignificantly changed with the increasing concentration of surfactant. Following this, the relative surface tension of the silica nanofluid samples was determined. The values of the CMC were further cross-checked by the electrical conductivity method [172]. This was performed using a Hanna Digital electrical conductivity meter (Model-HI98129, uncertainty $\pm 3\%$). To establish the CMC via the electrical conductivity method, the electrical conductivity of samples with varying surfactant concentration were measured. The CMC is the point at which a sharp change in the slope of the electrical conductivity values is observed [173]. To ensure the reproducibility of values, the entire exercise was repeated at least thrice for each of the nanofluid samples.

3.2.3 Additive adsorption in porous media

To establish the amount of polymer, NP and surfactant adsorption in porous media, static adsorption tests were performed by adding pretreated sand to a mix of fluid under

investigation and the entire mixture was stirred for 30 min at 1200 rpm in a centrifuge [174,175]. A rheological analysis of injection and effluent (obtained after the completion of sand adsorption) fluids was performed using a modular compact rheometer (MCR-52, Anton-Parr, Austria) utilized in our past studies. To perform these measurements, a small volume of the fluid under investigation (6-8 ml) was taken in a cup and bob assembly mated to the rheometer. A wide range of shear rate (20-2000 s⁻¹) was applied on the fluid and the entire experimental run took 9 minutes. Following this, the bob was lifted away from the cup and fluid was drained out of it. The cup and bob were carefully washed with toluene & water and dried before & after each investigation to minimize any instance of cross-contamination.

3.2.4 Oil recovery experiments using single-step silica nanofluids

To further validate the synergistic role that NPs and surfactants play in porous media which may be conducive to improving oil recovery from high temperature and adverse salinity formations, a set of flooding runs were performed in synthesized porous media. The synthetic porous media was prepared by wet-ramming pretreated sand of uniform shape (200-380 μm) and majorly quartz composition [109,176] in a sand-pack holder (length: 24 inches, diameter: 1.5 inches). The sand-pack was used as part of the experimental setup comprising of a syringe pump, fluid accumulators, heating jacket with integrated temperature controller and flow control valves. The entire setup was custom designed and manufactured by D-Cam Engineering, Ahmedabad and has been used to perform various oil recovery and flow behavior studies in past. The oil used in the study was obtained with the requisite permission of competent authorities of Tarapur Oilfield, India. Oil recovery tests were performed at two temperature conditions of 60 and 90 °C. No confining pressure was used on sand-packs during experiments and the pressure was thus kept ambient. The oil had a viscosity of 4.2 mPa.s at 60 °C and 2.8 mPa.s at 90 °C.

The porosity and permeability of the prepared sand-packs were obtained using standard oilfield procedure. The details about the crude oil have been provided in Table 3.1.

Table 3.1: Properties of crude oil used for flooding experiment

Pour Point	310 K
Viscosity (mPa.s) (at 333 K)	3.4
Density (gm/cc) (at 333 K)	0.85
Chemical composition (%)	
Saturates	64.6
Asphaltenes	18.4
Resins	12.9
Aromatics	4.1

3.3 Results and Discussion

In this section, initially, the shape and size of NPs in nanofluids were reported and discussed using SEM analysis and particle-size distribution. Following this, the results on nanofluid stability as a function of storage duration have been reported at various temperature and salt conditions using the DLS and zeta-potential measurements and the anticipated causes for the phase separation observed in the nanofluids are discussed. The effect of surfactant addition on the stability of the single-step silica nanofluids in the salt environment has also been reported and discussed. Finally, the role of polymer, surfactant and NP adsorption has also been investigated rheologically to establish the efficacy of surfactant treated silica nanofluids for oil recovery from high temperature, adverse salinity formations followed by the oil recovery studies using sole and surfactant treated single-step silica nanofluids.

3.3.1 Silica nanofluid degradation

Primarily, nanofluids tend to degrade if (1) stored for a long duration, (2) subjected to high temperature and (3) addition of salt. To perform these experiments, nanofluid

samples were kept in distinct conditions for the observation period and for measurement, a small volume from the nanofluid samples was removed from the stock solutions at regular intervals. The nomenclature of these samples has been provided in Table 3.2.

Table 3.2: Nomenclature, concentration, average particle size, and particle frequency of synthesized nanofluids

Sample no	Average particle size (nm)	NP concentration (wt%)	Size (30-40 nm) frequency (%)
S1	34 ± 6	0.1	82
S2	36 ± 4	0.5	80
S3	39 ± 5	1	74

The particle size measurements were performed to ascertain the size of the nanoparticle aggregates as a function of storage duration by placing the nanofluid samples in a quartz cuvette and the measurements were conducted at the various temperatures using a 173° scattering angle detector. The zeta-potential measurements were performed using a custom cuvette by taking a limited amount of sample and measuring the potential across the ends. These measurements were performed to observe if the NPs aggregate and develop into large clusters which may influence their performance when used in oilfield applications. All measurements were repeated at least five times to minimize errors and any deviations have been reported in the form of error bars. The single-step silica nanofluids (S1, S2, and S3) were observed using a DLS apparatus and their average particle size as a function of storage duration has been reported for the temperature range 30-90 °C as Figure 3.1.

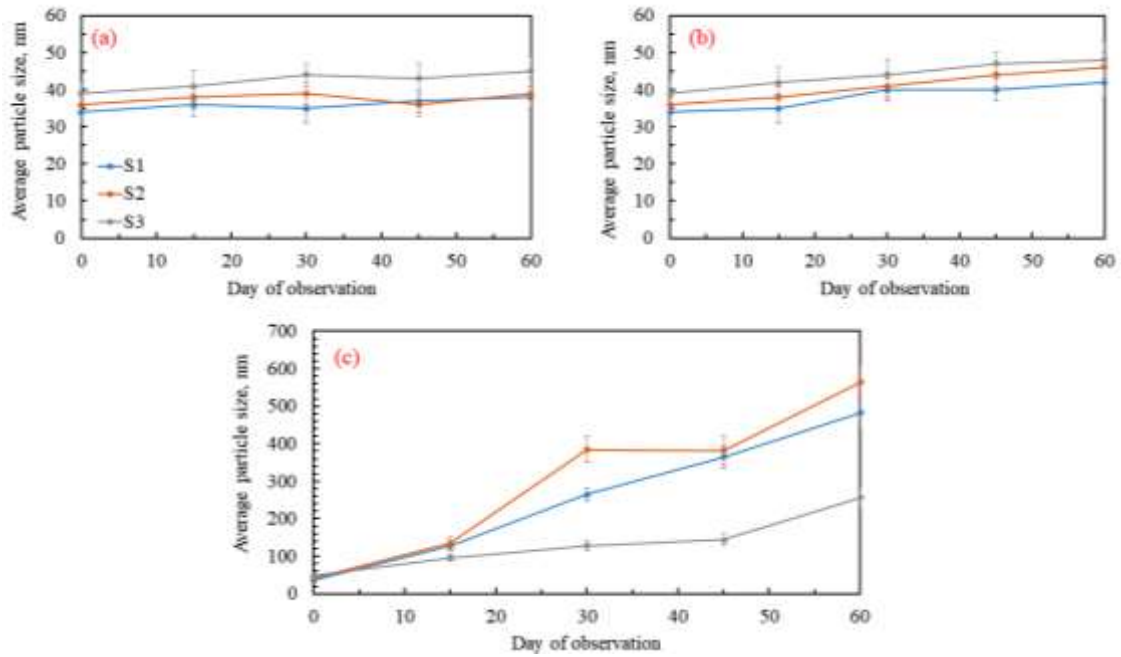


Figure 3.1: Average particle size observed for silica nanofluids as a function of storage duration at (a) 303 K, (b) 333 K and (c) 363 K.

At 303 K, it was observed that the nanofluid S1 exhibited a particle size of 34 nm while similar readings for S2 were 36 nm and S3 were 39 nm when the nanofluid samples were observed just after the completion of their synthesis. Over the entire period of observation, the nanofluids did not show any appreciable change and even at the end of 60 days, the average particle size recorded for S1 was 38 nm, S2 was 39 nm and S3 was 45 nm (Figure 3.1). The nanofluid samples were also kept in a glass vial inside an oven at 333 and 363 K and for measurements, the samples were withdrawn at regular intervals. At 333 K, the nanofluid samples did not show any change from the initial values throughout storage and near-similar values of 42, 46, and 48 nm were recorded at the end of the 333 K days (Figure 3.1). The average particle deviations were less than 5 nm. The observations at elevated temperatures indicate that the silica nanofluids resist agglomeration and remain stable even after being stored for a long duration (in this case, 60 days). This high stability of single-step silica nanofluids can be attributed to the presence of long PAM chains which

sterically stabilized the NPs allowing them to resist Brownian agglomeration. The increase in viscosity of the base fluid on the addition of PAM, resists the sedimentation of NPs, directly reducing their gravitational agglomeration.

However, when the experiments were repeated at 363 K, the nanofluids started to show agglomeration. Nanofluid sample S1 which had an average particle size of 34 nm after preparation increased in size to 128 ± 12 nm (Day 15), 264 ± 18 nm (Day 30), 364 ± 28 nm (Day 45) and 482 ± 42 nm (Day 60). Similarly, the NP size of S2 increased to 134 ± 16 nm (Day 15), 383 ± 34 nm (Day 30), 386 ± 36 nm (Day 45) and 564 ± 44 nm (Day 60). The average NP size observed in nanofluid S3 was 96 ± 10 nm (Day 15), 128 ± 14 nm (Day 30), 144 ± 16 nm (Day 45) and 256 ± 24 nm (Day 60) as observed in Figure 3.1.

At higher temperatures, PAM tends to degrade causing it to lose its viscous nature [88]. This was confirmed by the thermogravimetric analysis (TGA) of the base fluid (1000 ppm PAM dissolved in water) and the three nanofluid solutions (S1, S2, and S3). The thermogravimetric analysis results presented as the relative mass change observed in the solutions on an increase in temperature are presented as Figure 3.2. From Figure 3.2, it can be observed that PAM shows major degradation at 90 °C by losing over 65% of its mass. The addition of silica NPs was found to improve the thermal stability of the synthesized nanofluids (Figure 3.2). Silica NPs start to adhere to the surface of the polymer-nanocomposite due to their low surface energy [177]. Once present on the surface of the composites, they act as thermal insulating materials and hence, protect the inner polymer layer from heat degradation [178]. At 90 °C, the relative mass change observed was 58% in S1, 54% in S2 and 48% in S3. Thus, increasing the silica NP concentration (from S1:0.1 wt% to S2:0.5 wt% and then S3:1 wt%), further improved the thermal stability of nanofluids as more silica NPs were in the suspension to act as thermal insulators.

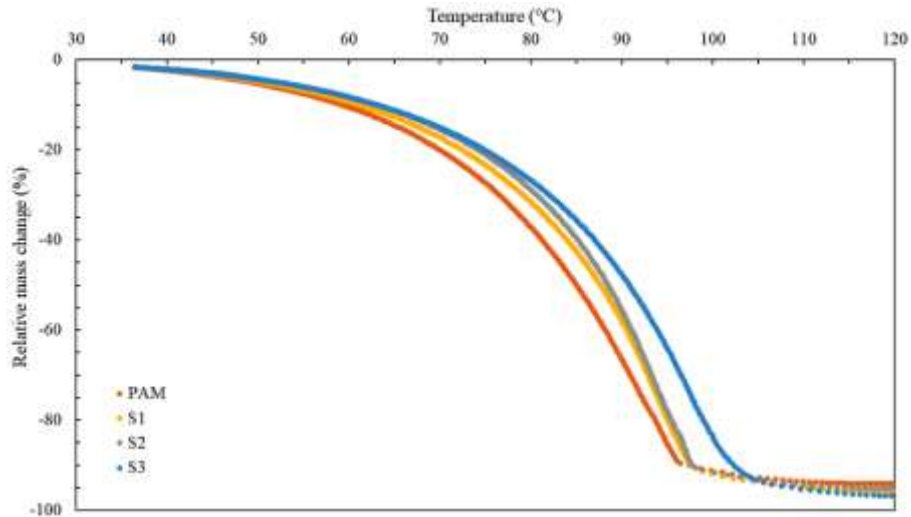


Figure 3.2: Thermogravimetric analysis of synthesized single step silica nanofluid samples.

However, the loss in mass (primarily, PAM) at elevated temperatures, reduced the steric stabilization of NPs which promotes agglomeration and eventual sedimentation, leading to the separation of phases in the nanofluid. The TGA results indicated that the polymeric solutions destabilized at higher temperatures. The inclusion of SiO₂ NPs stabilized the polymeric solutions and an increase in NP concentration was beneficial for further improving the stability of the solutions. The DLS measures the hydrodynamic diameter of the NPs. The measurement is indicative of the average size of particles suspended in the solution, not their concentration. At high temperature, the NP in the solution agglomerated rapidly and formed large clusters (which are themselves more prone to sedimentation). Thus, the NPs in S3 (which had the maximum concentration) agglomerated rapidly and due to weaker steric stabilization at higher temperature, settled rapidly. This ensured that most of the larger agglomerates (i.e. >300 nm) had settled before the second measurement of S3 could be taken after 15 days. Hence, the largest sizes recorded by the DLS were in the range of 200-300 nm while the larger NP aggregates had

settled on the base of the glass vial, in form of sediments and were thus, not part of the size measurements.

3.3.2 Single-step silica nanofluid degradation as a function of salinity

To ascertain the effect of salinity on the synthesized nanofluids, NaCl of varying wt% (0-8 wt%) was added to the nanofluids at ambient temperature. The observations obtained from the particle size measurements have been reported in Figure 3.3. When the particle size measurements were performed after adding NaCl salt (2 and 4 wt%), the observations varied significantly than those of nanofluids obtained without any salt. On adding 2 wt% salt, the particle sizes of S1 nanofluids were 156 ± 16 nm, 307 ± 12 nm in S2 nanofluids and 595 ± 43 nm in S3 nanofluids when the observations were performed 15 days after the addition of salt. When the observations were repeated after 30 days, the size of S1 nanofluids had increased to 294 ± 14 nm, the size of S2 was 1212 ± 59 nm and 1847 ± 48 nm in S3. The readings were then taken again on the 45th day and the particle size had changed to 368 ± 17 nm in S1, 1342 ± 34 nm in S2 and 206 ± 18 nm in S3 nanofluids. On the 60th day, the particle size had increased to 468 ± 27 nm in S1, 1785 ± 26 nm in S2 and 242 ± 16 nm in S3 nanofluids. When the salt concentration was increased from 2 to 4wt% NaCl, the particle sizes further increased to 284 ± 17 nm for S1 nanofluid, 482 ± 28 nm for S2 nanofluid, 1448 ± 48 nm for S3 nanofluids when the samples were observed on the 15th day. On the 30th day, the particle size had further increased to 388 ± 17 nm in S1 nanofluid, 643 ± 37 nm in S2 nanofluid and 168 ± 12 nm in S3 nanofluid. On the 60th day of observation, the particle size in S1 was 782 ± 42 nm, 265 ± 11 nm in S2 and 242 ± 16 nm in S3. The addition of 8 wt% NaCl promoted the instant formation of large aggregates in the solution which sediment rapidly and no observations could be taken. From the presented data, it is evident that the inclusion of salt had promoted rapid aggregation of the SiO₂ nanoparticles which is further amplified when the concentration of salt is increased in the solution. The aggregation can

be attributed to the dissolution of NaCl in water and the formation of Na⁺ and Cl⁻ ions. The presence of these electrolytes destabilizes the particle suspensions by compressing the extent electrical double layer. On an increase in electrolyte concentration, the present energy barrier is further lowered to such an extent that the extent of particle aggregation is dictated primarily by the kinetic energy in the particles. This leads to the formation of larger silica aggregates. Not only are the larger aggregates more prone to sedimentation which would reduce their applicability before flooding but they are also more likely to block the smaller pore throats once inside the sand-pack, further reducing the oil recovery. The drastic drop of size in nanofluids after being stored for some time after the addition of salt can be attributed to the sedimentation of all larger aggregates and only the smaller aggregates are left suspended (Figure 3.3). The formation of nanoparticle aggregates in PAM solution was ensured by DLS and SEM analysis, where nanofluid (S1) without salt exhibited average NP size of 34 nm and non-agglomerated structure, respectively.

However, S1 nanofluid (in presence of salt, 8 wt%) exhibited different SEM image and showed significant agglomeration as shown in Figure 3.4. From Figure 3.4, it is clear that silica NPs formed several clusters of larger size (> 3-4 μm). These nanofluid samples are separate from polymer aggregates. The polymer aggregates are solid transparent clumps, usually form during rapid polymer inclusion and non-uniform stirring in water. These factors may align polymer particulates to clump together and form an aggregate, that either floats to the top of surface or settle to the bottom of solution [179]. To avoid aggregates, polymer particulates were added progressively in water and thoroughly mixed using laboratory stirrer. Polymer solution is subsequently poured in other beakers for visualizing the flow profile. Interrupted flow is considered to be affected by the formation of PAM aggregates and this solution was not used for the synthesis of nanofluid. The effect of salt on nanofluid stability was also studied through zeta potential. Initially, after

synthesis, all nanofluid samples exhibited a stable zeta potential value in the range of -34 to -37 mV. A nanofluid exhibiting a value of greater than 30 mV and lower than -30 mV is stable and resists agglomeration [64]. Contrary to silica nanofluids prepared using the two-step method where an increase in particles number per unit volume increases the occurrence of particle agglomeration (which leads to unstable zeta-potential values), the single-step silica nanofluids did not show a deviation in values of zeta-potential when the concentration of NPs was increased, indicating that method of formulation plays a role in ensuring the stability of nanofluids. On the addition of salt, the zeta potential values of all nanofluids reduced substantially and fell in the unstable zone. Variation in zeta potential can be ascribed to the formation of the aggregates which leads to a charge depletion region forming around the particles.

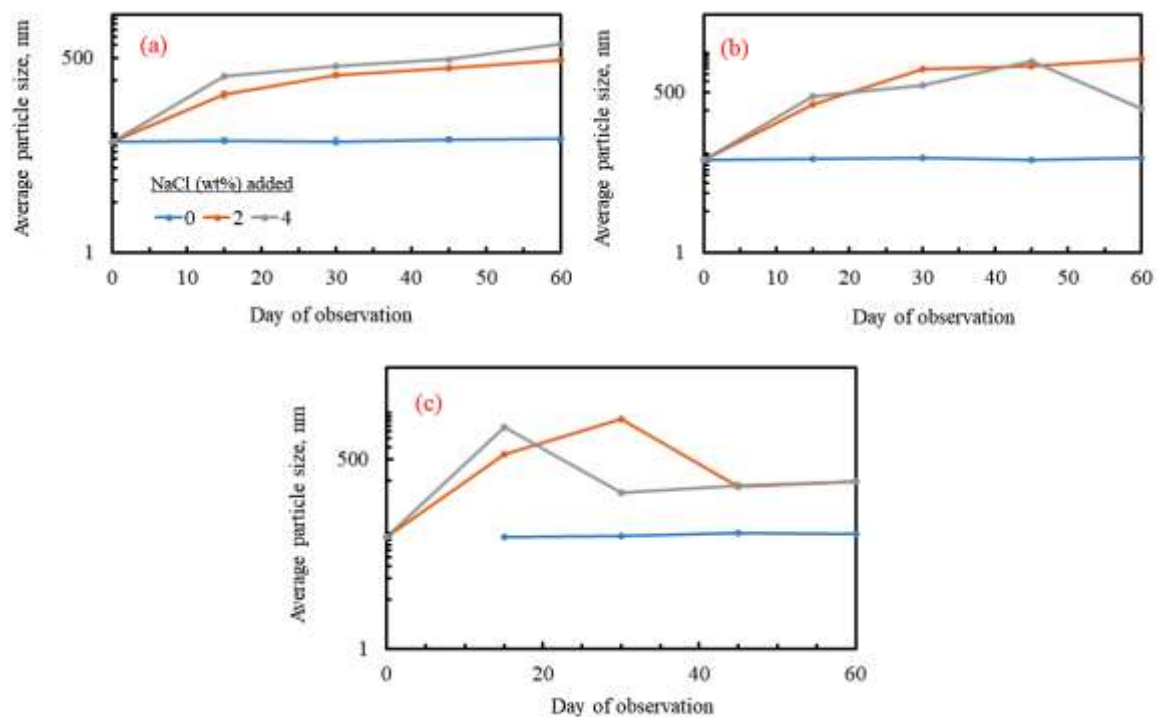


Figure 3.3: Average particle size observed for silica nanofluids as a function of salinity for (a) S1 (0.1 wt%), (b) S2 (0.5 wt%) and (c) S3 (1 wt%).

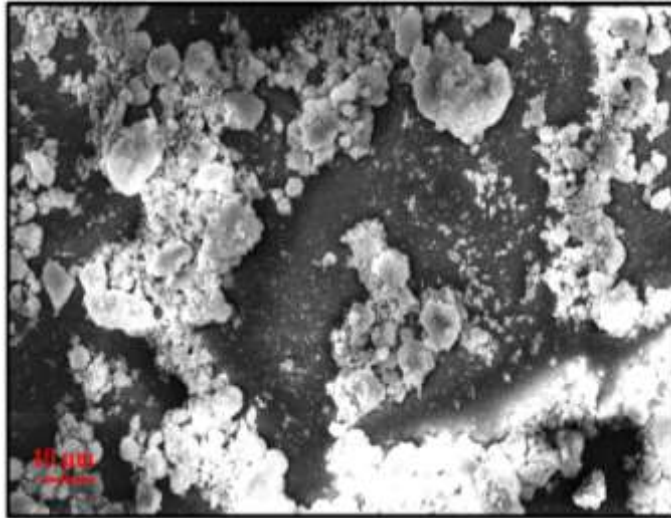


Figure 3.4: Aggregates formed in nanofluid S1 in the presence of 8 wt% NaCl.

The nanofluid samples also showed a surface charge inversion (from negative to positive) on adding salt which was due to the screening of surface charge of the particles for sample S3 when 2 wt% NaCl was added to the nanofluid. The DLS was used to measure the particle size of the nanofluids under varying conditions. It was observed that leaving the nanofluids over a period of time, adding salt to them or heating them induced aggregation and caused an increase in particle size. The increase in particle size, established by the DLS, made the nanofluids unstable which was also observed by the zeta-potential results (unstable region between -30 to 30 mV). Thus, it is not desirable that flooding with sole nanofluid solutions be performed in oil reservoirs where adverse high salinity is likely to be encountered as this would lead to the formation of large particle size aggregates which clog the pores, reduce formation permeability and reduce oil recovery.

3.3.3 Silica nanofluid stabilization by surfactant

Several studies have investigated the use of surfactants to stabilize silica nanofluids and found that when compared to cationic surfactants (like CTAB), anionic surfactants (SDS) are better in stabilizing nanofluids given their property to supercharge the surface of silica particles which leads to the development of a stronger negative charge and promotes

higher repulsive forces between individual NPs [163,168]. Conventionally, anionic surfactants such as SDS are preferred over cationic surfactants *i.e.* Cetrimonium bromide (CTAB) in oilfield applications [163,180]. In addition, anionic surfactants are recommended because of their negative charge and the potential to increase the zeta potential of particles in saline environment [163]. Thus, in this study, the role of anionic surfactant (SDS) was explored to stabilize silica nanofluids in saline environments. The stalagmometer method was used to determine the CMC of the anionic surfactant and the CMC value was determined to be around 0.18 wt%. This was further cross-verified by the electrical conductivity method to ascertain the CMC of the nanofluid-surfactant formulation. The electrical conductivity of the various surfactant wt% in S1 nanofluid was measured and the results as a function of surfactant wt% have been provided as Figure 3.5. The CMC is the point at which the electrical conductivity values exhibit a variation between the observed trendlines [172]. From Figure 3.5, the CMC value was obtained to be nearly 0.184 wt%, which is well in line with the results obtained from the stalagmometer method. However, multiple concentrations of surfactant and salt were investigated to comprehensively establish the stability of single-step silica nanofluids.

Initially, the surfactant was added to the nanofluid solutions in measured quantity (CMC + 20% absorption loss ~ 0.216 wt% SDS) immediately after preparation and before the addition of salt. The samples were then observed using a particle size analyzer and the observations have been reported in Figure 3.6.

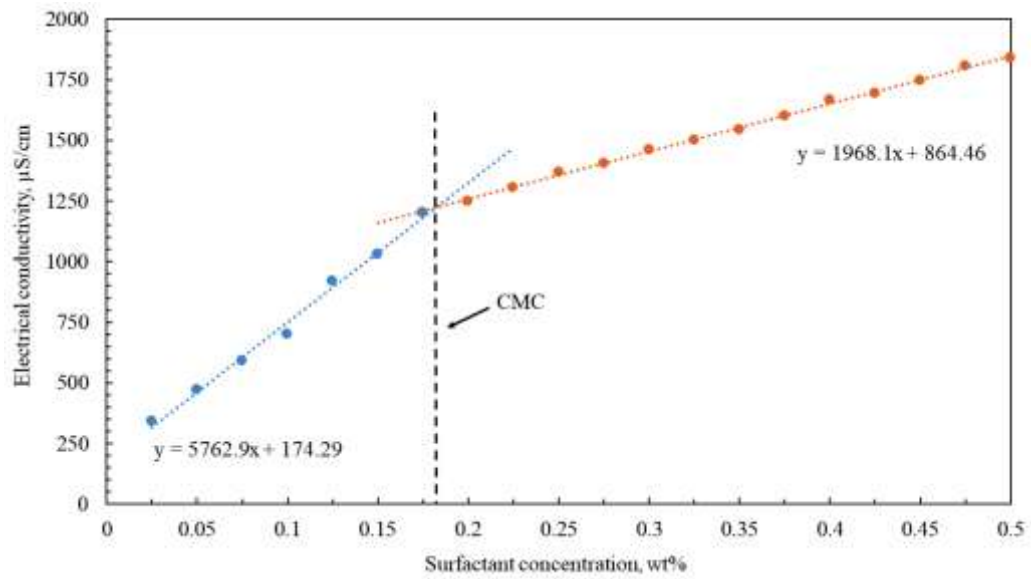


Figure 3.5: The electrical conductivity of silica nanofluid S1 as a function of surfactant treatment (wt%).

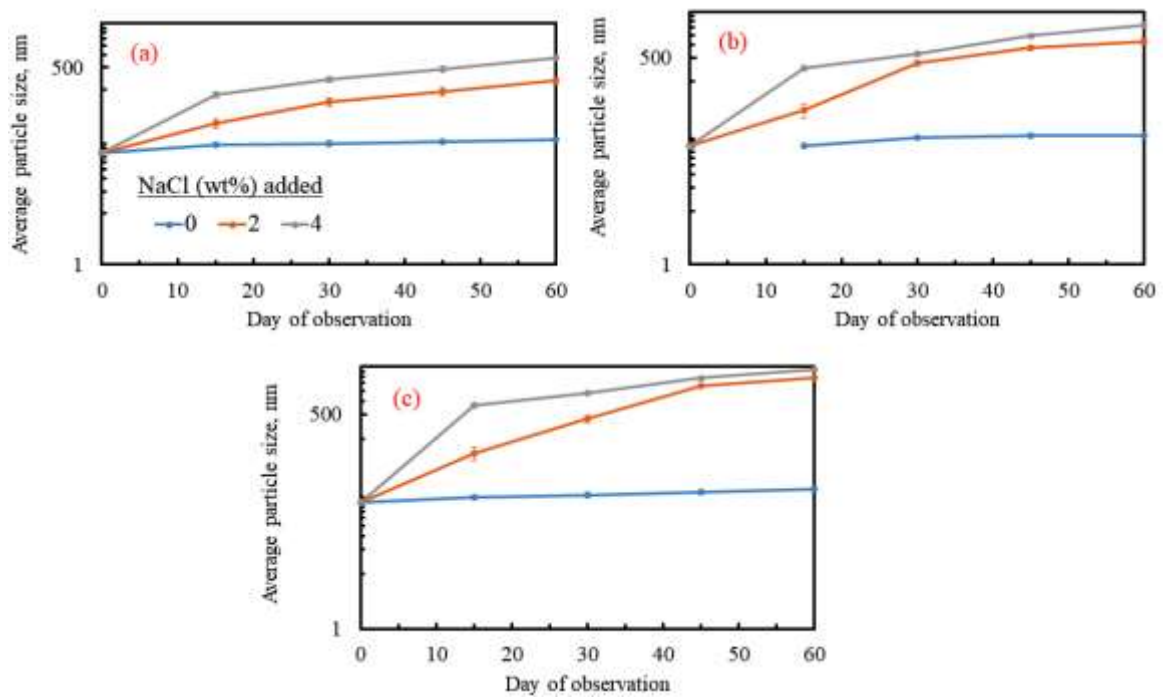


Figure 3.6: Average particle size observed for silica nanofluids with added surfactant (0.216 wt%) as a function of salinity for (a) S1 (0.1 wt%), (b) S2 (0.5 wt%) and (c) S3 (1 wt%).

In the surfactant laden solutions, the addition of 2 wt% salt did not destabilize the nanofluids as much as those without surfactants and the particle sizes were recorded to be 86 ± 12 nm (S1), 104 ± 22 nm (S2) and 164 ± 32 nm (S3) when the samples were observed 15 days after the addition of salt. The particle sizes gradually increased in the three silica nanofluids and after 60 days, the samples had a particle size of 329 ± 36 nm in S1, 824 ± 66 nm in S2, and 1447 ± 25 nm in S3 nanofluids. Further increase in salt concentration destabilized the silica nanofluids and the effect of surfactant addition was subdued. In the samples with 4 wt% salt added, the particle sizes were found to be 214 ± 22 nm (S1), 367 ± 26 nm (S2) and 648 ± 42 nm (S3) on the 15th day of observation. The particle size agglomeration was further observed on the 60th day of observation and the particle size in S1 was found to be 675 ± 34 nm, 1342 ± 16 nm (S2) and 1848 ± 68 nm in S3 nanofluid. In the sample with 8 wt% NaCl, no observations could be taken even after the addition of surfactant as large aggregates were formed in the solution which settled rapidly and no observations could be taken. Thus, from the presented data, it is evident that the use of surfactants in minute quantity cannot negate the salt-induced agglomeration effects in silica nanofluids. Hence, the concentration of surfactant was increased (from 0 to 0.8 wt%) in saline S1 nanofluid and the particle size observations have been presented in Figure 3.7.

Initially, the S1 nanofluid with no salt exhibited non-agglomerated particle size distribution in the range of 45 ± 12 nm when the surfactant was present in low quantity (≤ 0.35 wt%). However, on increasing the concentration of surfactants, the silica NPs started to show agglomeration and at higher concentrations of surfactants, the silica nanofluids showed high agglomeration (particle size: 228 ± 22 nm at 0.8 wt% SDS). This was cross-referenced by the zeta-potential values where initially, the addition of surfactant leads to a further decrease to -41 ± 3 mV (SDS: 0.3 wt%) (trending more towards stable region) in the silica nanofluid. However, on further increasing the surfactant concentration, the values of

zeta-potential started to change, recorded to be -24 ± 4 mV (SDS: 0.8 wt%) and began to fall in the unstable region (Figure 3.7).

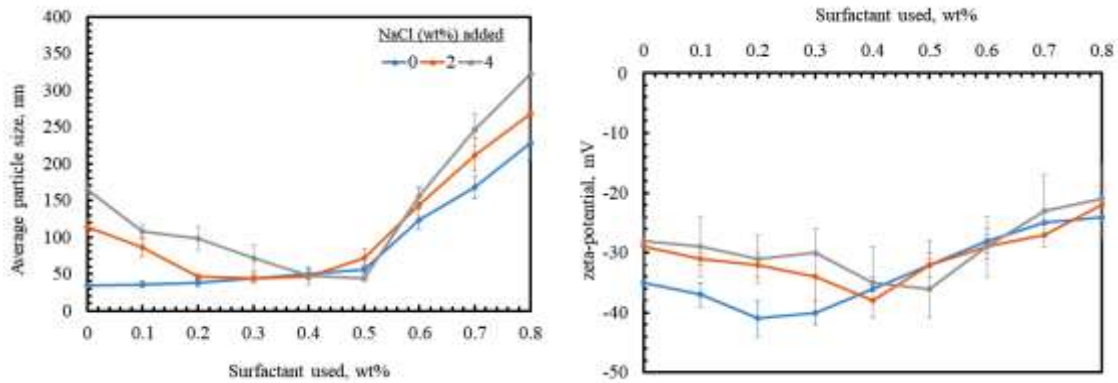


Figure 3.7: The effect of surfactant concentration on (left) average particle size and (right) zeta-potential values for silica nanofluid S1 in saline conditions.

The detrimental effect of high surfactant concentration on the stability of silica nanofluids has been widely explored in past works and hence, the use of surfactant with silica nanofluids must be curtailed to carefully measured quantities in oilfield field applications. When the salt concentration was increased, the use of surfactant did curtail the agglomeration due to salt induction in the nanofluids, though the effect was significantly muted for low surfactant concentrations. The addition of 0.5 wt% SDS was found to negate salt-induced agglomeration in 4 wt% NaCl laden silica nanofluid (0.216 wt% SDS had failed to stabilize this solution). The zeta-potential values in 0.5 wt% SDS laden silica nanofluid were recorded to be in the stable region even after the addition of 4 wt% NaCl salts, indicating that surfactant had stabilized the silica nanofluid (Figure 3.7). The use of surfactant reduced the aggregation of nanoparticles as the inclusion of SDS tends to re-establish the extent of electrostatic repulsion between the NPs which reduces the cluster size and increases the stability of the nanofluid for various applications. The zeta-potential values reduced depending on the salinity of the base fluid which indicates the

dependence of minimum zeta-potential value on the electrolyte concentration within the nanofluid. However, no amount of SDS added could stabilize the silica nanofluid when 8 wt% NaCl was added to the solution. Thus, from this study, it can be concluded that the use of a nanofluid solution in a saline reservoir can be promoted by adding surfactant (which is already a good foaming agent) to the suspension. Hence, the use of a suitable anionic surfactant (here, SDS) is very beneficial for this particular study.

3.3.4 Flow behavior study of surfactant treated nanofluids

One of the key parameters essential for consideration in the design of an EOR fluid is its ability to resist agglomeration/adsorption/retention within the porous media.

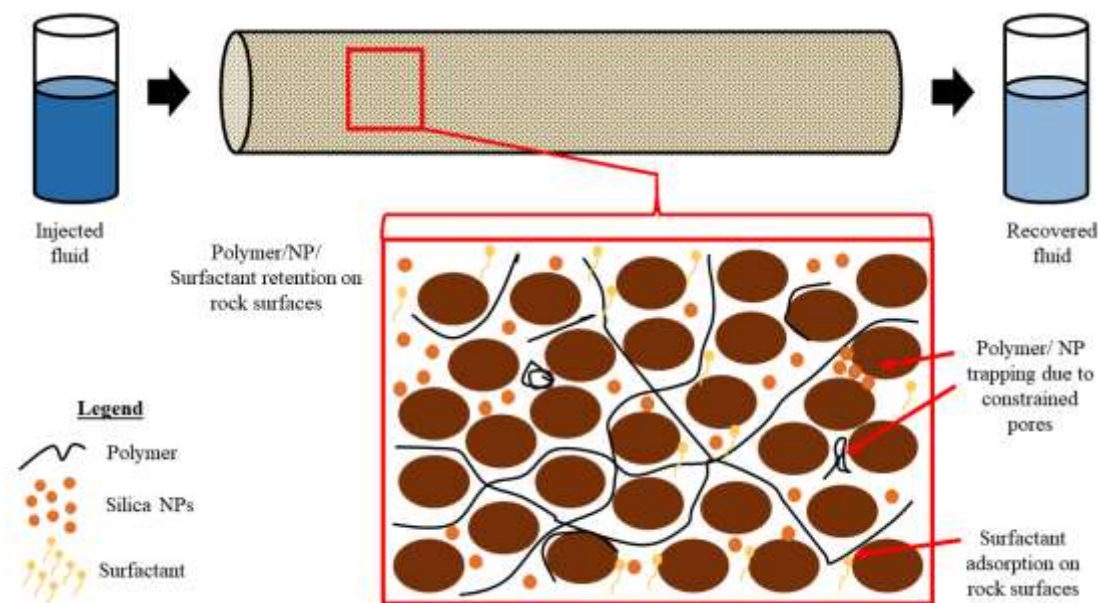


Figure 3.8: Schematic showing trapping/retention of injected fluids under different mechanisms during fluid injection in porous and permeable pore throats.

While there are several mechanisms which influence the adsorption of polymer, surfactant and NPs in porous media like rock surface adsorption, mechanical trapping, etc. (Figure 3.8), regardless of the cause of their occurrence, this leads to loss of vital fluid properties and reduces the efficacy of EOR. Surfactant adsorption usually takes place in

the form of monomers, instead of micelles [181]. Hence, it becomes essential to investigate this aspect before any wider field implementation. While past studies have focused on the role of surfactant absorption and their mitigation via any additive, in this study, the effect of retention/adsorption has been investigated via a rheological study. The rheology of the fluid is an important parameter in field studies and the retention of NPs or adsorption of surfactant/polymer would negatively impact the injected fluid viscosity, rendering it less capable to mobilize greater volumes of crude oil [182]. Initially, various fluids to be injected (i.e. 1000 ppm PAM, nanofluids S1-S3) with and without the addition of 0.216 wt% surfactant were analyzed using the rheometer and the resulting viscosity as a function of varying shear rate have been presented as Figure 3.9. The inclusion of NPs was found to increase the viscosity of the nanofluid over PAM and further increasing NP concentration, led to a greater increase in fluid viscosity which is under similar observations in past literature [183]. All fluids showed shear-thinning behavior on increasing shear rate and in PAM, the viscosity of 28.3 Pa.s at 22 s^{-1} fell to 3.82 Pa.s at 1840 s^{-1} . In S1, the viscosity at 22.3 s^{-1} was recorded to be 30.4 Pa.s which fell to 4.4 Pa.s at 1840 s^{-1} . For S2 and S3, the values of viscosity at the shear rate 22.3 s^{-1} were 35.5 and 39.5 Pa.s, respectively which reduced to 5 and 5.8 Pa.s, respectively at an applied shear rate of 1840 s^{-1} . The dependence of viscosity on the particle concentration of a colloidal solution was first correlated in Newton's correlation which has been well detailed in previous studies. As per this correlation, increasing particle volume concentration increases the viscosity of a fluid [184]. At 22.3 s^{-1} , the viscosity of PAM, S1, S2, and S3 were recorded to be 31, 32, 37 and 44 Pa.s respectively which at 1840 s^{-1} , fell sharply to 4.2, 4.5, 5.4 and 6.2 Pa.s, respectively.

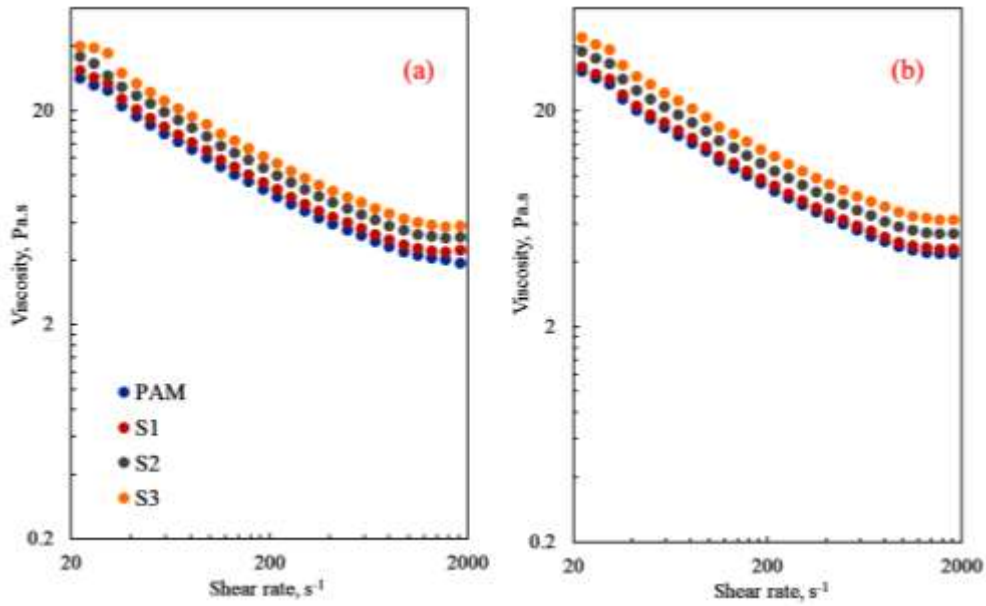


Figure 3.9: Viscosity versus shear rate profiles of polymer and sole silica nanofluids at 30 °C. (b) Viscosity versus shear rate profiles of polymer-surfactant and surfactant treated silica nanofluids at 30 °C. The pressure during measurement was 0.1 MPa.

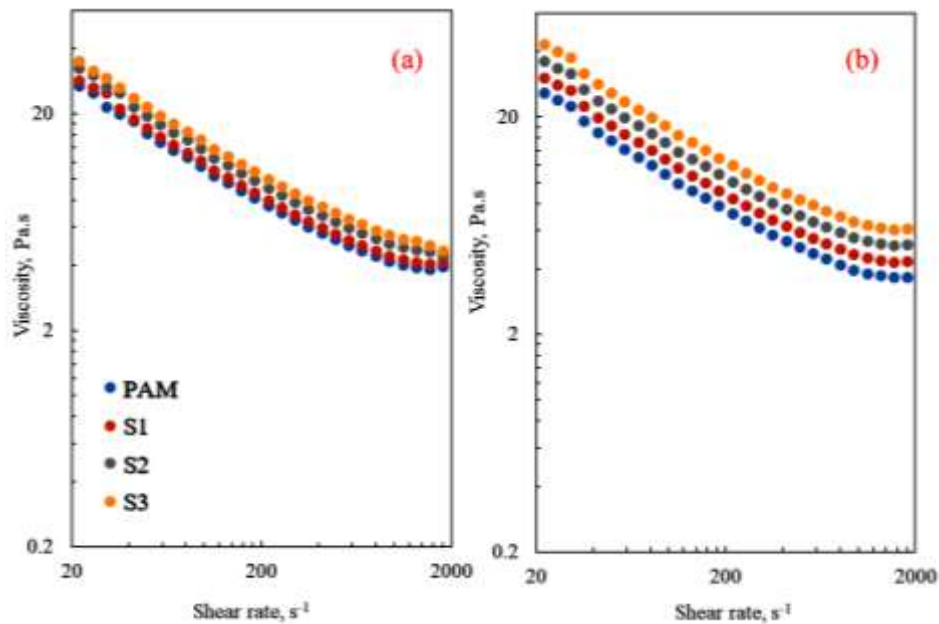


Figure 3.10: (a) Viscosity versus shear rate profiles of polymer & sole silica nanofluids and (b) polymer-surfactant & surfactant treated silica nanofluids obtained as effluent after centrifugation at 30 °C.

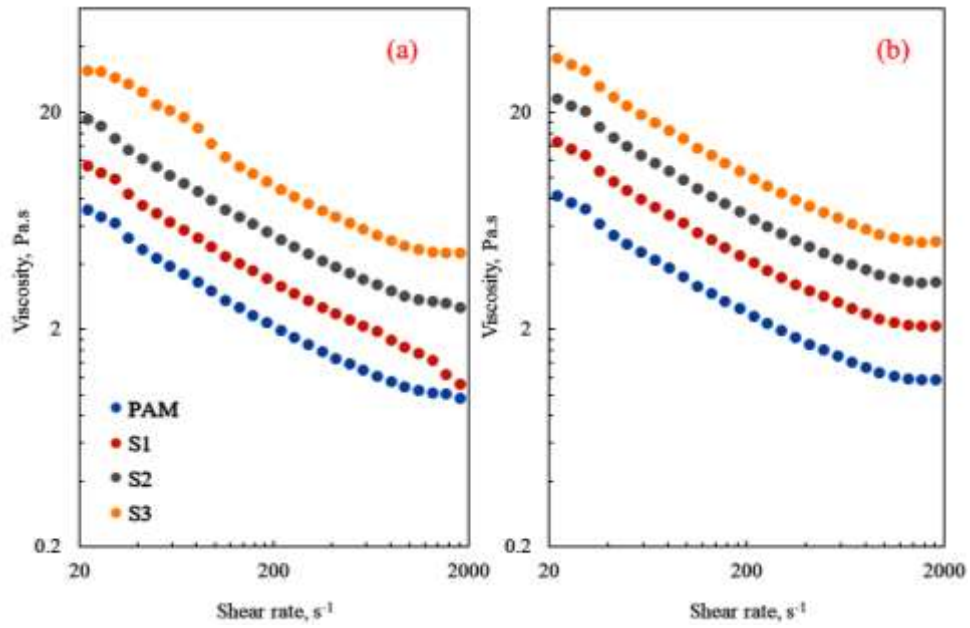


Figure 3.11: (a) Viscosity versus shear rate profiles of polymer & sole silica nanofluids and (b) polymer-surfactant & surfactant treated silica nanofluids obtained as effluent after centrifugation at 90 °C.

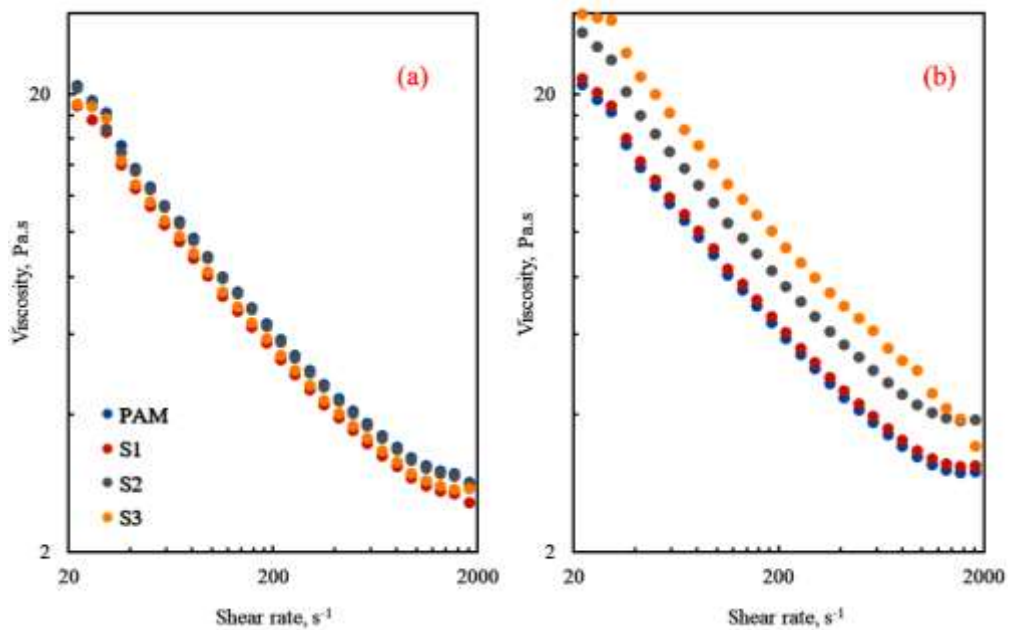


Figure 3.12: (a) Viscosity versus shear rate profiles of polymer & sole silica nanofluids and (b) polymer-surfactant & surfactant treated silica nanofluids obtained as effluent after centrifugation at 30 °C with 4 wt% NaCl solution saturated sand-packs.

The solutions were then mixed with sand at varying conditions and kept in a centrifuge. The solution was mixed at 1200 rpm for 30 min and the resulting fluid at the near the top (the effluent) was then extracted. The effluent was compared with the original injection fluids rheologically and the change in fluid viscosity was determined by comparing fluid viscosities (of original & effluent fluids) at every shear rate & obtaining their average. In Figure 3.10, the viscosity of injection fluids as a function of shear rate has been plotted for EOR fluids after centrifugation with sand at 30 °C while Figure 3.11 provides the data for tests performed after recovery from centrifuge at 90°C. Finally, in Figure 3.12, the data of viscosity as a function of shear rate has been provided after EOR fluids were mixed with 4 wt% NaCl solution before centrifugation (to simulate high salinity reservoirs). From Figure 3.10, it was observed that the viscosity of PAM at 22.3 s⁻¹ had insignificantly reduced to 26.2 Pa.s while at 1840 s⁻¹, the viscosity had further reduced to 4 Pa.s. The average fall in viscosity for PAM after centrifugation with sand at 30°C was 5%. Similarly, after centrifugation, the viscosity of nanofluids S1, S2, and S3 reduced by 6%, 8%, and 12%. While the decrease in polymer viscosity after injection in the sand-pack can be attributed to the retention of polymer inside, the fall in the viscosities of the nanofluid was due to the retention of both polymer and NPs inside the sand-pack. Compared to low concentration nanofluids, i.e. S1 and S2, higher concentration nanofluids (S3) are more prone to retention inside the sand-pack due to having a greater number of particles per unit volume. When surfactant treated solutions were used, the viscosity of PAM (surfactant-treated) was recorded to be 25.5 Pa.s at 22.3 s⁻¹ which reduced to 3.6 Pa.s at 1840 s⁻¹ (Figure 3.10), indicating an average reduction of 16% in viscosity of 16% which meant that a significant amount of surfactant was being lost in form of adsorption on rock surfaces inside the sand-pack. Similarly, at 22.3 s⁻¹, the viscosity of surfactant treated S1, S2 and S3 nanofluids were found to be 29.4, 30.1 and 42.1 Pa.s while at 1840 s⁻¹, these

values had reduced to 4.2, 5.1 and 6 Pa.s, respectively which indicated a fall of 6% for S1, 5% for S2 and 3% for S3. Interestingly, using surfactant treated nanofluids, reduces the retention of both surfactant and NPs inside the sand-pack, demonstrating great synergy and proves to be viable candidates for EOR use in oilfields.

When the experiments were repeated after centrifugation at a test temperature of 90 °C, the viscosity of PAM at 22.3 s⁻¹ was 7 Pa.s which reduced to 0.95 Pa.s at 1840 s⁻¹ (Figure 3.11), indicating that most of PAM had degraded at high temperature (the average loss in viscosity was a significant 75%) and contributed very less to maintain the viscosity of the fluid [88]. Similarly, the viscosities of nanofluids without surfactant treatment were recorded to be 11.2 Pa.s (S1), 18.4 Pa.s (S2) and 30.7 Pa.s (S3). The loss of viscosity after injection in a sand-pack at high temperature was 63% (for S1), 48% (for S2) and 24% (for S3). The inclusion of silica NPs, did lower the fall in viscosity by improving the stability of PAM at higher temperatures, also evident from the TGA results. The surfactant-treated PAM exhibited a viscosity of 8.16 Pa.s at 22.3 s⁻¹ which is slightly lower than sole PAM, indicating a reduction in viscosity of 68% and that the inclusion of surfactant, did stabilize the fluid, albeit minorly. The surfactant treated nanofluids exhibited a value of 14.2 Pa.s (S1), 22.8 Pa.s (S2) and 35.3 Pa.s (S3) at the shear rate of 22.3 s⁻¹ which significantly reduced to 2 Pa.s (S1), 3.2 Pa.s (S2) and 5 Pa.s (S3) at 1840 s⁻¹. This indicated that the viscosity of the surfactant treated nanofluids reduced by 52% (S1), 36% (S2) and 17% (S3). The surfactant treated nanofluids fared better than non-surfactant laden nanofluids which indicates a greater likelihood of surfactant use in higher temperature reservoirs where their use in judicious conjunction with NPs, may boost oil recovery.

Finally, the centrifugation runs were performed after 4 wt% NaCl had been added to the polymer, polymer-surfactant and the nanofluids to assess their viability in saline

reservoirs (Figure 3.12). The inclusion of such a higher concentration of salt-induced rapid agglomeration in the nanofluids (without surfactant treatment) and the polymer solution along with the three nanofluids (S1-S3) exhibited similar values of viscosity 18.4-20.5 Pa.s at 22.3 s^{-1} which reduced to between 2.55-2.75 Pa.s at 1840 s^{-1} indicating a loss of 26-52% in fluid viscosity on salt addition. Primarily, the nanofluid S3 which was most prone to salt-induced agglomeration exhibited a loss of 52% in fluid viscosity which can be attributed to a fall in particle concentration per unit volume as larger particle agglomerates (formed due to salt-action) may have been retained inside the constrained pores of the sand on centrifugation. The presented data indicates that silica nanofluids are not viable for EOR application in high salinity reservoirs without any surfactant treatment. However, when the surfactant was added to the mix, the rheological attributes of the injection fluids improved. Nanofluid S1 exhibited a viscosity of 21.5 Pa.s at 22.3 s^{-1} which reduced to 3.1 Pa.s at 1840 s^{-1} . The average fall in fluid viscosity due to salt-action was 18% (PAM), 28% (S1), 24% (S2) and 29% (S3). From the flow-behavior tests, it can be assessed that NPs and surfactants have great synergy and are viable candidates for use in high temperature and adverse salinity reservoirs when compared to sole polymer or polymer-NP solutions as they can retain their fluid attributes (here, viscosity) which allow for greater oil mobilization throughout the oil reservoir and may increase oil recovery.

3.3.5 Oil recovery runs

To understand the efficacy of EOR fluids under oilfield conditions, a set of injection runs were performed in porous media prepared using standard oilfield procedure. It has been established a moderate NP concentration is beneficial for better performance in oilfield application such as foam stabilization and carbonated water injection. Recently, other studies also endorsed the fact that moderate NP concentration of 0.1 wt% showed higher oil recovery (65% of original oil in place) during carbonated water injection in

loosely consolidated sandstones [54]. Initially, the sand-packs were prepared by wet-ramming and the fluids (connate water → crude oil → displacing fluid) were injected using a syringe pump at a constant flow rate (1 ml/min) to fully saturate the sand-pack. The porosity and permeability of the sand-packs were ascertained using conventionally documented methods. The flow behavior of the silica nanofluids (with and without surfactant treatment) was studied using synthetic sand-packs of fair porosity (28-31%) and permeability (600-780 md).

In each run, one of the EOR fluids was injected into the sand-pack and the resulting effluent was gathered at the outlet after the sand-packs were sufficiently saturated by the injection fluids (preferably, after the injection of 2.5 PV). The oil recovery runs were performed until a total of 5 PV (2 PV primary water flooding → 0.5 PV EOR slug → 2.5 PV chase water flooding) of fluid had been injected. The pore point of the crude oil used in the study was 37 °C, hence all experiments were performed above this temperature. A total of 4 different operating conditions: (1) 60 °C with pure water as a connate fluid, (2) 90 °C with pure water as a connate fluid, (3) 60 °C with 4 wt% NaCl solution as connate fluid and (4) 90 °C with 4 wt% NaCl solution as connate fluid were carried out. The oil recovery data (at 60 °C) as a function of fluid volume (PV) injected has been presented in Figure 3.13. In Figure 3.13, the results of oil recovery from sand-packs saturated with DI water have been provided along the data from the sand-packs were saturated with 4 wt% NaCl solution. From results, it could be observed that the injection of water yielded an oil recovery of 38-40% OOIP till 2 PV. This was followed by the injection of EOR slugs (0.5 PV of PAM/nanofluids). The injection of EOR slugs reintroduced oil recovery from sand-packs due to their superior viscosity and impact on oil mobilization. For PAM, oil recovery improved by 10% with resultant oil recovery of 49% OOIP while silica NPs exhibited further increase in oil recovery over PAM by 6% (S1), 7% (S2) and 10% (S3). Thus, S3

nanofluid yielded highest oil recovery of 59% OOIP. Nanofluid S3 mobilized oil for the longer duration as 100% water cut was seen after the completion of 3.75 PV. The amount of oil recovery with surfactant treated solutions has also been reported in Figure 3.13.

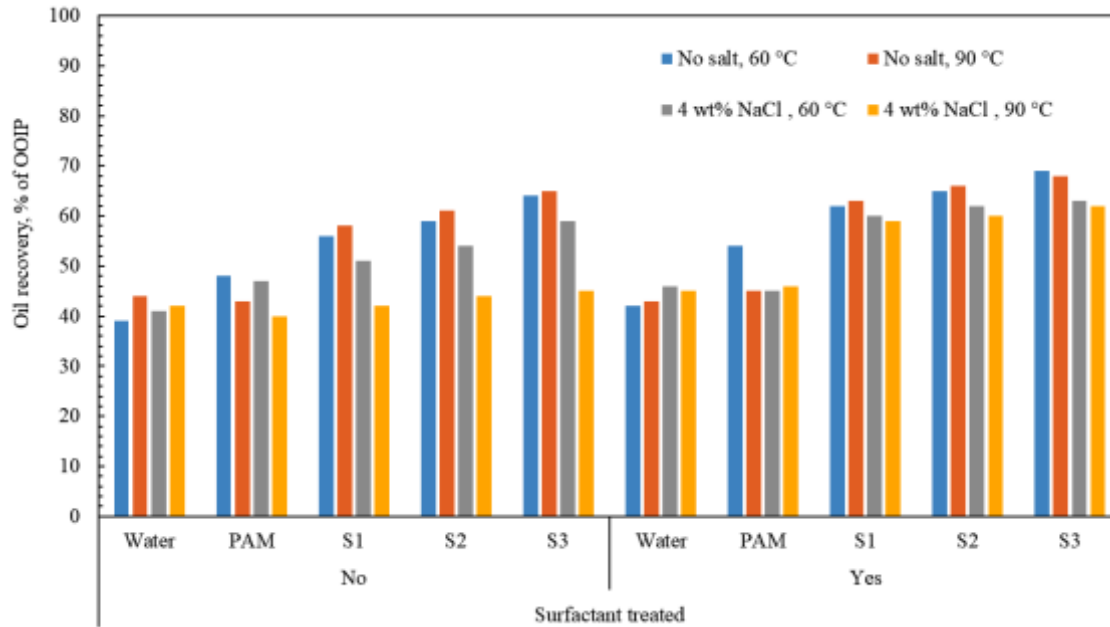


Figure 3.13: Cumulative oil recovery in varying temperature and salinity conditions by sole and surfactant treated single step silica nanofluids.

Expectedly, the nanofluid solutions (both with and without the surfactant treatment) outperformed both water and polymer-based injection under 60 °C with pure water as connate fluid conditions with a maximum oil recovery of 69% obtained with nanofluid S3 treated with surfactants due to a combination of several different incremental oil recovery mechanisms like disjoining pressure, IFT reduction and wettability alteration acting together in conjunction [56,57,185]. However, when the experiments were repeated at 90 °C with pure water as a connate fluid, the efficacy of the nanofluids came down significantly as the polymer, PAM deteriorated sharply at higher temperatures. The oil recovery by PAM injection at 90 °C with pure water as connate fluid was barely 43% of OOIP, even less than oil recovered by water (44% of OOIP) under the same operating

conditions. Interestingly, the amount of oil recovered by water improved at 90 °C was higher than the oil recovered at 60 °C (39% of OOIP) as increasing the temperature of sand-pack, reduces the density of the oil causing it to become less viscous and thus, more mobile [109]. All nanofluids, with and without surfactant treatment showed incremental oil recovery (higher than water and PAM) and the maximum amount of oil was recovered by surfactant treated S3 solution (68% of OOIP) at 90°C with pure water as connate fluid.

However, when 4 wt% NaCl solution was used as the connate water, the nanofluids (without surfactant treatment) performed much worse and the cumulative oil recovery was less than those obtained from sand-packs with pure water as connate fluid. For example, when solution S2 was injected in a sand-pack with water as a connate fluid, the amount of oil recovery at 60 °C was 59% of OOIP. However, when the experiment was performed with 4 wt% NaCl solution as connate fluid at the same temperature, the oil recovery reduced to 54% of OOIP, indicating that some of the NPs in the suspension may have gotten agglomerated and blocked off pores, reducing the amount of oil mobilization. This was especially true for nanofluid S3 (without surfactant treatment) where the oil recovery fell by 5% of OOIP (from 64 to 59%). When surfactant treated nanofluids were used, the amount of oil recovery was proportionally higher than those used without surfactants, indicating that surfactants had stabilized NPs in the saline environment. At 60 °C in sand-packs saturated by 4 wt% NaCl, S1 recorded oil production of 51 and 60% of OOIP, injection of S2 produced 54 and 62% of OOIP while S3 recorded an oil production of 59 and 63% of OOIP when injected without and with surfactant treatment, respectively. Finally, the oil recovery runs were performed at 90 °C with 4% NaCl solution as the connate fluid. The inclusion of surfactants and NPs demonstrated good synergy and the maximum amount of oil recovery was obtained when S3 nanofluids (with surfactant treatment) were injected (63% OOIP). All surfactant treated nanofluids outperformed sole silica nanofluids

in each test condition. From the presented results, surfactant treated single-step silica nanofluids prove to be viable candidates for use as EOR fluids in high-temperature saline reservoirs.

3.4 Conclusion

Single-step silica nanofluids can have wide-spread applications in several industries including the oil industry given their superior stability than two-step silica nanofluids in ambient conditions and size-control properties. However, their widespread adoption is constrained by the lack of understanding of silica nanofluid stability in adverse conditions like high temperature and salt environment. Thus, in this study, the stability of silica nanofluids was investigated in adverse temperature (30-90 °C) and salinity (0-8 wt% NaCl). While past studies have mostly focused on visual observations and zeta-potential investigations, given the scope of this study (to investigate silica nanofluids for oil field applications), the focus has been more on the particle size distribution of the silica nanofluids. Smaller particles can access smaller pores inside the reservoir and thus, have a larger areal coverage while larger particle clusters may block off pore channels causing formation damage and reduce oil recovery. The single-step silica nanofluids demonstrated excellent stability and did not show any agglomeration when left undisturbed for over 60 days. However, at higher temperatures (~90 °C), the solutions started to degrade due to the lack of thermal stability in PAM. The addition of salt aggravated particle agglomeration in the silica nanofluids and rendered the solutions unstable for use. At high salt concentration, the silica NPs in the nanofluids agglomerated rapidly and thus, were unviable for use in high salinity environments (reservoirs with salinity higher than 50,000 ppm NaCl). Finally, the silica solutions were stabilized by the addition of an anionic surfactant (SDS, commonly used as an oilfield foaming agent) which resisted particle agglomeration, to a certain extent, in low salt conditions (reservoirs with salinity lesser than 20,000 ppm NaCl). Increasing

the surfactant concentration allowed the silica nanofluids to exhibit enhanced stability in high salinity conditions though, at high surfactant concentrations, the silica nanofluid was destabilized by the addition of the surfactant itself. This was further understood by the flow behavior studies of the various silica solutions (with and without surfactant treatment) under varying temperature and salinity conditions. The inclusion of a surfactant was found to improve the properties of silica nanofluid under such adverse conditions as evident from the rheological data. However, the addition of surfactant too should be moderated to ensure that too much of it is not added which leads to instability in the silica nanofluids and reduces their efficacy in oilfield applications.

The specific results of this study are –

- ❖ Increasing temperature was found to have an adverse impact on the stability of the silica NPs as base fluid (PAM solution) stability was inversely proportional to temperature.
- ❖ Increasing salinity resulted in accelerated NP aggregation which quickly destabilized the nanofluids and rendered them unstable colloidal suspensions.
- ❖ Inclusion of an anionic surfactant, SDS, improved the stability of silica NPs and reduced the extent of salt-induced agglomeration.
- ❖ At high concentration, surfactant was not effective. Therefore, the concentration of surfactant to be added needs to be carefully optimized as high surfactant addition destabilized the nanofluids.

From the presented study, single-step silica nanofluids are viable candidates for application in oilfield applications.

Chapter 4

CO₂ Capturing Evaluation of Single-Step Silica Nanofluid for Carbon Utilization Applications

Abstract

Single-step silica nanofluids offer better stability and size-control due to less nanoparticle (NP) agglomeration. Uniform distribution and desired size of NP make nanofluid a rheologically modified fluid to be suitable for carbon utilization applications. Thus, in this work, single-step (sol-gel) technique is used to prepare silica nanofluids of different particle sizes (34-142 nm) in base of polyacrylamide (PAM, 1000 ppm). These nanofluids was tested for CO₂ capturing applications using rheological measurements (shear and dynamic) as a function of different conditions [particle concentration = 0.1, 0.5, and 1 wt% and temperature = 303, 323, and 353 K]. Increasing particle size was found to affect rheological properties insignificantly while increasing particle concentration led to increment in viscosity and viscoelastic moduli (elastic: G' and viscous: G''), good for nanofluid usage in oilfield practices where improved viscosity is required for higher oil recovery. The inclusion of CO₂ made nanofluid lighter and thus, viscosity and moduli values slightly reduced for CO₂ laden nanofluids. The effect of high temperature (353 K) on capturing potential of nanofluids was found marginal as viscosity and viscoelastic

properties and their flow trends remained almost similar at each test temperature, which indicates CO₂ capturing into the networks of NP and PAM was intact and even temperature could not deform it. However, a slight reduction in viscosity and moduli of nanofluids was attributed to temperature effect on PAM rheology. Thus, the synthesized nanofluids behaved almost thermally stable and showed marginal effects of flow conditions (shear rate, amplitude, and frequency) on rheological properties and CO₂ capturing potential of silica nanofluids, which is of key importance for various applications where conditions differ on a large scale.

4.1 Introduction

The rheological properties of a conventional fluid typically improves after the addition of a colloidal particle such as nanoparticle (NP) that possesses large surface area per unit volume [89], optical [91,186], and heat transfer properties [42,45,72,187,188]. Compared to conventional fluid, nanofluids are viscous colloidal suspensions and exhibit increased viscosity which leads to an increase in pumping power required for nanofluid injection in porous media [62,189]. However, nanofluids, due to improved rheological properties, have offered many advantages in several applications such as interfacial tension (IFT) reduction [62,190,191], solar water heating [53], oil recovery [192], and profile modification [118,193]. The rheological property of a nanofluid can be typically defined in terms of the relationship between shear stress (τ) and shear rate ($\dot{\gamma}$) where viscosity (η) is the ratio of shear stress to shear rate [194]. Separately, Brownian motion and NP aggregation have been found to affect the rheology of nanofluids [44]. Till date, a substantial amount of rheological data has been reported for nanofluids which make it possible to elucidate the particle size, concentration or the structure of a nanofluid from available data. Even, the improved viscosity of nanofluid is motivating researchers to investigate nanofluid potential for the vital areas such as carbon capturing where capturing

efficacy of conventional fluid is expected to improve by viscous nature and surface activity of charged NPs, which is limited in the literature as far as we are aware.

Together with the viscosity and shear stress data, the viscoelastic properties of a nanofluid are also important. A viscoelastic nanofluid is found to exhibit both elastic and viscous characteristics when it undergoes deformation and therefore, it is important to ascertain the viscoelasticity of a nanofluid before its industrial application. Several useful information like the evolution of dynamic viscoelastic properties, *viz.*, storage modulus (G') and loss modulus (G'') can be obtained from the viscoelastic study of a nanofluid [195]. Among nanofluids, silica nanofluids are easier and comparatively less expensive to synthesize and therefore, they have received widespread attention in the oilfield industry as agents for foam enhancement [97], low-salinity water flooding [196], wettability alteration [153] and improved CO₂ capture and retention [10]. In one study with concentrated colloidal suspensions of silica NPs, it was observed that G'' was larger than G' which indicates that a significant portion of energy will be dissipated by viscous forces when compared with the one stored in the structure of material [197]. The role of temperature (75 to 175 °F) on G' and G'' of a silica nanofluid was investigated and the results showed that the effect of temperature on them subdued above 100 °F [198]. In addition, the inclusion of silica NPs has been found to alter the viscoelasticity of a fluid system from liquid-like to a gel-like behavior which is desired for enhanced oil recovery applications in high-temperature reservoirs and has also been encountered in alumina-water based nanofluids [199,200]. Silica nanofluid is an excellent candidate for CO₂ absorbents in industrial processes like scrubbing, carbonated water flooding, foam flooding, supercritical CO₂ gas, and water-alternating gas injection due to improved rheological behavior [106,201–204]. In our previous work, we have reported the use of silica nanofluids for CO₂ capturing applications where nanofluid showed improved CO₂ molality,

better absorption kinetics, and longer CO₂ retention [10]. The application of CO₂-laden silica nanofluids has the potential to increase the oil recovery in two ways - the gradual expulsion and subsequent dissolution of CO₂ in oil and improved areal sweep of residual oil by the injected nanofluid [11,62]. Despite vital importance for silica nanofluids globally, none of the studies reported rheological investigation (viscosity and moduli) of silica nanofluids for carbon utilization applications. The knowledge of the viscoelastic properties of CO₂-laden silica nanofluids is essential while modeling the reservoir flow simulations for CO₂ sequestration studies. Mechanistically, reservoir engineers focus on injecting CO₂ for geological sequestration where CO₂ mobility and breakthrough can be controlled by suitable viscous candidates (e.g. silica nanofluids) *via* capturing in NP matrix [48,205]. This capturing potential of nanofluids is subjected to affect by the applied stresses/strains and rheological characterization is one of the effective techniques to understand these phenomena, on which we focus here.

The rheological properties of a silica nanofluid are also affected by its stability as nanofluids are meta-stable fluids where suspended silica NPs tend to form aggregates due to strong Van der Waals interactions between NPs [206]. The formation of large aggregates reduces the available surface area per unit volume of NP resulting NPs prefer to stay in bulk medium than participating for CO₂ absorption [10]. The aggregates settle on the bottom with time and nanofluid separates into two distinct phases of base fluid and aggregated silica NPs. Thus, a stable nanofluid of homogeneous NP distribution is essential for widespread industrial application. One method to prepare silica nanofluids of high stability is single-step technique as single-step method generates NPs within base fluid than mixing externally as the case with the two-step method [106]. Therefore, single-step synthesized nanofluids have been found to exhibit better stability and insignificant particle agglomeration which is proposed by the schematic in Figure 4.1 [70].

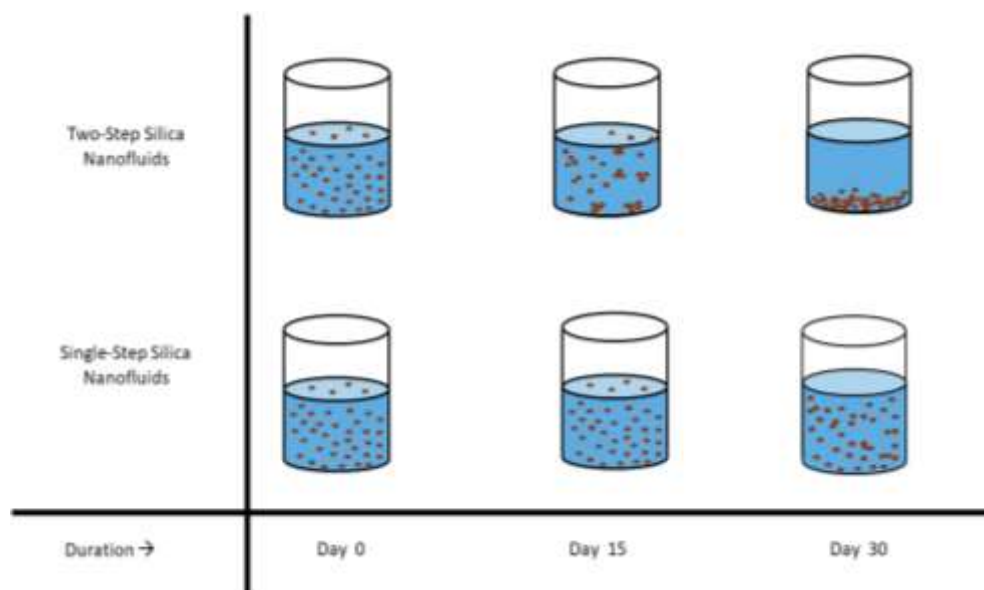


Figure. 4.1: Stability of single-step and two-step synthesized silica nanofluids as a function of storage period.

Thus, in this work, silica nanofluids of different sizes were prepared using single-step technique in base fluid of polyacrylamide (PAM, 1000 ppm), and further studied the rheological properties of these nanofluids with and without CO₂, to be applicable for carbon utilization applications. The role of NPs size (34-142 nm), NPs concentration (0.1-1 wt%) and temperature (303-353 K) on shear (viscosity and shear stress) and dynamic (moduli) properties of silica nanofluids is studied. Finally, the effect of different parameters on rheological properties of CO₂ laden silica nanofluids was discussed and compared to examine CO₂ capturing potential of silica nanofluid for complex conditions.

4.2 Materials and Methods

4.2.1 Materials

The materials used in the synthesis of the single-step nanofluids have been reported before in Chapter 3.

4.2.2 Preparation and characterization of nanofluid

Single-step silica nanofluids were prepared using Stober sol-gel method [105,106]. The volume of each constituent to prepare nanofluids and their nomenclature has been listed in Table 4.1. The detailed preparation and characterization of these nanofluids has been reported before in Chapter 2 and Chapter 3.

Table 4.1: Nomenclature, concentration, average particle size and pH of synthesized silica nanofluids

Nanofluid nomenclature	Average particle size (nm)	NP concentration (wt%)	pH [§]
S1	34 ± 6	0.1	8.22
S2	82 ± 14	0.1	8.23
S3	142 ± 16	0.1	8.20
S4	36 ± 4	0.5	8.26
S5	39 ± 5	1	8.27

[§]standard uncertainties in pH measurement: $u(\text{pH}) = 0.05$

The pH of the nanofluid samples was measured using a Hanna Digital pH meter (Model-HI98129, range 0-14) was used after calibration with provided buffer solutions.

4.2.3 Preparation of CO₂ laden silica nanofluids

CO₂ in silica nanofluid was purged using a custom build equilibrium cell which was also utilized in our previous CO₂ absorption studies [10,11]. For the sake of brevity, a brief description of the apparatus has been provided. The experimental setup comprises of a 25 ml stainless steel equilibrium cell. To maintain the test temperature inside the equilibrium

cell, a thermal jacket with a temperature circulator (HRC2, IKA) was attached to the cell. The pressure inside the cell was measured by a digital pressure gauge (Broil Sensotek BT DPG 100/100D, 0-100 bar, accuracy $\pm 0.15\%$ of span). The temperature of the fluid inside the equilibrium cell was measured by a thermocouple (RTD PT 100, 273-673 K, accuracy ± 0.2 K). The entire setup was mounted on a magnetic stirrer (IKA-C-MAG-HS7). CO₂ mixing in the solvent was performed using magnetic stirrer at two stirring speeds of 300 and 600 rpm inside the equilibrium cell. Initially, 10 ml of known solvent was taken via a calibrated pipette in the cell and the sealed cell was mounted on the stirrer. The cell was then degassed using a vacuum pump (ESCY India) and then, a measured amount of CO₂ was carefully introduced in the cell. CO₂ gas, under pressure, begins to solvate in the body of the fluid until an equilibrium pressure is reached after which no further amount of CO₂ will enter the body of the fluid. CO₂ enriched nanofluid was taken from the cell in a measuring cylinder for further investigations.

4.2.4 Rheological investigation of CO₂-loaded silica nanofluids

A detailed rheological investigation of the synthesized nanofluids was carried out using a compact rheometer (MCR-52, Anton Paar[®], Physica, Austria). The rheological investigations were conducted using a bob and cup arrangement of the rheometer. To perform the measurements, 6 ml of nanofluid was carefully poured in the cup and the bob was slowly lowered till it was entirely submerged in the fluid. After every measurement, the cup and bob were removed from the rheometer followed by cleaning using laboratory solvent toluene and water. The entire experimental run took 9 min and the time per measurement point was 10 second. The rheological investigation was performed in both shear (viscosity and yield stress) and dynamic modes (storage modulus: G' and viscous modulus: G'') for silica nanofluids before and after CO₂ capturing. A wide range of shear rates from 20 to 2000 s⁻¹ was varied to perform shear measurements on nanofluid samples.

Dynamic tests were conducted for both strain-sweep and frequency-sweep measurements. Strain-sweep were performed to obtain G' and G'' vs. strain amplitude (0.1 to 100%) results where the frequency was kept constant at 10 rad s^{-1} [207]. These measurements are useful in the determination of Linear Viscoelastic (LVE) region (G' remains constant with strain amplitude) and the critical strain (cross-over point) of viscoelastic nature in nanofluids. Frequency-sweep measurements typically performed at an applied strain within the LVE region. Thus, frequency-sweep measurements were performed in the range of 1-100 rad/s of angular frequency while amplitude is fixed at a particular value within LVE range of strain-sweep analysis of nanofluids. All rheological experiments (shear and oscillatory) were repeated thrice to establish repeatability in results and the standard deviation was calculated by accounting the values of all 3 runs. The experimental uncertainty of 1.5-4% and 2-9% is estimated for oscillatory and shear flow experiments, respectively. Various parts of the rheometer (bob, cup, and spindle) were cleaned after each sample study with DI water and subsequently dried with the air blower to reduce cross-contamination and improve the quality of results.

4.3 Results and Discussion

First, the discussion on rheological properties into two sections; shear and dynamic modes. In each section, the effect of particle size, concentration, and temperature (303, 323, and 353 K) on rheological properties nanofluids is discussed. Finally, CO_2 capturing and retaining potential of nanofluid is examined *via* viscosity and viscoelastic results at different rpm (300/600) and temperature (303 and 353 K).

4.3.1 Shear rheological behavior of nanofluids

The effect of particle size, concentration, and temperature on viscosity and shear stress of silica nanofluids is studied at varying shear rates ($20\text{-}2000 \text{ s}^{-1}$). All tests related to particle size and concentration were carried out at 303 K and 0.1 MPa. The effect of varying

temperatures (303-353 K) was investigated on the rheological properties of nanofluid S1. Nanofluid, being viscous, possesses yield strength and thus, to induce any deformation in solution, an externally applied shear rate must be higher than the yield strength of the solution [11]. It was observed that shear rate less than 20 s^{-1} was not sufficient enough to induce deformation in nanofluid and hence, the shear rheological data for shear rate $< 20 \text{ s}^{-1}$ were not reported.

Figure 4.2 shows the shear rheological analysis for the effect of particle size on viscosity and shear stress profiles of S1, S2, and S3, respectively.

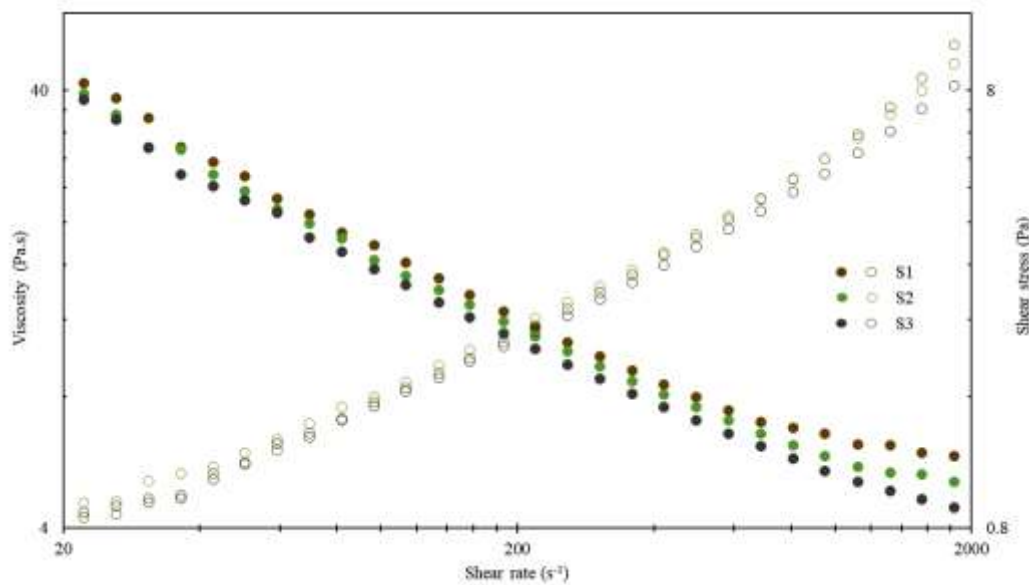


Figure 4.2: Plots of viscosity (closed symbols: ●) and shear stress (open symbols:○) vs. shear rate experiments of silica nanofluids as a function of particle size at 303 K and 0.1 MPa.

It was observed that the viscosity for sample S1 was 41.3 Pa.s at shear rate of 22.3 s^{-1} which significantly reduced to 13.6 Pa.s at 158 s^{-1} . Finally, it reached to a minimum value of 5.8 Pa.s at 1860 s^{-1} . For S2 nanofluid (particle size $\sim 82 \text{ nm}$), the viscosity was observed to be 38 Pa.s at 22.3 s^{-1} which reduced to 12.8 Pa.s at 158 s^{-1} followed by 5 Pa.s at 1860 s^{-1} . For S3 nanofluid (particle size $\sim 142 \text{ nm}$), the viscosity reduced from 37.8 Pa.s

at 22.3 s^{-1} to $4.4 \text{ Pa}\cdot\text{s}$ at 1860 s^{-1} . Thus, the increase in particle size causes a reduction in viscosity of nanofluids even though they exhibit a similar concentration of 0.1 wt% (Table 4.1). A similar trend for increasing particle size on viscosity was observed for Al_2O_3 and ZnO nanofluids prepared in base fluid of ethylene glycol [189]. Minakov et al. [208] also found similar viscosity trend for silica NPs dispersed in water. This can be attributed to the fact, for a given mass concentration in a nanofluid, the relative viscosity decreases on increasing the particle size due to a decrease in the interfacial area. This reduces the hydrodynamic interactions between the solid and fluid phases, which results in lower resistance to flow [209]. Another possible explanation for this can be supported by the fact that reduced particle size increases the inter-particle forces that tend to dominate the applied shear forces and thus, the viscosity increases, consistent with viscosity results of S1. It is also to be noted here that the nanofluids exhibited shear-thinning nature with an increasing shear rate. Shear-thinning is the reduction in suspension viscosity with increasing shear rate, which is often found in colloidal systems [210]. For nanofluid, it is also established that shear thinning behavior depends on particle concentration, the applied shear rate, and viscosity of the base fluid [211].

In addition, S1 (i.e. nanofluid with the smallest size) exhibited shear stress of 0.85 Pa (at 22.3 s^{-1}) which continued to increase with increasing shear rate. The effect of increasing particle size on shear stress was insignificant for both S2 and S3 nanofluids, consistent with viscosity results in Figure 4.2. Almost similar values of shear stress were obtained over the entire range of shear rate; 0.9 (S2) and 0.86 Pa (S3) at 22.3 s^{-1} and 1.92 (S2) and 1.9 Pa (S3) at 158 s^{-1} . However, at a high shear rate (at 1860 s^{-1}), the shear stress was found to reduce slightly with increasing particle size and shear stress value of 10.1, 9.1, and 8.2 Pa was determined for S1, S2, and S3, respectively. Thus, a small amount of

variation ($\sim 6\%$) was observed for shear stress data of nanofluids, consistent with previous findings [49].

The effect of increasing particle concentration on viscosity of nanofluid is provided in Figure 4.3 for S1, S4, and S5. S1 has a particle concentration of 0.1 wt% while the concentration of S4 and S5 is 0.5 and 1 wt%, respectively. For S4, the viscosity was determined as 42.1 Pa.s (at 22.3 s^{-1}) which is higher than the viscosity of S1. This increase in viscosity of S4 can be attributed to a higher concentration of NP (0.5 wt%) in suspension. With increasing shear rate, the viscosity decreases to 14.5 Pa.s at 158 s^{-1} followed by 5.9 Pa.s at 1860 s^{-1} . For S5, the viscosity further increased to 48.2 Pa.s at 22.3 s^{-1} .

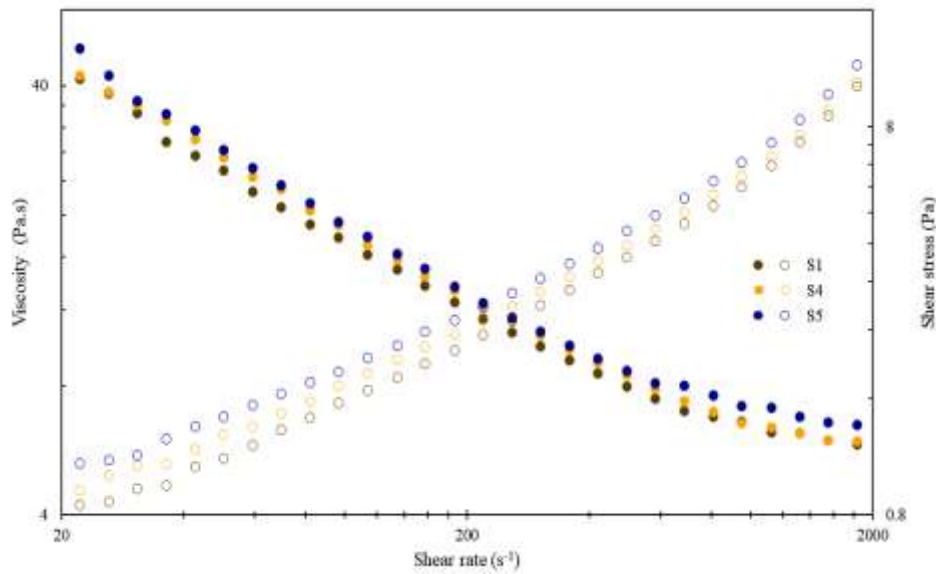


Figure 4.3: Effect of increasing shear rate on viscosity (closed symbols:●) and shear stress (open symbols:○) vs. shear rate profiles of silica nanofluids as a function of particle concentration at 303 K and 0.1 MPa.

Even, the viscosity at high shear rate of 1860 s^{-1} (6.5 Pa.s) was greater than the ones of S4 and S1 at the corresponding shear rate. The increase in viscosity of a nanofluid with increasing particle concentration is in accordance with the literature [183]. Thus, the increase in NP concentration causes an increase in the density due to a greater number of

particles present in the system which consequently made more particles to become the part of fluid and solid phase interactions resulting viscosity of the nanofluid increases [205]. One of the earliest correlations establishing a relation between the volume fraction of particles in a suspension and the viscosity was developed by Einstein [212]. Thus, the relationship between viscosity and the suspended solid concentration can be expressed as $\eta = \eta_0 (1 + 2.5 \varphi)$ where η is the viscosity of colloidal suspension, η_0 is the viscosity of water, and φ is the particle volume fraction [213]. According to the relation, increasing particle volume fraction (φ) will increase the viscosity of suspension (η). This is in line with our viscosity results where NP concentration increases the viscosity of nanofluid [184]. Thus, the viscosity of a silica nanofluid system can be increased by adding more NPs to the system. However, the enhancement of viscosity is not valid in all cases as an increase in viscosity increases the need for pumping power and wears them out faster.

Shear stress value of 0.92 and 1.1 Pa (at 22.3 s^{-1}) was measured for S4 and S5 (NP concentration of 0.5 and 1.0 wt%), respectively, which is slightly higher than the one of S1 at corresponding shear rate. Even, shear stress value at a high shear rate (1860 s^{-1}) remained higher for these nanofluids with 11.5 and 10.3 Pa, respectively, which might be possible due to the higher concentration of NPs in the system. Overall, a variation of $\sim 6\%$ was determined for shear stress data of these nanofluids. Thus, the results indicate that the effect of shear deformation on shear stress data of nanofluids was marginal and almost similar trends were obtained for both cases of particle size and particle concentration.

4.3.2 Effect of temperature on rheological properties

The effect of temperature (303-353 K) on the viscosity and shear stress of water and silica nanofluid S1 is provided in Figure 4.4. It can be observed that the viscosity for sample S1 was 41.3 Pa.s at shear rate of 22.3 s^{-1} which significantly reduced to 13.6 Pa.s at 158 s^{-1} and finally reached to a minimum value of 5.8 Pa.s at 1860 s^{-1} . With increasing

temperature from 303 to 323 K, the viscosity decreased to 36 Pa.s at 22.3 s^{-1} which further reduced to 4 Pa.s at 1860 s^{-1} for nanofluid S1. At 353 K, the viscosity further reduced to 28.3 Pa.s at 22.3 s^{-1} and reached to 3.4 Pa.s at a high shear rate of 1860 s^{-1} . From these results, it is evident that the nanofluid viscosity decreases with increasing temperature. For nanofluid synthesis in polymer solution, there can be two causes for the decrease in nanofluid viscosity with temperature. One, the viscosity of PAM solution exhibits a tendency to get negatively influenced by an increase in temperature. With increasing temperature, the time of interaction between neighboring molecules of PAM decreases due to an increase in surface velocities, which in turn causes a decrease in intermolecular forces and thus, it reduces the viscosity of the system [214]. Second, the intermolecular attraction between the NPs and base fluid weakens with increasing temperature [215].

It was observed that the effect of increasing temperature on shear stress of nanofluid S1 was marginal and almost similar profiles were obtained at each test temperature till the shear rate of $\sim 200 \text{ s}^{-1}$. After 200 s^{-1} , the shear stress profiles of nanofluid is different where stress value progressively decreased with increasing temperature. At 1860 s^{-1} , the value of stress was measured to be around 10.1, 9, and 7.2 Pa for temperature 303, 323, and 353 K, respectively.

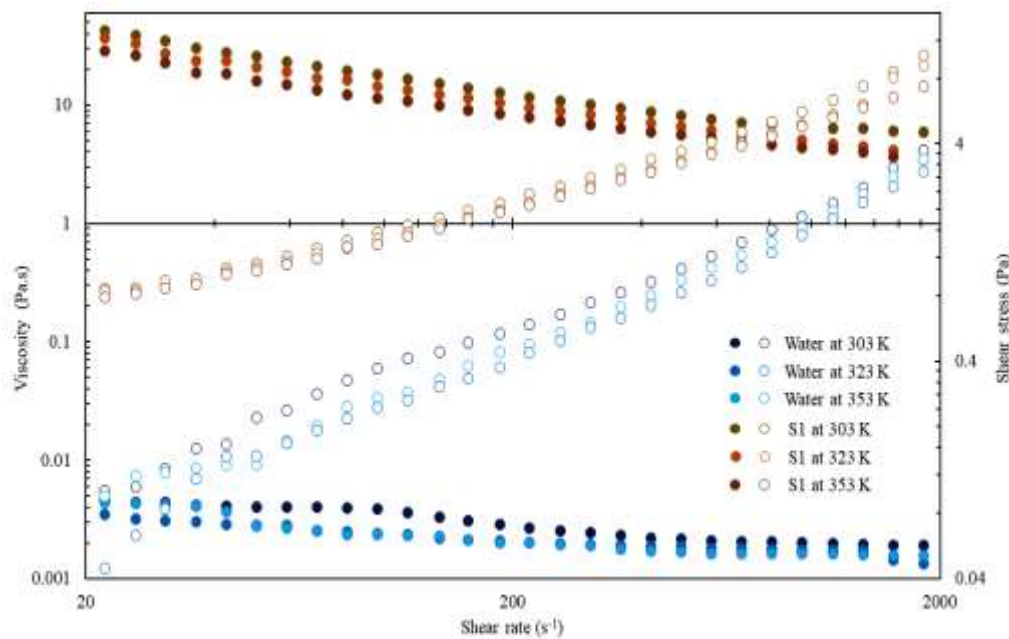


Figure 4.4: Effect of increasing temperature (303, 323, and 353 K) on viscosity (closed symbols:●) and shear stress (open symbols:○) data of nanofluid S1 and compared with the ones of water.

With increasing temperature, the decreases in stress value of nanofluid are in support of viscosity results where PAM viscosity is regarded as the crucial factor for viscosity reduction in nanofluids.

To validate these results, a comparative analysis with DI water was performed under identical conditions and the results have been included in Figure 4.4. It was observed that water viscosity was significantly lower than the viscosity of nanofluids. The value of viscosity of water at 303 K was 0.097 Pa.s (at 22.3 s⁻¹) which reduced with increasing shear rate. As a result, water viscosity reached to 0.002 Pa.s at 1860 s⁻¹. With increasing temperature, water viscosity value of 0.097 Pa.s decreased to 0.092 (323 K) and 0.003 Pa.s at 353 K. Similarly, near identical shear stress profiles (similar to S1) were obtained for water. For water, the value of shear stress was measured to be around 0.10, 0.09 and 0.04 Pa at 303, 323, and 353 K, respectively. These values steadily increased with increasing

applied shear rate, consistent with stress profiles of nanofluids. At 1860 s^{-1} , shear stress value was measured to be 3.7, 3.3 and 2.9 Pa at 303, 323, and 353 K, respectively. Compared to water, the nanofluid S1 exhibited superior rheological properties, which is of key importance for nanofluid use at high temperature applications.

4.3.3 Dynamic rheological behavior

Silica nanofluids are viscoelastic materials, possessing both elastic (G') and viscous (G'') nature. The viscoelastic nature of nanofluid is subjected to change at any applied strain amplitude [127]. It is worth noting that larger the viscoelasticity of a solution, greater will be its sweep efficiency for oil recovery applications. A nanofluid solution tends to agglomerate resulting in it exhibiting nonlinear viscoelasticity during deformational strain; this can be ascertained from their rheological behavior where their character is characterized by elastic nature at low strain rates, which rapidly drops when strain is increased. This sudden decrease in the moduli can be linked to the breakdown of NPs interactions in the system [216]. Hence, to understand the viscoelasticity of silica nanofluids, there is a need to ascertain the dependence of G' and G'' on the strain.

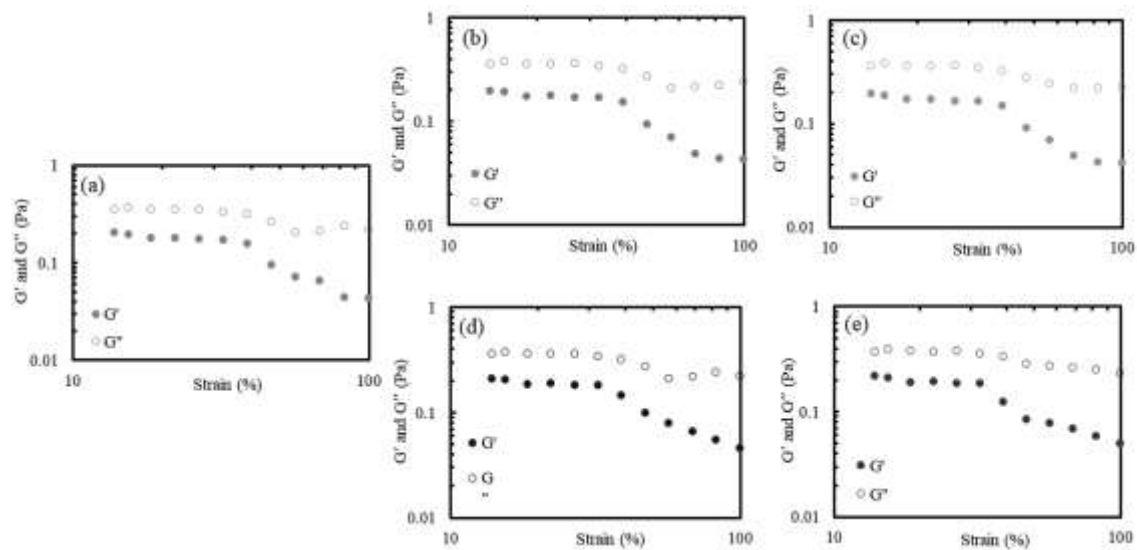


Figure 4.5: Strain-sweep analysis (at angular frequency of 10 rad.s^{-1}) showing effect of different particle (a-c) size and (d-e) concentration on viscoelastic properties (G' and G'') of nanofluids [a: S1 (34 nm, 0.1 wt%); b: S2 (82 nm, 0.1wt%); c: S3 (142 nm, 0.1 wt%); d: S4 (36 nm, 0.5 wt%); e: S5 (39 nm, 1 wt%)] at 303 K.

Thus, Figure 4.5 (a-e) represents strain-sweep measurements of silica nanofluids (S1, S2, S3, S4, and S5) at an angular frequency of 10 rad.s^{-1} [207]. From this figure, it can be inferred that the nanofluids exhibited viscoelastic behavior due to the presence of both G' and G'' over the entire range of strain explored. Both linear and nonlinear regions are evident and the nonlinearity in the viscoelasticity of nanofluids is attributed to the presence of fillers that probably change the polymer matrix structure *via* the formation of NPs agglomerates, adsorption of polymeric chains on NPs, and increase of chain entanglements [170,217]. It is to be noted here that G'' is higher than G' . In addition, G'' exhibited almost plateau over the entire range of strain for all nanofluids. This suggests that the characteristic behavior of nanofluids is liquid-like which is favorable for oil recovery applications with easy flow. At initial strain (14%), the value of G' was found to be 0.19 Pa. G' variation is rather nonlinear; G' remains almost constant during low to intermediate strain (\sim till 34%) however, high strain ($\geq 65\%$) significantly affected G' trend and its value reach to a minimum level of 0.04 Pa at 100% strain for nanofluid S1. With increasing particle concentration, the amount of NPs in nanofluids (S4 and S5) increased resulting magnitude of deformational strain required to break the particle-polymer structure increases as evident from a slight increase in G' . For S4 (NP = 0.5 wt%), the value of G' was measured as 0.2 Pa at 14% strain which was recorded to be 0.22 Pa for S5 at 14% (NP = 1 wt%). Thus, on increasing NP concentration, G' increases. Since increasing NPs concentration results in the formation of stronger NP-NP bonds, the formed network structure becomes the most

important mechanism to signify viscoelasticity in solution [170]. Also, it is to be noted that the slope of the nonlinear part for G' increases and the length of linear region decreases; the strain at which S4 and S5 nanofluids exhibited transition from linear to nonlinear elastic nature was measured ~32% which was higher in case of S1 (around 40%). From strain-sweep results, it is clear that the linear viscoelastic (LVE) region of nanofluids is very small as G' and G'' tend to merge at a very low value of strain amplitude (<10%) as predicted by Figure 4.5a. Mechanistically, this value might be around 1-2% which is in line with the literature value of LVE range for other NP based systems [207,218]

Figure 4.6 shows the effect of increasing temperature (323 and 353 K) on strain-sweep measurements for nanofluid S1. It is to be noted here that increasing temperature leads to a marginal reduction in G' and G'' values of S1; a decrease of only 10% between 303-323 K and 18% between 303-353 K was observed for moduli values. In addition, the trends of moduli profiles did not change and remained similar to the ones obtained for S1 at 303 K. The decrease in viscoelastic properties of nanofluid S1 is attributed to the reduction in viscosity of PAM at high temperature, indicating a characteristic feature of thermal stability in silica nanofluid. Therefore, polymer methods usually show challenges in high-temperature applications. Moreover, these results indicate that the thermal stability of PAM methods can be improved by introducing silica NPs that interact with PAM chains and improve the rheological properties of simple polymer methods.

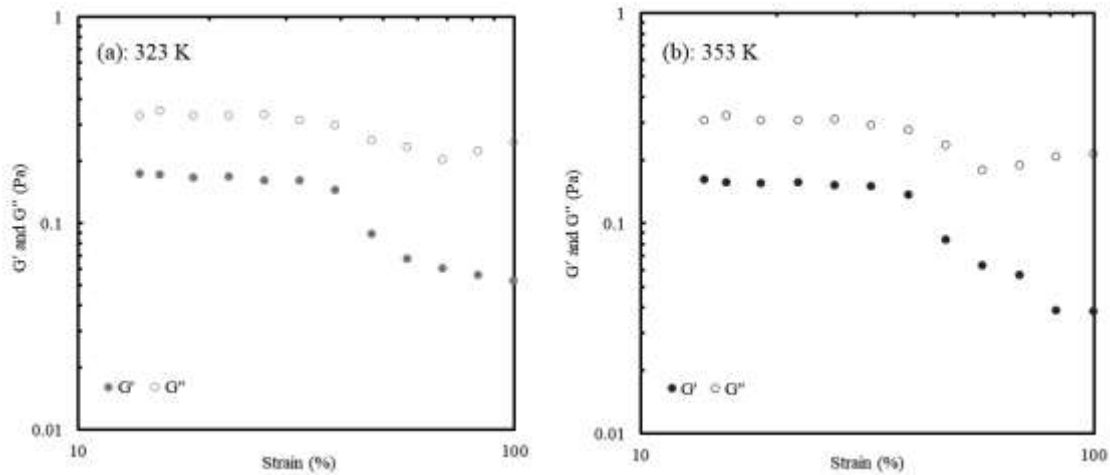


Figure 4.6: Temperature dependence (a: 323 and b: 353 K) strain-sweep measurements (G' and G'') of nanofluid S1, exhibiting NP size of 34 nm and concentration 0.1 wt%.

The results of frequency-sweep measurements for silica nanofluids were performed with a constant strain amplitude of 2% as applied strain within LVE region and the results are shown in Figure 4.7 where G' and G'' were plotted as a function of angular frequency (1-100 $\text{rad}\cdot\text{s}^{-1}$). Irrespective of particle size and concentration, all nanofluids showed strong viscoelastic nature due to the presence of both G' and G'' . In addition, both G' and G'' greatly increased with increasing frequency (i.e. greater than 20 $\text{rad}\cdot\text{s}^{-1}$) which indicates that both elastic and viscous nature dominates in nanofluids.

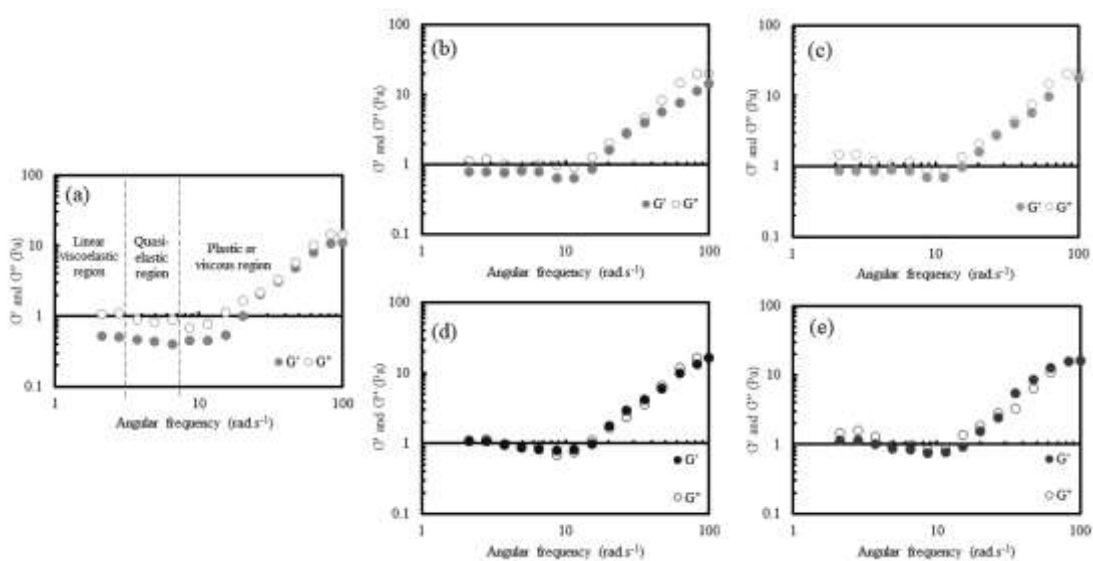


Figure 4.7: Frequency based viscoelastic response (G' and G'' vs. frequency), at constant strain amplitude (2%), of different silica nanofluids (a: S1; b: S2; c: S3; d: S4; e: S5) as a function of different particle (a-c) size and (d-e) concentration. Different flow regimes showing dominance of viscous (G'') /elastic (G') nature in nanofluid are also evident from Figure.

However, G'' remained slightly higher than G' for S1, S2, and S3 nanofluids, consistent with strain-sweep results for these nanofluids. For S4 and S5, G' slightly increased and almost match with G'' values over the entire range of frequency. This indicates S4 and S5 exhibited a slight increase in elastic nature (G') than S1-S3 nanofluids, which is credited to the presence of a higher concentration of NPs (0.5 and 1 wt%) in suspension consistent with strain-sweep results of S4 and S5 nanofluids. Based on the oscillatory response, three distinct regions could be defined for each of the nanofluids. The region in which the values of moduli exhibited a plateau is referred to LVE region (frequency $\leq 2 \text{ rad.s}^{-1}$). LVE region refers to the region in which moduli values exhibit insignificant change with increasing frequency [207]. In Figure 4.7, LVE region was small as moduli showed plateau till frequency $\sim 2 \text{ rad.s}^{-1}$. After 2 rad.s^{-1} , moduli values showed steady decrease in QE region before passing through a minimum value at 10 rad.s^{-1} , and finally moduli increase in plastic region. This is followed by a small but steady moduli decrease in the quasi-elastic (QE) region (frequency $\sim 2\text{-}8 \text{ rad.s}^{-1}$). After reaching a minimum value ($G' \sim 0.4 \text{ Pa}$ at 6 rad.s^{-1}), both the moduli increase in plastic or viscous region (frequency $\geq 10 \text{ rad.s}^{-1}$) as shown in Figure 4.7, which is in line with previous findings [207]. It is clear that increasing particle size and concentration marginally affected ($\sim 6\%$) the viscoelastic properties of nanofluids and nanofluids showed identical rheological behavior.

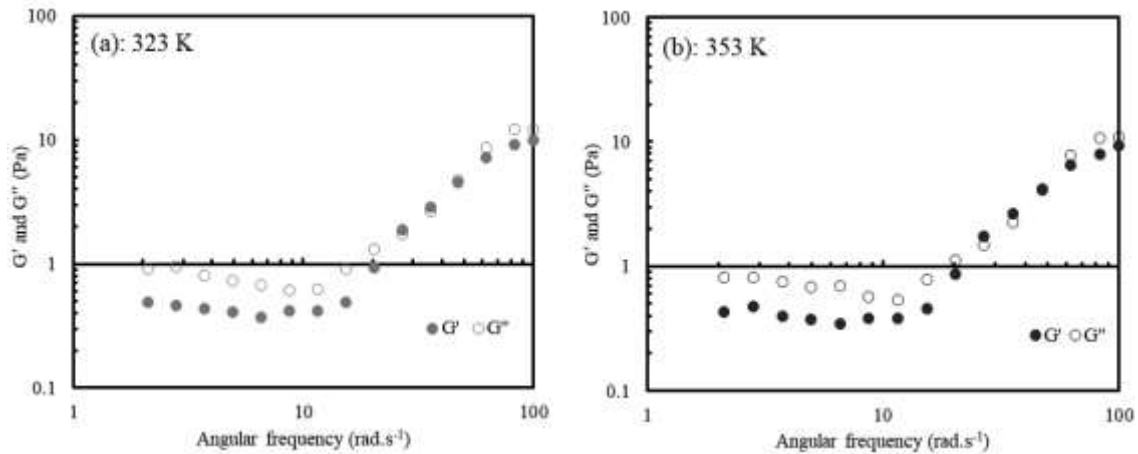


Figure 4.8: Effect of high temperature (a: 323 and b: 353 K) on frequency based viscoelastic properties (G' and G'') of nanofluid S1.

The effect of temperature on viscoelastic properties (G' and G'') of nanofluid S1 was investigated and the results are presented in Figure 4.8. It can be inferred that viscoelastic response of nanofluid is least dependent on temperature and therefore, nanofluid behaved almost as thermally stable fluid resulting G' and G'' decreased by only $\sim 8\%$ between 303-323 K and $\sim 17\%$ between 303-353 K. G' and G'' reached to minimum values of 0.34 and 0.53 Pa at 353 K, respectively, which are comparable with moduli values at 303 K. This is in accordance with temperature assisted decrease in viscosity of nanofluid S1, where PAM viscosity was considered to be the main factor for changes in rheological properties of nanofluid. From these results, it can be inferred that, at low-frequency levels, rheological behavior of nanofluid S1 is liquid-like ($G'' > G'$) while at high-frequency levels, it exhibited both (viscoelastic) due to almost equal values of G' and G'' at each test temperature. Thus, compared to a conventional fluid, the thermally stable viscoelastic response of nanofluid can offer promising solutions for high-temperature oil recovery applications.

4.3.4 Effect of CO₂ capturing on shear rheology of nanofluids

The structure formed by mixed entanglements of SiO₂ NPs and PAM chains creates a steric barrier to captured CO₂ bubbles as a result, nanofluid offers promising solutions for CO₂ utilization than conventional fluid. The images of silica nanofluid S1 before and after CO₂ capturing test (at 300 rpm) is shown in Figure 4.9.

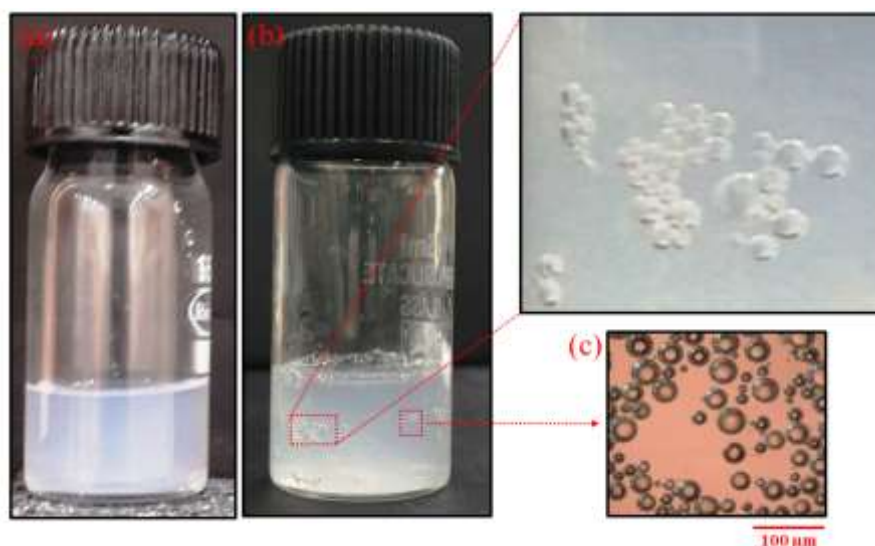


Figure 4.9: Visual appearance of nanofluid S1 (a) before and (b) after CO₂ capturing experiment at 300 rpm. The presence of CO₂ bubbles in the aqueous phase of S1 is shown by microscopic image.

It is clear that the inclusion of CO₂ slightly increased the volume of nanofluid in the vial and CO₂ remained suspended in the form of bubbles in the body of nanofluid (Figure 4.9). The presence of CO₂ bubbles in the aqueous phase of nanofluid is also confirmed by microscopic analysis; CO₂ bubbles were circular in size and sparsely distributed in nanofluid as shown by a microscopic image in Figure 4.9. In the oilfield, silica nanofluid flow through pore throats is subjected to varying shear deformation, which may impair its rheological properties resulting CO₂ capturing potential of nanofluid and the purpose of CO₂ utilization face challenges. Thus, it becomes essential to investigate the rheological

properties of silica nanofluid before and after CO₂ capturing and compare to find nanofluid potential in CO₂ utilization applications.

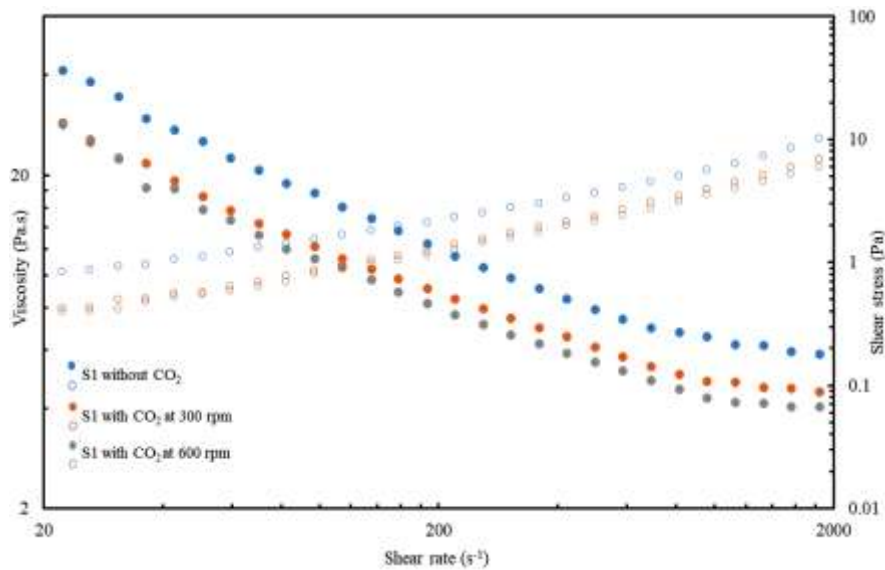


Figure 4.10: Effect of CO₂ inclusion, at different stirring rates (300 and 600 rpm), on shear rheological properties e.g. viscosity (solid symbols) and shear stress (open symbols) measurements of nanofluid S1 at ambient conditions (303 K and 0.1 MPa).

Figure 4.10 represents the effect of shear rate (s^{-1}) on viscosity and shear stress of nanofluid S1 (with and without CO₂) at 303 K, where viscosity and shear stress are denoted by solid and open symbols, respectively. CO₂ capturing tests were performed at two different stirring speeds of 300 and 600 rpm as CO₂ capturing is directly proportional to the stirring rate [11]. The viscosity of nanofluid S1 before capturing was 41.3 Pa.s at 22.3 s^{-1} which decreases to 5.8 Pa.s at 1860 s^{-1} . After CO₂ capturing at 300 and 600 rpm, the viscosity of S1 was measured as 28.7 and 28.1 Pa.s, respectively. At 1860 s^{-1} , these values were determined as 4.4 and 4 Pa.s, respectively. It was observed that nanofluid S1 with CO₂ exhibited lower viscosity than the one without CO₂. This reduction in viscosity of silica nanofluid S1 was due to the influx of lighter gas (CO₂ as small bubbles) in suspension. This drop-in viscosity is further compounded on increasing stirring rate (600 rpm) which

leads to a higher CO₂ influx in the nanofluid phase. It is to be noted here that nanofluid viscosity with CO₂ (for 300/600 rpm) always remained lower than the one without CO₂ over the entire range of shear rate. This indicates that CO₂ did not deform (i.e. coalescence, escape, etc.) by increasing shear rate which made nanofluid S1 a rheologically stable fluid for CO₂ capturing at varying flow conditions. Otherwise, CO₂ may coalesce and escape from the matrix of NP-PAM under increasing shear deformation resulting nanofluid phase will free from CO₂ and viscosity becomes equal to the viscosity of nanofluid without CO₂. However, this was not observed as evident from stable shear thinning response of nanofluid at both 300 and 600 rpm (Figure 4.10). The experiments were repeated for shear stress vs. shear rate for nanofluid S1 before and after CO₂ capturing at 300/600 rpm and the results were reported in Figure 4.10. The shear stress for S1 without CO₂ was 0.84 Pa (at 22.3 s⁻¹) which increased to 10.12 Pa at 1860 s⁻¹. After CO₂ capturing, the values of shear stress for S1 were measured as 0.41 (for 300 rpm) and 0.39 Pa (for 600 rpm) at 22.3 s⁻¹ which further increased to only 6.8 and 5.9 Pa at 1860 s⁻¹, respectively. These results also confirm the presence of CO₂ in the nanofluid phase. Silica nanofluids are viscous suspensions and at the same time, they have surface active agent (NP) to reduce IFT of CO₂. It is well established that CO₂, being lighter phase, is tended to escape from the solution which significantly affects the CO₂ capturing potential of a fluid system [38]. This can be controlled by nanofluid as its viscous nature can reduce gravitational action on captured CO₂ bubbles. This can be attributed to steric hindrance (due to the polymer chains) and enhanced absorption of silica NPs at the interface of gas-liquid [10]. Increasing number of NPs will create more IFT reduction which is desirable for CO₂ capturing, as smaller CO₂ bubbles are better stabilized than large size bubbles in NP entanglements of nanofluid [11]. Therefore, nanofluids are preferable for improved CO₂ capturing.

4.3.5 Effect of CO₂ capturing on the viscoelasticity of silica nanofluids

Strain-sweep analysis of nanofluid S1 after CO₂ capturing as a function of stirring rate (300 and 600 rpm) at 303 K is shown in Figure 4.11. Effect of high temperature (353 K) on CO₂ capturing potential of S1 was also investigated. At 300 rpm and 303, it was observed that G' and G'' values for S1 were 0.18 and 0.33 Pa (at 14%), respectively, lower than the values without CO₂ (Figure 4.11). This was observed the entire range of applied strain. However, the level of reduction was not severe due to a lower amount of CO₂ solvated in the solution. At 600 rpm, these values reached were measured as 0.16 and 0.28 Pa, respectively (Figure 4.11). This suggests that, at 600 rpm, more CO₂ captured into the bulk phase and made nanofluid lighter, therefore, moduli values were lower at 600 rpm than 300 rpm (graphically compared with S1) (Figure 4.11). This is in accordance with viscosity results where nanofluid with 600 rpm exhibited lower viscosity than 300 rpm (Figure 4.10). With increasing strain, G'' value did not reduce much and its value remained significantly higher [0.19 Pa (300 rpm) and 0.16 Pa (600 rpm)] at 100% strain. This indicates that viscous property of nanofluid S1 improved in presence of turbulence (i.e. 600 rpm) which favors nanofluid application for CO₂ capturing projects in tortuous reservoirs full of complex pore throats. However, G' changed significantly from 0.18 Pa (at 14%) to 0.02 Pa (at 100%). For 600 rpm, these values were 0.16 Pa (at 14%) and 0.018 Pa (100%). Thus, the elastic property of nanofluid for CO₂ capturing is greatly affected by applied strain which might be possible if CO₂ increases the inter-particle distance between NPs resulting network strength of the system reduces.

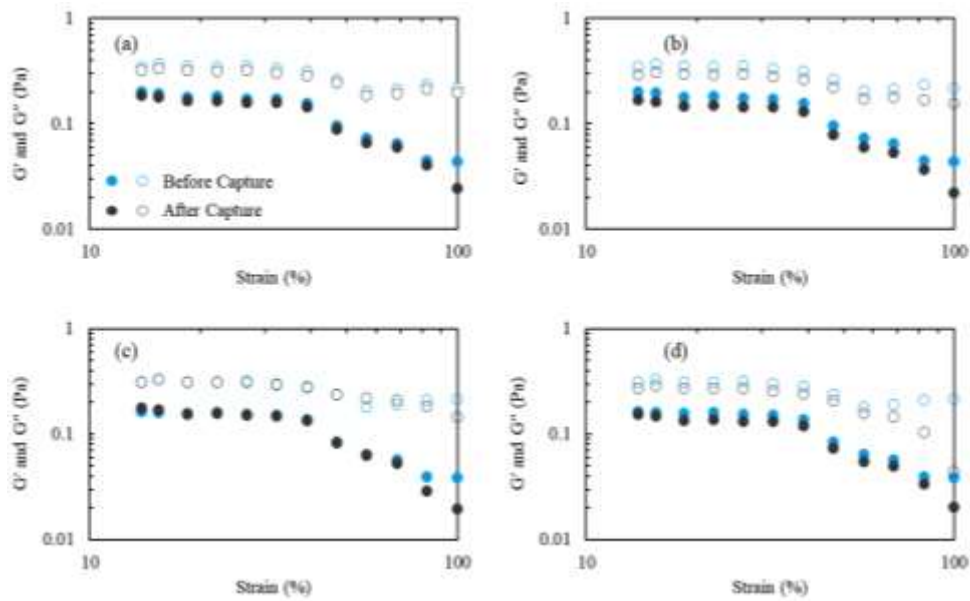


Figure 4.11: Strain-sweep measurements (G' and G'' vs. strain) to determine the impact of high temperature 353 K (c, d) on CO_2 capturing potential of nanofluid S1 at different stirring rates (a: 300 rpm and b: 600 rpm). G' (solid symbols) and G'' (open symbols).

The effect of high temperature (353 K) on CO_2 capturing potential of nanofluid S1 is shown in Figure 4.11c (300 rpm) and Figure 4.11d (600 rpm). In Figure 4.11c, G'' value was determined as 0.3 Pa (at 14%) and 0.14 Pa (at 100%) while G' value was 0.17 Pa (at 14%) and 0.017 Pa (at 100%). The values did not change much at the high temperature because of the very low amount of CO_2 loaded at high temperatures [10]. Similarly, for 600 rpm, the values of G' and G'' were determined as 0.15 and 0.26 Pa at 14% and 0.015 and 0.43 Pa at 100%. It can be inferred that moduli values slightly reduced at 353 K which might be associated to the effect of temperature on nanofluid viscosity however, their trends remained almost similar as obtained at 303 K. Thus, the insignificant variation in viscoelastic trends of moduli proposes that CO_2 capturing in S1 phase was stable against temperature resulting CO_2 bubbles neither coalesce nor escape from networks created by SiO_2 NP and PAM entanglements. Since CO_2 under temperature can coalesce and convert into a large bubble, premature escaping may occur between CO_2 and nanofluid due to

gravitational action. This will make nanofluid phase free from CO₂ and nanofluid will receive original moduli values obtained for S1 without CO₂. Thus, nanofluid showed enhanced potential for CO₂ capturing which was least affected by conditions (strain and temperature), consistent with shear rheology data of CO₂ laden nanofluid S1.

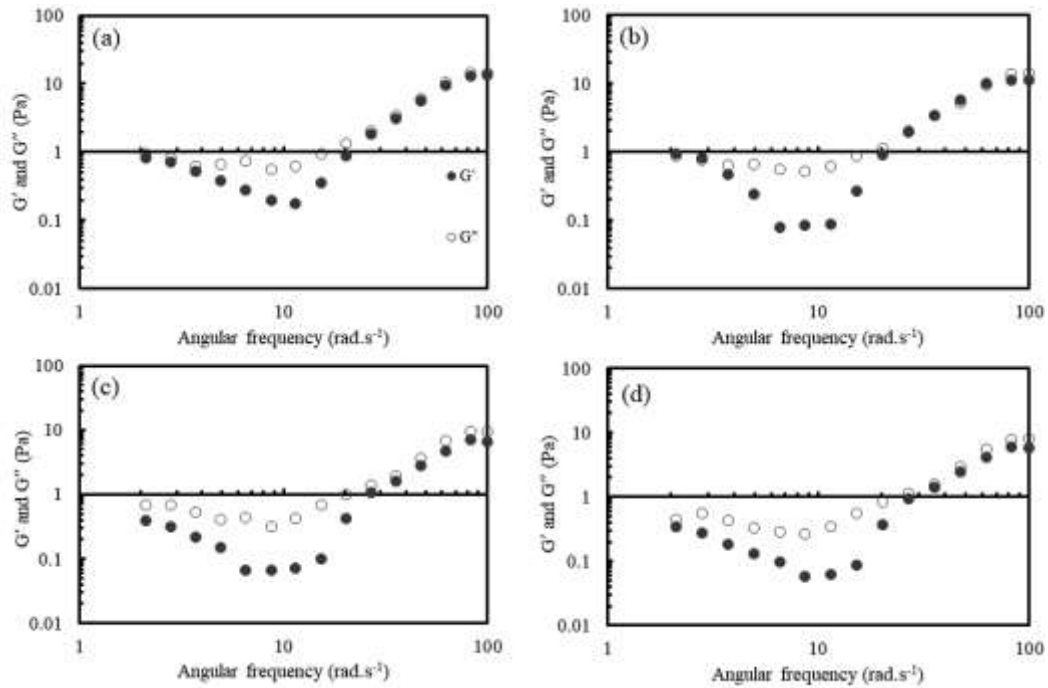


Figure 4.12: Frequency-sweep analysis (G' and G'' vs. frequency) to measure effect of high temperature 353 K (c, d) on CO₂ capturing potential of nanofluid S1 at different stirring rates (a: 300 rpm and b: 600 rpm). G' (solid symbol) and G'' (open symbols).

Similarly, frequency-sweep results confirmed enhanced CO₂ capturing at 600 rpm (Figure 4.12b) than 300 rpm (Figure 4.12a) at 303 K. Therefore, G' values (at 600 rpm) were lower than G'' over the entire range of frequency consistent with strain-sweep results at 600 rpm. The inclusion of CO₂ in the system has a more pronounced impact on the elastic modulus of nanofluid which signifies that including CO₂ in a nanofluid would yield to its liquid-like behavior as observed by an insignificant change in G'' . With CO₂ capturing, a higher portion of the energy will be dissipated by viscous forces when compared to energy

stored in structure of the material. This will predominantly favor viscous behavior of the suspension [197]. Even, high temperature (353 K) did not affect the viscoelastic response and almost similar G' and G'' trends were obtained at both the test temperature. The viscoelastic results are promising for improved CO₂ capturing in nanofluid phase as CO₂ loaded in nanofluid phase retained in the body of nanofluid, and no change in rheological properties was observed during application of any strain amplitude and angular frequency. This is promoting the likelihood of using silica nanofluid for carbon transport and utilization in subsurface formations.

4.4 Conclusion

The shear and dynamic rheological properties of single-step silica nanofluids have been investigated for CO₂ capturing applications under different conditions *viz.*, varying particle size (34-142 nm), concentration (0.1, 0.5, 1 wt%), and test temperature (303, 323, and 353 K). All nanofluids exhibited shear-thinning non-Newtonian behavior which was found to be affected by particle concentration than size. As a result, nanofluid viscosity, G' , and G'' values increased from 41.3 Pa.s, 0.2 Pa, and 0.37 Pa (S1, NP = 0.1 wt%) to 48.2, 0.26 Pa, and 0.39 Pa (S5, NP = 1 wt%), respectively. The viscosity of nanofluid S1 decreased with increasing temperature and at 353 K, nanofluid viscosity was determined as 28.3 Pa.s (31% decrease). The decrease in nanofluid viscosity is linked with temperature assisted drop in PAM viscosity because flow profile and shear thinning in S1 were similar to the ones at 303 K. This indicates that the molecular structure of NPs in nanofluid did not change, however, drop-in PAM viscosity recorded was responsible for the drop-in nanofluid viscosity. Dynamic investigations *viz.*, strain-sweep and frequency-sweep measurements were conducted and nanofluids exhibited viscoelastic nature (presence of both G' and G''). The dynamic results were in line with shear results where only particle concentration and temperature affected the viscoelastic response of nanofluids. Further,

CO₂ capturing potential of nanofluid S1 was measured through rheological investigation on viscosity and moduli. The inclusion of CO₂ in S1 leads to a drop in viscosity and moduli values which was proportional to the degree of CO₂ capturing (for high stirring rate e.g. 600 rpm) in nanofluid. In addition, CO₂ capturing in nanofluid was intact as CO₂ did not deform with increasing temperature (for both stirring rates *viz.*, 300 and 600 rpm) resulting viscoelastic response of CO₂ laden S1 remained similar to the ones at ambient temperature (303 K), and slight % drops in G' [(5.5% (300 rpm) and 6.2% (600 rpm)] and G'' [(9% (300 rpm) and 7.1% (600 rpm)] values were again credited to temperature effect on PAM properties. Thus, the formulated silica nanofluids may offer excellent rheological advantages at high shear deformation and temperature, which makes them suitable candidates for carbon utilization and storage applications at complex conditions.

Chapter 5

In-Situ Formulation of Pickering CO₂ Foam for Enhanced Oil Recovery and Improved Carbon Storage in Sandstone Formation

Abstract

Compared to sole gas flooding, foam flooding provides superior mobility control, enhanced sweep, and greatly improved oil recovery from depleted oil reservoirs. However, since most modern oil reservoirs are located at higher depths and further away from foam generation units, it is becoming increasingly difficult to maintain foam stability, especially in modern deeper oil wells. Thus, in this study, an alternative study in foam formulation has been reported. Instead of preparing the foam at the surface and injecting it down the oil well, into the subsurface, the foam can be formed “in situ” by saturating the porous media downhole by foaming agents. The foaming agents in this study consisted of an anionic surfactant, sodium dodecyl sulfate (SDS), and the whole solution was stabilized by the addition of 1000 ppm PAM and varying concentrations of silica nanoparticles (NPs). The formed foam can then be pushed conventionally by chase water and provide increased oil recovery. Increasing NP concentration, initially improved foam stability as a higher number of NPs participated in strengthening the gas bubble. In-situ foam formation was also investigated for improving carbon storage in depleted oilfields. The injection rate of gas and the slug size of the foaming agent were varied to determine gas storage before the

breakthrough. A lower flow rate was found to be more conducive for foam formation while increasing slug size had little effect on gas storability in the reservoir.

5.1 Introduction

Primarily, driven by the need to enhanced recovery of oil from fast-depleting oil fields and the accompanying challenge to reduce anthropogenic carbon dioxide (CO₂) in the atmosphere, the use of CO₂ as an injection fluid for enhanced oil recovery (EOR) has gained significant attention within the hydrocarbon industry. When compared with the other more pre-dominantly used injection fluids (primarily water) for pressure maintenance, the application of CO₂ has the added benefit of reducing the viscosity of residual oil by causing it to swell and become mobile, which significantly improves oil recovery [16,219]. However, like all gases (CO₂, N₂, CH₄) used for injection, the efficacy of CO₂ flooding is significantly hampered by the extant challenges like viscous fingering, channeling to bypass residual oil, and gravity override [220–222]. The poor performance of gas injection-based enhanced oil recovery (EOR) can be attributed mainly to the low density and significantly lesser viscosity (compared to water, formation brine, and crude oil) of CO₂ gas exuberating the challenges of gravity segregation and undesired mobility ratio contrast, respectively [223–225]. Thus, to overcome these challenges, one of the most promising methods for EOR can be the use of CO₂ foam flooding. Conventionally, foams are defined to be a dispersion of gas/gases in a carrying liquid where the liquid phase is interconnected and at-least some of the gas flow paths are inhibited by the presence of a lamella [226]. The mobility of the gas bubbles is reduced by trapping them in porous media, mainly water which increases their viscosity [227]. Primarily, the foams are stabilized by a chemical surfactant which is a molecule that has low energy, and its presence at the gas-liquid interface reduces the surface tension [228,229]. Availability of the surfactant is an essential condition for the generation of foam and while the formation of foam and its

eventual decay is governed by separate mechanisms, the distance of foam propagation is dictated by the amount of retained surfactants. The inclusion of a surfactant and formation of foam, both increase the viscosity of the solution which is highly conducive for improved oil recovery [62,109,139,230]. One unique attribute of foams is that they can block off layers of highly permeable rock (already swept by preceding injection fluid) and divert the incoming injection fluid towards paths left unswept by the preceding injection fluid, improving its applicability to heterogeneous reservoirs [231–233]. Foams can also directly improve the front profile control with insignificant formation damage making them more viable for damage-prone formations. Consequently, the sweep efficiency of foam flooding is improved and incremental oil recovery is higher than CO₂ flooding [201,203,225]. This also has the advantage of improved carbon storage inside the oil reservoir as many more inaccessible pores, bypassed during CO₂ flooding are now accessed and become available for gas storage [234,235]. One commonly overlooked advantage of using CO₂ foams over other gases is their potential for selective mobility reduction (SMR) which allows the foam flooding to be viable even in high permeability reservoirs [236,237]. Commonly used surfactants for foam formulation in the hydrocarbon industry are sodium dodecyl sulfate (SDS), dioctyl sodium sulfosuccinate (AOT), and cetyl trimethyl ammonium bromide (CTAB) [135,238–241]. However, a major drawback associated with foams is that they are a thermodynamically and kinetically unstable system that causes rapid phase separation in the foam between liquid & gaseous components [242,243]. This reduces the efficacy of foam for various industrial applications and has led to the use of other chemicals like improved surfactants, polymers, or nanoparticles (NPs) to stabilize the foam for longer durations [10,95,129,165,242]. Some studies have also proposed the role of ionic liquids as an additive for foam stabilization [244,245].

The inclusion of a viscosifying polymer increases the fluid viscosity which in-turn prevents the gas from escaping from the foam and decreases the rate of film drainage [246]. Conventionally, the most common polymers used are PAM (polyacrylamide) and HPAM (hydrolysed-polyacrylamide) [247]. There have been several studies that have reported that foams stabilized by NPs are comparatively more stable than sole surfactant/surfactant-polymer stabilized foams [99,248–250]. A study on the applicability of Laponite particles and C₁₂E₄ (tetramethylene glycol monododecyl ether) on the stability of foams by varying the concentration of components in the mixture was performed by Zhang et al. (2008) who concluded that the foam stability was positively impacted by the increasing concentration of C₁₂E₄. The use of nanoparticle for stabilizing foams can improve the sweep efficiency and also, mitigate the gravity segregation [99]. Even at relatively higher concentrations (~1.5 wt%), higher oil recovery could be achieved using silica nanoparticles, sodium dodecyl sulfate, and N₂ gas [251]. The use of nanoparticle (NP)-surfactant solutions generate a more uniform and smaller foam. Conventionally, NP- stabilized foams have been found to perform better than polymer or surfactant enhanced foams in terms of oil recovery and CO₂ retention in the reservoir.

However, even with the use of foam stabilizing chemicals & NPs, the stability of foam cannot be extended indefinitely. Modern wells are located in difficult to access locations, with very narrow pore throats and are deeper than most historical wells. Under most of these conditions, the stability of foam from the surface to the formation can-not be surely assured for it to perform its function. Thus, there is a need to re-think the current approach towards CO₂ foam flooding and explore newer methods to ensure that significant amounts of oil can be recovered from the modern fields while ensuring that most of the injected CO₂ remains left behind in the reservoir. Thus, in this study, we have conducted a comprehensive experimental investigation of a novel approach towards CO₂ foam flooding.

In a sandstone sand-pack prepared using sand of size 0.2-0.38 mm, various fluids including water, polymer (PAM) solution, surfactant-polymer (PAM-SDS) solution, and NP-polymer-surfactant (SiO₂-PAM-SDS) solutions were injected after the completion of primary water-flooding. This was followed by the injection of CO₂ gas and was left for a specified duration to stimulate the generation of in-situ foam within the reservoir. The foam prepared in-situ, is expected to remain stable for a longer duration and hence, recover a greater amount of oil than the conventional foam flooding process. Following foam formation, chase water flooding was performed and corresponding, oil recoveries were tabulated. To analyze the effect of NP concentration on oil recovery, the varying wt% (0.5-2) of nanoparticles were added to the base solutions (1000 ppm PAM) and the resultant oil recoveries were compared to optimize the nanoparticles. The amount of carbon retention & storage by in-situ foam formation was also tabulated by a set of flow behaviour studies under varying flow rates and slug-sizes. All studies were performed using deionized water and at a test temperature of 333 K.

5.2 Materials & Methods

5.2.1 Materials

To prepare the nanoparticles, liquid tetraethylorthosilicate (TEOS, purity~99%) obtained from Merck was used as a precursor. Other chemicals used for this experiment without any purification were liquid ammonia solution (25%) obtained from Merck-Millipore, Ethanol (absolute, assay~99.9%) obtained from Changshu Hongsheng Fine Chemicals. To prepare foams, a commonly used surfactant SDS (purity~90%) was used. The SDS contains ingredients such as 5–15% anionic surfactants; oxygen-based bleaching agents, viz., <5% nonionic surfactants, phosphonates, polycarboxylates; and zeolites in very less amount. The salt used for the preparation of reservoir brines was NaCl (purity 99.5%) which was obtained in powder form from Sisco Research Laboratories,

India. DI water was used to prepare all aqueous formulations like the Polymer (P), Surfactant-polymer (SPAM), and Surfactant-nanofluids (SNF) solutions used during this study. For the oil recovery experiments, crude oil obtained from Tarapur oilfield (Ahmedabad, India) was used.

5.2.2 Preparation of injection solutions

The polymer solution was prepared by dispersing 1 g of PAM in 1000 ml of water taken in a glass flask. This flask was mounted on a magnetic stirrer and a magnetic bead was put in it to ensure stirring. To ensure a stable vortex, the solution was initially stirred at 150 RPM for 6 hours and then at 650 RPM for the next 6 hours. The solution was then checked by hand to ensure that no flocculates remained in the system. The polymer-surfactant solution was prepared by taking a measured amount of SDS (0.125 wt%, 0.25 wt% or 0.5 wt%) and adding it slowly to the polymer/nanofluid system while stirring it at 350 RPM for 30 mins. The prepared solution was then left to stabilize in a glass cylinder.

The 1000 ppm PAM solution was then used to prepare single-step silica nanofluids which remain stable for longer durations using the well-reported Stober sol-gel method [105,106]. However, for the sake of brevity, a brief discussion is provided as under. First, a defined volume of PAM/ethanol solution was taken in a glass beaker and sonicated for 10 min. Following this, TEOS of specified volume (to control the concentration) was added to the mixture and the solution further sonicated for 20 min. After this, ammonium hydroxide was added to the mixture and the solution sonicated for 60 min till the mixture in the beaker turned milky white. This indicated the presence of silica nanoparticles. To this mix, the surfactant solution of the desired quantity was added and slowly stirred at 350 RPM for 30 mins to prepare the SNF solution. The prepared solution was then left to stabilize in a glass cylinder before use.

5.2.3 Porous media investigations

To mimic a sand-stone reservoir, an artificial sand-pack was synthesized using commonly available sand bought from a commercial retailer. The sand used for preparing the sand-pack was initially cleaned using a reagent grade solvent (toluene) and was then dried in an oven for 96 h (at 250 °C). This was done to ensure any residual impurities were removed. After removing the sand from the oven before use, the sand was observed under a scanning electron microscopy (SEM) (SEM, Quanta 450, FEI, image processor up to 6144 x 4096 pixels) to ascertain the size of sand particles. To establish the size of the sand-particles, 4 separate micrographs were obtained and the average size of the sand particles was found to be between 0.2-0.38 mm. To obtain the mineralogical composition of the XRD data, an X-ray diffractometer (X-Ray Diffractometer D8 Advance, Bruker®, India) was used. The sand composition was found to consist of main quartz (88 wt%), kaolinite (6 wt%), feldspar (2 wt%), and chlorite (1 wt%), and others (3 wt%). For all oil recovery experiments, the sand-packs were prepared manually in a custom-built sand-pack holder. This was prepared using stainless steel (diameter: 1.5 inches and length: 24 inches), by D-CAM Engineering (Ahmedabad, India). To establish the porosity of the sand-pack, water of a known quantity (300 ml) was measured in a graduated cylinder and stored in a wash-bottle. While preparing the sand-pack, water and sand were simultaneously added and rammed continuously using a custom-ramming rod. This process was repeated until the sand-pack holder was completely saturated with water and sand. All oil recovery experiments were performed using a customized sand-pack flooding set-up comprising two syringe pumps, three fluid accumulators, and a sand-pack holder. In all the flooding experiments, one syringe pump was used to inject the fluids *viz.*, water, crude oil, PAM, SPAM & SNF-0.5-2.0 solutions & for chase water flooding, and the other syringe pump

was exclusively used for CO₂ injection in the sand-pack. The oil recovered during each flooding run is referred to as the resultant oil recovery.

5.3 Results and discussion

In this section, the observations related to the formation of in-situ foam inside the sand-pack and the resultant oil recovery have been provided. Primarily, the focus has been on investigating the mechanism of foam formation inside the sand-pack and exploring the role of NP concentration in improving produced foam stability leading to improved oil recovery. This has been followed by the use of in-situ formulated foam for improving carbon storage in oilfields. The amount of carbon storage under varying injection flow rates, slug size, and surfactant concentration has been investigated and a discussion provided on them.

5.3.1 Sand pack flooding results

To assess the viability of various injection fluids for in-situ foam formation and subsequently, the resulting oil recovery-several flooding tests (runs 1-6) at temperature 333 K were performed using each of the suspensions used immediately after preparation. These sand pack flooding runs were performed by following a well-established oilfield procedure [11]. The nomenclature, porosity, and permeability of each of the sand-packs have been provided in Table 5.1. After saturating the sand-packs with oil and establishing the irreducible water saturation, the sand packs were left to age for 10 days following which initial waterflooding at 30 ml/hr was performed till a volume equal to 1.5 PV had been obtained at the outlet. This was followed by injecting the EOR slug “S” (0.3 PV) and immediately followed by a gas slug “G” (0.3 PV) at 30 ml/hr. The sand packs were then left undisturbed for 3 days following which chase water flooding of further 1.9 PV at 60 ml/hr was performed. During the entire injection sequence, the pressure drop, amount of oil recovered and obtained water-cut was carefully measured.

Table 5.1: Petro physical properties and oil recovery obtained during flooding runs

Run	Porosity (%)	Permeability (md)	Initial water flooding	Oil recovery (% of OOIP)			Total oil recovery
				EOR slug	Gas slug	Chase water flooding	
1	32.4	642	33	--	3	3	39
2	33.1	656	32	7	3	10	52
3	32.8	648	34	8	4	12	58
4	32.6	643	33	10	6	22	71
5	33.5	672	34	11	6	23	74
6	33.6	681	33	10	5	18	66

The solutions used for injection were water, PAM (1000 ppm PAM), SPAM (0.5 wt% SDS in 1000 ppm PAM) and SNF 0.5-2.0 (0.5, 1 and 2 wt% silica NPs in 0.5 wt% SDS and 1000 ppm PAM solution). All silica solutions were investigated for their particle size and zeta stability before injection. The silica nanofluids had an average particle size of 36 ± 6 nm and the zeta-potential between -32 and -36 mV before injection.

Conventionally, the injection of any fluid inside a porous media creates some amount of back-pressure (due to resistance to flow by materials inside sand-pack) which was measured using a pressure transducer. The formation of foam inside the sand-pack was established by the pressure-drop profile observed during the injection of gas. The pressure drop profile is obtained between as the sand-packs being consolidated porous mediums, offer some amount of resistance to the inflow of the injection fluids. The resistance is directly proportional to the density and viscosity of the injected fluids. A solution having higher density/viscosity (say PAM solution) than water will require a greater amount of

energy to displace and will consequently have a higher pressure drop profile. The pressure profiles for each of the flooding runs have been provided in Figure 5.1. In the initial run (run-1), when only water was injected, the pressure profile did not show many fluctuations and the value of pressure drop remained between 8 psi to 9 psi over the entire course of the oil recovery run with an exception of the gas injection duration. During the gas injection, the pressure profile reduced significantly as the pressure required to move a specified volume of gas is much lower than the same volume of another fluid (on account of the gases lower density than water). When the oil recovery with performed with a polymer solution (run-2), the value of pressure drop jumped significantly during the injection of the polymer slug to 34.2 psi (as PAM is more difficult to displace than water). When the gas injection was performed, the value of pressure drop fell significantly to 12.4 psi when gas injection was initiated (at 1.9 PV) and slightly increased to 16.7 psi when gas injection was stopped (at 2.1 PV). While chase water flooding, the pressure increased continuously, and once, the slug was able to completely traverse the sand-pack, the pressure dropped to 8.4 psi. The sawtooth profile observed during the injection represents the areal coverage of the slug before its breakthrough at the outlet of the sand-pack. When the surfactant-polymer (SPAM) slug was injected into the sand-pack, the pressure slightly increased to 36.8 psi (run 3, at 1.8 PV) which fell similarly when CO₂ was injected. A bigger, wider sawtooth profile was formed on injecting SPAM which indicated that the injected fluids covered a wider areal range inside the sand-pack. The greater extent of the pressure profile also indicates that foam was formed inside the porous media. Conventionally, foams are formed in the presence of surfactants and this would be established by determining the residence time & the pressure drop profile during their injection. When the three NSP solutions were injected, the sawtooth type profile was also observed during each of the subsequent runs. However, the inclusion of NPs increased both the maximum value of pressure and the area

under the curve. The maximum pressure was observed for the SNF-2.0 solution as it has the maximum viscosity (on account of a greater number of particles suspended in the solution). Higher NP loading was also found to increase the CO₂ residence time inside the sand-pack (evident from the area under the curve, Figure 5.1). The saw tooth type profile observed on the injection of CO₂ indicates that of foam must have been formed, inside the sand-pack. These observations may further be correlated by the oil recovery studies.

The amount of fluid displaced by the injected fluid was obtained as a function injected pore volume (PV) and has been provided in Figure 5.2. First, the injection of water was performed which yielded an oil recovery of 33% of the original oil in place (OOIP). Then, CO₂ was injected in the sand-pack which was able to move another 3% of OOIP.

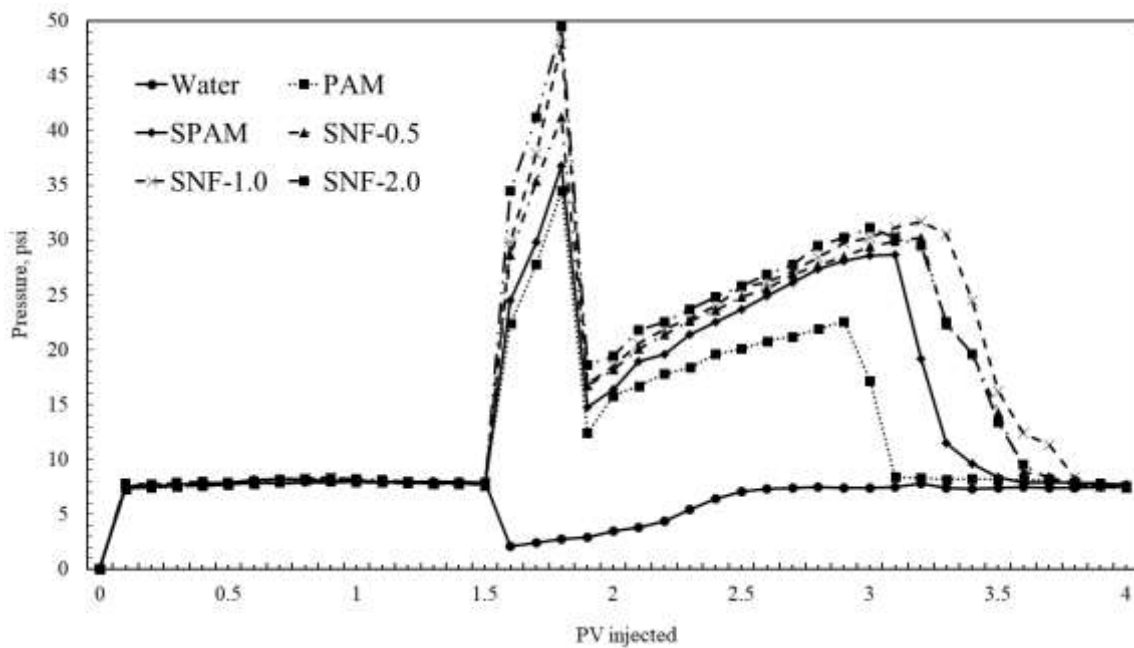


Figure 5.1: Pressure drop as a function of fluid injected (PV) in sand-packs for various runs at temperature 333 K.

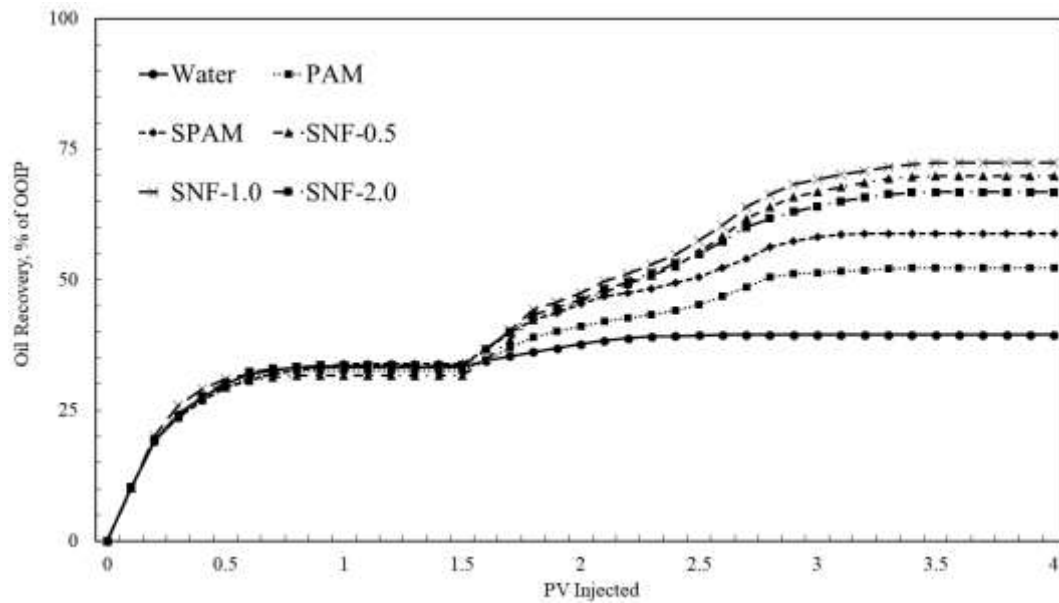


Figure 5.2: Resultant oil recovery (% OOIP) as a function of fluid injected (PV) in sand-packs for different flooding experiments at the test temperature of 333 K.

The injection of CO₂ can increase oil recovery as the injected CO₂ disperses into the residual crude oil, thereby making it easier to flow. However, since true miscibility conditions were not achieved in this study, the quantum of oil recovery (due to CO₂ injection) remained low [77]. This was followed by chase water flooding which mobilized 3% of OOIP more from the sand-pack (Figure 5.3). Thus, in the run-1, where only water and CO₂ were used, the cumulative oil recovery was 39% of OOIP (Table 5.1). In run-2, after the initial water flooding (which mobilized 32% of OOIP), a PAM was injected which displaced 7% of OOIP on account of its higher viscosity and greater oil mobilization capacity than conventional water. When CO₂ was injected after the PAM slug, it was also able to mobilize an additional 2% of OOIP. However, when the chase water flooding was performed, the greater amount of mobility control and better sweep performance (obtained from the conjunction of PAM and CO₂), more than 10% of OOIP of oil was mobilized for a total amount of 52% of OOIP (in run-2). These observations indicate that the mobility of CO₂ was controlled by the presence of PAM, causing it to preferentially solvate in crude

oil due to its higher residence time and massively increase oil recovery [252]. There are mainly three displacement processes which mobilize oil when the injection of CO₂ is followed by the injection of water or PAM solution. These are (a) CO₂ displacement by water by a two-phase drainage process, (b) oil displacement by water (two-phase drainage process), and (c) CO₂ displacement by water which then further displaces oil (double-drainage process). Hence, while mobility control of CO₂ by any fluid should residually trap CO₂ and increase oil production, it also displaces a significant portion of the earlier injected CO₂ (upto 70%) which is beneficial for oil recovery but requires further refinement for carbon storage. Thus, it is desirable that additional chemical additives be explored to increase the residual trapping of injected CO₂ within the reservoir.

The trapping of CO₂ may be increased by the use of surfactant-treated injection fluids. Hence, on run-3, the SPAM solution was injected after initial water flooding (Figure 5.2). The SPAM solution was able to mobilize over 8% of OOIP, in part due to the presence of surfactant (SDS) which tends to lower the Interfacial tension (IFT) that is responsible for an increase in oil recovery [175]. When CO₂ injection was performed in this sand-pack, it was able to mobilize 4% of OOIP and on chase water flooding, another 12% of OOIP was recovered. Hence, on the injection of SPAM and CO₂ slugs in run-3, a total of 58% of OOIP was mobilized which indicates greater suitability of surfactant solutions for oil recovery in conjunction with gas-based EOR methods.

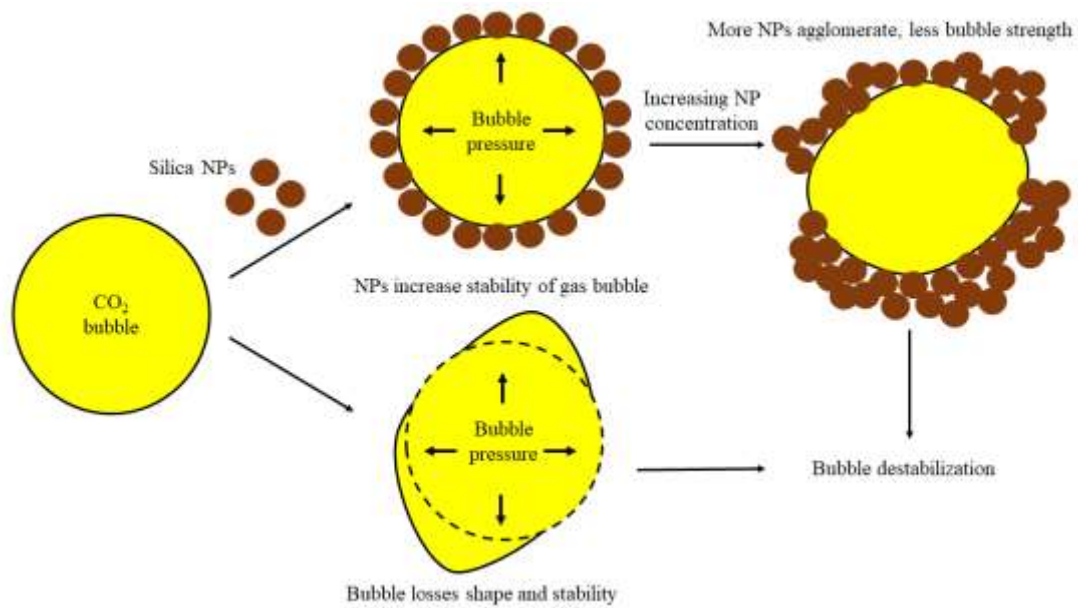


Figure 5.3: Schematic showing dependence of bubble gas strength on NP presence. At higher NP concentrations, NPs participate less in increasing bubble strength due to higher agglomeration.

When the surfactant-treated silica nanofluid solutions (SNF-0.5-2.0) were used, the amount of oil recovery due to their injection was in the range of 10-12% of OOIP. Compared to polymer and surfactant solutions, the silica nanofluids were able to mobilize a greater amount of oil due to the presence of nano-sized silica NPs which can mobilize additional oil due to a combination of wettability alternation, disjoining pressure, and IFT reduction [253,254]. They also benefit from the synergy between polymer, surfactant, and silica NPs, which has been explored and discussed in past studies [255]. The injection of CO₂ was able to move between 5-6% of OOIP, indicating the superior viability of surfactant-treated silica nanofluids for mobility control in gas-based EOR. Finally, when chase water flooding was performed, an additional 18-22% of OOIP was recovered in the runs 4-6. The maximum amount of oil recovery (74% of OOIP) was obtained in the run-5 where the SNF-1.0 solution was used. Compared to other solutions, the polymeric surfactant treated silica nanofluids (SNF 0.5-2.0) were able to perform more effectively in

oil mobilization due to the formation of foam which will be stabilized by the addition of both polymer and silica NPs. The polymer, PAM improves foam stability by causing its molecules to adsorb on the surface of the CO₂-water interface which greatly increases its strength and improves its life by reducing the liquid drainage. Furthermore, past studies have established that NPs have a tendency to adhere to the CO₂-water interface, which was evident by the remnants of silica NPs found at the edges of the residue CO₂ bubble under SEM [10]. The presence of silica NPs at the interface acts as an armour and resists bubble deformation and eventual break. Increasing the NP concentration further improves the stability of the bubbles as more NPs are present to strengthen its interface (Figure 5.3). A thicker layer of NPs (single-layer to double-layer to multi-layer) strengthens the foam and reduces its disintegration by countering the bubble burst pressure and the collapse pressure. The higher foam stability is one of the reasons why the SNF-1.0 solution yields a higher amount of oil recovery than the SNF-0.5 solution. However, at higher concentrations, NPs are highly prone to agglomeration which reduces their stability and impacts their foam strengthening ability [47,256]. This reduces the stability of formed foam which is evident by the decrease in oil recovery (66%) observed in SNF-2.0 when compared to SNF-1.0 (74% of OOIP) and SNF-0.5 (71%). However, additional studies on the mechanisms and quantum of residual trapping need to be explored, which are planned to be conducted in a separated study.

5.3.2 Evaluation of surfactant-treated solutions for carbon storage

Since the surfactant-treated solutions were able to form in-situ foam and mobilize a greater amount of oil in the oil recovery tests, they were then explored for carbon storage in depleted sandstone reservoirs. Given that CO₂ is a major greenhouse irritant and its subsurface storage has the potential to negate the ongoing climate change, carbon storage in depleted hydrocarbon reservoirs is a fast emerging area of study [234,257].

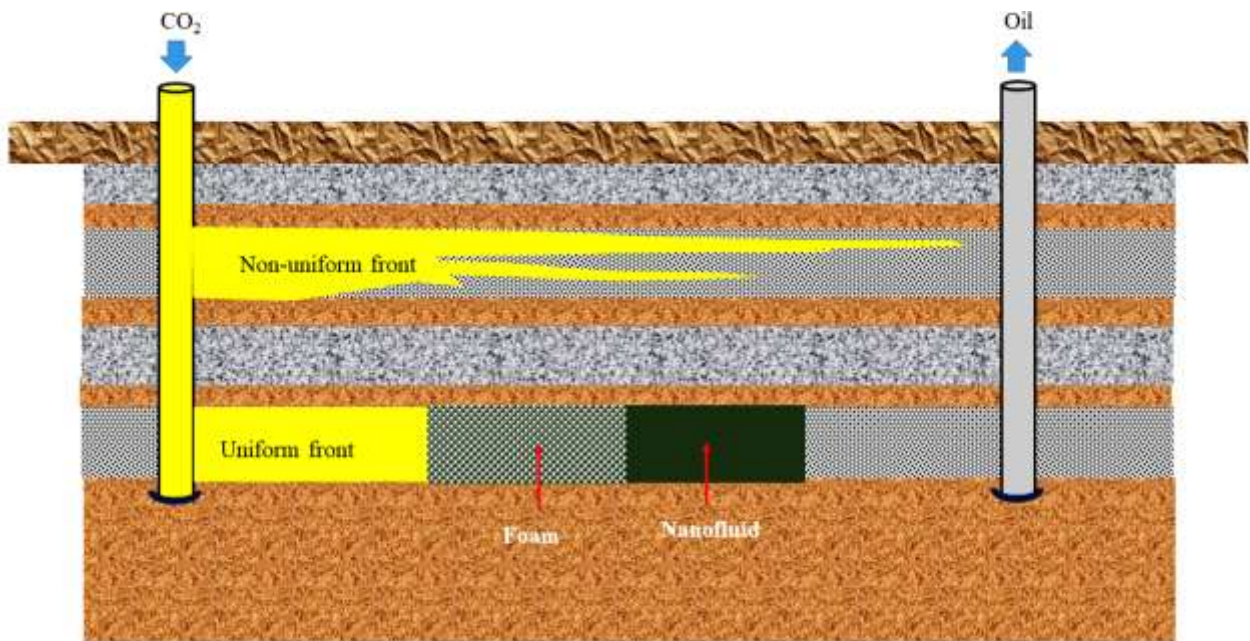


Figure 5.4: Comparative front formation while (top) sole gas injection and (bottom) nanofluid injection followed by gas injection.

However, its implementation is plagued by issues like mobility contrast leading to viscous fingering, premature escape, low areal sweep efficiency, etc., all of which reduce the efficacy of storage (Figure 5.4). Hence, in this study, the role of a surfactant-treated solution (SNF 1.0) was explored for controlling the mobility of CO₂ in the subsurface. It is expected that the SNF-1.0 will be able to form a front of foam on the injection of CO₂ which would reduce the premature breakthrough of CO₂ and improve its storability in the subsurface. For this study, sand-packs were fabricated using the procedure established in section 2.4. These sand-packs were found to have a porosity in the range of 32-34% and permeability between 642-698 mD. They were then saturated (i.e. water and then required amount of SNF-1.0) before CO₂ injection was initiated. The role of CO₂ injection flow rate, size of SNF-1.0 slug, and surfactant concentration were investigated separately. The pressure drop and the amount of fluid recovered at the outlet were carefully noted for each run. All experiments were performed at 333 K.

Initially, the amount of carbon storage in the sand-pack was investigated for varying flow-rates of CO₂. The sand-packs in this study had been pre-injected with 0.5 PV SNF-1.0 nanofluid. The gas injection flow rate was varied between 30-150 ml/hr and the observations of the pressure drop have been presented in Figure 5.5. From the pressure drop, it can be observed that when the injection was performed at 30 ml/hr, the area under the curve was maximum and the pressure drop took place after 2.1 PV of gas had been injected. This indicates the formed foam inside the sand-pack was able to negate the early escape of CO₂ and a greater area inside the reservoir was touched. On increasing the flow rate, the area under the curve fell progressively, indicating CO₂ was able to escape from the sand-pack at a much quicker pace. When CO₂ injection was performed at a flow rate of 150 ml/hr, the breakthrough took place after the injection of just 0.8 PV of CO₂ (Figure 5.5), indicating the nonviability of higher flow rates for carbon storage.

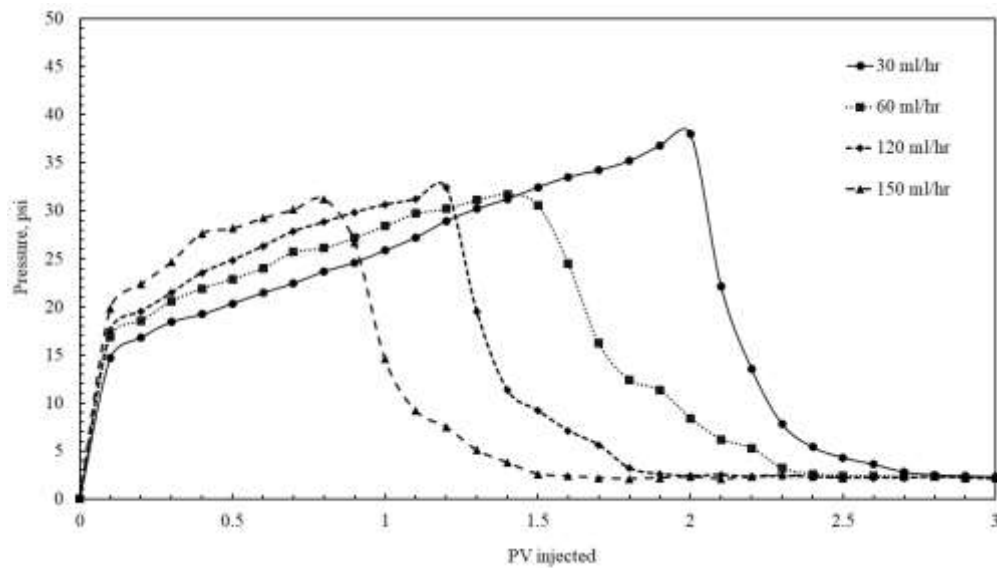


Figure 5.5: Pressure drop as a function of fluid injected (PV) in oil depleted sand-packs for flow behavior runs at varying flow rates. The test temperature was 333 K.

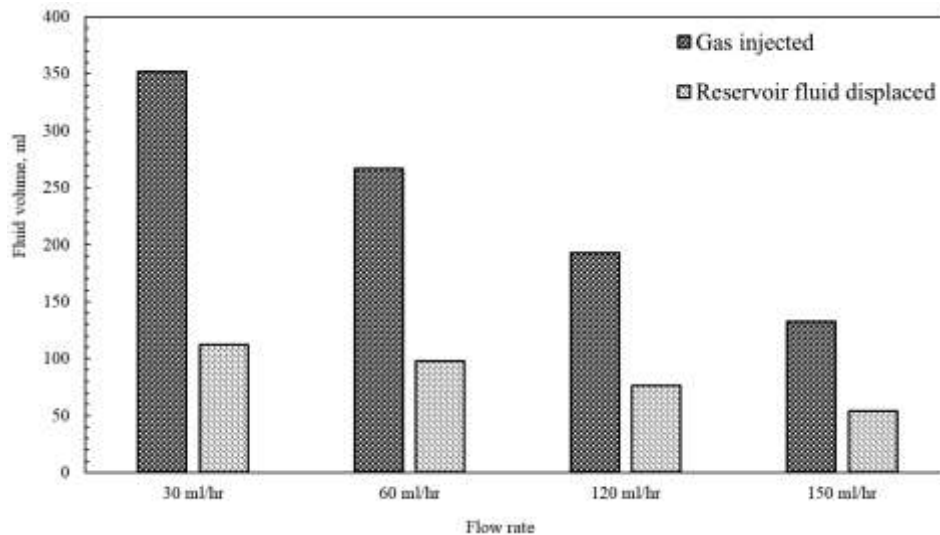


Figure 5.6: The amounts of gas injected and liquid recovered at varying flow rates in oil depleted sand-packs saturated with 0.5 PV SNF-1.0.

This may be attributed to lack of foam formation at higher flow rates due to increasing gas turbulence [258]. This was also evident in the gas injected and the reservoir fluid displaced observations (Figure 5.6). Increasing the gas flow rate progressively reduced the amount of gas injected (i.e. retained by the sand-pack before a steady stream of gas was obtained at the outlet, indicated by no more effluent liquid) from 352 (for 30 ml/hr) ml to 134 ml (150 ml/hr). The displacement of the reservoir fluid (i.e. water and SNF-1.0) from the reservoir also fell progressively from 112 ml (for 30 ml/hr) to 54 ml (for 150 ml/hr). The displacement of reservoir fluid is a crucial indicator as it shows that majority of the reservoir was touched by accessed at lower flow rates, which is not the case on increasing flow rate of CO₂ as less amount of residual reservoir fluid is displaced.

Next, the effect of the silica nanofluid (SNF-1.0) slug size was varied between 0.25 to 1 PV inside the sand-pack, and the CO₂ was injected at a flow rate of 30 ml/hr. The observations of the pressure drop and the gas injected have been provided in Figure 5.7 and 5.8, respectively. Increasing the size of the slug of the SNF-1.0 was found to greatly

increase the area under the curve. This may be attributed to a higher amount of silica NPs, polymers, and surfactants available for foam formation and stabilization. The area under the curve and the maximum pressure obtained progressively increases from 0.25 PV (maximum pressure = 27 psi) to 0.5 PV (maximum pressure = 38 psi) and 1 PV (maximum pressure = 49 psi). This also led to an increase in gas injected and retained in the sand-pack from 209 ml (when 0.25 PV was injected) to 425 ml (when 1 PV was injected). The presented results indicate the superior viability of a higher volume of SNF-1.0 solution for carbon storage. However, given the increasing expense of the fabricating silica nanofluids, the volume of usage must be carefully optimized to establish the best economic and environmental results.

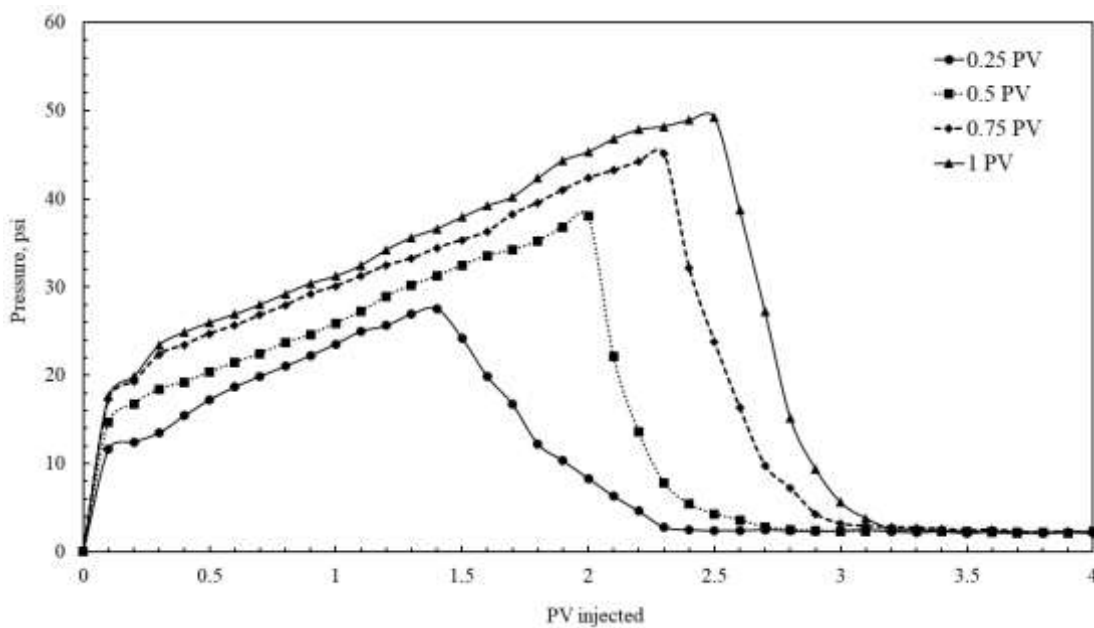


Figure 5.7: Pressure drop as a function of fluid injected (PV) in oil depleted sand-packs for flow behaviour runs after injection of varying slug-sizes of SNF-1.0. The test temperature was 333 K.

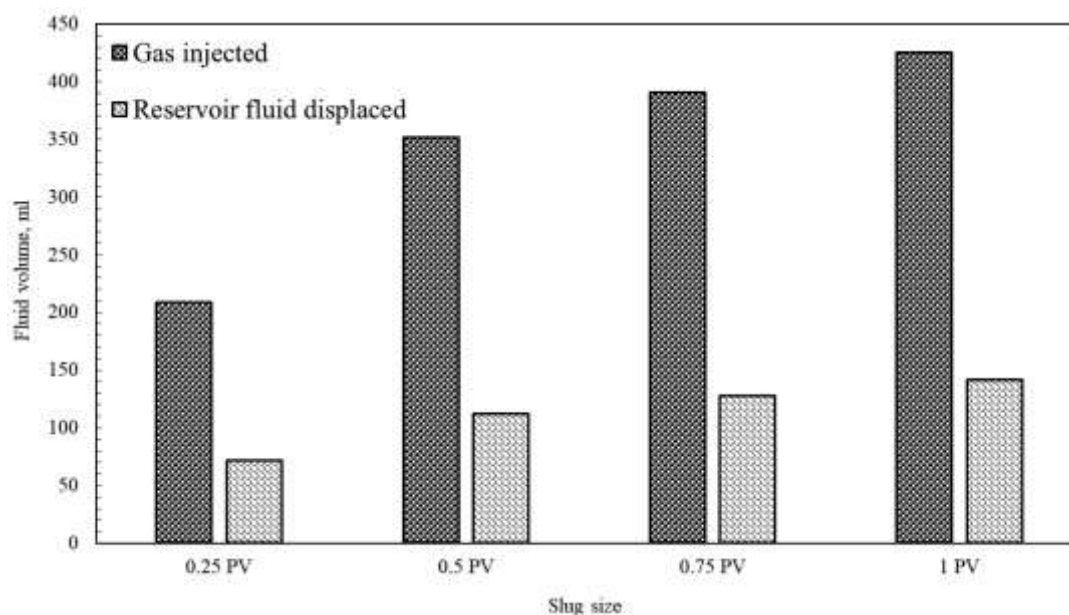


Figure 5.8: The amounts of gas injected and liquid recovered after injection of slug sizes in oil depleted sand-packs saturated with SNF-1.0. The flow rate was 30 ml/hr.

5.4 Conclusion

In this study, the role of surfactant-treated silica nanofluids, prepared in 1000 ppm PAM solution using Stober sol-gel method, was explored to generate in-situ (inside pore) CO₂ foam for oil recovery and effective carbon storage in a depleted sandstone reservoir. A sand-pack prepared using sand of known composition and size was used to denote a sandstone reservoir. The silica NPs had an average size of 35±6 nm and a zeta-potential between -32-36 mV after preparation, which indicates that they exhibited good stability for subsurface injection. The use of 0.5 wt% surfactant solutions (i.e. PAM and the silica nanofluids) greatly increased oil recovery in conjunction with CO₂ injection due to in-situ foam formation. With 1 wt% silica nanofluid (SNF-1.0), the maximum amount of oil recovery was obtained. Increasing NP concentration (from 0.5 wt% to 1 wt %) initially increased oil recovery (due to the formation of more stable foam). However, on further increasing NP concentration (from 1 to 2 wt%), the oil recovery reduced which may be attributed to NP agglomeration and insufficient foam stabilization inside the reservoir.

Given the superior performance of SNF-1.0 solution in oil recovery, they were then used in carbon storage under varying CO₂ injection rates (30-150 ml/hr) and slug size (0.25-1 PV). While increasing the CO₂ injection rate was found to reduce the carbon storage due to premature breakthrough from the reservoir, increasing the slug size and surfactant concentration increased the amount of carbon retention inside the sand-pack. Based on the observations of this study, the application of surfactant treated silica nanofluids may be proposed for increasing carbon storage in sandstone reservoirs. However, it is recommended that the operating conditions be optimized before application for attaining the perfect balance between the economic and the environmental applicability of the project.

Experimental Investigations to Evaluate Surfactant Role on Absorption Capacity of Nanofluid for CO₂ Utilization in Sustainable Crude Mobilization

Abstract

Carbon dioxide (CO₂) utilization for oilfield applications is affected by viscous fingering which leads to premature breakthrough without showing any appreciable impact on oil recovery and storage. Therefore, to control these issues, CO₂ is often injected with high viscous fluid such as nanofluid. However, nanofluid efficacy can be further improved by the inclusion of a surfactant that not only increases specific area of CO₂ [*via* interfacial tension (IFT) reduction] but also increases CO₂ absorption capacity of nanofluid through the formation of foam. Thus, in this study, an anionic surfactant (i.e. sodium dodecyl sulfate, SDS) of critical micelle concentration (CMC, 0.16-0.24 wt%) was added to polymer based single-step silica nanofluid of varying concentration (0.1-1.0 wt%) and, utilized in CO₂ absorption, IFT reduction of crude oil, and fossil fuel displacement. CO₂ absorption experiments showed that absorption was positively influenced by pressure and NP concentration, while increasing temperature showed reverse impact on CO₂ absorption. In addition, SDS ensured the formation of a Pickering foam which made CO₂ to retain inside for over 10 days (an increase of 67%) in SDS treated nanofluid, higher than 6 days

of simple nanofluid. Pickering CO₂ foam of SDS treated nanofluids was also envisaged for IFT reduction of crude oil, to identify the role of these nanofluids in crude mobilization from porous reservoir. CO₂ absorption capacity of nanofluid exhibited inverse relationship with IFT value of crude oil. Finally, displacement experiments were conducted which also support the inclusion of SDS in silica nanofluid for reduced water cut and higher fossil fuel recovery from porous media. From the results, it can be inferred that highest oil recovery (61%) was achievable with NP+SDS combination of 1/0.16 wt%, respectively, which was only 42% with water and 52% with NP concentration of 1 wt%.

6.1 Introduction

Energy reliance on fossil fuels is a potential source of carbon dioxide (CO₂) emission and it is responsible for widespread fluctuations in global climatic conditions [1–3]. Current atmospheric concentration of CO₂ is already higher than permissible limit of 350 ppm [4]. One solution regarding CO₂ reduction which holds great promise is subsurface injection of CO₂ which also allows for mitigation of CO₂ emissions *via* geo-storage [5–9]. This is an effective technique to work with CO₂ utilization provided injected CO₂ does not exhibit premature breakthrough, viscous fingering and premature CO₂ escape [10–14]. CO₂, being lighter, tends to move faster and bypasses significant area in the reservoir which not only reduces oil recovery but also reduces the storage volume during sequestration operations. This can be mitigated by a process known as carbonated fluid injection (CFI) where CO₂ is made to absorb/dissolve in water (CWI). With CFI, CO₂ interaction with oil is expected to increase due to its greater solubility in oil than water and CO₂ solvated oil is easier to displace [15]. Past studies on CWI/CFI for oil recovery applications have shown higher oil production by a margin of 12-30% of original oil in place (OOIP) [16,17]. Also, CFI allows for safer sequestration of carbon by mitigating any concerns of buoyancy driven leakages [18]. Seyyedi et al.[19] investigated use of

carbonated sea brine for rock wettability alteration and concluded that absorbed CO₂ had a major effect on oil recovery and wettability alteration of oil bearing reservoir. CO₂ requirement of CWI is comparatively much lesser than pure CO₂, which makes it attractive for field trials lacking major suppliers of CO₂ [20]. Use of CWI for CO₂ absorption and transport is constrained by low CO₂ carrying and retention capacity of water, which have forced researchers to seek alternate solutions for effective CO₂ utilization in oilfield applications. When CO₂ is injected for sequestration in subsurface formations, it causes the formation of a weak acid (carbonic acid) which along with present organic acids, affect the viability of long-term CO₂ storage [21–24]. The presence of these acids influences rock wettability, the effect of which needs to be carefully calibrated to mitigate rock dissolution and trap degradation. Along with CO₂, other gases like hydrogen may also be affected by the adverse acid reductive behavior when stored in the subsurface [25]. CO₂ presence also effects the rock-wettability which can be altered to more favorable for long term sequestration in the presence of nanofluids [26].

Nanofluids are colloidal suspensions of nanoparticles (NPs, size < 100 nm) [27]. Nanofluids possess desirable chemical and rheological properties due to their superior surface-to-volume ratio [28–33]. Silica (SiO₂) NPs are widely used due to their (1) eco-friendly nature (sandstone and silica particles have similar composition), (2) synthesis scheme, and (3) cost-effectiveness than other NPs [30,34–36]. In addition, nanofluids like silica/alumina have shown superior efficacy for EOR and carbon sequestration in sandstone formations due to their role in altering the wettability from oil-wet to water-wet. It minimizes the reductive conditions due to injected CO₂ which reverses the adverse effect of organic acids on CO₂ storage capacity [37–39]. Their use has been widely explored in chemical oil recovery projects for designing simple nanofluid, polymer enhanced nanofluid, and foam stabilizing agent [40–43]. Independently, silica nanofluids exhibit high

potential to load and retain CO₂ [30,44]. A comprehensive review investigated the application of nanofluids for mass-transfer enhancement and CO₂ absorption to reduce carbon emissions from industrial systems and reported their superior performance in this role [45]. Carbonated nanofluids offer potential to improve oil recovery and possibility of encapsulating CO₂ in cross-links of embedded constituents and NPs. However, conventional nanofluids tend to show premature agglomeration which leads to NP settlement. The rate of agglomeration can be controlled by the optimization of pH (as pH increase alters the electrostatic forces acting on NPs in the solution) [46–49]. This increases extent of phase separation in a nanofluid [50]. While conventional nanofluids are obtained through mixing of silica nano-powder in a base fluid (referred to as two-step nanofluid) and are unstable, single-step generates non-agglomerated and uniform NP dispersion with high stability. However, two-step silica nanofluids have been focus of many studies due to its ease of formulation [51]. But single-step silica nanofluids exhibit improved CO₂ absorption by 10-16% than two-step silica nanofluids [44,52].

Efficacy of CO₂ absorption of nanofluids can be further increased by inclusion of a surface active agent i.e. surfactant [53]. Typically, surfactant can modify wettability of dispersed NPs and increase their adsorption on CO₂ bubble surface. Typically, surfactant can modify wettability of dispersed NPs and increase their adsorption on CO₂ bubble surface [54–56]. Additionally, surfactant can reduce interfacial tension of CO₂ and make CO₂ foam where CO₂ bubbles of smaller size and higher specific area are packed in a steric barrier of surfactant-NP links (Figure 6.1) [57].

CO₂ absorption in nanofluid systems

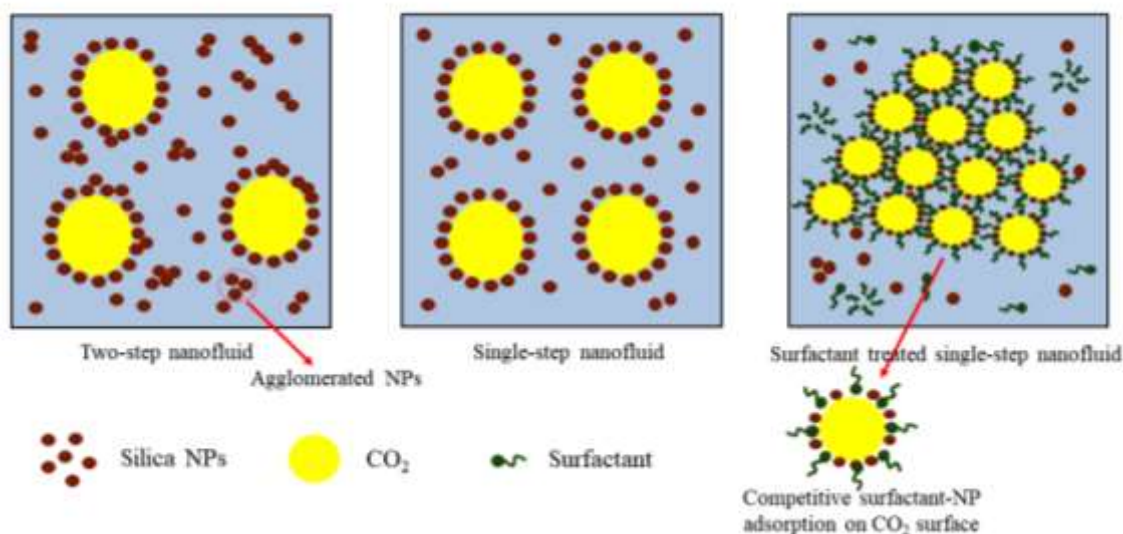


Figure 6.1: Competitive surfactant-NP adsorption on CO₂ surface in surfactant treated silica nanofluid.

Silica NP inclusion in CO₂ foam (hereafter, Pickering foam) is advantageous as resistance to destabilization in crude oil presence and at reservoir conditions is increased [58]. It is also more stable and viscous than sole CO₂ foam yielding better control on CO₂ mobility and retention time [59]. Surfactant inclusion also leads to interfacial tension (IFT) reduction of crude oil [60–63]. Addition of anionic surfactant in CW leads to development of an active carbonated water (ACW), increasing oil recovery [64]. Greater CO₂ absorption further increased extent of oil recovery by 6-8%, indicating a greater likelihood for field scale adoption. Optimum slug size, as ascertained by experimental data, was reported to be 0.6 PV [64], in line with reported slug size of other enhanced oil recovery (EOR) methods [65]. Thus, novel aspect of current work is inclusion of anionic surfactant (sodium dodecyl sulfate, SDS) with single-step silica NP for effective CO₂ utilization. For nanofluids, use of anionic surfactant is known to reduce extent of NP agglomeration [66,67], which may increase dispersion stability. Also, while silica nanofluids have demonstrated excellent CO₂ absorption in previous studies, their application as mobility control agents in carbon

sequestration projects (which hold immense importance in upcoming years) is yet to be explored. Moreover, the performance of single-step silica nanofluids, which have demonstrated superior stability and efficacy than two-step nanofluids, is yet to be explored in subsurface carbon utilization applications where investigation in the presence of common oilfield chemicals (i.e. anionic surfactant and high molecular weight polymer) makes the process more sustainable and effective.

In this study, single-step silica NPs were synthesized in viscous base fluid of polyacrylamide (PAM) of 1000 ppm and their use in improving absorption capacity of simple water is subsequently examined for effective CO₂ utilization in subsurface applications (hereafter referred to as carbonated nanofluids, CN). SDS was used to formulate surfactant-treated carbonated nanofluids (ACN) and amount of CO₂ loading in silica nanofluids was determined under varying operating conditions (i.e. pressure, temperature, and NP concentration). To establish role of SDS, IFT investigations were performed for silica nanofluids and CO₂. Finally, displacement tests were performed to establish role of ACN in CO₂ utilization for oil recovery and storage prospects. A previous study focused on the role of anionic surfactant [sodium dodecyl sulfate (SDS), 0-0.8 wt%] to negate salt induced agglomeration (a population reducing but mass conserving phenomenon) in single-step silica nanofluid for enhanced oil recovery (EOR) applications [66]. However, the current study has focused on anionic surfactant [SDS, 0-0.3 wt%] role on improving CO₂ absorption potential of silica nanofluids for effective carbon utilization in EOR and sequestration applications. The results presented in the previous study were based on zeta-potential, average particle size, viscosity, and oil recovery while in this study, results on CO₂ molality, retention, interfacial tension (IFT) are discussed and presented.

6.2 Experimental work

6.2.1 Materials

Nanofluids were synthesized by laboratory grade Tetraethylorthosilicate (TEOS), ammonium hydroxide (NH₄OH), ethanol (EtOH), and Polyacrylamide (PAM). All aqueous solutions were prepared using deionized (DI) water, which was obtained from a water purification system (Millipore[®] Elix-10). Sodium dodecyl sulfate (SDS) was purchased from Sisco Research Lab Pvt. Ltd. India. Equipment used for fabrication of nanofluid were magnetic stirrers (IKA-C-MAG-HS7) and particle homogenizers (Rivotek Ultrasonic). Nanofluid synthesis has been reported in Chapter 2. Nanofluids were characterized using a particle size analyzer (Malvern Nano ZS, UK) to ascertain their particle size and zeta-potential. IFT measurements of crude oil and nanofluids were measured using dynamic tensiometer (KRUSS K9), based on a standard Wilhelmy plate method [41,69]. At interface, plate was locked and IFT was measured automatically on measurement unit.

6.2.2 Experimental set-up for CO₂ absorption

CO₂ absorption is the encapsulation of CO₂ bubbles in fluid interstices [70,71]. CO₂ absorption studies were performed using a standard pressure decay method in which solvent and gas are kept in an enclosed chamber under a confining pressure. The experimental setup used was similar to one reported in previous studies [52,72]. During the absorption experiment, pressure reduction indicates absorption of gas inside fluid. The saturation of CO₂ absorption into fluid was confirmed by no further reduction in pressure which was maintained for 6 h to ensure that no further absorption of CO₂ takes place.

6.2.3 Microscopic characterization of nanofluid samples

Presence of absorbed CO₂ in nanofluid was established by an optical microscope (Motic Microscope, Hong Kong). To obtain image, a small volume of carbonated nanofluid (1.5 µl) was taken on a glass slide. To obtain bubble size distribution of CO₂ in nanofluid,

an advanced image analysis software (ImageJ) was used. Using image scale bar, size of individual bubbles was extracted and a frequency distribution was provided.

6.2.4 Fabrication of sand-pack for displacement studies

A series of sand-packs were prepared by using sand, collected from a commercial retailer. Its characterization details, properties, and morphology of sand has been provided in our previous studies [73,74]. The sand was then manually rammed into sand-pack holder (diameter: 1.5 inch and length: 24 inch) to ensure tight packing of sand grains.

Porosity (available void space) was measured by saturating sand-pack with water at 100% condition. After a steady state flow from sand-pack (*i.e.* volume injected at inlet = volume obtained at outlet), pore volume (PV) of sand-pack was calculated by reducing total volume of water recovered at outlet from total volume of water injected into sand-pack. Permeability of sand-pack was measured by flowing water through sand-pack at a constant rate of 20 ml/h, consistent with flow rate used for determination of permeability in sand-pack in literature [74]. Pressure drop, across inlet and outlet of sand-pack, was measured simultaneously during injection of fluid. Pressure drop was used to calculate permeability of sand-pack using Darcy's law [41]. In each sand-pack, permeability tests were repeated till obtained results attained a degree of precision ($> 5\%$ deviation from a base value). sand-pack was then flooded with crude oil for displacement test using experimental set-up which is similar to set-up used for displacement experiments in our previous study [74]. Total amount of oil which was retained inside sand-pack is known as original oil in place (OOIP) while oil recovered during experimental run is referred to as cumulative oil recovery [74]. The injection scheme involves 2 PV of water-flooding followed by injection 0.5 PV of carbonated fluid. Finally, 2.5 PV of chase water was used to sweep displaced oil from sand-pack. For each experimental run, a total of 5 PV fluid was injected in sand-pack. Fraction of oil recovered in cylinder at end of injection is referred to as oil cut.

6.3 Results and discussion

6.3.1 IFT studies with nanofluid and crude oil

Without surfactant, IFT value between crude oil and nanofluid S1 was determined to be 10.8 mN/m (Figure 6.2) which is in line with research findings of IFT in literature [77]. Similarly, nanofluid S2 and S3 showed IFT value between 9.6-9.8 mN/m. Reducing IFT will lead to an increase in oil recovery as lower values of IFT are more conducive for EOR [78]. Similarly, nanofluid S2 and S3 showed IFT value between 9.6-9.8 mN/m. With 0.04 wt% of SDS addition, IFT value of nanofluid S1 decreased to 8.92 mN/m. It is to be noted here that SDS concentration of 0.24 wt% suggested least IFT value as further increase did not cause any appreciable change in IFT value of S1. For nanofluids (S2 and S3) of higher NP concentration, CMC was determined at lower SDS concentration of 0.2 and 0.16 wt%, respectively, as evident from insignificant IFT change beyond these concentrations in Figure 6.2. The reduction in CMC (in S2 & S3) can be attributed to corresponding increase in surface activity of nanofluid. As a result, space available for SDS monomers to adsorb at interface of crude oil and nanofluid reduced and SDS monomers aggregated into micelles at lower surfactant concentration [79].

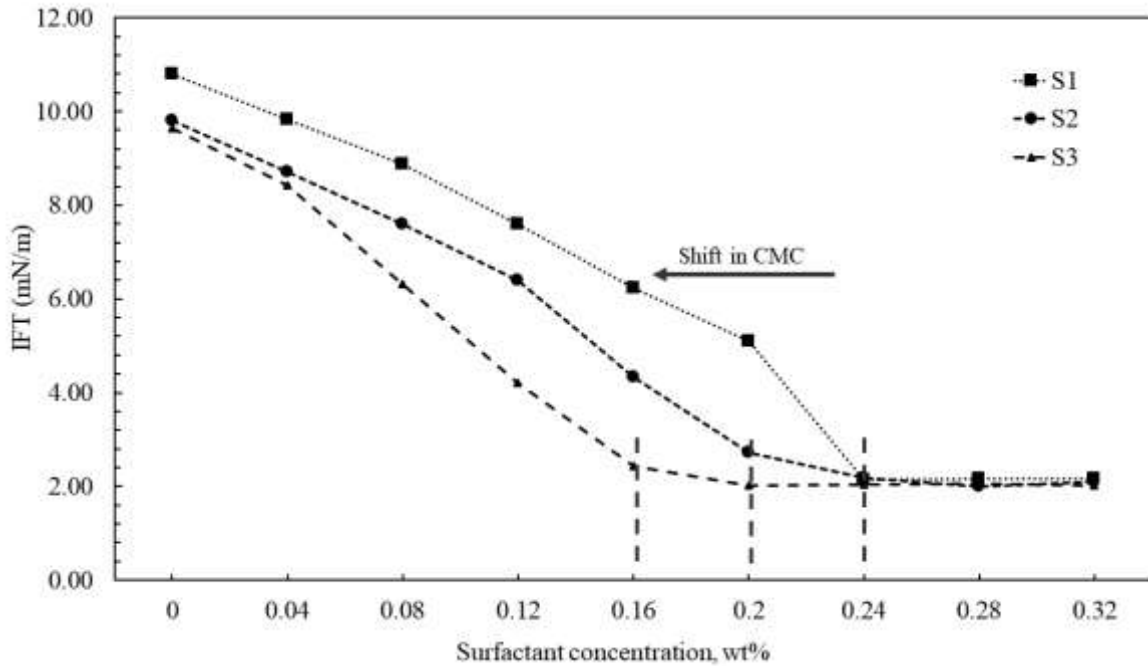


Figure 6.2: Selection of CMC value of SDS through IFT measurements between crude oil and different nanofluids (S1: 0.1 wt%; S2: 0.5 wt%; S3: 1.0 wt%). Increasing nanofluid concentration (0.1 to 1 wt%) showed reduction in CMC requirement of SDS.

It is essential to understand the affinity between surfactants and NPs as for high affinity, the surfactant molecules will remain adsorbed on NP surface even after coming in contact with crude oil [80]. This tends to affect their nature in IFT reduction of crude oil. All experiments were carried out with corresponding CMC value of SDS determined for surfactant treated nanofluids.

6.3.2 Microscopic characterization of nanofluids

For all fluid systems, absorption experiments were performed using widely-practiced pressure decay method [52,65,72,81]. Different fluids i.e. polymer (P), surfactant-polymer (SP), nanofluid (N), and surfactant-treated nanofluid (AN) were chosen, where nomenclature of carbonated fluids is denoted by CP, CSP, CN, and ACN, respectively. Absorption in water was unsuccessful as absorbed CO₂ bubbles rapidly escaped after removing confining pressure [70]. For CP and nanofluid CN (0.1-1 wt%), absorbed CO₂

was non-uniformly distributed in form of large bubbles most of which were adhered to sides of glass vial, consistent with research findings of our previous work based on CO₂ absorption in fluid systems [70,71]. This might be credited to presence of SDS. Since SDS of CMC value was added, CO₂ inclusion resulted into a foam which was lighter than liquid therefore, it remained at top of liquid layer. In addition, it is clear that SDS made CO₂ to exhibit a uniform distribution in foam structure which was further analyzed through microscopic study in Figure 6.3.

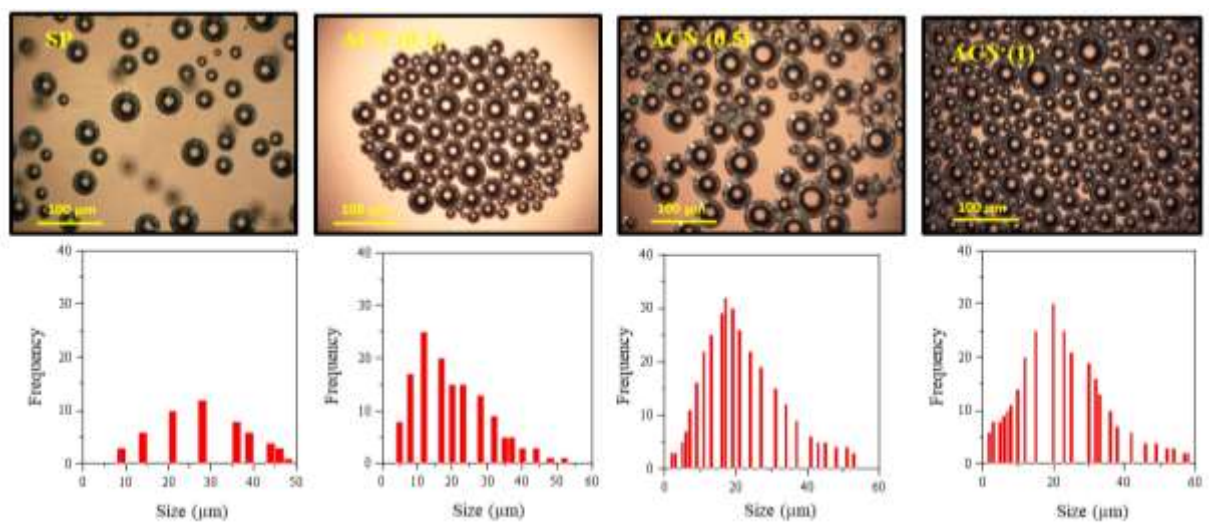


Figure 6.3: Microscopic images of surfactant-treated PAM fluid and nanofluids (0.1-1 wt%) after CO₂ absorption experiments at 323 K and 12 bar.

Microscopic characterization of CO₂ absorption in polymer and commercial silica nanofluid has been studied in previous works [70,71]. Microscopic images showed uniform CO₂ distribution throughout fluid with an increasing CO₂ population from SP to ACS(0.1) followed by ACS(0.5). A greater population of CO₂ bubbles (of different sizes) was observed for ACS(1.0) as evident from size distribution chart in Figure 6.3. A denser packing (due to greater population) of CO₂ foam was observed in presence of ACS(1.0). The average size of CO₂ bubbles was determined to be in range of 25-35 µm. CO₂ bubble of smaller size is desirable as smaller bubble can easily access greater areal extent in

reservoir. These small CO₂ microbubbles have good gas-blocking potential which reduces gas mobility inside subsurface. Thus, active carbonated nanofluid (ACN) showed greater affinity for absorption.

6.3.3 Surfactant role on CO₂ absorption of nanofluids

CO₂ absorption capacity of a fluid is often measured in terms of molality (gas moles absorbed/kg. of solvent) which represents gas concentration in a solution. Solvents used in this study are water, P, SP, nanofluids without surfactant [N(0.1-1)], and nanofluids with surfactant [AN(0.1-1)], and results of molality for these fluids as a function of varying pressure (4-12 bar) and temperature (323 and 353 K) are shown in Figure 6.4. From results, it can clearly be inferred that CO₂ absorption in water was least in all conditions. Inclusion of PAM slightly increased CO₂ loading as more CO₂ get entrapped in entanglements of PAM. As a result, P fluid exhibited 6-10 % higher molality than water. Furthermore, inclusion of silica NPs increased CO₂ loading and molality increased to 0.44 and 0.5 mol/kg. of solvent for N (0.1) and AN (0.1), respectively (at 12 bar and 323 K). It is to be noted here that increasing NP concentration increased CO₂ absorption capacity and a maximum molality of 0.532 mol/kg. of solvent was found for AN (0.1) nanofluid. An increase in CO₂ absorption capacity can be attributed to Brownian motion of NPs in fluid. The rapid formation and breaking of CO₂ bubbles inside body of a nanofluid increased CO₂ absorption which is consistent with research findings in literature [44,52,70].

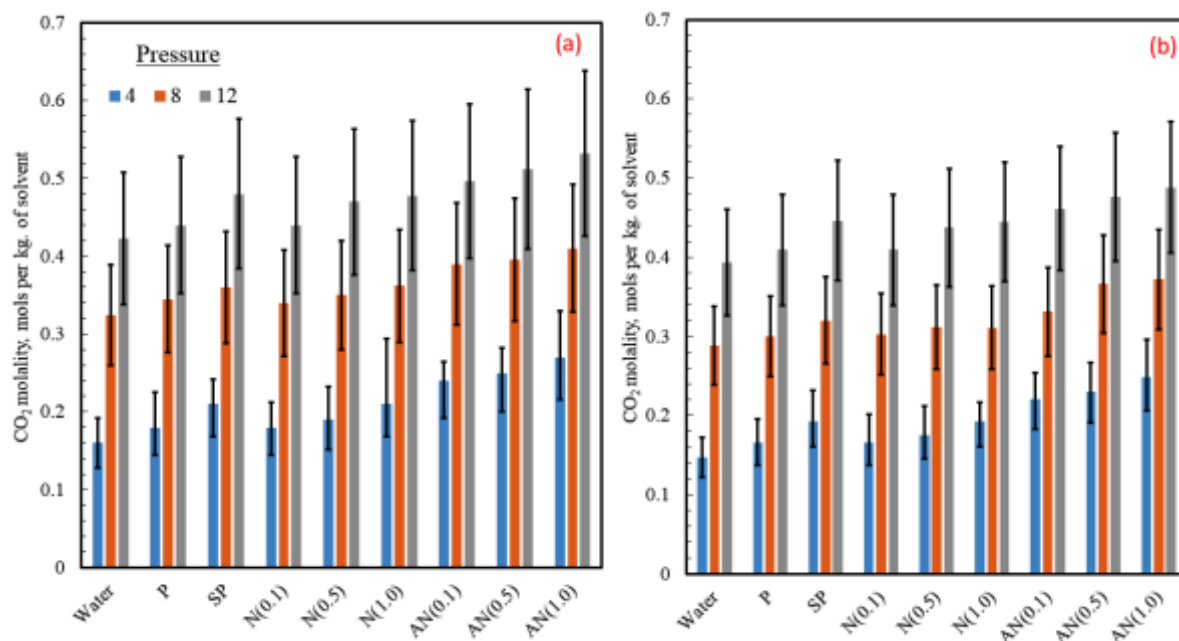


Figure 6.4: CO₂ molality results for DI water, PAM fluid, and different nanofluids with and without surfactant at (a): 323 K and (b): 353 K. Unit of values in plot is mol. of absorbed CO₂/kg of solvent.

CO₂ tends to separate from liquid phase and it can be controlled through deformation of CO₂ into smaller bubbles, which increases possibility of get absorbed into entanglements of NP-PAM in nanofluid N. It is also evident from results that CO₂ absorption increased with increasing NP concentration in nanofluid N(1.0), exhibiting higher CO₂ molality of 0.48 mol/kg. of solvent (at 12 bar and 323 K) than 0.44 mol/kg. of solvent [N(0.1)] and 0.47 mol/kg. of solvent [N(0.5)]. Process of CO₂ absorption in water-based silica nanofluid is predominately physical and NPs increase this absorption by providing agitation and steric stabilization to absorbed gas bubbles [52,85]. The single-step silica nanofluids showed greater increase (more than 9-12%) in CO₂ absorption than nanofluids prepared with commercial silica NPs [70]. Since commercial silica nanofluid prepared by two-step process exhibit NP aggregation, it reduces interfacial area available for CO₂ absorption which is consistent with the research findings in literature [45,86].

These larger silica NP clusters do not participate in CO₂ absorption process rather they tend to either remain suspended in body of nanofluid or settle under action of gravitational forces [70]. In single-step technique, process of agglomeration greatly slowed and nanofluids usually do not show any sign of agglomeration, significantly increasing CO₂ absorption [66]. As a result, single-step silica nanofluids showed superior CO₂ absorption due to their higher stability, in line with the research findings of carbon nanotube (CNT) based nanofluids in literature [81]. In this study, the increase in CO₂ absorption has remained between 6-24% which is within the range of reported data for CO₂ absorption in previous studies [45,52,70,71]. These studies have reported an increase in CO₂ absorption by a margin of only 2-3% while other studies have reported an increase of up to 80% [45]. It is also essential to note that increasing NP concentration may not always provide increase in CO₂ absorption as higher NP population may accelerate agglomeration and reduce available surface area for CO₂ absorption [45].

CO₂ absorption can be further accelerated by inclusion of SDS. Typically, surfactant helps to make foam of gases where gas bubbles are encapsulated in cross links of added substituents and foams are capable of retaining absorbed CO₂ for a longer duration [87]. This might be case of with AN nanofluids which showed greater CO₂. It was observed that maximum CO₂ loading of 0.532 mol/kg. of solvent was observed for AN(1.0) nanofluid at 323 K. From results, it also clear that CO₂ molality in fluids is dictated by both pressure and temperature. An increasing pressure positively influences CO₂ capturing while increment in temperature reduces CO₂ loading capacity of all fluid systems. Thus, increase in confining pressure forces more CO₂ molecules to solvate inside body of fluid. On other hand, increasing temperature possibly increases kinetic energy of system which reduces CO₂ absorption capacity of fluids. Compared to water, P and SP fluids exhibited 5% and 14%, respectively, higher CO₂ absorption. Similarly, N and AN fluids showed 6-

15% and 18-24%, respectively, higher CO₂ absorption under similar conditions. Thus, as compared to an increase of 1.18 in AN(0.1) and 1.22 in AN(0.5), increase in molality (1.24 times) of AN(1.0) nanofluid remained higher even at 353 K, which is of key importance for these nanofluids in effective CO₂ utilization at high temperature conditions.

6.3.4 Effect of absorption on IFT of crude oil

IFT tests were performed to understand role of carbonated nanofluids in crude mobilization and compared with ones without absorption. Since surfactant-treated nanofluids showed better performance in absorption, these tests were conducted only for these nanofluids. IFT measurements between crude oil and surfactant-treated nanofluids AN(0.1-1) are provided in Figure 6.5. These nanofluids without CO₂ loading exhibited an IFT of 2.23, 2.18, and 2.15 mN/m for AN(0.1), AN(0.5) and AN(1.0), respectively. In these nanofluids, interface of crude oil is saturated by two surface-active agents (NP and surfactant micelles). Thus, if crude interface is only shared by single entity (NP/surfactant), IFT measurements of higher value are expected [88]. Similarly, inclusion of CO₂ (as Pickering foam) results in formation of two separate interfaces; one between foam and nanofluid and other between foam and crude oil. The presence of NP/SDS at interface between foam/nanofluid reduces IFT while interface of crude oil and foam shared by NPs which stabilize foam from deformation by crude oil molecules [30,89].

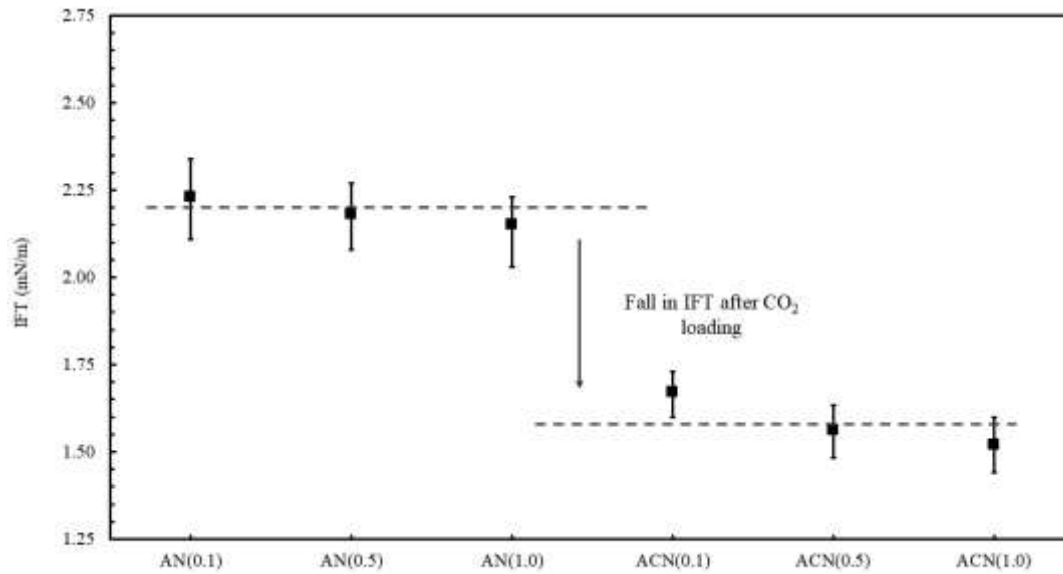


Figure 6.5: IFT measurements between crude oil and surfactant-treated nanofluids before and after CO₂ absorption experiments in equilibrium cell at 323 K and 4 bar.

It was found that inclusion of CO₂ (after CO₂ absorption at 4 bar) lowered IFT value to 1.69 mN/m in ACN(0.1). Similarly, IFT value for crude oil-carbonated nanofluid ACN(0.5) and ACN(1.0) was found to be 1.56 and 1.54 mN/m which indicates that higher CO₂ loading of ACN(1.0) is favorable to IFT reduction. Similarly, when amount of absorbed CO₂ was increased in nanofluid *via* confining pressure, IFT value reduced to 1.56 mN/m (CO₂ absorption at 8 bar) and 1.44 mN/m (CO₂ absorption at 12 bar) in silica nanofluid ACN (0.1). Hence, reduction in IFT was found proportional to amount of absorbed CO₂. It is well established that CO₂ is used in oil recovery process as gas injection method [15], where it mobilizes oil through miscibility. But, CO₂ based oil recovery projects are affected by premature CO₂ breakthrough and viscous fingering [18]. These results showed that CO₂ injection along with AN nanofluids can provide both benefits of controlled fingering/breakthrough and IFT reduction. A lower IFT translates into a higher amount of fossil fuel displacement. Additionally, higher absorption capacity of surfactant treated nanofluids favors use of SDS for CO₂ sequestration. The effect of CO₂ on IFT

reduction for crude oil and different fluid systems has also summarized for previous studies which are majorly in line with obtained results of this study. This makes carbonated fluids highly attractive for crude mobilization and CO₂ sequestration.

6.3.5 Fluid displacement studies

Finally, to assess viability of carbonated nanofluids in oilfield applications, 9 displacement experiments were performed in synthetic sand-packs at 323 K using standard oil recovery process [74]. Since, several studies have already investigated the application of sole CO₂ injection for oil recovery, no such experiment was performed in this study [96–98]. Thus, the study has been limited to establishing the efficacy of carbonated nanofluids for EOR in sandstone reservoirs. The sand-packs had a porosity of 29-31% and a permeability of 623-748 md (quite similar to actual rock samples) [65,99]. First, sand-pack was saturated with crude oil and after aging period of 10 days, primary water flooding (of 2 PV) was performed. After that, carbonated fluid (i.e. CP, CSP, CN, and ACN) of 0.5 PV was injected in sand-pack and experiments were stopped for 5 days to offer nanofluid sufficient time in porous media with crude oil. Finally, chase water flooding (2.5 PV) was performed. All injection was performed at 20 ml/hr [71]. During injection process, fluid at outlet was continuously collected and measured. displacement experiments were conducted for water cut and resultant oil recovery and these results as a function of fluid injection (PV) were measured.

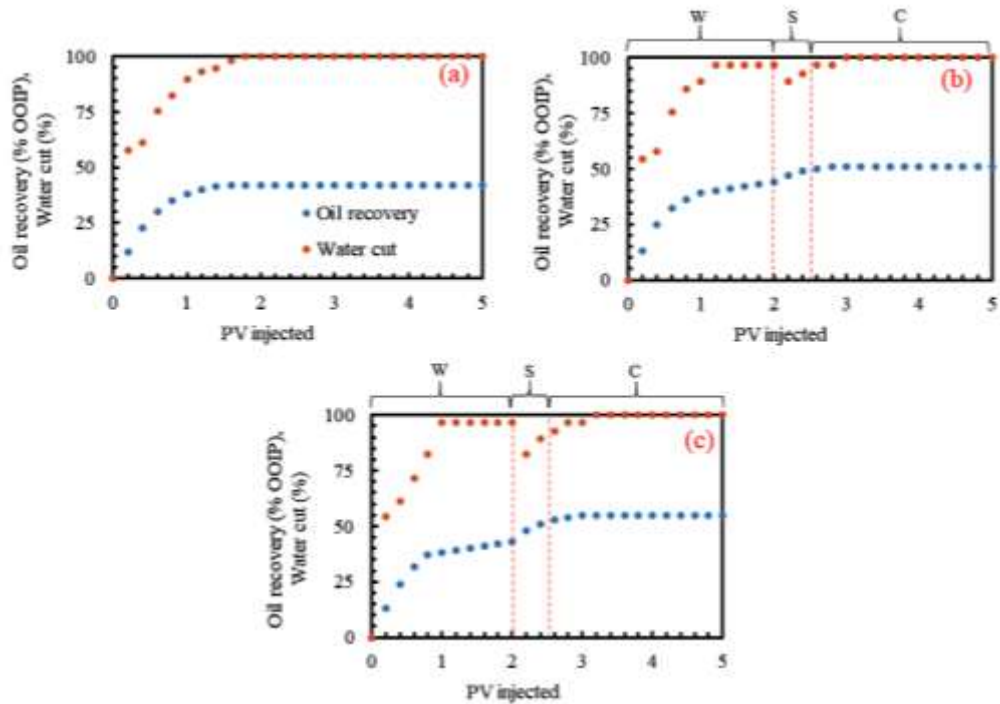


Figure 6.6: Water cut and resultant oil recovery (% OOIP) results for (a): water; (b): carbonated polymer (CP), and (c): carbonated surfactant-polymer (CSP) fluids as a function of fluid injected (PV) in sand-pack at test temperature of 323 K. EOR slug S (0.5 PV) was injected after a primary water flooding (W) of 2 PV. Displacement experiment is ended with chase water flooding (C) of 2.5 PV.

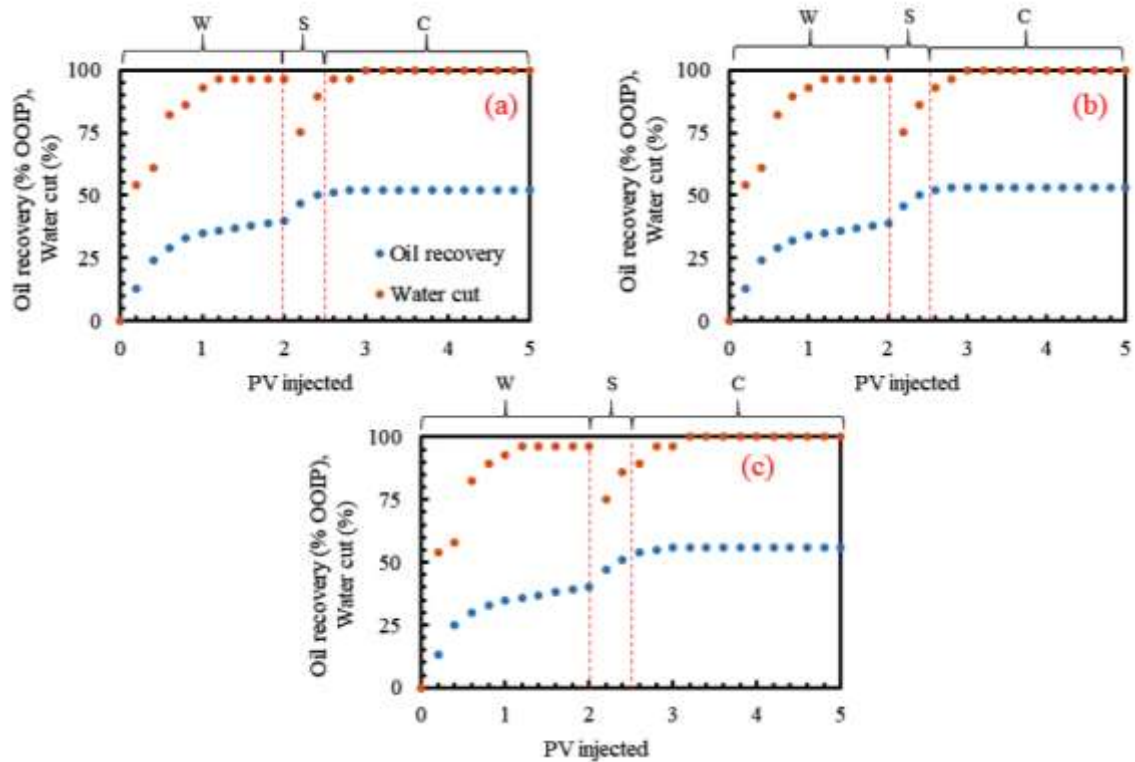


Figure 6.7: Water cut and resultant oil recovery (% OOIP) results for carbonated nanofluids (CN) of varying NP concentration (a: 0.1; b: 0.5; and c: 1.0 wt%) as a function of fluid injected (PV) in sand-pack at test temperature of 323 K.

For run-1, injection of water was found to displace over 42% of original oil in place (OOIP) (see Figure 6.6). For CP (run-2), resultant oil recovery measured to be 51% OOIP, consistent with water cut result. Thus, oil recovery increased by 9% for CP as it is more viscous than water, thus, able to displace more oil from sand-pack [74]. Injection of CSP fluid further increased oil recovery to 56% of OOIP (see Figure 6.6). This clearly supports role of SDS in oil recovery applications. CSP has a better areal sweep capacity than water or carbonated-polymer (CP) fluid. Then, injection of carbonated silica nanofluids [CN(0.1-1)] yielded an oil recovery between 51-55% of OOIP (see Figure 6.6). The superior performance of silica nanofluids for oil recovery is in line with previous studies which have explored their viability for EOR from adverse formations [100]. With higher NP concentration, amount of CO₂ absorption was also higher. Higher CO₂ absorption is linked

to higher oil recovery as more CO₂ is transported to subsurface and more oil is pushed forward [15,65]. It is to be noted here that oil recovery of CN(1.0) nanofluid (56% OOIP) is almost equal to oil recovery of CSP fluid (55% OOIP), which indicates that 1 wt% NP in CN (run-6) technically created same effect on oil recovery as that of 0.16 wt% of SDS in CSP (run-3). Thus, combination of NP and SDS can offer favorable increment in rate of oil recovery.

Finally, oil recovery was reported for carbonated nanofluids [ACN (0.1-1)] in Figure 6.7. SDS reduced IFT between crude oil-injected fluid, which probably mobilized a greater volume of oil (57-61% OOIP) than carbonated nanofluid (51-56% OOIP). ACN were also able to displace more oil than CSP fluid as NP stabilized bubbles were more stable than SDS stabilized bubbles when they came in contact with crude oil [53,101]. These NP-stabilized CO₂ bubbles (Pickering foam) is more stable and resistant to destabilization [102]. Highest amount of oil recovery (61% OOIP) was obtained in ACN(1.0) where higher NP concentration and SDS together greatly affected CO₂ absorption capacity and its associated oil recovery. The experimental results of this study can ascertain; (1) CO₂ absorption and retention depends on NP population and its agglomeration in solution, (2) oil recovery is positively influenced by increasing CO₂ absorption in solution, and (3) optimum surfactant concentration (CMC) is dependent on NP concentration in solution.

6.4 Conclusion

In this work, the role of an anionic surfactant (SDS) was explored on CO₂ absorption capacity of polymer based single-step silica nanofluids of varying size (34-42 nm) and varying NP concentration (0.1-1 wt%). SDS was used at CMC level, which was determined separately for each nanofluid. It was found that increasing NP concentration reduced the requirement of CMC in system [79], which is of key importance in surfactant

based chemical EOR as it reduces surfactant adsorption on rock surface. The minimum value of SDS that stabilizes nanofluid N(1.0) was 0.16 wt% [a decrease of 34%]. Increasing NP concentration increases CO₂ absorption capacity of nanofluid as demonstrated by molality results. CO₂ absorption capacity of N(1.0) nanofluid was 9% higher than the one of simple PAM fluid. SDS inclusion further improved the CO₂ absorption and nanofluid AN(1.0) exhibited maximum CO₂ absorption (24% higher than water), indicating synergistic interaction between surfactant and NPs may improve the performance of surfactant-treated carbonated solutions in carbon utilization. In addition, the role of CO₂ absorption on IFT reduction of crude oil was investigated. IFT was found to reduce with increase in CO₂ absorption, which is of significant worth for carbon utilization in oil recovery from marginal fields as lower values of IFT have been correlated an increase in oil recovery [61]. As a result, a minimum IFT value of 1.54 mN/m was obtained for ACN(1.0), which in line with results obtained from expensive ionic-liquid based surfactant [103]. Thus, adding surfactant greatly enhanced CO₂ absorption and retention capacity of silica nanofluids [88,90,91] which made silica nanofluids suitable for effective CO₂ utilization. Finally, displacement tests were conducted using surfactant based carbonated nanofluids to justify their role on oil recovery from sand-packs, exhibiting 29-31% porosity and 623-748 mD permeability. The resultant oil recovery of simple carbonated nanofluid did not increase more than 56% OOIP [for CN(1.0)] while surfactant treated nanofluid ACN(1.0) showed resultant oil recovery of 61% OOIP, an increase of 5% OOIP which is higher than oil recovery by nanofluid injection. Thus, the proposed use of surfactant treated nanofluid is noteworthy for CO₂ utilization in subsurface formations, where other EOR methods like polymer/surfactant may show challenges for field implementation [104,105].

Effect of Single-Step Silica Nanoparticle on Rheological Characterization of Surfactant Based CO₂ Foam for Effective Carbon Utilization in Subsurface Applications

Abstract

In this study, the role of single-step silica nanofluids (size ~ 30-150 nm) on rheological behavior of surfactant based carbon dioxide (CO₂) foams was investigated for effective carbon utilization in porous media. The nanofluids were synthesized in base solution of polyacrylamide (1000 ppm) by Stober sol-gel method in which nanoparticle growth was controlled by a precursor (tetraethyl orthosilicate). Stable nanofluids, of varying nanoparticle size (36-148 nm) and concentration (0.1-1 wt%), displayed excellent dispersion stability and potential for foam stabilization. Pickering CO₂ foams of varying size (20-40 μm) were developed. CO₂ foams, after preparation, were analyzed for foam volume, stability, and rate of liquid drainage. Increasing silica size was found to show a detrimental effect on foam stability while increasing concentration improved foam stability by reducing the extent of liquid drainage. The foam stability was found to be greatly dependent on test temperature and above 90 °C, Pickering foam exhibited higher foam degradation with coalescence stability of only 2 h. For foam, the rheological measurements were conducted at 1 bar as a function of wide range of temperature (30-90 °C). Pickering CO₂ foams showed non-Newtonian shear thinning behavior where increasing nanoparticle

concentration (0.5-1 wt%) yielded 6-13% increase in foam viscosity. The foams also showed strong viscoelastic nature with the presence of both G' and G'' over the entire range of investigated strain and amplitude sweep. From the viscoelastic characterization of CO_2 foams, it was established that foam behavior was dominated by elastic nature ($G' > G''$) at low stress values (10-20 strain %) while increasing stress (> 20 strain %) produced liquid like ($G'' > G'$) dominance in the behavior of foam. Finally, hysteresis analysis was reported to understand the role of heterogeneous pore environment (where varying shear conditions usually prevail) on flow properties of CO_2 foams.

7.1 Introduction

Rheologically stable foams (pockets of gas entrapped between layers of liquid or solids) show insignificant changes in viscosity and moduli profiles under varying shear flow conditions [296]. Conventionally, a rheologically stable foam is able to retain its viscosity and viscoelastic nature (with minimal degradation) over varying shear conditions. This is of key importance for foam utilization in subsurface applications where variable porosity (pore throats of uneven size/holding capacity) of heterogeneous reservoirs will not be a limitation [98,297]. Compared to gas or water-alternating gas (WAG) injection, rheologically stable foams exhibit greater mobility control, allowing them to access a greater volume of the reservoir for improved oil recovery and carbon storage [134,298]. In addition, these foams may show extensive industrial applications as drilling fluid additive, enhanced oil recovery (EOR) agents, and mobility control agents for CO_2 storage and utilization in subsurface porous and permeable formations [249,299–302]. The use of foams in heterogeneous formations is highly attractive as foams generate better flow resistance in high permeable zones (due to Jamin effect), which leads to foam diversion into zones of low permeability [303,304]. Rheologically stable foams also resist gravity segregation and water channeling as a result, they show improved displacement efficiency

at microscale level [305–307]. However, for widespread utilization, these foams should be tested for real field conditions such as moderate to high temperature, salinity, and non-polar phase (oil) [40,134,308,309]. These conditions have imparted significant changes in foam stability by either increasing bubble coalescence or decreasing viscosity to low levels [40,134,308,309]. Hence, there is a pertinent need to increase the stability of foams for complex conditions so that metastable foam systems find suitability in subsurface applications.

Previous research activities have focused on the use of polymer and binary surfactant-polymer solutions to impart rheological stability to foam systems and increase their longevity for industrial application [290,310]. The application of viscosifying agent, i.e., polymer holds significant promise to improve the stability of foam as demonstrated [305]; this study highlighted positive effects of polymer (partially hydrolyzed polyacrylamide, HPAM) on foam stability through the improvements in film coarsening, drainage, and bubble coalescence [305]. These instability issues can be addressed by increasing the compression modulus (surface) of foam, which further improves the yield stress of foam films by making them thick and rigid [311–313]. Core flood studies have revealed that polymer-enhanced foam (PEF) yielded higher oil recovery (24%) than surfactant-polymer based foam system [305]. Additionally, with competitive adsorption at bubble surface, polymer can reduce adsorption loss of surfactant which helps to preserve the performance of foam inside porous media [314]. However, polymer performance is subjected to decrease at high temperature, reducing its viscosifying effect and efficacy to adsorb on bubble surface [88,315–317].

In recent years, the use of nanoparticles (NPs) to stabilize foams has gained much attention due to their higher stability [96,250,318]. These foams are also referred to as Pickering foams where solid NPs tend to adsorb on interface of two phases involved

[165,299]. Also, NP addition has been found to increase their thermal stability, allowing them to perform better in presence of higher temperature [319,320]. As compared to conventional polymer enhanced foams (PEFs), Pickering foams can display higher stability and more resistance to destabilization induced by salinity, temperature, and non-polar crude oil [98,273,321]. Solid NPs tend to prevent coarsening and coalescence of foam bubbles, indicating delayed phase separation between phases at elevated temperature [322–324]. In Pickering foams, NPs provide strong viscoelastic film through the creation of a steric barrier which slows down the rate of film rupturing and liquid drainage [325,326]. While several NPs have been used for foam stabilization, silica NPs have gained much prominence due to their ease of fabrication, neutral chemistry, and favorable economics [99,225,250]. Also, the wettability of silica NPs can be easily modified to make them viable for enhanced adsorption at liquid-gas interface [327]. Pickering foams, stabilized by silica NPs, exhibited excellent stability in presence of high temperature, salinity, crude oil, and pH [165,310,328]. In Pickering foams, silica NP not only ensures the formation of 3D networks of bubbles but also controls the rate of bubble coalescence [329,330]. Stable supercritical CO₂-in-water foams were developed by Espinoza et al. [331] who utilized polyethylene glycol (PEG) treated silica NPs (5 nm) in foam stabilization. This study found that resistance to fluid flow increased by a factor of 2-18 and stable Pickering foams were generated at a temperature of 95 °C. In another study, Bayat et al. [332] compared foam stability and oil recovery potential of oxides, i.e., silica (SiO₂), aluminum (Al₂O₃), titanium (TiO₂), and copper (CuO) of varying concentration (0.002-0.1 wt%) and found that higher foam stability was obtained at 0.008 wt% for all NPs. Also, as compared to other NPs, silica showed superior performance in increasing stability of foams and associated oil recovery [332]. The effect of high salinity on foam behavior of silica NPs (size ~ 5-80 nm) was investigated by Kim et al. [165]. The effect of NP size (20-500 nm) on foam property

of different surfactants [sodium dodecylsulfate (SDS) and cetyltrimethylammonium bromide (CTAB)] was investigated by Hu et al. [180]. They found that NP reduced the liquid drainage and simultaneously helped foams to maintain their dynamic stability. In another study, pH-responsive Pickering foams, of silica NPs and cationic carboxyl betaine, showed superior stability between pH range of 4-10 [333]. The positive effect of NP concentration on foam stability was established by Li et al. [334], who found that silica NP (size ~ 65 nm) of concentration > 0.7 wt% was able to improve the viscosity (up to 80 mPa.s) and resistance factor (by a margin of 200) of supercritical CO₂ foam.

Though silica based suspensions can offer several advantages in foam and oil production, NP agglomeration and premature sedimentation are two important instability issues of nanofluids [66,67]. Agglomeration causes an increase in NP size that leads to the development of large NP clusters in suspension. This negatively impacts foam stability by increasing the rate of sedimentation, entrapment in subsurface, and block pore throats resulting it reduces NP migration and areal coverage in porous media [165,273,335]. Several methods have been incorporated to improve the stability of silica nanofluids; the most promising method to develop stable nanofluids with long dispersion stability is single-step synthesis of NPs [69,117,279]. In previous studies, it has been established that single-step silica nanofluids can remain stable for over 60 days with negligible change in particle size and zeta-potential [273]. The effect of increasing shear (Figure 7.1) also needs to be understood for complex system polymer-surfactant-NP in Pickering CO₂ foams as liquid drainage tends to increase with increasing shear-thinning, usually occurs at high shear rate [336].

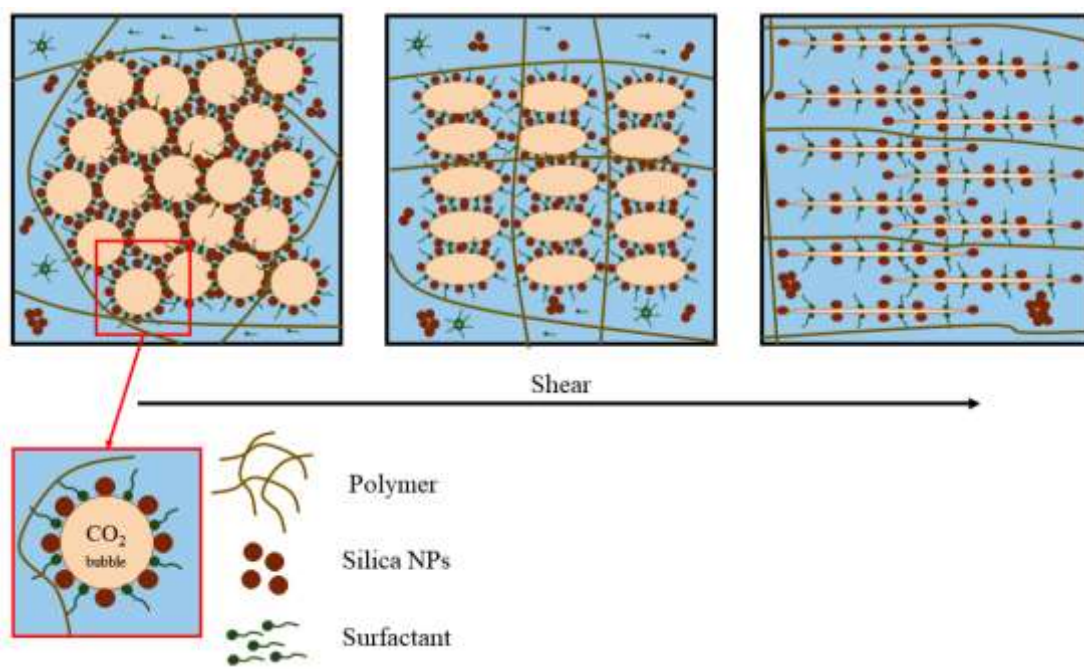


Figure 7.1: Schematic showing anticipated effect of increasing shear on the bubble shape in Pickering foams.

Hence, in this study, the role of single-step silica nanofluid on stability and properties of sodium dodecyl sulfate (SDS) based CO₂ foams was reported for nanotechnology impact in carbon utilization. The effect of varying NP size and concentration was investigated on stability and decay mechanism of CO₂ foam. The effect of NP size (36-148 nm) and concentration (0.1-1 wt%) on adsorption scheme at gas-liquid interface was also investigated using pendant drop method. This was followed by shear rheological and viscoelastic analysis of synthesized CO₂ foam using a modular compact rheometer. Finally, the rheological hysteresis of CO₂ foam was investigated under varying shear rate to find suitability of CO₂ foam for carbon sequestration and mobility control in heterogeneous formations. The rheological hysteresis was conducted by varying shear rate from low to high (i.e. 1 to 1000 s⁻¹), where it was held for 60 s following which shear rate was reduced from high to low (1000 to 1 s⁻¹). The viscosity was plotted for the entire cycle of shear rate investigated.

7.2 Materials and Methods

7.2.1 Materials

To synthesize the silica NPs, liquid tetraethyl orthosilicate (TEOS, purity ~ 99%) was obtained from Merck and used as a precursor without any treatment. Other chemicals were liquid ammonia solution (NH₄OH, purity ~ 25%, Merck-Millipore), ethanol (EtOH, absolute assay ~ 99.9%, Changshu Hongsheng Fine Chemicals), and polyacrylamide (PAM, molecular weight = 10 mD, SNF Floerger). All experiments were performed using deionized (DI) water which was obtained from Millipore[®] Elix-10 purification apparatus. All aqueous solutions were prepared after careful weigh measurement of solutes by an accurate analytical weighing balance (Mettler Toledo, United States). All chemicals were used as received to keep the scope of study in line with literature [273,279]. CO₂ (purity ~ 99.95%) was obtained from Sigma Gases Limited, India. Anionic surfactant, SDS, was purchased from Sisco Research Lab Pvt. Ltd. India and SDS has purity and an alkalinity of 85% and 5 Meq/ml, respectively.

7.2.2 Preparation and characterization of nanofluids

The methodology for the preparation of silica nanofluids has been reported in Chapter 2.

7.2.3 Methodology for foam formulation

The foams were formulated using tailor made set-up, manufactured by D-CAM Engineering, India. The schematic of experimental set-up has been provided in Figure 7.2.

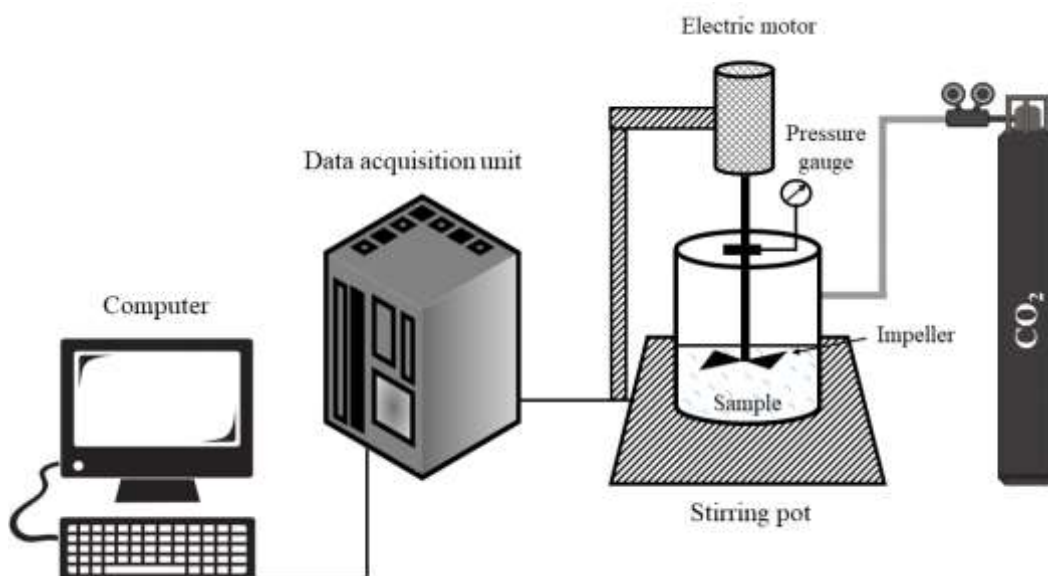


Figure 7.2: Figure 7.2: Experimental schematic showing equipment assembly utilized for foam generation. The viscosity of the foam is a strong function of its quality with good quality foams displaying superior viscosity than foams of inferior quality.

The experimental set-up comprised of a stirring pot with an internal volume of 100 ml. The entire system was mounted inside a temperature controlled bath to minimize any fluctuation of temperature during test. The temperature of pot was maintained using a temperature controller, ESCI, India, which used silicon oil as heat conducting fluid. The temperature was measured with the help of a thermocouple (accuracy ± 0.002 °C), equipped within the system. For measurement, 20 ml of fluid was taken inside the stirring pot and the vacuum was create using a vacuum pump (SSU India, flow rate ~ 50 L/min). CO₂ was introduced into the stirring pot with the help of a valve at predetermined pressure of 6 bar (to understand the effect of pressure other than atmospheric, on foam stability). CO₂ and nanofluid were thoroughly mixed at rpm value of 600 for 15 min. After each measurement, the stirring pot was carefully cleaned using DI water, dried, and vacuumed to ensure no residual gas left in cell.

7.2.4 Visual and microscopic characterization of nanofluids

After preparation, the foams were decanted into graduated glass cylinders of 100 ml with an accuracy of 0.5 ml. Glass stoppers were attached to ensure no atmospheric contamination took place during storage. Images of glass cylinders were obtained at regular intervals using a handheld camera (Samsung M11).

For microscopic characterization, a small quantity of foam (1.5 μ l) was taken on a glass slide and observed under optical microscope (Motic, Hong Kong). The microscopic images of the foam samples were envisaged using an inbuilt camera and imaging software (Moticam-10). The obtained images were then analyzed by Image J software to obtain average bubble size in foam. The microscope was also equipped with a thermal stage, attached to necessary temperature control and measurement units. This arrangement was utilized in thermal stability tests of Pickering foam.

7.2.5 Measurement of IFT of CO₂-nanofluid system

Interfacial tension (IFT) of CO₂-nanofluid system was measured using pendent drop method. The method of IFT measurement has been detailed in our recent study [19]. Initially, nanofluid sample was extruded into a pressurized cell containing CO₂. The nanofluid took the shape of a pendent drop which was captured using a high resolution camera (Phantom Camera VEO 1010). In current work, CO₂-nanofluid system has been taken as reference system in which CO₂ is considered as one phase and nanofluid being the other phase to determine IFT. PVT-cell was first filled with CO₂ at required test pressure (12 bar) using CO₂ cylinder, connected inline to a syringe pump which helped to maintain test pressure in cell. Then, a drop of nanofluid was carefully maintained at the tip of capillary tube in cell. An image was carefully captured at the moment nanofluid finally detached from the tip of tube in cell. This image was further analyzed using ImageJ software to obtain IFT between CO₂ and nanofluid. This method was established in a

previous study [337]. To minimize data aberrations, every reading was repeated at least 5 times.

7.2.6 Rheological investigation of Pickering foam

A modular compact rheometer (MCR-52, Anton Paar, Austria) was used to characterize CO₂ foams. For these tests, double gap cylinder assembly (a modified variant of bob and cup) was used. For analysis, a small volume (6 ml) of foam was filled within concentric cup and bob was attached on cup. Bob and cup assembly was then mounted on rheometer stand for further analysis. An inbuilt software, Rheo Compass, was used for the analysis of rheological measurements. During shear rheological analysis, the total time taken by experimental run was 9 min with test tie of 10 s between two consequent measurements. The shear rate was varied from 20 to 2000 s⁻¹ to cover a wide range of shear deformation on foam. The dynamic viscoelastic measurements were conducted using strain-sweep and frequency-sweep analysis. Strain-sweep measurements were performed to obtain elastic modulus (G') and viscous modulus (G'') as a function of strain amplitude (0.1-100%) at constant frequency of 10 rad/s [207]. An essential requirement of these measurements was to determine linear viscoelastic (LVE) region. In LVE region, G' and G'' remain independent of applied strain amplitude. Another useful information is to establish the presence of critical strain where crossover between G' and G'' takes place. Frequency-sweep (1-100 rad.s⁻¹) measurements were performed at applied strain within LVE region. All experiments were repeated at least twice to ensure no aberrations took place. After each investigation, the various parts of rheometer were cleaned using DI water and dried to ensure no cross-contamination occurred during the study [63].

7.3 Results & Discussion

First, the effect of varying NP size (36-148 nm) and concentration (0.1-1 wt%) on foam quality, quantity, and rate of liquid drainage was investigated followed by the

discussion on microscopic characterization of foams at different test temperature (30-90 °C). Next, rheological properties (viscosity and moduli) of Pickering foams were studied *via* both shear and dynamic modes. Finally, hysteresis results [shear rate (increasing and decreasing) *vs.* stress profiles] were presented.

7.3.1 Stability analysis of Pickering CO₂ foams

To prepare CO₂ foams, surfactant SDS (of critical micelle concentration, ~0.22 wt%) and single step nanofluids of varying concentration were used. CMC value of SDS was determined using electrical conductivity measurements [279]. The visual appearance images of CO₂ foams (of different composition) are provided in Figure 7.3. These foams were regularly monitored for any change in their appearance. The visual appearance images of foams are provided in Figure 7.4. As evident from Figure 7.4, foam volume was found to decrease with time resulting liquid drained from the foam and collected in bottom of glass vials. The total volume of generated foam was recorded and the results are provided in Table 7.1 (along with NP size, concentration, and nomenclature). Initially, S1 nanofluid (36 nm, 0.1 wt%) resulted into the development of 155 ml of foam volume. With increasing NP size (> 36 nm), the foam volume reduced to 106 and 88 ml in S2 (size = 82 nm) and S3 (size = 146 nm) nanofluids, respectively.

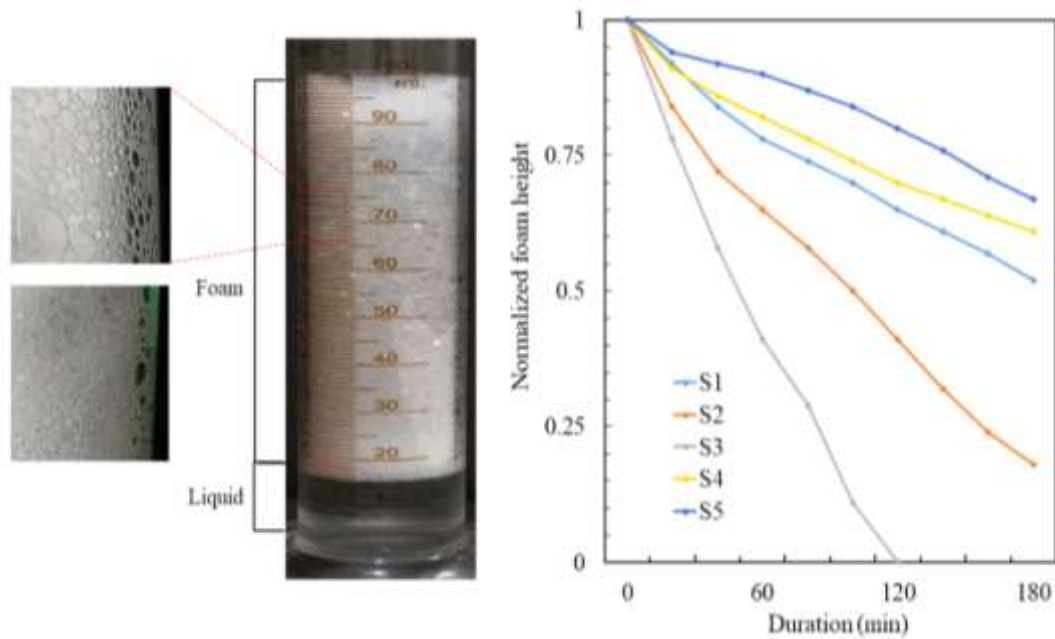


Figure 7.3: Representative image showing distinct foam and liquid phases in the glass cylinder (left). Normalized height of foam generated from various silica nanofluids as a function of time (right).

However, increasing NP concentration (>0.1 wt%) showed increase in foam volume resulting foam volume of 107 ml was obtained with nanofluid S4 (35 nm, 0.5 wt%) while nanofluid S5 (37 nm, 1 wt%) suggested foam volume of 102 ml. From the results, it is evident that increasing NP size suggested reduction in foam volume (for similar NP concentrations). This can be attributed to the fact that NPs of large size usually prefer to stay in bulk phase resulting fewer NPs participate in the development of foam and this might be the possible reason of drop in foam volume [38]. On the other hand, increasing NP concentration suggested availability of more NPs in the system and consequently, increased the volume of foam.

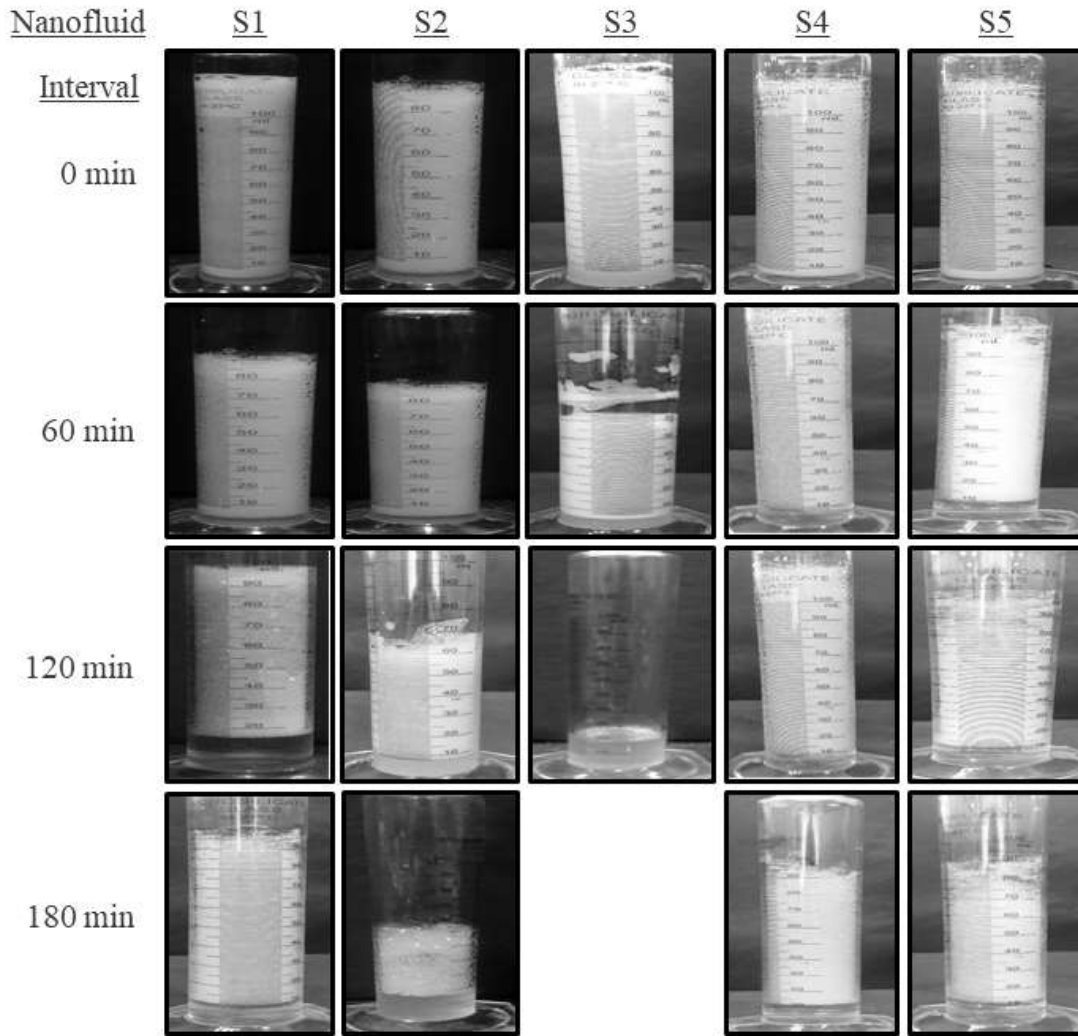


Figure 7.4: Visual appearance images of foams in graduated glass vials as a function of time.

Next, half-life of Pickering foam was determined. Half-life of a foam is defined as the time taken by half of the foam to disappear and convert into a liquid phase. To calculate half-life, a normalized foam height was obtained by selecting the initial amount of foam in glass cylinder as 1. The normalized foam height at instance t was determined using the following formula:

$$\text{Normalized foam height}(t) = \frac{\text{Foam volume at time } t}{\text{Initial foam volume}}$$

The half-life of various Pickering foams has been plotted as a function of time in Figure 7.3. For nanofluid S1(36 nm, 0.1 wt%), the value of half-life was determined as 194 min.

Table 7.1: Nomenclature and foam volume of the Pickering foams stabilized using single-step silica nanofluids.

Size (nm)	Concentration (wt%)	Nomenclature	Foam Volume (ml)
36		S1	115
82	0.1	S2	106
146		S3	88
35	0.5	S4	107
37	1	S5	102

Conventionally, it has been found that the inclusion of silica NP increases the half-life of foam and makes them more stable against the severity of destabilization [338]. Since NP size yields inverse relationship with the stability of foam, minimum half-life of 56 min was obtained with largest silica NP (142 nm) of S3 nanofluid. Maximum half-life of 237 min was obtained with S5 nanofluid, consistent with foam volume results. Thus, as compared to NP size, increasing NP concentration offered foam formulation of superior stability.

7.3.2 Microscopic characterization of Pickering CO₂ foams

Microscopic images of foams and their associated bubble size distribution are provided in Figure 7.5 and 7.6, respectively. It was observed that CO₂ foam of nanofluid S1 (36 nm, 0.1 wt%) exhibited average bubble size of 20 μm. The bubble size progressively increased with time as evident from microscopic images in Figure 7.5; the average bubble size increased from 90 μm to 115 μm (after 60 min) and finally increased to 160 μm after

120 min (Figure 7.5). The value of average bubble size was determined a 180 μm after 180 min. This indicates that smaller bubbles coalesce and converted into larger bubbles, which was evident by the significant decrease in bubble population in size distribution chart of Figure 7.5. The increased coalescence between bubbles is a sign of inferior foam stability because CO_2 foam of large bubbles tends to separate faster than the one of smaller bubbles [339]. It is well established that foam bubbles are thermodynamically unstable and thus, foams are subjected to experience coalescence due to gas diffusion and capillary suction [243]. Also, a continuous change in the thickness of bubble is responsible for foam degradation. Mechanistically, the difference in pressure that exists between the gas and liquid (also referred to as the capillary pressure P_c) is found to occur at the curved interface. The presence of this difference in pressure moves the liquid to borders of the foam plateau which in turn causes the liquid content to be drained (liquid drainage) and rupturing the thin film. Another mechanism influencing bubble/foam coalescence is Oswald ripening, which is the result of gas diffusion between foam bubbles of unequal size [277,340]. Conventionally, smaller bubbles are absorbed into larger bubbles due to the chemical potential difference between gases trapped within bubbles of unequal size.

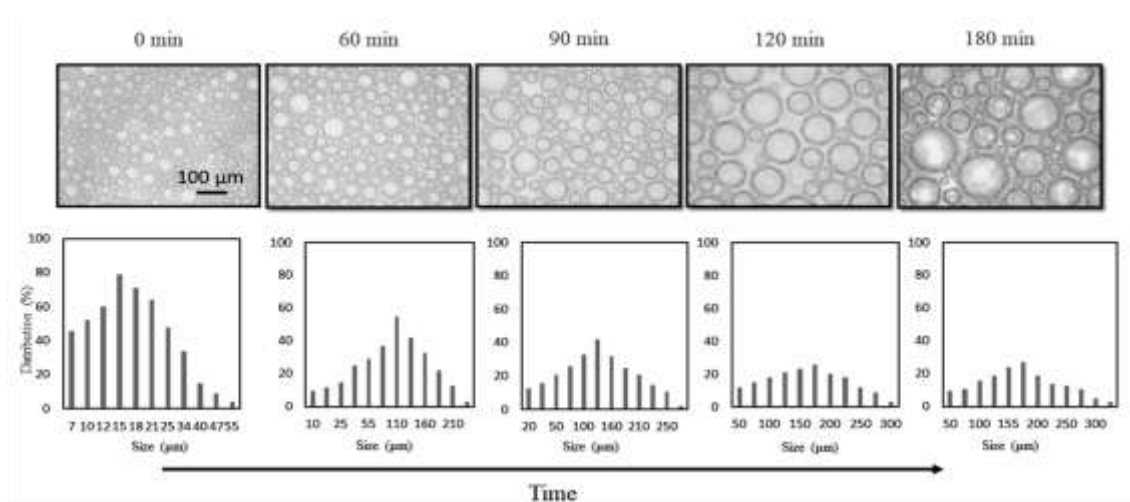


Figure 7.5: Microscopic image and bubble size distribution of Pickering foam prepared using silica nanofluid S1. The glass slide was kept open to the atmosphere

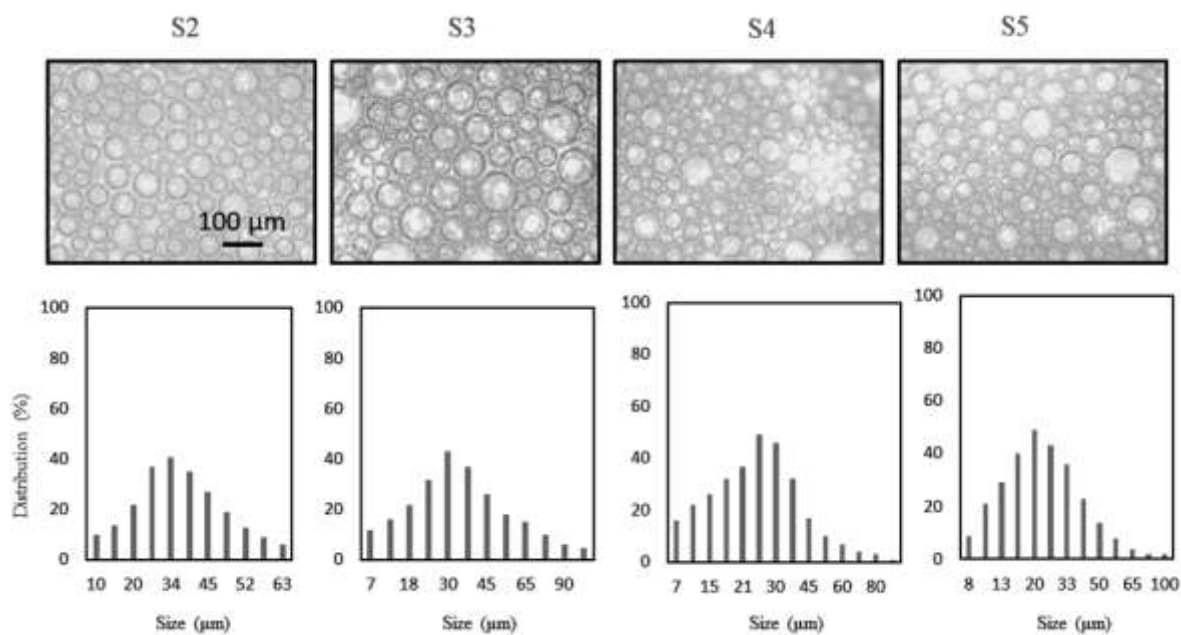


Figure 7.6: Microscopic image and bubble size distribution of Pickering foam prepared using silica nanofluid S2-S5, immediately after preparation. The observations were performed at ambient pressure and temperature.

When the microscopic investigations were also repeated for other nanofluids (S2-S5), it was observed that the average bubble size of the Pickering foams varied between 22-36 µm. It was observed that highest bubble size of 38 µm was found for CO₂ foam of nanofluid S3, indicating CO₂ foam of this composition will destabilize faster than foams of other composition (Figure 7.6).

7.3.3 Thermal stability of Pickering foams

For a foam, thermal stability is desirable trait that widens foam utilization for high temperature application [165]. NP adsorption on bubble surface can make foam stable by creating a steric barrier that resists bubble coalescence [250]. The effect of temperature on stability of Pickering foam was investigated *via* microscopic characterization. First, Pickering foam of nanofluid S1 (36 nm, 0.1 wt%) was kept on a glass slide and temperature was progressively increased to determine average bubble size at each test temperature. It

was observed that size of foam increased with increasing temperature as evident from Figure 7.7. This is credited to increase in bubble coalescence as a result, smaller bubbles converted into large size bubbles. Therefore, the average bubble size of 20 μm (at 25 $^{\circ}\text{C}$) increased to ~ 180 μm at 50 $^{\circ}\text{C}$ (moderate temperature) and 260 μm at 90 $^{\circ}\text{C}$ (high temperature) (Figure 7.7). A similar increase was observed for all nanofluids where CO_2 foam of nanofluid S3 showed maximum increase in foam size. The thermal stability of Pickering foams is also affected by the rate of collision and aggregation between NPs [161]. At high temperature, the rate of collision and agglomeration usually increases due to increase in kinetic energy of NPs and consequently, it reduces NP participation in bubble stabilization. For CO_2 foam of nanofluid S1 (36 nm, 0.1 wt%), the effect of temperature > 90 $^{\circ}\text{C}$ (100 $^{\circ}\text{C}$) was also explored (Figure 7.7). It was observed that gas bubbles rapidly deformed (< 5 min) at 100 $^{\circ}\text{C}$ and after the evaporation of liquid, a solid white cake left behind on the glass slide (Figure 7.7).

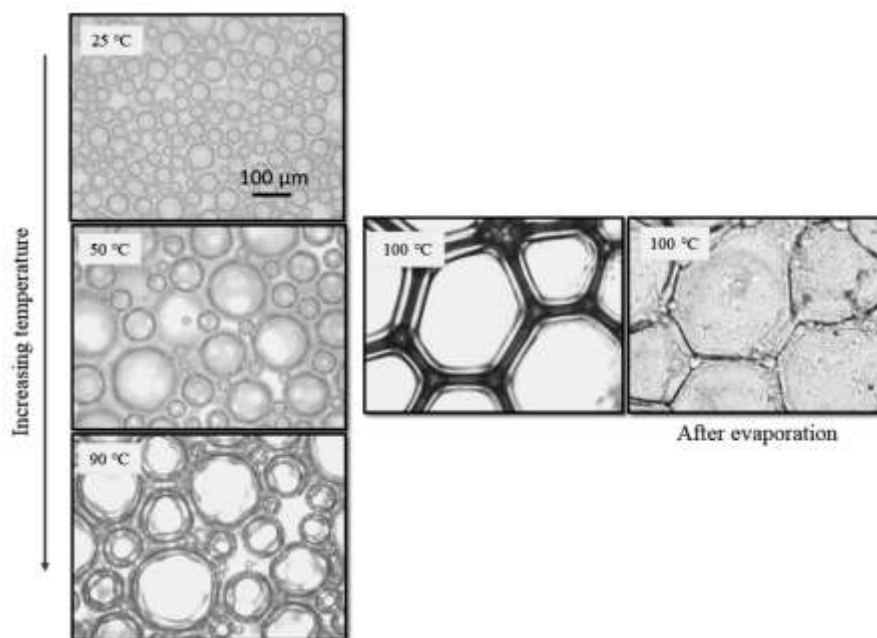


Figure 7.7: Thermal stability of Pickering foam prepared using silica nanofluid S1, immediately after preparation. The bubble size increased on increasing temperature and after evaporation, a solid layer of deposition was found on the location of the foam lamella.

However, the presence of lamella around foam bubbles could be readily identified from the residue of foam bubbles. This can be attributed to the adherence of silica NPs on foam boundaries and this might be the possible reason of additional stability at high temperature [250].

7.3.4 Interfacial tension between silica nanofluid and CO₂

Interfacial tension (IFT) measurements between silica nanofluid and CO₂ were conducted to understand NP adsorption on CO₂ surface which is essential to reduce CO₂ globules into stable small size bubbles. This is of key importance for the successful CO₂ capturing and storage (CCS) in constricted pore throats or low permeable reservoir. This is in agreement with the fact that interfacial properties of solid/fluid often influence carbon trapping and storage potential [341]. For IFT measurements, CO₂ was pressurized into a cell to desired pressure (12 bar) and a drop of nanofluid (S1-S5) was introduced using a syringe pump, similar to what was practiced in a previous study for low salinity brine solution [19]. The nanofluid droplet was allowed to stabilize with surrounding CO₂ and IFT was measured before the detachment of nanofluid from needle [342]. The image of droplet was captured using a camera followed by its analysis to determine IFT between CO₂-nanofluid (for actual image, see Figure 7.8; for schematic, see Figure 7.9).



Figure 7.8: Actual images of the nanofluid droplets in CO₂ environment obtained using Phantom VCC camera and adjustable height arrangement.

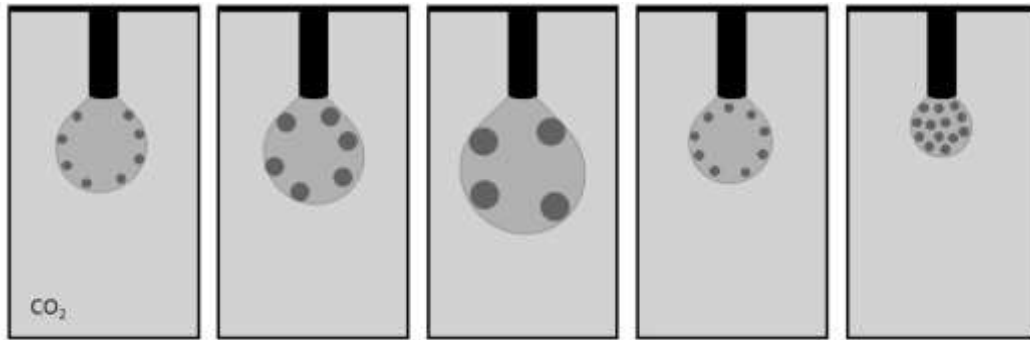


Figure 7.9: Representative image showing the droplet shape of nanofluids in an atmosphere of CO₂. These images were used to obtain the IFT of the CO₂-fluid system.

Similarly, IFT measurements were conducted for the effects of varying NP size and concentration and these results are provided in Table 7.2.

Table 7.2: Interfacial tension measurements of CO₂-water/nanofluid system at ambient temperature (303 K) and pressure= 12 bar. The values provided are the average of 5 measurements.

Fluid	IFT (mN/m)
Water	68
S1	52
S2	57
S3	60
S4	50
S5	49

IFT value of DI water-CO₂ system was found to be 68 mN/m. IFT value dropped to 52 mN/m when S1 (36 nm, 0.1 wt%) nanofluid was introduced into the cell. Further, with increase in particle size (>36 nm), IFT value increased to 57 and 60 mN/m for S2-CO₂

and S3-CO₂ systems, respectively. However, increasing NP concentration (>0.1 wt%) led to reduction in IFT value. Thus, IFT value of 50 and 49 mN/m were recorded for S4-CO₂ and S5-CO₂ systems, respectively. From these results, it can be stated that increasing NP concentration is relatively more advantageous in IFT reduction of nanofluid-CO₂ system than NP size. In nanofluid with large size NPs, the quantum of IFT reduction is limited due to the presence of fewer NPs at the interface as most of the NPs prefer to stay in bulk liquid phase. This is in line with the fact that NP adsorption on liquid-gas interface causes reduction in IFT. Thus, with high NP concentration, a significant IFT reduction can be obtained as the interface is optimally saturated by NPs (Figure 7.9). But, it is also true that increasing NP concentration beyond a limit will have no further pronounced impact on IFT reduction of CO₂-nanofluid system, since optimal NP saturation leaves no place for further adsorption [343,344].

7.3.5 Shear rheological behavior of Pickering foams

The effect of NP size, NP concentration, and test temperature on shear rheological behavior (viscosity) of the Pickering foams was reported as a function of varying shear rate (20-2000 s⁻¹). The test pressure was chosen as 1 bar. The effect of NP size on viscosity of Pickering foams is provided in Figure 7.10a. It was observed that all foams exhibited shear-thinning behavior with increasing shear rate as evident from viscosity profiles at high shear rate. The viscosity of Pickering foam of nanofluid S1 (36 nm, 0.1 wt%) was found to be 50 mPa.s at 22 s⁻¹ which reduced to 7 mPa.s at 1860 s⁻¹ (Figure 7.10a). The viscosity of foam reduced with increase in NP size and as a result, its value reached to 43 and 39 mPa.s for Pickering foams of S2 (82 nm, 0.1 wt%) and S3 (146 nm, 0.1 wt%), respectively (Figure 7.10a). It is to be noted here that S3 exhibited maximum viscosity reduction and its viscosity reached to lowest level of 4.67 mPa.s at 1860 s⁻¹. When NP concentration was increased, the viscosity of Pickering foam slightly increased to 52 and 58 mPa.s (at 22 s⁻¹)

for nanofluid S4 (35 nm, 0.5 wt%) and S5 (37 nm, 1 wt%), respectively. Thus, for high NP size, the reason of decrease in foam viscosity can be credited to the tendency of NP preference for bulk liquid than CO₂ surface, consistent with foam stability results of this study and research findings in literature [63].

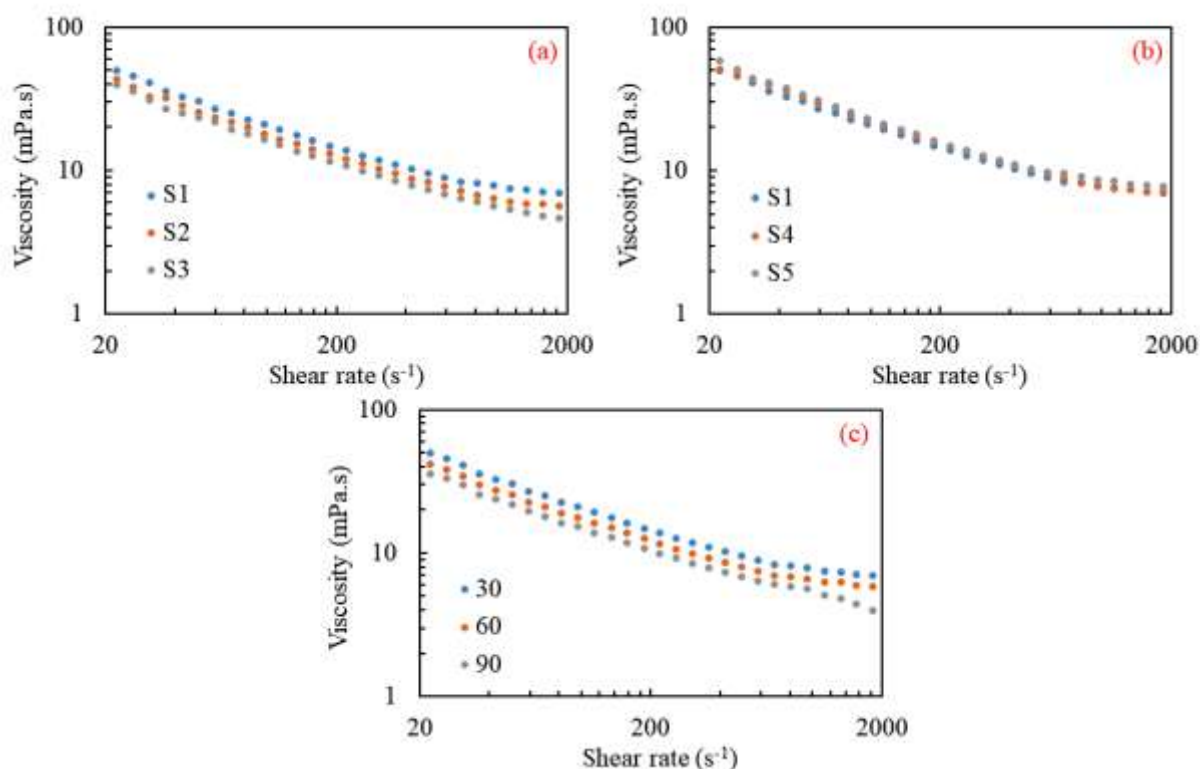


Figure 7.10: The effect of increasing NP size (a), concentration (b), and temperature (c) on viscosity data of Pickering foams prepared using nanofluid S1-S5.

The effect of temperature (30-90 °C) on viscosity of Pickering foam of nanofluid S1 (36 nm, 0.1 wt%) is shown in Figure 7.10c. It was observed that the viscosity of S1-foam decreased with increasing temperature. As a result, the viscosity of foam was measured to be 42 and 36 mPa.s at test temperature of 60 and 90 °C, respectively. The relation between temperature and colloidal systems is well established in literature [212], where aqueous phase viscosity is reported to be a responsible factor in the performance of foam at high temperature. With further increase in shear rate to 1860 s⁻¹, the viscosity of

Pickering foam dropped to 5.8 and 4 mPa.s at 60 and 90 °C, respectively. Thus, these results indicate that foam application at high temperature requires careful selection and design of aqueous phase in which nanofluid is synthesized.

7.3.6 Dynamic rheological behavior of Pickering foams

Pickering foams are complex viscoelastic suspensions with the presence of both G' (elastic) and G'' (viscous) components [63]. Their complex rheological behavior paves a way for their application in various industries including EOR and carbon storage [345].

Strain-sweep measurements were performed for Pickering foams at an angular frequency of 10 rad.s^{-1} and these results are provided in Figure 7.11. Frequency value of 10 rad.s^{-1} was chosen from the literature [207]. The presence of G' and G'' can help to infer the viscoelastic behavior of foams over the range of strain explored. It was observed that the value of G'' was higher than G' over the entire range of strain explored, indicating dominance of liquid-like behavior in foam. Also, it is important to note that increasing NP concentration suggested increase in G' value (Figure 7.11c and 11d) while increasing NP size showed decrease in G' value (Figure 7.11b and 11c). This is attributed to higher viscosity of foams (as evident from Figure 7.10). With increasing strain, drop in G' and G'' value is the sign of decrease in viscoelasticity of foams. The transition from linear to elastic nature (around 25-30%) can be observed in Figure 7.11(a) for foam prepared using nanofluid S1 (36 nm, 0.1 wt%). For elastic region, a plateau (similar values of G') was observed while above yield strain (20%), G' decreases in accordance to power law [346]. Figure 7.11 (e-f) show the effect of temperature on Pickering foam of nanofluid S1. With increase in temperature, a minor reduction in G' and G'' value was obtained, in line with viscosity results of foam. With increasing temperature, the inter-molecular attraction between NPs and base fluid reduces [215]. This, along with weakening of PAM chains, reduces the viscosity of nanofluid [214]. Given G' and G'' dependency on viscosity of

solution, the decrease in viscosity causes reduction in values of both G' and G'' . However, the general trend of G' and G'' profiles remain similar even at high temperature (90 °C), indicating that Pickering foam retains its viscoelastic nature.

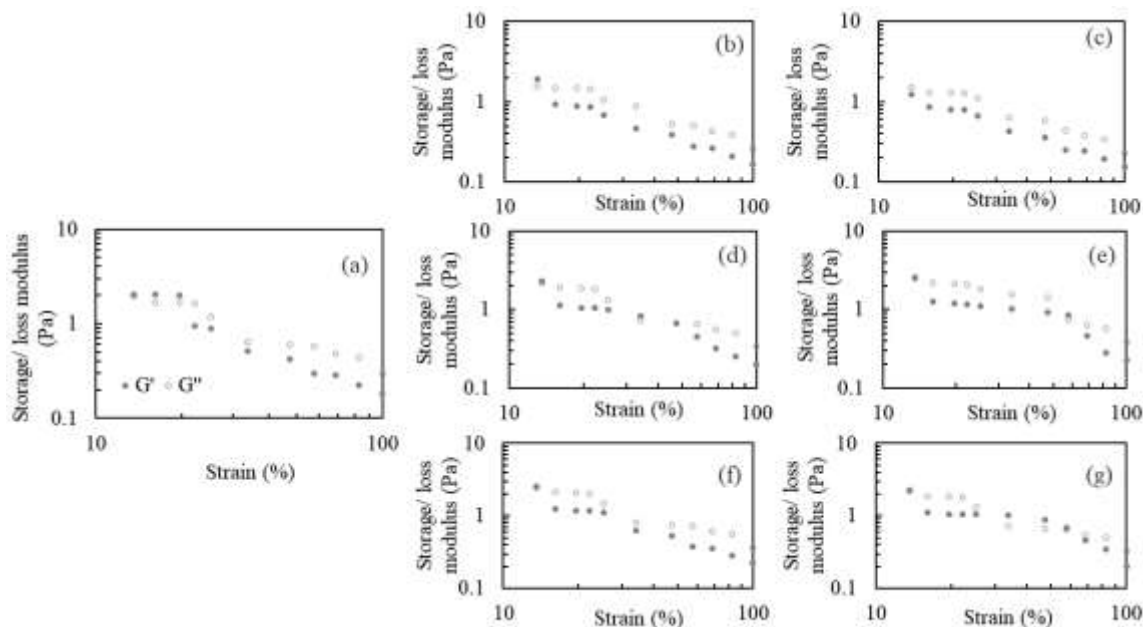


Figure 7.11: Plots of strain-sweep analysis (at angular frequency of 10 rad.s^{-1}) illustrating effect on viscoelastic properties (G' and G'') of nanofluids of different particle (a–c) size and (d–e) concentration [a: S1 (36 nm, 0.1 wt%); b: S2 (82 nm, 0.1 wt%); c: S3 (147 nm, 0.1 wt%); d: S4 (35 nm, 0.5 wt%); e: S5 (37 nm, 1 wt%)]. The effect of temperature 60 °C (f) and 90 °C (g) on the Pickering foam of silica nanofluid S1 has also been reported.

The frequency-sweep measurements for Pickering foams were conducted at constant strain amplitude of 2% [207]. The results of frequency-sweep measurements are given in Figure 7.12. For Pickering foam of nanofluid S1, G' and G'' values were measured to be 7 Pa and 2.5 Pa (at 2 rad.s^{-1}), respectively (Figure 7.10a). Additionally, with increasing frequency, G'' value increases while G' exhibited slight reduction. This indicates that foam behavior was dominated by liquid effects with increasing angular frequency. At 94 rad.s^{-1} , G' and G'' values were measured to be 5 and 3.6 Pa, respectively (Figure 7.12a). Similar

was observed for other Pickering foams [Figure 7.12 (b-e)]. It is to be noted here that G' was dependent on the viscosity of foam as increasing NP concentration showed increase in G' value [see Figure 7.12(a-e)] and increasing NP size showed reverse behavior. The trait of enhancement in viscoelastic response of foam is credited to colloids and PAM chains those formulate a strong lamella around the interface of bubble and thus, a strong viscoelastic response followed the order of $S5 > S4 > S1 > S2 > S3$. Also, for foams of nanofluids S4 and S5, G'' became greater than G' at angular frequency around 40-60 rad.s^{-1} . As a result, the cross-over (between G' and G'') was only present for foams of S4 (35 nm, 0.5 wt%) and S5 (37 nm, 1 wt%) while other nanofluids exhibited no sign of cross-over. When frequency-sweep measurements for foam of S1 were repeated at 90 °C, a drop in G' and G'' value was obtained which is in accordance with effect of high temperature on viscosity of S1-foam.

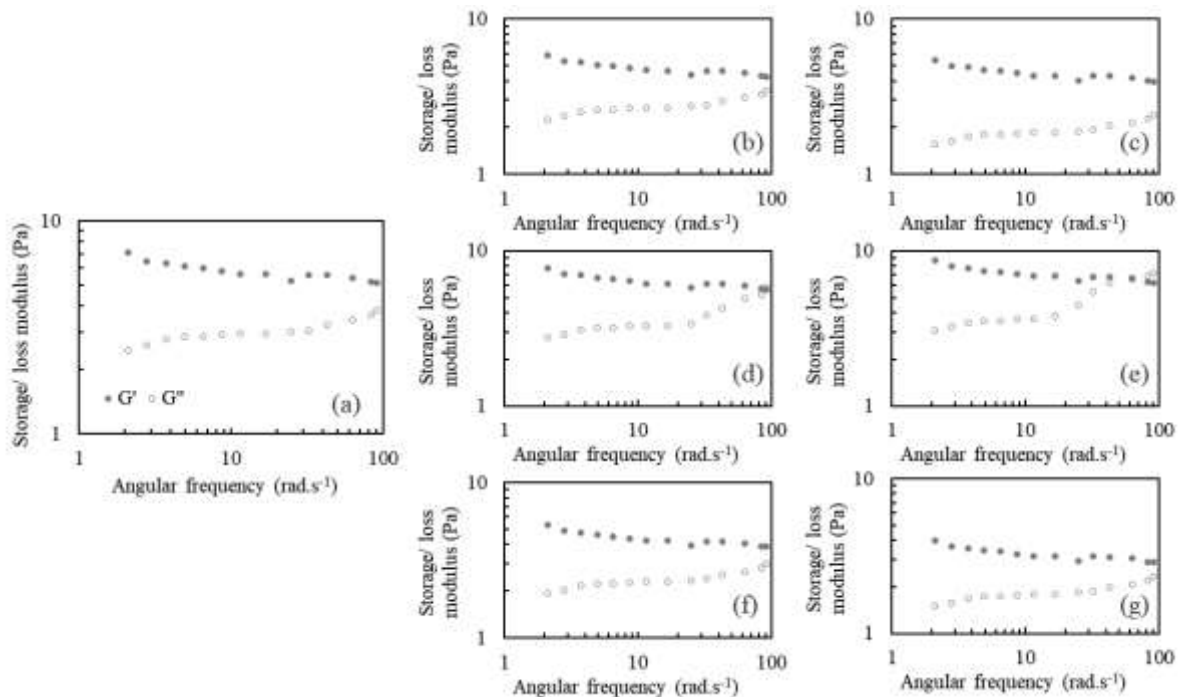


Figure 7.12: Plots of the frequency based response (at angular strain amplitude of 2%) illustrating effect on viscoelastic properties (G' and G'') of nanofluids of different particle

(a–c) size and (d–e) concentration. The effect of temperature 60 °C (f) and 90 °C (g) on the Pickering foam of silica nanofluid S1 is also reported.

7.3.7 Hysteresis analysis of Pickering foams

Pickering foams hold immense potential as agents of mobility control in carbon sequestration and utilization (CSU) applications. NP presence ensures that synthesized Pickering foams are more stable (than conventional foams) in complex subsurface environment [250,332,333]. Heterogeneous formations are complex rocks of varying flow paths in which most of the injected slugs either deform or fail prematurely. Additionally, heterogeneous formations exert an unequal shear on injected foam (even in very short intervals) [347,348]. The unequal shear may impair the rheology of foam, causing it to deform and negate the favorable mobility ratio of injected gas (Figure 7.13).

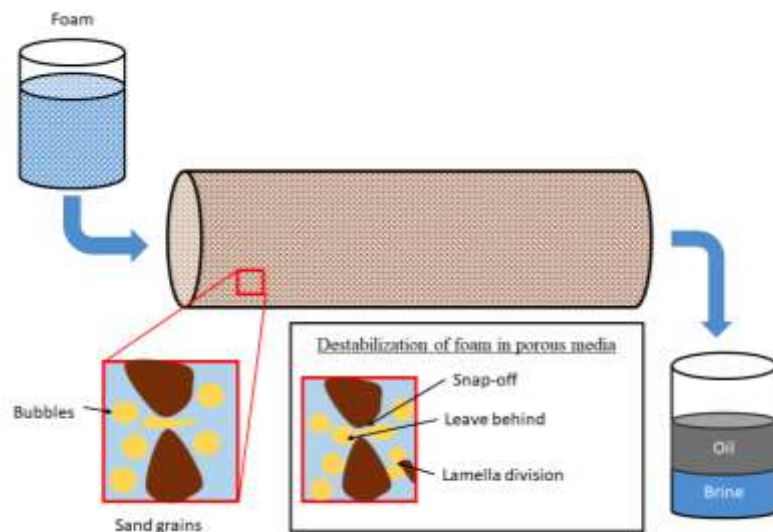


Figure 7.13: Schematic showing various stages of foam destabilization in porous media due to constrained pore throats.

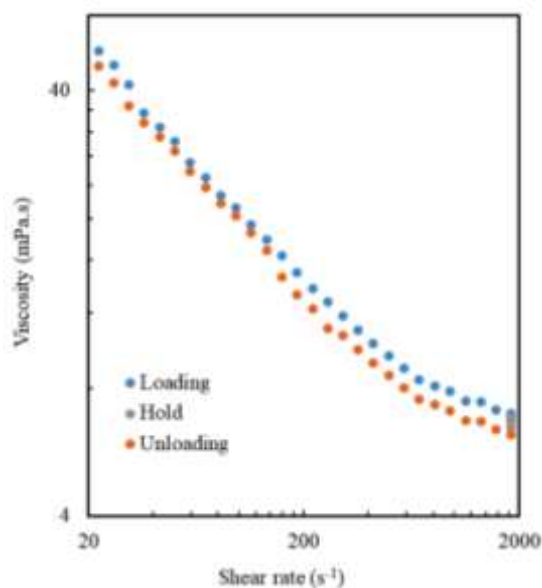


Figure 7.14: Plot of values of viscosity obtained during loading (increasing shear rate) and unloading (reducing shear rate) in Pickering foam prepared using silica nanofluid S1 (36 nm, 0.1 wt%). (Temperature = 30 °C).

Hence, it is important to investigate the impact of varying shear conditions on stability of injected foam and hysteresis analysis is one of the effective tools to perform these studies. The hysteresis behavior of Pickering foam of S1 (36 nm, 0.1 wt%) was investigated for shear rate ranges from 20-2000 s^{-1} at test temperature of 30 °C and results are provided in Figure 7.14. Conventionally, hysteresis is defined as the variation between different cycles of loading and unloading (or in case of rheology, the variation of shear rate). Thus, it is an ideal method to characterize and compare efficacy of Pickering foams for low permeable rocks. Initially, shear rate was increased from 20-2000 s^{-1} (known as loading cycle) and the shear rate was maintained at 2000 s^{-1} for 1 min where 5 measurement points were recorded. The shear rate was reduced from 2000 to 20 s^{-1} (the unloading cycle). The values of loading and unloading cycles were plotted to report the difference between two cycles, known as hysteresis loss. From Figure 7.14, it can be observed that Pickering foam (of nanofluid S1) did not show any significant change in viscosity values during

loading and unloading cycles. Therefore, the hysteresis loss was lower than 5% in S1-foam, which indicates potential of Pickering foam for heterogeneous formations.

7.4 Conclusion

This study has investigated the effect of NP size, NP concentration, and test temperature on synthesis, stability, and rheology of Pickering foams, stabilized by nanofluid of different compositions. Silica NPs were prepared in-situ in 1000 ppm PAM solution using Stober sol-gel method utilizing tetra-ethyl orthosilicate (TEOS) as precursor and ethanol as medium. Foam was prepared in a stirring pot and volume and half-life of foam were measured. Increase in NP concentration increased foam stability by delaying the rate of half-life of foam, while increasing NP size suggested insignificant improvement in foam stability. The maximum foam stability was obtained for nanofluid S5 (size 37 nm, 1 wt %) with half-life of 237 min. On the other hand, the lowest foam stability was associated with nanofluid S3 (size 146 nm, 0.1 wt%) which had half-life of lower than 1 h. The average bubble size of Pickering foams was determined to be in the range of 20-40 μm . With increase in storage duration and test temperature, the bubble size increased and large size bubbles were found to be more susceptible to phase separation and destabilization. IFT measurements, conducted for CO₂-nanofluid system, demonstrated that the presence of silica NP offered significant reduction in IFT value. Additionally, the drop in IFT value was found dependent on the population of suspended NPs. Furthermore, increasing NP concentration beyond an optimum value (>0.1 wt%) did not show pronounced IFT reduction between CO₂-nanofluid system. Shear rheological analysis demonstrated that the viscosity of Pickering foams reduced with increasing NP size and test temperature while increasing NP concentration increased the viscosity of system. Foams also exhibited viscoelastic response with both elastic ($G' > G''$) and viscous effects ($G' < G''$), where viscoelasticity was found to vary with foam viscosity. Hysteresis analysis showed that

Pickering foam (of nanofluid S1) exhibited minimum hysteresis loss in the presence of varying shear rate (20-2000 s⁻¹) and hysteresis loss of 5% was determined after loading and unloading cycles. Thus, stability and rheological behavior of conventional CO₂ foams can be improved by the inclusion of single-step size controlled silica nanofluids and these foams can be an alternative solution for CO₂ utilization in EOR and carbon sequestration.

8.1 Conclusion

This work reports the synthesis of a stable silica nanofluid formulated via the single-step route via the *Stober* sol-gel. The size of particles was controlled via increasing or decreasing the amount of ammonium hydroxide added to the solution while varying the amount of precursor (TEOS) yielded an increase or decrease in particle concentration. In this study, the nanofluids were prepared of size between 30-150 nm and of concentration ranging from 0.1-1 wt%. The formulated NPs had a spherical shape and were widely dispersed in the polymer matrix as observed from advanced imaging techniques like SEM and TEM. These nanofluids retained their stability for a duration of over 60 days without any severe signs of agglomeration or sedimentation, as established from dynamic light scattering and zeta-potential results. The formulated nanofluids were planned for use in brownfield applications like enhanced oil recovery and carbon storage. For this, the flow behavior of CO₂ was evaluated in a synthetic porous media (to mimic a sandstone reservoir) in presence of the silica nanofluids. The use of nanofluids was able to increase the duration of retention and areal coverage of CO₂ within the sand-pack by three fold (as established by the pressure drop profiles and the amount of fluid mobilized at the other end of the sand-pack). The use of nanofluids also improved the fluid displacement ratio and thus, showed superior efficacy for mobility control applications of CO₂. The formulated nanofluids also showed negligible sedimentation in porous media (attributed to their high resistance to

agglomeration) during flow operations with NP retention being found to directly depend on rate of injection and length of the sand-pack while temperature of the sand-pack and NP concentration having no significant role in NP retention.

To evaluate the nanofluid stability in saline mediums, salt, i.e. NaCl was added to the solutions and the increase in NP size was carefully observed using a dynamic light scattering unit as a function of time. Since salt suppresses inter-particle repulsion behavior, the NPs agglomerated rapidly in saline medium with higher NP concentration solutions being particularly more vulnerable to sedimentation and phase separation. To minimize NP agglomeration, an anionic surfactant, SDS was used and the nanofluids showed significantly improved dispersion stability in their presence. The silica nanofluids also showed superior oil mobilization tendency which was further improved in the presence of surfactant as synergy between NPs and surfactant enabled higher oil mobilization than possible in either of the two methods. The silica nanofluids were also evaluated to establish their rheological behavior. This analysis was carried out using both shear and dynamic rheology routes. These nanofluids displayed a shear-thinning behavior wherein viscosity was found to decrease on the increase of shear rate applied on the solution. The nanofluids also showed stable viscoelastic behavior with the presence of both G' and G'' over the entire investigated range. The inclusion of CO_2 in the silica nanofluid was found to reduce the nanofluid's viscosity in proportion to the amount of CO_2 absorbed in the solution. However, the nanofluids were able to retain the absorbed CO_2 within the solution even at high shear rates, demonstrating their superior retention ability for CO_2 transport within the formation, wherein non-uniform shear is likely to be encountered due to varying pore-throat size and reservoir heterogeneity.

The silica nanofluids were also evaluated to establish their carbon storage ability in a formation in conjunction with surfactants and the results demonstrated that higher carbon

storage (for the same pore volume) is possible when silica nanofluids or surfactant treated silica nanofluids are used as mobility and conformance control fluids in place of water. These nanofluids also exhibited higher CO₂ absorption (by a factor of 18-32%) in comparison with water when absorption studies were performed using the pressure decay method. These solutions also showed higher IFT reduction and CO₂ retention, which enable higher oil mobilization from sand-packs. Finally, the silica nanofluids were used for Pickering foam formulation which were investigated via rheological measurements. The inclusion of the silica NPs improved the stability of the foam solutions which resisted degradation under adverse conditions. Thus, the formulated silica nanofluids were found to be effective carbon utilization agents for use in brownfield oil reservoirs.

8.2 Proposed industrial applications

This nanofluid has shown high efficacy in lab-scale testing. Thus, its utilization is proposed in the following areas for field applications-

- Chemical EOR (as nanofluid flooding)
- Chemical EOR (in conjunction with surfactant/polymer flooding)
- Carbonated water injection
- Carbon sequestration (mobility/conformance control)
- Gas storage in porous media and hydrates

8.3 Future research direction

While this work has focused on the synthesis and experimental characterization of a novel silica nanofluid, wider scale studies incorporating the use of reservoir simulation (for field scale applications) and molecular dynamics studies (for micro-scale understanding) can be performed in the future to better understand the various mechanisms and their efficacies more broadly. For this, the use of any industry grade reservoir simulator

is proposed for reservoir simulation studies with data like IFT, relative permeability, petro physical properties and initial water saturation obtained from the experimental work performed in this study. Furthermore, the use of a molecular dynamics software will enable the understanding of the physical movements between the various constituents at the molecular level. Additionally, simulations can be used to understand the flow behavior of nanofluids in pore channels of small size under different velocities and shear.

The role of other common oilfield chemicals can also be explored in conjunction with these silica nanofluids to establish their compatibility and explore their synergy for field applications. Finally, the role of these silica nanofluids can be explored to establish gas storage in porous media. This holds immense potential as future energy basket will contain hydrogen which comes with unique storage and distribution problems. The formulated nanofluids might just be the right answer to the question of hydrogen storage.

References

- [1] T.R. Anderson, E. Hawkins, P.D. Jones, CO₂, the greenhouse effect and global warming: from the pioneering work of Arrhenius and Callendar to today's Earth System Models, *Endeavour*. 40 (2016) 178–187. doi:10.1016/j.endeavour.2016.07.002.
- [2] B. Ekwurzel, J. Boneham, M.W. Dalton, R. Heede, R.J. Mera, M.R. Allen, P.C. Frumhoff, The rise in global atmospheric CO₂, surface temperature, and sea level from emissions traced to major carbon producers, *Clim. Change*. 144 (2017) 579–590. doi:10.1007/s10584-017-1978-0.
- [3] Y. Zhang, B. Zhao, J. Jiang, Y. Zhuo, S. Wang, The use of TiO₂ nanoparticles to enhance CO₂ absorption, *Int. J. Greenh. Gas Control*. 50 (2016) 49–56. doi:10.1016/j.ijggc.2016.04.014.
- [4] K.Z. House, D.P. Schrag, C.F. Harvey, K.S. Lackner, Permanent carbon dioxide storage in deep-sea sediments, *Proc. Natl. Acad. Sci. U. S. A.* 103 (2006) 12291–12295. doi:10.1073/pnas.0605318103.
- [5] M. Bui, C.S. Adjiman, A. Bardow, E.J. Anthony, A. Boston, S. Brown, P.S. Fennell, S. Fuss, A. Galindo, L.A. Hackett, J.P. Hallett, H.J. Herzog, G. Jackson, J. Kemper, S. Krevor, G.C. Maitland, M. Matuszewski, I.S. Metcalfe, C. Petit, G. Puxty, J. Reimer, D.M. Reiner, E.S. Rubin, S.A. Scott, N. Shah, B. Smit, J.P.M. Trusler, P. Webley, J. Wilcox, N. Mac Dowell, Carbon capture and storage (CCS): The way forward, *Energy Environ. Sci.* 11 (2018) 1062–1176. doi:10.1039/c7ee02342a.
- [6] J. Machale, S.K. Majumder, P. Ghosh, T.K. Sen, Development of a novel biosurfactant for enhanced oil recovery and its influence on the rheological properties of polymer, *Fuel*. 257 (2019) 116067. doi:10.1016/j.fuel.2019.116067.
- [7] C. Zou, Q. Zhao, G. Zhang, B. Xiong, Energy revolution: From a fossil energy era

- to a new energy era, *Nat. Gas Ind. B.* 3 (2016) 1–11. doi:10.1016/j.ngib.2016.02.001.
- [8] V. Núñez-López, E. Moskal, Potential of CO₂-EOR for Near-Term Decarbonization, *Front. Clim.* 1 (2019) 5. doi:10.3389/fclim.2019.00005.
- [9] A. Sanna, L. Steel, M.M. Maroto-Valer, Carbon dioxide Sequestration using NaHSO₄ and NaOH: A dissolution and carbonation optimisation study, *J. Environ. Manage.* 189 (2017) 84–97. doi:10.1016/j.jenvman.2016.12.029.
- [10] K.R. Chaturvedi, R. Kumar, J. Trivedi, J.J. Sheng, T. Sharma, Stable Silica Nanofluids of an Oilfield Polymer for Enhanced CO₂ Absorption for Oilfield Applications, *Energy and Fuels.* 32 (2018) 12730–12741. doi:10.1021/acs.energyfuels.8b02969.
- [11] K.R. Chaturvedi, J. Trivedi, T. Sharma, Evaluation of Polymer-Assisted Carbonated Water Injection in Sandstone Reservoir: Absorption Kinetics, Rheology, and Oil Recovery Results, *Energy and Fuels.* 33 (2019) 5438–5451. doi:10.1021/acs.energyfuels.9b00894.
- [12] B. Honarvar, A. Azdarpour, M. Karimi, A. Rahimi, M. Afkhami Karaei, H. Hamidi, J. Ing, E. Mohammadian, Experimental Investigation of Interfacial Tension Measurement and Oil Recovery by Carbonated Water Injection: A Case Study Using Core Samples from an Iranian Carbonate Oil Reservoir, *Energy Fuels.* 31 (2017) 2740–2748. doi:10.1021/acs.energyfuels.6b03365.
- [13] E.M. Ruidiaz, A. Winter, O. V. Trevisan, Oil recovery and wettability alteration in carbonates due to carbonate water injection, *J. Pet. Explor. Prod. Technol.* 8 (2018) 249–258. doi:10.1007/s13202-017-0345-z.
- [14] S. Lee, S.I. Kam, *Enhanced Oil Recovery by Using CO₂ Foams: Fundamentals and Field Applications*, First Edit, Elsevier Inc., 2013. doi:10.1016/B978-0-12-386545-8.00002-6.

- [15] X. Xu, A. Saeedi, K. Liu, Bulk phase Behavior and displacement performance of CO₂ foam induced by a combined foaming formulation, *J. Pet. Sci. Eng.* 147 (2016) 864–872. doi:10.1016/j.petrol.2016.09.045.
- [16] M. Cao, Y. Gu, Oil recovery mechanisms and asphaltene precipitation phenomenon in immiscible and miscible CO₂ flooding processes, *Fuel*. 109 (2013) 157–166. doi:10.1016/j.fuel.2013.01.018.
- [17] S.A. Farzaneh, M. Sohrabi, Experimental investigation of CO₂-foam stability improvement by alkaline in the presence of crude oil, *Chem. Eng. Res. Des.* 94 (2015) 375–389. doi:10.1016/j.cherd.2014.08.011.
- [18] Z. Kargozarfard, M. Riazi, S. Ayatollahi, Viscous fingering and its effect on areal sweep efficiency during waterflooding: an experimental study, *Pet. Sci.* 16 (2019) 105–116. doi:10.1007/s12182-018-0258-6.
- [19] K.R. Chaturvedi, D. Ravilla, W. Kaleem, P. Jadhawar, T. Sharma, Impact of Low Salinity Water Injection on CO₂ Storage and Oil Recovery for Improved CO₂ Utilization, *Chem. Eng. Sci.* 229 (2021) 116127. doi:10.1016/j.ces.2020.116127.
- [20] G. Bisweswar, A. Al-Hamairi, S. Jin, Carbonated water injection: an efficient EOR approach. A review of fundamentals and prospects, *J. Pet. Explor. Prod. Technol.* 10 (2019) 673–685. doi:10.1007/s13202-019-0738-2.
- [21] K.R. Chaturvedi, T. Sharma, Enhanced carbon capture and storage in depleted sandstone reservoirs using silica nanofluids, *Mater. Today Proc.* 46 (2021) 5298–5303. doi:10.1016/J.MATPR.2020.08.782.
- [22] S. Zhang, Y. She, Y. Gu, Evaluation of polymers as direct thickeners for CO₂ enhanced oil recovery, *J. Chem. Eng. Data.* 56 (2011) 1069–1079. doi:10.1021/je1010449.
- [23] W. Wang, Y. Liu, Y. Gu, Application of a novel polymer system in chemical

- enhanced oil recovery (EOR), *Colloid Polym. Sci.* 281 (2003) 1046–1054. doi:10.1007/s00396-003-0873-6.
- [24] D.B. Siano, J. Bock, Viscosity of mixtures of polymers and microemulsions - the Huggins interaction coefficient, *Colloid Polym. Sci.* 264 (1986) 197–203. doi:10.1007/BF01414953.
- [25] A.D.K. Wibowo, L.A. Yoshi, A.S. Handayani, Joelianingsih, Synthesis of polymeric surfactant from palm oil methyl ester for enhanced oil recovery application, *Colloid Polym. Sci.* 299 (2021) 81–92. doi:10.1007/s00396-020-04767-5.
- [26] K. Xie, B. Cao, X. Lu, W. Jiang, Y. Zhang, Q. Li, K. Song, J. Liu, W. Wang, J. Lv, R. Na, Matching between the diameter of the aggregates of hydrophobically associating polymers and reservoir pore-throat size during polymer flooding in an offshore oilfield, *J. Pet. Sci. Eng.* 177 (2019) 558–569. doi:10.1016/j.petrol.2019.02.076.
- [27] S.H. Talebian, R. Masoudi, I.M. Tan, P.L.J. Zitha, Foam assisted CO₂-EOR: A review of concept, challenges, and future prospects, *J. Pet. Sci. Eng.* 120 (2014) 202–215. doi:10.1016/j.petrol.2014.05.013.
- [28] M. Mohajeri, M. Hemmati, A.S. Shekarabi, An experimental study on using a nanosurfactant in an EOR process of heavy oil in a fractured micromodel, *J. Pet. Sci. Eng.* 126 (2015) 162–173. doi:10.1016/j.petrol.2014.11.012.
- [29] S.M. Hosseini-Nasab, P.L.J. Zitha, Investigation of certain physical–chemical features of oil recovery by an optimized alkali–surfactant–foam (ASF) system, *Colloid Polym. Sci.* 295 (2017) 1873–1886. doi:10.1007/s00396-017-4162-1.
- [30] A. Bera, T. Kumar, K. Ojha, A. Mandal, Adsorption of surfactants on sand surface in enhanced oil recovery: Isotherms, kinetics and thermodynamic studies, *Appl. Surf. Sci.* 284 (2013) 87–99. doi:10.1016/j.apsusc.2013.07.029.

- [31] G. Shu, M. Dong, S. Chen, P. Luo, Improvement of CO₂ EOR performance in water-wet reservoirs by adding active carbonated water, *J. Pet. Sci. Eng.* 121 (2014) 142–148. doi:10.1016/j.petrol.2014.07.001.
- [32] B. Xiong, R.D. Loss, D. Shields, T. Pawlik, R. Hochreiter, A.L. Zydney, M. Kumar, Polyacrylamide degradation and its implications in environmental systems, *Npj Clean Water*. 1 (2018). doi:10.1038/s41545-018-0016-8.
- [33] B. Huang, X. Hu, C. Fu, W. Zhang, L. Wang, Effect of a Partial Pressure Tool on Improving the Heterogeneous Oil Recovery and Polymer Solution Microstructure, *ACS Omega*. 5 (2020) 7002–7010. doi:10.1021/acsomega.0c00362.
- [34] A. Sugar, V. Torrealba, U. Buttner, H. Hoteit, Assessment of polymer-induced formation damage using microfluidics, in: *Proc. - SPE Annu. Tech. Conf. Exhib., Society of Petroleum Engineers (SPE)*, 2020. doi:10.2118/201626-ms.
- [35] F. Zhao, H. Hao, J. Hou, L. Hou, Z. Song, CO₂ mobility control and sweep efficiency improvement using starch gel or ethylenediamine in ultra-low permeability oil layers with different types of heterogeneity, *J. Pet. Sci. Eng.* 133 (2015) 52–65. doi:10.1016/j.petrol.2015.05.014.
- [36] O. Rahmani, Mobility control in carbon dioxide-enhanced oil recovery process using nanoparticle-stabilized foam for carbonate reservoirs, *Colloids Surfaces A Physicochem. Eng. Asp.* 550 (2018) 245–255. doi:10.1016/j.colsurfa.2018.04.050.
- [37] A.S. Elhag, Y. Chen, P.P. Reddy, J.A. Noguera, A.M. Ou, G.J. Hirasaki, Q.P. Nguyen, S.L. Biswal, K.P. Johnston, Switchable diamine surfactants for CO₂ mobility control in enhanced oil recovery and sequestration, in: *Energy Procedia*, Elsevier Ltd, 2014: pp. 7709–7716. doi:10.1016/j.egypro.2014.11.804.
- [38] A. Haghtalab, M. Mohammadi, Z. Fakhroueian, Absorption and solubility measurement of CO₂ in water-based ZnO and SiO₂ nanofluids, *Fluid Phase Equilib.*

- 392 (2015) 33–42. doi:10.1016/j.fluid.2015.02.012.
- [39] D. Rousseau, S. Renard, B. Prempain, C. Féjean, S. Betouille, CO₂ mobility control with dissolved polymers: A core-scale investigation of polymer-rock and polymer-oil interactions, in: SPE - DOE Improv. Oil Recover. Symp. Proc., Society of Petroleum Engineers (SPE), 2012: pp. 791–803. doi:10.2118/154055-ms.
- [40] M. Sagir, I.M. Tan, M. Mushtaq, M. Pervaiz, M.S. Tahir, K. Shahzad, CO₂ mobility control using CO₂ philic surfactant for enhanced oil recovery, *J. Pet. Explor. Prod. Technol.* 6 (2016) 401–407. doi:10.1007/s13202-015-0192-8.
- [41] T. Føyen, Z.P. Alcorn, M.A. Fernø, A. Barrabino, T. Holt, CO₂ mobility reduction using foam stabilized by CO₂- and water-soluble surfactants, *J. Pet. Sci. Eng.* 196 (2021) 107651. doi:10.1016/j.petrol.2020.107651.
- [42] S.U.S. Choi, J.A. Eastman, Enhancing thermal conductivity of fluids with nanoparticles, in: Am. Soc. Mech. Eng. Fluids Eng. Div. FED, ASME, 1995: pp. 99–105.
- [43] M.S. Liu, M.C.C. Lin, I. Te Huang, C.C. Wang, Enhancement of thermal conductivity with CuO for nanofluids, *Chem. Eng. Technol.* 29 (2006) 72–77. doi:10.1002/ceat.200500184.
- [44] L. Wang, H. Chen, S. Witharana, Rheology of nanofluids: a review., *Recent Pat. Nanotechnol.* 7 (2013) 232–46. <http://www.ncbi.nlm.nih.gov/pubmed/24330046> (accessed October 8, 2019).
- [45] X. Wei, L. Wang, Synthesis and thermal conductivity of microfluidic copper nanofluids, *Particuology.* 8 (2010) 262–271. doi:10.1016/j.partic.2010.03.001.
- [46] C. Negin, S. Ali, Q. Xie, Application of nanotechnology for enhancing oil recovery – A review, *Petroleum.* 2 (2016) 324–333. doi:10.1016/j.petlm.2016.10.002.
- [47] I. Gosens, J.A. Post, L.J. de la Fonteyne, E.H. Jansen, J.W. Geus, F.R. Cassee, W.H.

- de Jong, Impact of agglomeration state of nano- and submicron sized gold particles on pulmonary inflammation, *Part. Fibre Toxicol.* 7 (2010) 37. doi:10.1186/1743-8977-7-37.
- [48] A.K. Sharma, A.K. Tiwari, A.R. Dixit, Rheological behaviour of nanofluids: A review, *Renew. Sustain. Energy Rev.* 53 (2016) 779–791. doi:10.1016/j.rser.2015.09.033.
- [49] A. V. Minakov, V.Y. Rudyak, M.I. Pryazhnikov, About rheology of nanofluids, in: *AIP Conf. Proc.*, American Institute of Physics Inc., 2018. doi:10.1063/1.5065235.
- [50] A. Zamani, B. Maini, P.P. Almaso, Propagation of nanocatalyst particles through Athabasca sands, in: *J. Can. Pet. Technol.*, Society of Petroleum Engineers, 2013: pp. 279–288. doi:10.2118/148855-PA.
- [51] A. Wahab, A. Hassan, M.A. Qasim, H.M. Ali, H. Babar, M.U. Sajid, Solar energy systems – Potential of nanofluids, *J. Mol. Liq.* 289 (2019). doi:10.1016/j.molliq.2019.111049.
- [52] H.D. Koca, S. Doganay, A. Turgut, I.H. Tavman, R. Saidur, I.M. Mahbubul, Effect of particle size on the viscosity of nanofluids: A review, *Renew. Sustain. Energy Rev.* 82 (2018) 1664–1674. doi:10.1016/j.rser.2017.07.016.
- [53] E. Natarajan, R. Sathish, Role of nanofluids in solar water heater, *Int. J. Adv. Manuf. Technol.* (2009). doi:10.1007/s00170-008-1876-8.
- [54] K.R. Chaturvedi, T. Sharma, Carbonated polymeric nanofluids for enhanced oil recovery from sandstone reservoir, *J. Pet. Sci. Eng.* 194 (2020) 107499. doi:10.1016/j.petrol.2020.107499.
- [55] S.F. Tolesorkhi, F. Esmaeilzadeh, M. Riazi, Experimental and theoretical investigation of CO₂ mass transfer enhancement of silica nanoparticles in water, *Pet. Res.* 3 (2018) 370–380. doi:10.1016/j.ptlrs.2018.09.002.

- [56] B.A. Suleimanov, F.S. Ismailov, E.F. Veliyev, Nanofluid for enhanced oil recovery, *J. Pet. Sci. Eng.* 78 (2011) 431–437. doi:10.1016/j.petrol.2011.06.014.
- [57] B. Wei, Q. Li, F. Jin, H. Li, C. Wang, The Potential of a Novel Nanofluid in Enhancing Oil Recovery, *Energy and Fuels*. 30 (2016) 2882–2891. doi:10.1021/acs.energyfuels.6b00244.
- [58] H. Ehtesabi, M. Mahdi Ahadian, V. Taghikhani, Enhanced heavy oil recovery using TiO₂ nanoparticles: Investigation of deposition during transport in core plug, *Energy and Fuels*. 29 (2015) 1–8. doi:10.1021/ef5015605.
- [59] Z. Zhang, W. He, J. Zheng, G. Wang, J. Ji, Rice Husk Ash-Derived Silica Nanofluids: Synthesis and Stability Study, *Nanoscale Res. Lett.* 11 (2016) 502. doi:10.1186/s11671-016-1726-9.
- [60] H. Chen, A.S. Elhag, Y. Chen, J.A. Noguera, A.M. AlSumaiti, G.J. Hirasaki, Q.P. Nguyen, S.L. Biswal, S. Yang, K.P. Johnston, Oil effect on CO₂ foam stabilized by a switchable amine surfactant at high temperature and high salinity, *Fuel*. 227 (2018) 247–255. doi:10.1016/j.fuel.2018.04.020.
- [61] M. Khajepour, S. Reza Etminan, J. Goldman, F. Wassmuth, Nanoparticles as foam stabilizer for steam-foam process, in: *Soc. Pet. Eng. - SPE EOR Conf. Oil Gas West Asia, OGWA 2016*, Society of Petroleum Engineers, 2016. doi:10.2118/179826-ms.
- [62] T. Sharma, S. Iglauer, J.S. Sangwai, Silica Nanofluids in an Oilfield Polymer Polyacrylamide: Interfacial Properties, Wettability Alteration, and Applications for Chemical Enhanced Oil Recovery, *Ind. Eng. Chem. Res.* 55 (2016) 12387–12397. doi:10.1021/acs.iecr.6b03299.
- [63] K.R. Chaturvedi, R. Narukulla, T. Sharma, CO₂ capturing evaluation of single-step silica nanofluid through rheological investigation for nanofluid use in carbon utilization applications, *J. Mol. Liq.* 304 (2020) 112765.

- doi:10.1016/j.molliq.2020.112765.
- [64] H. Setia, R. Gupta, R.K. Wanchoo, Stability of nanofluids, *Mater. Sci. Forum.* 757 (2013) 139–149. doi:10.4028/www.scientific.net/MSF.757.139.
- [65] S.U. Ilyas, R. Pendyala, N. Marneni, Stability of Nanofluids, (2017) 1–31. doi:10.1007/978-3-319-29761-3_1.
- [66] H. Loria, P. Pereira-Almao, C.E. Scott, Determination of Agglomeration Kinetics in Nanoparticle Dispersions, *Ind. Eng. Chem. Res.* 50 (2011) 8529–8535. doi:10.1021/ie200135r.
- [67] K.H. Solangi, S.N. Kazi, M.R. Luhur, A. Badarudin, A. Amiri, R. Sadri, M.N.M. Zubir, S. Gharekhani, K.H. Teng, A comprehensive review of thermo-physical properties and convective heat transfer to nanofluids, *Energy.* 89 (2015) 1065–1086. doi:10.1016/j.energy.2015.06.105.
- [68] S. Chakraborty, P.K. Panigrahi, Stability of nanofluid: A review, *Appl. Therm. Eng.* 174 (2020) 115259. doi:10.1016/j.applthermaleng.2020.115259.
- [69] Z. Haddad, C. Abid, H.F. Oztop, A. Mataoui, A review on how the researchers prepare their nanofluids, *Int. J. Therm. Sci.* 76 (2014) 168–189. doi:10.1016/j.ijthermalsci.2013.08.010.
- [70] W. Yu, H. Xie, A review on nanofluids: Preparation, stability mechanisms, and applications, *J. Nanomater.* 2012 (2012) 435873. doi:10.1155/2012/435873.
- [71] B. Nazarian, R. Held, L. Høier, P. Ringrose, Reservoir management of CO₂ injection: Pressure control and capacity enhancement, in: *Energy Procedia*, Elsevier Ltd, 2013: pp. 4533–4543. doi:10.1016/j.egypro.2013.06.360.
- [72] A.S. Haddad, I. Gates, CO₂-based heavy oil recovery processes for post-CHOPS reservoirs, *J. CO₂ Util.* 19 (2017) 238–246. doi:10.1016/j.jcou.2017.03.019.
- [73] P. Zuloaga, W. Yu, J. Miao, K. Sepehrnoori, Performance evaluation of CO₂ Huff-

- n-Puff and continuous CO₂ injection in tight oil reservoirs, *Energy*. 134 (2017) 181–192. doi:10.1016/j.energy.2017.06.028.
- [74] H. Yu, Z. Rui, Z. Chen, X. Lu, Z. Yang, J. Liu, X. Qu, S. Patil, K. Ling, J. Lu, Feasibility study of improved unconventional reservoir performance with carbonated water and surfactant, *Energy*. 182 (2019) 135–147. doi:10.1016/j.energy.2019.06.024.
- [75] F. van Bergen, J. Gale, K.J. Damen, A.F.B. Wildenborg, Worldwide selection of early opportunities for CO₂-enhanced oil recovery and CO₂-enhanced coal bed methane production, *Energy*. 29 (2004) 1611–1621. doi:10.1016/j.energy.2004.03.063.
- [76] N. Mosavat, F. Torabi, Performance of secondary carbonated water injection in light oil systems, *Ind. Eng. Chem. Res.* 53 (2014) 1262–1273. doi:10.1021/ie402381z.
- [77] M.K. Emera, H.K. Sarma, Prediction of CO₂ solubility in oil and the effects on the oil physical properties, *Energy Sources, Part A Recover. Util. Environ. Eff.* 29 (2007) 1233–1242. doi:10.1080/00908310500434481.
- [78] X. Zhou, Q. Yuan, Y. Zhang, H. Wang, F. Zeng, L. Zhang, Performance evaluation of CO₂ flooding process in tight oil reservoir via experimental and numerical simulation studies, *Fuel*. 236 (2019) 730–746. doi:10.1016/j.fuel.2018.09.035.
- [79] G. Lv, Q. Li, S. Wang, X. Li, Key techniques of reservoir engineering and injection-production process for CO₂ flooding in China's SINOPEC Shengli Oilfield, *J. CO₂ Util.* 11 (2015) 31–40. doi:10.1016/j.jcou.2014.12.007.
- [80] H. Hao, J. Hou, F. Zhao, Z. Song, L. Hou, Z. Wang, Gas channeling control during CO₂ immiscible flooding in 3D radial flow model with complex fractures and heterogeneity, *J. Pet. Sci. Eng.* 146 (2016) 890–901. doi:10.1016/j.petrol.2016.07.034.

- [81] Y. Zhang, M. Gao, Q. You, H. Fan, W. Li, Y. Liu, J. Fang, G. Zhao, Z. Jin, C. Dai, Smart mobility control agent for enhanced oil recovery during CO₂ flooding in ultra-low permeability reservoirs, *Fuel*. (2019) 442–450. doi:10.1016/j.fuel.2018.12.069.
- [82] M. Motealleh, R. Kharrat, A. Hashemi, An experimental investigation of water-alternating-CO₂ coreflooding in a carbonate oil reservoir in different initial core conditions, *Energy Sources, Part A Recover. Util. Environ. Eff.* 35 (2013) 1187–1196. doi:10.1080/15567036.2010.516315.
- [83] M. Sagir, I.M. Tan, M. Mushtaq, M. Pervaiz, M.S. Tahir, K. Shahzad, CO₂ mobility control using CO₂ philic surfactant for enhanced oil recovery, *J. Pet. Explor. Prod. Technol.* 6 (2016) 401–407. doi:10.1007/s13202-015-0192-8.
- [84] H. Yu, S. Hermann, S.E. Schulz, T. Gessner, Z. Dong, W.J. Li, Optimizing sonication parameters for dispersion of single-walled carbon nanotubes, *Chem. Phys.* 408 (2012) 11–16. doi:10.1016/j.chemphys.2012.08.020.
- [85] M. Sohrabi, M. Riazi, M. Jamiolahmady, N. Idah Kechut, S. Ireland, G. Robertson, Carbonated water injection (CWI)—A productive way of using CO₂ for oil recovery and CO₂ storage, *Energy Procedia*. 4 (2011) 2192–2199. doi:10.1016/J.EGYPRO.2011.02.106.
- [86] A. Khezrnejad, L.A. James, T.E. Johansen, Water Enhancement Using Nanoparticles in Water Alternating Gas (WAG) Micromodel Experiments, in: Society of Petroleum Engineers (SPE), 2014. doi:10.2118/173484-stu.
- [87] M. Lv, S. Wang, Studies on CO₂ foam stability and the influence of polymer on CO₂ foam properties, *Int. J. Oil, Gas Coal Technol.* 10 (2015) 343–358. doi:10.1504/IJOGCT.2015.072077.
- [88] K.G. Uranta, S. Rezaei-Gomari, P. Russell, F. Hamad, Studying the Effectiveness of

- Polyacrylamide (PAM) application in hydrocarbon reservoirs at different operational conditions, *Energies*. 11 (2018). doi:10.3390/en11092201.
- [89] L.S. Semko, S. V. Khutornoi, N. V. Abramov, P.P. Gorbik, Synthesis, structure, and properties of large surface area Fe₃O₄/SiO₂ nanocomposites, *Inorg. Mater.* 48 (2012) 374–381. doi:10.1134/S0020168512040127.
- [90] D.T. Wasan, A.D. Nikolov, Spreading of nanofluids on solids, *Nature*. 423 (2003) 156–159. doi:10.1038/nature01591.
- [91] P.T. Leung, N. Do, L. Klees, W.P. Leung, F. Tong, L. Lam, W. Zapka, A.C. Tam, Transmission studies of explosive vaporization of a transparent liquid film on an opaque solid surface induced by excimer-laser-pulsed irradiation, *J. Appl. Phys.* 72 (1992) 2256–2263. doi:10.1063/1.351619.
- [92] J. Yuan, M.-P. Yang, W.-Y. Zhi, H. Wang, H. Wang, J.-X. Lu, Efficient electrochemical reduction of CO₂ to ethanol on Cu nanoparticles decorated on N-doped graphene oxide catalysts, *J. CO₂ Util.* 33 (2019) 452–460. doi:10.1016/j.jcou.2019.07.014.
- [93] N. Yekeen, M.A. Manan, A.K. Idris, A.M. Samin, A.R. Risal, Experimental investigation of minimization in surfactant adsorption and improvement in surfactant-foam stability in presence of silicon dioxide and aluminum oxide nanoparticles, *J. Pet. Sci. Eng.* 159 (2017) 115–134. doi:10.1016/j.petrol.2017.09.021.
- [94] C. Fu, J. Yu, N. Liu, The effect of foam quality, particle concentration and flow rate on nanoparticle-stabilized CO₂ mobility control foams, *RSC Adv.* 9 (2019) 9313–9322. doi:10.1039/c8ra10352f.
- [95] F. Guo, S.A. Aryana, Nanoparticle-Stabilized CO₂ Foam Flooding, in: 2019: pp. 61–63. doi:10.1007/978-3-030-01578-7_15.

- [96] F. Guo, S. Aryana, An experimental investigation of nanoparticle-stabilized CO₂ foam used in enhanced oil recovery, *Fuel*. 186 (2016) 430–442. doi:10.1016/j.fuel.2016.08.058.
- [97] M.A. Manan, S. Farad, A. Piroozian, M.J.A. Esmail, Effects of Nanoparticle Types on Carbon Dioxide Foam Flooding in Enhanced Oil Recovery, *Pet. Sci. Technol.* 33 (2015) 1286–1294. doi:10.1080/10916466.2015.1057593.
- [98] A.R. Risal, M.A. Manan, N. Yekeen, N.B. Azli, A.M. Samin, X.K. Tan, Experimental investigation of enhancement of carbon dioxide foam stability, pore plugging, and oil recovery in the presence of silica nanoparticles, *Pet. Sci.* 16 (2019) 344–356. doi:10.1007/s12182-018-0280-8.
- [99] S. Alzobaidi, M. Lotfollahi, I. Kim, K.P. Johnston, D.A. DiCarlo, Carbon Dioxide-in-Brine Foams at High Temperatures and Extreme Salinities Stabilized with Silica Nanoparticles, *Energy and Fuels*. 31 (2017) 10680–10690. doi:10.1021/acs.energyfuels.7b01814.
- [100] A. Zamani, B. Maini, P. Pereira-Almao, Flow of nanodispersed catalyst particles through porous media: Effect of permeability and temperature, *Can. J. Chem. Eng.* 90 (2012) 304–314. doi:10.1002/cjce.20629.
- [101] S. Al-Anssari, A. Barifcani, S. Wang, L. Maxim, S. Iglauer, Wettability alteration of oil-wet carbonate by silica nanofluid, *J. Colloid Interface Sci.* 461 (2016) 435–442. doi:10.1016/j.jcis.2015.09.051.
- [102] S. Le Van, B.H. Chon, Chemical flooding in heavy-oil reservoirs: From technical investigation to optimization using response surface methodology, *Energies*. 9 (2016). doi:10.3390/en9090711.
- [103] N. Ali, J.A. Teixeira, A. Addali, A Review on Nanofluids: Fabrication, Stability, and Thermophysical Properties, *J. Nanomater.* 2018 (2018). doi:10.1155/2018/6978130.

- [104] W. Stober, A. Fink, D. Ernst Bohn, Controlled Growth of Monodisperse Silica Spheres in the Micron Size Range 1, 1968.
- [105] K.S. Rao, K. El-Hami, T. Kodaki, K. Matsushige, K. Makino, A novel method for synthesis of silica nanoparticles., *J. Colloid Interface Sci.* 289 (2005) 125–31. doi:10.1016/j.jcis.2005.02.019.
- [106] S.H. Kim, W.G. Kim, H.U. Kang, K.M. Jung, Synthesis of silica nanofluid and application to CO₂ absorption, *Sep. Sci. Technol.* 43 (2008) 3036–3055. doi:10.1080/01496390802063804.
- [107] J.K. Bailey, M.L. Mecartney, Formation of colloidal silica particles from alkoxides, *Colloids and Surfaces.* 63 (1992) 151–161. doi:10.1016/0166-6622(92)80081-C.
- [108] A. Thomas, Polymer Flooding, in: *Chem. Enhanc. Oil Recover. - a Pract. Overv.*, InTech, 2016. doi:10.5772/64623.
- [109] R. Goswami, K.R. Chaturvedi, R.S. Kumar, B.H. Chon, T. Sharma, Effect of ionic strength on crude emulsification and EOR potential of micellar flood for oil recovery applications in high saline environment, *J. Pet. Sci. Eng.* 170 (2018) 49–61. doi:10.1016/j.petrol.2018.06.040.
- [110] S. Bhakta, C.K. Dixit, I. Bist, K.A. Jalil, S.L. Suib, J.F. Rusling, Sodium hydroxide catalyzed monodispersed high surface area silica nanoparticles, *Mater. Res. Express.* 3 (2016). doi:10.1088/2053-1591/3/7/075025.
- [111] S. Santra, R. Tapeç, N. Theodoropoulou, J. Dobson, A. Hebard, W. Tan, Synthesis and characterization of silica-coated iron oxide nanoparticles in microemulsion: The effect of nonionic surfactants, *Langmuir.* 17 (2001) 2900–2906. doi:10.1021/la0008636.
- [112] X. Li, D. Zhu, X. Wang, Evaluation on dispersion behavior of the aqueous copper nano-suspensions, *J. Colloid Interface Sci.* 310 (2007) 456–463.

- doi:10.1016/j.jcis.2007.02.067.
- [113] X. Wei, H. Zhu, T. Kong, L. Wang, Synthesis and thermal conductivity of Cu₂O nanofluids, *Int. J. Heat Mass Transf.* 52 (2009) 4371–4374. doi:10.1016/j.ijheatmasstransfer.2009.03.073.
- [114] E. V. Timofeeva, M.R. Moravek, D. Singh, Improving the heat transfer efficiency of synthetic oil with silica nanoparticles, *J. Colloid Interface Sci.* 364 (2011) 71–79. doi:10.1016/j.jcis.2011.08.004.
- [115] O. Weichold, B. Tigges, M. Bertmer, M. Möller, A comparative study on the dispersion stability of aminofunctionalised silica nanoparticles made from sodium silicate, *J. Colloid Interface Sci.* 324 (2008) 105–109. doi:10.1016/j.jcis.2008.04.060.
- [116] M. Zhao, W. Lv, Y. Li, C. Dai, H. Zhou, X. Song, Y. Wu, A Study on Preparation and Stabilizing Mechanism of Hydrophobic Silica Nanofluids, *Materials (Basel)*. 11 (2018) 1385. doi:10.3390/ma11081385.
- [117] A. Ghadimi, R. Saidur, H.S.C. Metselaar, A review of nanofluid stability properties and characterization in stationary conditions, *Int. J. Heat Mass Transf.* 54 (2011) 4051–4068. doi:10.1016/j.ijheatmasstransfer.2011.04.014.
- [118] R.O. Afolabi, Enhanced oil recovery for emergent energy demand: challenges and prospects for a nanotechnology paradigm shift, *Int. Nano Lett.* 9 (2019) 1–15. doi:10.1007/s40089-018-0248-0.
- [119] T. Zhang, D. Davidson, S.L. Bryant, C. Huh, Nanoparticle-Stabilized Emulsions for Applications in Enhanced Oil Recovery, in: *SPE Improv. Oil Recover. Symp.*, Society of Petroleum Engineers, 2010. doi:10.2118/129885-MS.
- [120] C. Bantz, O. Koshkina, T. Lang, H.-J. Galla, C.J. Kirkpatrick, R.H. Stauber, M. Maskos, The surface properties of nanoparticles determine the agglomeration state

- and the size of the particles under physiological conditions, *Beilstein J. Nanotechnol.* 5 (2014) 1774–1786. doi:10.3762/bjnano.5.188.
- [121] P. Zhang, J. Xia, S. Luo, Generation of Well-Defined Micro/Nanoparticles via Advanced Manufacturing Techniques for Therapeutic Delivery, *Materials* (Basel). 11 (2018) 623. doi:10.3390/ma11040623.
- [122] X. Zhu, C. Vo, M. Taylor, B.R. Smith, Non-spherical micro- and nanoparticles in nanomedicine, *Mater. Horizons.* 6 (2019) 1094–1121. doi:10.1039/c8mh01527a.
- [123] C.M. Lee, J.D. Kubicki, B. Fan, L. Zhong, M.C. Jarvis, S.H. Kim, Hydrogen-Bonding Network and OH Stretch Vibration of Cellulose: Comparison of Computational Modeling with Polarized IR and SFG Spectra, *J. Phys. Chem. B.* 119 (2015) 15138–15149. doi:10.1021/acs.jpcc.5b08015.
- [124] M. Hernández-Ortiz, L.S. Acosta-Torres, G. Hernández-Padrón, A.I. Mendieta, R. Bernal, C. Cruz-Vázquez, V.M. Castaño, Biocompatibility of crystalline opal nanoparticles, *Biomed. Eng. Online.* 11 (2012). doi:10.1186/1475-925X-11-78.
- [125] D.B. Stojanović, L. Brajović, A. Orlović, D. Dramlić, V. Radmilović, P.S. Uskoković, R. Aleksić, Transparent PMMA/silica nanocomposites containing silica nanoparticles coating under supercritical conditions, *Prog. Org. Coatings.* 76 (2013) 626–631. doi:10.1016/j.porgcoat.2012.12.002.
- [126] I.A. Rahman, P. Vejayakumaran, C.S. Sipaut, J. Ismail, C.K. Chee, Size-dependent physicochemical and optical properties of silica nanoparticles, *Mater. Chem. Phys.* 114 (2009) 328–332. doi:10.1016/j.matchemphys.2008.09.068.
- [127] R.S. Kumar, T. Sharma, Stability and rheological properties of nanofluids stabilized by SiO₂ nanoparticles and SiO₂-TiO₂ nanocomposites for oilfield applications, *Colloids Surfaces A Physicochem. Eng. Asp.* 539 (2018) 171–183. doi:10.1016/j.colsurfa.2017.12.028.

- [128] R. Phukan, S.B. Gogoi, P. Tiwari, Enhanced oil recovery by alkaline-surfactant-alternated-gas/CO₂ flooding, *J. Pet. Explor. Prod. Technol.* 9 (2019) 247–260. doi:10.1007/s13202-018-0465-0.
- [129] J.A. Clark, E.E. Santiso, Carbon Sequestration through CO₂ Foam-Enhanced Oil Recovery: A Green Chemistry Perspective, *Engineering*. 4 (2018) 336–342. doi:10.1016/j.eng.2018.05.006.
- [130] L. Sun, W. Pu, J. Xin, P. Wei, B. Wang, Y. Li, C. Yuan, High temperature and oil tolerance of surfactant foam/polymer-surfactant foam, *RSC Adv.* 5 (2015) 23410–23418. doi:10.1039/c4ra17216g.
- [131] M.V. Bennetzen, K. Mogensen, Novel Applications of Nanoparticles for Future Enhanced Oil Recovery, in: *Int. Pet. Technol. Conf., International Petroleum Technology Conference, 2014*. doi:10.2523/IPTC-17857-MS.
- [132] C. Huang, M. Cui, Z. Sun, F. Liu, B.A. Helms, T.P. Russell, Self-Regulated Nanoparticle Assembly at Liquid/Liquid Interfaces: A Route to Adaptive Structuring of Liquids, *Langmuir*. 33 (2017) 7994–8001. doi:10.1021/acs.langmuir.7b01685.
- [133] X. Sun, Y. Zhang, G. Chen, Z. Gai, Application of Nanoparticles in Enhanced Oil Recovery: A Critical Review of Recent Progress, *Energies*. 10 (2017) 345. doi:10.3390/en10030345.
- [134] Y. Wang, Y. Zhang, Y. Liu, L. Zhang, S. Ren, J. Lu, X. Wang, N. Fan, The stability study of CO₂ foams at high pressure and high temperature, *J. Pet. Sci. Eng.* 154 (2017) 234–243. doi:10.1016/j.petrol.2017.04.029.
- [135] A.S. Aronson, V. Bergeron, M.E. Fagan, C.J. Radke, The influence of disjoining pressure on foam stability and flow in porous media, *Colloids Surfaces A Physicochem. Eng. Asp.* 83 (1994) 109–120. doi:10.1016/0927-7757(94)80094-4.

- [136] V.G. Babak, M.-J. Stébé, Highly Concentrated Emulsions: Physicochemical Principles of Formulation, *J. Dispers. Sci. Technol.* 23 (2002) 1–22. doi:10.1080/01932690208984184.
- [137] N.D. Denkov, Mechanisms of Foam Destruction by Oil-Based Antifoams, *Langmuir*. 20 (2004) 9463–9505. doi:10.1021/LA049676O.
- [138] L. Minssieux, OIL DISPLACEMENT BY FOAMS IN RELATION TO THEIR PHYSICAL PROPERTIES IN POROUS MEDIA., *JPT, J. Pet. Technol.* 26 (1974) 100–108. doi:10.2118/3991-PA.
- [139] A. Telmadarreie, J. Trivedi, Static and Dynamic Performance of Wet Foam and Polymer-Enhanced Foam in the Presence of Heavy Oil, *Colloids and Interfaces*. 2 (2018) 38. doi:10.3390/colloids2030038.
- [140] P.R. Garrett, The Mode of Action of Antifoams, in: *Defoaming*, CRC Press, 2018: pp. 1–118. doi:10.1201/9781315140827-1.
- [141] J. V. Robinson, W.W. Woods, A method of selecting foam inhibitors, *J. Soc. Chem. Ind.* 67 (1948) 361–365. doi:10.1002/jctb.5000670908.
- [142] H.C. Lau, S.M. O'Brien, Effects of spreading and nonspreading oils on foam propagation through porous media, *SPE Reserv. Eng. (Society Pet. Eng.* 3 (1988) 893–896. doi:10.2118/15668-PA.
- [143] K. Koczó, L.A. Lobo, D.T. Wasan, Effect of oil on foam stability: Aqueous foams stabilized by emulsions, *J. Colloid Interface Sci.* 150 (1992) 492–506. doi:10.1016/0021-9797(92)90218-B.
- [144] R. Aveyard, B.P. Binks, P.D.I. Fletcher, T.G. Peck, P.R. Garrett, Entry and spreading of alkane drops at the air/surfactant solution interface in relation to foam and soap film stability, *J. Chem. Soc. Faraday Trans.* 89 (1993) 4313–4321. doi:10.1039/FT9938904313.

- [145] K. Osei-Bonsu, N. Shokri, P. Grassia, Foam stability in the presence and absence of hydrocarbons: From bubble- to bulk-scale, *Colloids Surfaces A Physicochem. Eng. Asp.* 481 (2015) 514–526. doi:10.1016/j.colsurfa.2015.06.023.
- [146] G.C. Wang, A Study of Crude Oil Composition During CO₂ Extraction Process, in: Calif. Reg. Meet., Society of Petroleum Engineers, 1986: pp. 423–426. doi:10.2118/15085-MS.
- [147] K.D. Hagedorn, F.M. Orr, Component partitioning in CO₂/crude oil systems: effects of oil composition on CO₂ displacement performance, *SPE Adv. Technol. Ser.* 2 (1994) 177–184. doi:10.2118/25169-pa.
- [148] P. Diwu, T. Liu, Z. You, G. Hou, R. Qiao, L. Zhao, Study on pulse characteristic of produced crude composition in CO₂ flooding pilot test, *Geofluids*. 2018 (2018). doi:10.1155/2018/2968629.
- [149] M. Bickle, N. Kampman, H. Chapman, C. Ballentine, B. Dubacq, A. Galy, T. Sirikitputtisak, O. Warr, M. Wigley, Z. Zhou, Rapid reactions between CO₂, brine and silicate minerals during geological carbon storage: Modelling based on a field CO₂ injection experiment, *Chem. Geol.* 468 (2017) 17–31. doi:10.1016/j.chemgeo.2017.07.031.
- [150] T. Zhou, X. Liu, Z. Yang, X. Li, S. Wang, Experimental analysis on reservoir blockage mechanism for CO₂ flooding, *Pet. Explor. Dev.* 42 (2015) 548–553. doi:10.1016/S1876-3804(15)30048-3.
- [151] M. Al-Hindi, F. Azizi, Absorption and desorption of carbon dioxide in several water types, *Can. J. Chem. Eng.* 96 (2018) 274–284. doi:10.1002/cjce.22901.
- [152] X. Ma, Y. Abe, A. Kaneko, S. Fujimoto, C. Murakami, Study on Dissolution Process of Liquid CO₂ into Water under High Pressure Condition for CCS, in: *Energy Procedia*, Elsevier Ltd, 2017: pp. 5430–5437. doi:10.1016/j.egypro.2017.03.1687.

- [153] M. Franco-Aguirre, R.D. Zabala, S.H. Lopera, C.A. Franco, F.B. Cortés, Interaction of anionic surfactant-nanoparticles for gas - Wettability alteration of sandstone in tight gas-condensate reservoirs, *J. Nat. Gas Sci. Eng.* 51 (2018) 53–64. doi:10.1016/j.jngse.2017.12.027.
- [154] A.U. Rognmo, H. Horjen, M.A. Fernø, Nanotechnology for improved CO₂ utilization in CCS: Laboratory study of CO₂-foam flow and silica nanoparticle retention in porous media, *Int. J. Greenh. Gas Control.* 64 (2017) 113–118. doi:10.1016/j.ijggc.2017.07.010.
- [155] P. Babakhani, J. Bridge, R. an Doong, T. Phenrat, Continuum-based models and concepts for the transport of nanoparticles in saturated porous media: A state-of-the-science review, *Adv. Colloid Interface Sci.* 246 (2017) 75–104. doi:10.1016/j.cis.2017.06.002.
- [156] P. Babakhani, The impact of nanoparticle aggregation on their size exclusion during transport in porous media: One- and three-dimensional modelling investigations, *Sci. Rep.* 9 (2019). doi:10.1038/s41598-019-50493-6.
- [157] J. Bowers, H. Cao, G. Qiao, Q. Li, G. Zhang, E. Mura, Y. Ding, Flow and heat transfer behaviour of nanofluids in microchannels, *Prog. Nat. Sci. Mater. Int.* 28 (2018) 225–234. doi:10.1016/j.pnsc.2018.03.005.
- [158] P. Christian, F. Von Der Kammer, M. Baalousha, T. Hofmann, Nanoparticles: Structure, properties, preparation and behaviour in environmental media, *Ecotoxicology.* 17 (2008) 326–343. doi:10.1007/s10646-008-0213-1.
- [159] R.S. Kumar, T. Sharma, Stable SiO₂–TiO₂ composite-based nanofluid of improved rheological behaviour for high-temperature oilfield applications, *Geosystem Eng.* (2020) 1–11. doi:10.1080/12269328.2020.1713909.
- [160] T. Sharma, G. Suresh Kumar, J.S. Sangwai, Enhanced oil recovery using oil-in-

- water (o/w) emulsion stabilized by nanoparticle, surfactant and polymer in the presence of NaCl, *Geosystem Eng.* 17 (2014) 195–205. doi:10.1080/12269328.2014.959622.
- [161] C.O. Metin, R.T. Bonnecaze, L.W. Lake, C.R. Miranda, Q.P. Nguyen, Aggregation kinetics and shear rheology of aqueous silica suspensions, *Appl. Nanosci.* 4 (2014) 169–178. doi:10.1007/s13204-012-0185-6.
- [162] A. Behzadi, A. Mohammadi, Environmentally responsive surface-modified silica nanoparticles for enhanced oil recovery, *J. Nanoparticle Res.* 18 (2016) 1–19. doi:10.1007/s11051-016-3580-1.
- [163] S. Al-Anssari, M. Arif, S. Wang, A. Barifcani, S. Iglauer, Stabilising nanofluids in saline environments, *J. Colloid Interface Sci.* 508 (2017) 222–229. doi:10.1016/j.jcis.2017.08.043.
- [164] H. Pham, Q.P. Nguyen, Effect of silica nanoparticles on clay swelling and aqueous stability of nanoparticle dispersions, *J. Nanoparticle Res.* 16 (2014) 1–11. doi:10.1007/s11051-013-2137-9.
- [165] I. Kim, A.J. Worthen, K.P. Johnston, D.A. DiCarlo, C. Huh, Size-dependent properties of silica nanoparticles for Pickering stabilization of emulsions and foams, *J. Nanoparticle Res.* 18 (2016) 1–12. doi:10.1007/s11051-016-3395-0.
- [166] G.M. El-sayed, M.M. Kamel, N.S. Morsy, F.A. Taher, Encapsulation of nano Disperse Red 60 via modified miniemulsion polymerization. I. Preparation and characterization, *J. Appl. Polym. Sci.* 125 (2012) 1318–1329. doi:10.1002/app.35102.
- [167] H. Shamsijazeyi, C.A. Miller, M.S. Wong, J.M. Tour, R. Verduzco, Polymer-coated nanoparticles for enhanced oil recovery, *J. Appl. Polym. Sci.* 131 (2014) 40576. doi:10.1002/app.40576.

- [168] S. Ahualli, G.R. Iglesias, W. Wachter, M. Dulle, D. Minami, O. Glatter, Adsorption of anionic and cationic surfactants on anionic colloids: Supercharging and destabilization, *Langmuir*. 27 (2011) 9182–9192. doi:10.1021/la201242d.
- [169] T. Sharma, G.S. Kumar, J.S. Sangwai, Comparative effectiveness of production performance of Pickering emulsion stabilized by nanoparticle-surfactant-polymer over surfactant-polymer (SP) flooding for enhanced oil recovery for Brownfield reservoir, *J. Pet. Sci. Eng.* 129 (2015) 221–232. doi:10.1016/j.petrol.2015.03.015.
- [170] A. Haghtalab, S. Rahimi, Study of viscoelastic properties of nanocomposites of SiO₂-acrylonitrile-butadiene-styrene, *J. Appl. Polym. Sci.* 127 (2013) 4318–4327. doi:10.1002/app.38041.
- [171] F. Devínsky, L. Masárová, I. Lacko, Surface activity and micelle formation of some new bisquaternary ammonium salts, *J. Colloid Interface Sci.* 105 (1985) 235–239. doi:10.1016/0021-9797(85)90363-7.
- [172] K. Rahimi, M. Adibifard, Experimental study of the nanoparticles effect on surfactant absorption and oil recovery in one of the Iranian oil reservoirs, *Pet. Sci. Technol.* 33 (2015) 79–85. doi:10.1080/10916466.2014.950382.
- [173] M.A. Ahmadi, S.R. Shadizadeh, Induced effect of adding nano silica on adsorption of a natural surfactant onto sandstone rock: Experimental and theoretical study, *J. Pet. Sci. Eng.* 112 (2013) 239–247. doi:10.1016/j.petrol.2013.11.010.
- [174] G. Cheraghian, S.S. Khalili Nezhad, M. Kamari, M. Hemmati, M. Masihi, S. Bazgir, Adsorption polymer on reservoir rock and role of the nanoparticles, clay and SiO₂, *Int. Nano Lett.* 4 (2014) 1–8. doi:10.1007/s40089-014-0114-7.
- [175] T. Amirianshoja, R. Junin, A. Kamal Idris, O. Rahmani, A comparative study of surfactant adsorption by clay minerals, *J. Pet. Sci. Eng.* 101 (2013) 21–27.

- doi:10.1016/j.petrol.2012.10.002.
- [176] K.R. Chaturvedi, A.K. Singh, T. Sharma, Impact of shale on properties and oil recovery potential of sandstone formation for low-salinity waterflooding applications, *Asia-Pacific J. Chem. Eng.* 14 (2019). doi:10.1002/apj.2352.
- [177] V. Arabli, A. Aghili, The effect of silica nanoparticles, thermal stability, and modeling of the curing kinetics of epoxy/silica nanocomposite, *Adv. Compos. Mater.* 24 (2015) 561–577. doi:10.1080/09243046.2014.944254.
- [178] G.H. Hsiue, Y.L. Liu, H.H. Liao, Flame-retardant epoxy resins: An approach from organic-inorganic hybrid nanocomposites, *J. Polym. Sci. Part A Polym. Chem.* 39 (2001) 986–996. doi:10.1002/1099-0518(20010401)39:7<986::aid-pola1074>3.0.co;2-w.
- [179] V. Vajihinejad, S.P. Gumfekar, B. Bazoubandi, Z. Rostami Najafabadi, J.B.P. Soares, Water Soluble Polymer Flocculants: Synthesis, Characterization, and Performance Assessment, *Macromol. Mater. Eng.* 304 (2019) 1800526. doi:10.1002/mame.201800526.
- [180] N. Hu, Y. Li, Z. Wu, K. Lu, D. Huang, W. Liu, Foams stabilization by silica nanoparticle with cationic and anionic surfactants in column flotation: Effects of particle size, *J. Taiwan Inst. Chem. Eng.* 88 (2018) 62–69. doi:10.1016/j.jtice.2018.04.008.
- [181] A.F. Belhaj, K.A. Elraies, S.M. Mahmood, N.N. Zulkifli, S. Akbari, O.S.E. Hussien, The effect of surfactant concentration, salinity, temperature, and pH on surfactant adsorption for chemical enhanced oil recovery: a review, *J. Pet. Explor. Prod. Technol.* 10 (2020) 125–137. doi:10.1007/s13202-019-0685-y.
- [182] Z. Wu, X. Yue, T. Cheng, J. Yu, H. Yang, Effect of viscosity and interfacial tension of surfactant-polymer flooding on oil recovery in high-temperature and high-salinity

- reservoirs, *J. Pet. Explor. Prod. Technol.* 4 (2014) 9–16. doi:10.1007/s13202-013-0078-6.
- [183] R. Saidur, K.Y. Leong, H.A. Mohammad, A review on applications and challenges of nanofluids, *Renew. Sustain. Energy Rev.* 15 (2011) 1646–1668. doi:10.1016/j.rser.2010.11.035.
- [184] S.K. Das, N. Putra, W. Roetzel, Pool boiling characteristics of nano-fluids, *Int. J. Heat Mass Transf.* 46 (2003) 851–862. doi:10.1016/S0017-9310(02)00348-4.
- [185] N.A. Ogolo, O.A. Olafuyi, M.O. Onyekonwu, Enhanced oil recovery using nanoparticles, in: *Soc. Pet. Eng. - SPE Saudi Arab. Sect. Tech. Symp. Exhib. 2012*, Society of Petroleum Engineers, 2012: pp. 276–284. doi:10.2118/160847-ms.
- [186] J. Shah, S. Kumar, M. Ranjan, Y. Sonvane, P. Thareja, S.K. Gupta, The effect of filler geometry on thermo-optical and rheological properties of CuO nanofluid, *J. Mol. Liq.* 272 (2018) 668–675. doi:10.1016/j.molliq.2018.09.117.
- [187] R. Essajai, A. Mzerd, N. Hassanain, M. Qjani, Thermal conductivity enhancement of nanofluids composed of rod-shaped gold nanoparticles: Insights from molecular dynamics, *J. Mol. Liq.* 293 (2019) 111494. doi:10.1016/j.molliq.2019.111494.
- [188] D. Lee, J.W. Kim, B.G. Kim, A new parameter to control heat transport in nanofluids: Surface charge state of the particle in suspension, *J. Phys. Chem. B.* 110 (2006) 4323–4328. doi:10.1021/jp057225m.
- [189] R. Bardool, A. Bakhtyari, F. Esmaeilzadeh, X. Wang, Nanofluid viscosity modeling based on the friction theory, *J. Mol. Liq.* 286 (2019). doi:10.1016/j.molliq.2019.110923.
- [190] L. Bai, C. Li, C. Korte, B.M.J. Huibers, A.R. Pales, W. Liang, D. Ladner, H. Daigle, C.J.G. Darnault, Effects of silica-based nanostructures with raspberry-like morphology and surfactant on the interfacial behavior of light, medium, and heavy

- crude oils at oil-aqueous interfaces, *Appl. Nanosci.* 7 (2017) 947–972.
doi:10.1007/s13204-017-0630-7.
- [191] M. Mohebbifar, M.H. Ghazanfari, M. Vossoughi, Experimental Investigation of Nano-Biomaterial Applications for Heavy Oil Recovery in Shaly Porous Models: A Pore-Level Study, *J. Energy Resour. Technol.* 137 (2015) 014501.
doi:10.1115/1.4028270.
- [192] Q. Meng, H. Liu, J. Wang, H. Liu, Effect of fluid viscosity on correlation of oil recovery by linear counter-current spontaneous imbibition, *J. Pet. Sci. Eng.* 151 (2017) 341–347. doi:10.1016/j.petrol.2017.01.008.
- [193] A. Bila, J.Å. Stensen, O. Torsæter, Experimental investigation of polymer-coated silica nanoparticles for enhanced oil recovery, *Nanomaterials.* 9 (2019).
doi:10.3390/nano9060822.
- [194] S. Thankappan, J. Abraham, S.C. George, S. Thomas, Rheological Characterization of Nanocomposites, in: *Charact. Nanomater.*, Elsevier, 2018: pp. 167–189.
doi:10.1016/b978-0-08-101973-3.00006-7.
- [195] T. Sharma, G.S. Kumar, J.S. Sangwai, Viscoelastic properties of oil-in-water (o/w) pickering emulsion stabilized by surfactant-polymer and nanoparticle-surfactant-polymer systems, *Ind. Eng. Chem. Res.* 54 (2015) 1576–1584.
doi:10.1021/ie504501a.
- [196] A.H.S. Dehaghani, R. Daneshfar, How much would silica nanoparticles enhance the performance of low-salinity water flooding?, *Pet. Sci.* (2019). doi:10.1007/s12182-019-0304-z.
- [197] M. Hasanzadeh, V. Mottaghitlab, M. Rezaei, Rheological and viscoelastic behavior of concentrated colloidal suspensions of silica nanoparticles: A response surface methodology approach, *Adv. Powder Technol.* 26 (2015) 1570–1577.

- doi:10.1016/j.appt.2015.08.011.
- [198] M.F. Fakoya, S.N. Shah, Effect of Silica Nanoparticles on the Rheological Properties and Filtration Performance of Surfactant-Based and Polymeric Fracturing Fluids and Their Blends, *SPE Drill. Complet.* 33 (2018) 100–114. doi:10.2118/163921-PA.
- [199] D. Zhu, L. Wei, B. Wang, Y. Feng, Aqueous hybrids of silica nanoparticles and hydrophobically associating hydrolyzed polyacrylamide used for EOR in high-temperature and high-salinity reservoirs, *Energies*. 7 (2014) 3858–3871. doi:10.3390/en7063858.
- [200] C.T. Nguyen, F. Desgranges, G. Roy, N. Galanis, T. Maré, S. Boucher, H. Angue Mintsa, Temperature and particle-size dependent viscosity data for water-based nanofluids - Hysteresis phenomenon, *Int. J. Heat Fluid Flow*. 28 (2007) 1492–1506. doi:10.1016/j.ijheatfluidflow.2007.02.004.
- [201] C. Esene, N. Rezaei, A. Aborig, S. Zendehboudi, Comprehensive review of carbonated water injection for enhanced oil recovery, *Fuel*. 237 (2019) 1086–1107. doi:10.1016/j.fuel.2018.08.106.
- [202] J. Wang, G. Xue, B. Tian, S. Li, K. Chen, D. Wang, Y. Sun, H. Xu, J.T. Petkov, Z. Li, Interaction between surfactants and SiO₂ nanoparticles in multiphase foam and its plugging ability, *Energy and Fuels*. 31 (2017) 408–417. doi:10.1021/acs.energyfuels.6b02592.
- [203] D. Li, B. Ren, L. Zhang, J. Ezekiel, S. Ren, Y. Feng, CO₂-sensitive foams for mobility control and channeling blocking in enhanced WAG process, *Chem. Eng. Res. Des.* 102 (2015) 234–243. doi:10.1016/j.cherd.2015.06.026.
- [204] E. Mahdavi, R. Khaledialidusti, A. Barnoush, Rheological properties of super critical CO₂ with Al₂O₃: Material type, size and temperature effect, *J. Mol. Liq.* 289 (2019). doi:10.1016/j.molliq.2019.111037.

- [205] A.K. Tiwari, P. Ghosh, J. Sarkar, Heat transfer and pressure drop characteristics of CeO₂/water nanofluid in plate heat exchanger, *Appl. Therm. Eng.* 57 (2013) 24–32. doi:10.1016/j.applthermaleng.2013.03.047.
- [206] S.M. Gatica, M.W. Cole, D. Velegol, Designing van der Waals forces between nanocolloids, *Nano Lett.* 5 (2005) 169–173. doi:10.1021/nl048265p.
- [207] R.R. Ujjwal, T. Sharma, J.S. Sangwai, U. Ojha, Rheological investigation of a random copolymer of polyacrylamide and polyacryloyl hydrazide (PAM-ran-PAH) for oil recovery applications, *J. Appl. Polym. Sci.* 134 (2017). doi:10.1002/app.44648.
- [208] A. V. Minakov, D. V. Guzei, M.I. Pryazhnikov, V.A. Zhigarev, V.Y. Rudyak, Study of turbulent heat transfer of the nanofluids in a cylindrical channel, *Int. J. Heat Mass Transf.* 102 (2016) 745–755. doi:10.1016/j.ijheatmasstransfer.2016.06.071.
- [209] E. V Timofeeva, D.S. Smith, W. Yu, D.M. France, D. Singh, J.L. Routbort, Particle size and interfacial effects on thermo-physical and heat transfer characteristics of water-based alpha-SiC nanofluids., *Nanotechnology.* 21 (2010) 215703. doi:10.1088/0957-4484/21/21/215703.
- [210] A. Vázquez-Quesada, R.I. Tanner, M. Ellero, Shear Thinning of Noncolloidal Suspensions., *Phys. Rev. Lett.* 117 (2016) 108001. doi:10.1103/PhysRevLett.117.108001.
- [211] H. Chen, Y. Ding, C. Tan, Rheological behaviour of nanofluids, *New J. Phys.* 9 (2007). doi:10.1088/1367-2630/9/10/367.
- [212] P.C. Mishra, S. Mukherjee, S.K. Nayak, A. Panda, A brief review on viscosity of nanofluids, *Int. Nano Lett.* 4 (2014) 109–120. doi:10.1007/s40089-014-0126-3.
- [213] L. Spinoso, A. Ayol, Rheological characterization of sludge, in: *Ind. Munic. Sludge*, Elsevier, 2019: pp. 225–252. doi:10.1016/b978-0-12-815907-1.00011-8.

- [214] J. Jung, J. Jang, J. Ahn, Characterization of a polyacrylamide solution used for remediation of petroleum contaminated soils, *Materials (Basel)*. 9 (2016). doi:10.3390/ma9010016.
- [215] S. Thomas, C.B. Panicker Sobhan, A review of experimental investigations on thermal phenomena in nanofluids, *Nanoscale Res. Lett.* 6 (2011) 1–21. doi:10.1186/1556-276X-6-377.
- [216] M. Kamibayashi, H. Ogura, Y. Otsubo, Rheological behavior of suspensions of silica nanoparticles in associating polymer solutions, *Ind. Eng. Chem. Res.* 45 (2006) 6899–6905. doi:10.1021/ie0512486.
- [217] A.J. Zhu, S.S. Sternstein, Nonlinear viscoelasticity of nanofilled polymers: Interfaces, chain statistics and properties recovery kinetics, *Compos. Sci. Technol.* 63 (2003) 1113–1126. doi:10.1016/S0266-3538(03)00032-0.
- [218] T. Sharma, J.S. Sangwai, Effects of electrolytes on the stability and dynamic rheological properties of an oil-in-water pickering emulsion stabilized by a nanoparticle-surfactant-polymer system, *Ind. Eng. Chem. Res.* 54 (2015) 5842–5852. doi:10.1021/acs.iecr.5b00734.
- [219] S.M. Seyyedsar, M. Sohrabi, Visualization observation of formation of a new oil phase during immiscible dense CO₂ injection in porous media, *J. Mol. Liq.* 241 (2017) 199–210. doi:10.1016/j.molliq.2017.05.146.
- [220] Z. Wu, H. Liu, Z. Pang, Y. Wu, X. Wang, M. Gao, Visualized Study on Blocking Characteristics and EOR Mechanisms of High-Temperature Gel During Steam Injection Process, (2016). doi:10.2523/iptc-18622-ms.
- [221] H. Wang, X.W. Liao, X.L. Zhao, The influence of CO₂ solubility in reservoir water on CO₂ flooding and storage of CO₂ injection into a water flooded low permeability reservoir, *Energy Sources, Part A Recover. Util. Environ. Eff.* 36 (2014) 815–821.

- doi:10.1080/15567036.2012.741654.
- [222] X. Xu, A. Saeedi, K. Liu, An experimental study of combined foam/surfactant polymer (SP) flooding for carbone dioxide-enhanced oil recovery (CO₂-EOR), *J. Pet. Sci. Eng.* 149 (2017) 603–611. doi:10.1016/j.petrol.2016.11.022.
- [223] F. Khalil, K. Asghari, Application of CO₂-foam as a means of reducing carbon dioxide mobility, *J. Can. Pet. Technol.* 45 (2006) 37–42. doi:10.2118/06-05-02.
- [224] E.A. Chukwudeme, A.A. Hamouda, Enhanced oil recovery (EOR) by miscible CO₂ and water flooding of asphaltenic and non-asphaltenic oils, *Energies.* 2 (2009) 714–737. doi:10.3390/en20300714.
- [225] A.F. Ibrahim, A. Emrani, H. Nasraldin, Stabilized CO₂ foam for EOR applications, in: *Carbon Manag. Technol. Conf. C. 2017 Glob. CCUS Innov. Nexus, AIChE, 2017*: pp. 264–282. doi:10.7122/486215-ms.
- [226] A.A.A. Hussain, S. Vincent-Bonnieu, R.Z. Kamarul Bahrim, R.M. Pilus, W.R. Rossen, Impact of Crude Oil on Pre-Generated Foam in Porous Media, *J. Pet. Sci. Eng.* 185 (2020) 106628. doi:10.1016/j.petrol.2019.106628.
- [227] A.H. Falls, G.J. Hirasaki, T.W. Patzek, D.A. Gauglitz, D.D. Miller, T. Ratulowski, Development of a mechanistic foam simulator: The population balance and generation by snap-off, *SPE Reserv. Eng. (Society Pet. Eng.* 3 (1988) 884–892. doi:10.2118/14961-PA.
- [228] R. Farajzadeh, A. Andrianov, R. Krastev, G.J. Hirasaki, W.R. Rossen, Foam-oil interaction in porous media: Implications for foam assisted enhanced oil recovery, *Adv. Colloid Interface Sci.* 183–184 (2012) 1–13. doi:10.1016/j.cis.2012.07.002.
- [229] J.S. Solbakken, A. Skauge, M.G. Aarra, Foam performance in low permeability laminated sandstones, *Energy Fuels.* 28 (2014) 803–815. doi:10.1021/ef402020x.
- [230] G.J. Hirasaki, J.B. Lawson, Mechanisms of foam flow in porous media: Apparent

- viscosities in smooth capillaries, *Soc. Pet. Eng. J.* 25 (1985) 176–190.
doi:10.2118/12129-PA.
- [231] J.F. Casteel, N.F. Djabbarah, Sweep improvement in the CO₂ flooding by use of foaming agents, *SPE Reserv. Eng. (Society Pet. Eng.* 3 (1988) 1186–1192.
doi:10.2118/14392-PA.
- [232] J. Jin, Y. Wang, M. Wei, H. Ma, K. Wang, Coreflooding and Pore-Scale Visualization of Foamed Gel Flowed in Porous Network Media, *J. Dispers. Sci. Technol.* 37 (2016) 1436–1443. doi:10.1080/01932691.2015.1111146.
- [233] Y. Zhang, Y. Wang, F. Xue, Y. Wang, B. Ren, L. Zhang, S. Ren, CO₂ foam flooding for improved oil recovery: Reservoir simulation models and influencing factors, *J. Pet. Sci. Eng.* 133 (2015) 838–850. doi:10.1016/j.petrol.2015.04.003.
- [234] R.C. Ferguson, C. Nichols, T. Van Leeuwen, V.A. Kuuskraa, Storing CO₂ with enhanced oil recovery, in: *Energy Procedia*, 2009: pp. 1989–1996.
doi:10.1016/j.egypro.2009.01.259.
- [235] A.U. Rognmo, S. Heldal, M.A. Fernø, Silica nanoparticles to stabilize CO₂-foam for improved CO₂ utilization: Enhanced CO₂ storage and oil recovery from mature oil reservoirs, *Fuel*. 216 (2018) 621–626. doi:10.1016/j.fuel.2017.11.144.
- [236] A. Dixit, J.S. Tsau, J.P. Heller, Laboratory Study on Surfactant-Based Selective Mobility Control, in: *Permian Basin Oil Gas Recover. Conf.*, Society of Petroleum Engineers (SPE), Midland, Texas, 1994. doi:10.2118/27729-ms.
- [237] J.-S. Tsau, J.P. Heller, How Can Selective Mobility Reduction of CO₂ Foam Assist in Reservoir Floods?, in: *Permian Basin Oil Gas Recover. Conf.*, Society of Petroleum Engineers, Midland, Texas, 1996. doi:10.2118/35168-MS.
- [238] S. Kumar, A. Mandal, Investigation on stabilization of CO₂ foam by ionic and nonionic surfactants in presence of different additives for application in enhanced

- oil recovery, *Appl. Surf. Sci.* 420 (2017) 9–20. doi:10.1016/j.apsusc.2017.05.126.
- [239] W. Yang, T. Wang, Z. Fan, Q. Miao, Z. Deng, Y. Zhu, Foams Stabilized by in Situ-Modified Nanoparticles and Anionic Surfactants for Enhanced Oil Recovery, *Energy Fuels*. 31 (2017) 4721–4730. doi:10.1021/acs.energyfuels.6b03217.
- [240] C. Zhang, Z. Li, Q. Sun, P. Wang, S. Wang, W. Liu, CO₂ foam properties and the stabilizing mechanism of sodium bis(2-ethylhexyl)sulfosuccinate and hydrophobic nanoparticle mixtures, *Soft Matter*. 12 (2016) 946–956. doi:10.1039/c5sm01408e.
- [241] S. Li, C. Qiao, Z. Li, S. Wanambwa, Properties of Carbon Dioxide Foam Stabilized by Hydrophilic Nanoparticles and Hexadecyltrimethylammonium Bromide, 31 (2017) 1478–1488. doi:10.1021/acs.energyfuels.6b03130.
- [242] R.G. Alargova, D.S. Warhadpande, V.N. Paunov, O.D. Velev, Foam superstabilization by polymer microrods, *Langmuir*. 20 (2004) 10371–10374. doi:10.1021/la048647a.
- [243] A. Bhakta, E. Ruckenstein, Decay of standing foams: Drainage, coalescence and collapse, *Adv. Colloid Interface Sci.* 70 (1997) 1–124. doi:10.1016/s0001-8686(97)00031-6.
- [244] A.S. Hanamertani, R.M. Pilus, N.A. Manan, M.I.A. Mutalib, The use of ionic liquids as additive to stabilize surfactant foam for mobility control application, *J. Pet. Sci. Eng.* 167 (2018) 192–201. doi:10.1016/j.petrol.2018.04.010.
- [245] A.O. Gbadamosi, R. Junin, M.A. Manan, A. Agi, A.S. Yusuff, An overview of chemical enhanced oil recovery: recent advances and prospects, *Int. Nano Lett.* 9 (2019) 171–202. doi:10.1007/s40089-019-0272-8.
- [246] S.A. Farzaneh, M. Sohrabi, A Review of the Status of Foam Application in Enhanced Oil Recovery, in: *EAGE Annu. Conf. Exhib. Inc. SPE Eur.*, Society of Petroleum Engineers (SPE), London, UK, 2013. doi:10.2118/164917-ms.

- [247] X. Xu, A. Saeedi, K. Liu, Laboratory studies on CO₂ foam flooding enhanced by a novel amphiphilic ter-polymer, *J. Pet. Sci. Eng.* 138 (2016) 153–159. doi:10.1016/j.petrol.2015.10.025.
- [248] R. Singh, K.K. Mohanty, Foam flow in a layered, heterogeneous porous medium: A visualization study, *Fuel*. 197 (2017) 58–69. doi:10.1016/j.fuel.2017.02.019.
- [249] D. Lee, H. Cho, J. Lee, C. Huh, K. Mohanty, Fly ash nanoparticles as a CO₂ foam stabilizer, *Powder Technol.* 283 (2015) 77–84. doi:10.1016/j.powtec.2015.05.010.
- [250] R. Singh, K.K. Mohanty, Synergy between nanoparticles and surfactants in stabilizing foams for oil recovery, *Energy and Fuels*. 29 (2015) 467–479. doi:10.1021/ef5015007.
- [251] Q. Sun, Z. Li, S. Li, L. Jiang, J. Wang, P. Wang, Utilization of surfactant-stabilized foam for enhanced oil recovery by adding nanoparticles, *Energy and Fuels*. 28 (2014) 2384–2394. doi:10.1021/ef402453b.
- [252] D. Yang, P. Tontiwachwuthikul, Y. Gu, Interfacial tensions of the crude oil + reservoir brine + CO₂ systems at pressures up to 31 MPa and temperatures of 27°C and 58°C, *J. Chem. Eng. Data*. 50 (2005) 1242–1249. doi:10.1021/je0500227.
- [253] L. Hendraningrat, S. Li, O. Torsæter, A coreflood investigation of nanofluid enhanced oil recovery, *J. Pet. Sci. Eng.* 111 (2013) 128–138. doi:10.1016/j.petrol.2013.07.003.
- [254] A. Ahmed, I.M. Saaid, A.A. Ahmed, R.M. Pilus, M.K. Baig, Evaluating the potential of surface-modified silica nanoparticles using internal olefin sulfonate for enhanced oil recovery, *Pet. Sci.* 17 (2020) 722–733. doi:10.1007/s12182-019-00404-1.
- [255] R.S. Kumar, K.R. Chaturvedi, S. Iglauer, J. Trivedi, T. Sharma, Impact of anionic surfactant on stability, viscoelastic moduli, and oil recovery of silica nanofluid in

- saline environment, *J. Pet. Sci. Eng.* 195 (2020) 107634.
doi:10.1016/j.petrol.2020.107634.
- [256] Y. Wang, X. Wu, W. Yang, Y. Zhai, B. Xie, M. Yang, Aggregate of nanoparticles: Rheological and mechanical properties, *Nanoscale Res. Lett.* 6 (2011).
doi:10.1186/1556-276X-6-114.
- [257] C. Gough, State of the art in carbon dioxide capture and storage in the UK: An experts' review, *Int. J. Greenh. Gas Control.* 2 (2008) 155–168. doi:10.1016/S1750-5836(07)00073-4.
- [258] M. Bui, I. Gunawan, T. V. Verheyen, E. Meuleman, Dynamic operation of liquid absorbent-based post-combustion CO₂ capture plants, in: *Absorption-Based Post-Combustion Capture of Carbon Dioxide*, Elsevier Inc., 2016: pp. 589–621.
doi:10.1016/B978-0-08-100514-9.00024-X.
- [259] L. Zhang, L. Yang, J. Wang, J. Zhao, H. Dong, M. Yang, Y. Liu, Y. Song, Enhanced CH₄ recovery and CO₂ storage via thermal stimulation in the CH₄/CO₂ replacement of methane hydrate, *Chem. Eng. J.* 308 (2017) 40–49.
doi:10.1016/j.cej.2016.09.047.
- [260] J. Baltrusaitis, J. Schuttlefield, E. Zeitler, V.H. Grassian, Carbon dioxide adsorption on oxide nanoparticle surfaces, *Chem. Eng. J.* 170 (2011) 471–481.
doi:10.1016/j.cej.2010.12.041.
- [261] D. Yue, J. Gong, F. You, Synergies between geological sequestration and microalgae biofixation for greenhouse gas abatement: Life cycle design of carbon capture, utilization, and storage supply Chains, *ACS Sustain. Chem. Eng.* 3 (2015) 841–861.
doi:10.1021/sc5008253.
- [262] J.C.M. Pires, F.G. Martins, M.C.M. Alvim-Ferraz, M. Simões, Recent developments on carbon capture and storage: An overview, *Chem. Eng. Res. Des.* 89 (2011) 1446–

1460. doi:10.1016/j.cherd.2011.01.028.
- [263] R.J. Stewart, R.S. Haszeldine, Can producing oil store carbon? greenhouse gas footprint of CO₂EOR, offshore north sea, *Environ. Sci. Technol.* 49 (2015) 5788–5795. doi:10.1021/es504600q.
- [264] J. Liu, L. Xie, Y. Yao, Q. Gan, P. Zhao, L. Du, Preliminary Study of Influence Factors and Estimation Model of the Enhanced Gas Recovery Stimulated by Carbon Dioxide Utilization in Shale, *ACS Sustain. Chem. Eng.* 7 (2019) 20114–20125. doi:10.1021/acssuschemeng.9b06005.
- [265] P. Zhao, L. Xie, B. He, J. Liu, Strategy Optimization on Industrial CO₂Sequestration in the Depleted Wufeng-Longmaxi Formation Shale in the Northeastern Sichuan Basin, SW China: From the Perspective of Environment and Energy, *ACS Sustain. Chem. Eng.* 8 (2020) 11435–11445. doi:10.1021/acssuschemeng.0c04114.
- [266] X. Zhang, B. Wei, J. Shang, K. Gao, W. Pu, X. Xu, C. Wood, L. Sun, Alterations of geochemical properties of a tight sandstone reservoir caused by supercritical CO₂-brine-rock interactions in CO₂-EOR and geosequestration, *J. CO₂ Util.* 28 (2018) 408–418. doi:10.1016/j.jcou.2018.11.002.
- [267] A. Dindi, D.V. Quang, L.F. Vega, E. Nashef, M.R.M. Abu-Zahra, Applications of fly ash for CO₂ capture, utilization, and storage, *J. CO₂ Util.* 29 (2019) 82–102. doi:10.1016/j.jcou.2018.11.011.
- [268] R.W. Klusman, Evaluation of leakage potential from a carbon dioxide EOR/sequestration project, *Energy Convers. Manag.* 44 (2003) 1921–1940. doi:10.1016/S0196-8904(02)00226-1.
- [269] N.I. Kechut, M. Jamiolahmady, M. Sohrabi, Numerical simulation of experimental carbonated water injection (CWI) for improved oil recovery and CO₂ storage, *J. Pet. Sci. Eng.* 77 (2011) 111–120. doi:10.1016/j.petrol.2011.02.012.

- [270] M. Seyyedi, P. Mahzari, M. Sohrabi, A comparative study of oil compositional variations during CO₂ and carbonated water injection scenarios for EOR, *J. Pet. Sci. Eng.* 164 (2018) 685–695. doi:10.1016/j.petrol.2018.01.029.
- [271] M. Seyyedi, M. Sohrabi, A. Farzaneh, Investigation of Rock Wettability Alteration by Carbonated Water through Contact Angle Measurements, *Energy and Fuels*. 29 (2015) 5544–5553. doi:10.1021/acs.energyfuels.5b01069.
- [272] T. Babadagli, Philosophy of EOR, *J. Pet. Sci. Eng.* 188 (2020) 106930. doi:10.1016/j.petrol.2020.106930.
- [273] K.R. Chaturvedi, J. Trivedi, T. Sharma, Single-step silica nanofluid for improved carbon dioxide flow and reduced formation damage in porous media for carbon utilization, *Energy*. 197 (2020) 117276. doi:10.1016/j.energy.2020.117276.
- [274] M.B. Moghaddam, E.K. Goharshadi, M.H. Entezari, P. Nancarrow, Preparation, characterization, and rheological properties of graphene-glycerol nanofluids, *Chem. Eng. J.* 231 (2013) 365–372. doi:10.1016/j.cej.2013.07.006.
- [275] A. Mohammadi, M. Manteghian, A. Haghtalab, A.H. Mohammadi, M. Rahmati-Abkenar, Kinetic study of carbon dioxide hydrate formation in presence of silver nanoparticles and SDS, *Chem. Eng. J.* 237 (2014) 387–395. doi:10.1016/j.cej.2013.09.026.
- [276] S. Al-Ansari, A. Barifcani, A. Keshavarz, S. Iglauer, Impact of nanoparticles on the CO₂-brine interfacial tension at high pressure and temperature, *J. Colloid Interface Sci.* 532 (2018) 136–142. doi:10.1016/j.jcis.2018.07.115.
- [277] Z. Xue, A. Worthen, A. Qajar, I. Robert, S.L. Bryant, C. Huh, M. Prodanović, K.P. Johnston, Viscosity and stability of ultra-high internal phase CO₂-in-water foams stabilized with surfactants and nanoparticles with or without polyelectrolytes, *J. Colloid Interface Sci.* 461 (2016) 383–395. doi:10.1016/j.jcis.2015.08.031.

- [278] X. Duan, J. Hou, T. Cheng, S. Li, Y. Ma, Evaluation of oil-tolerant foam for enhanced oil recovery: Laboratory study of a system of oil-tolerant foaming agents, *J. Pet. Sci. Eng.* 122 (2014) 428–438. doi:10.1016/j.petrol.2014.07.042.
- [279] K.R. Chaturvedi, T. Sharma, Rheological analysis and EOR potential of surfactant treated single-step silica nanofluid at high temperature and salinity, *J. Pet. Sci. Eng.* 196 (2021) 107704. doi:10.1016/j.petrol.2020.107704.
- [280] S. Sakthivel, S. Velusamy, R.L. Gardas, J.S. Sangwai, Use of Aromatic Ionic Liquids in the Reduction of Surface Phenomena of Crude Oil–Water System and their Synergism with Brine, *Ind. Eng. Chem. Res.* 54 (2015) 968–978. doi:10.1021/ie504331k.
- [281] M.B. Haider, D. Jha, B. Marriyappan Sivagnanam, R. Kumar, Thermodynamic and Kinetic Studies of CO₂ Capture by Glycol and Amine-Based Deep Eutectic Solvents, *J. Chem. Eng. Data.* 63 (2018) 2671–2680. doi:10.1021/acs.jced.8b00015.
- [282] S.K. Mofrad, A.H.S. Dehaghani, An experimental investigation into enhancing oil recovery using smart water combined with anionic and cationic surfactants in carbonate reservoir, *Energy Reports.* 6 (2020) 543–549. doi:10.1016/j.egyr.2020.02.034.
- [283] K. Abdalla, I.M. Tan, The Application of a New Polymeric Surfactant for Chemical EOR, in: *Introd. to Enhanc. Oil Recover. Process. Bioremediation Oil-Contaminated Sites*, InTech, 2012. doi:10.5772/47975.
- [284] M.A. Ahmadi, J. Sheng, Performance improvement of ionic surfactant flooding in carbonate rock samples by use of nanoparticles, *Pet. Sci.* 13 (2016) 725–736. doi:10.1007/s12182-016-0109-2.
- [285] E. Nagy, T. Feczko, B. Koroknai, Enhancement of oxygen mass transfer rate in the presence of nanosized particles, *Chem. Eng. Sci.* 62 (2007) 7391–7398.

- doi:10.1016/j.ces.2007.08.064.
- [286] J. Buongiorno, Convective transport in nanofluids, *J. Heat Transfer*. 128 (2006) 240–250. doi:10.1115/1.2150834.
- [287] H.D. Do, W. V. Pinczewski, Diffusion-controlled swelling of reservoir oil by indirect contact with injection gas, *Chem. Eng. Sci.* 48 (1993) 3243–3252. doi:10.1016/0009-2509(93)80208-8.
- [288] A.S. Emrani, H.A. Nasr-El-Din, An experimental study of nanoparticle-polymer-stabilized CO₂ foam, *Colloids Surfaces A Physicochem. Eng. Asp.* 524 (2017) 17–27. doi:10.1016/j.colsurfa.2017.04.023.
- [289] Q. Lan, F. Yang, S. Zhang, S. Liu, J. Xu, D. Sun, Synergistic effect of silica nanoparticle and cetyltrimethyl ammonium bromide on the stabilization of O/W emulsions, *Colloids Surfaces A Physicochem. Eng. Asp.* 302 (2007) 126–135. doi:10.1016/j.colsurfa.2007.02.010.
- [290] L. Hernando, B. Satken, A. Omari, H. Bertin, Transport of polymer stabilized foams in porous media: Associative polymer versus PAM, *J. Pet. Sci. Eng.* 169 (2018) 602–609. doi:10.1016/j.petrol.2018.05.066.
- [291] B.P. Binks, T.S. Horozov, Aqueous Foams Stabilized Solely by Silica Nanoparticles, *Angew. Chemie Int. Ed.* 44 (2005) 3722–3725. doi:10.1002/anie.200462470.
- [292] S. Zhang, D. Sun, X. Dong, C. Li, J. Xu, Aqueous foams stabilized with particles and nonionic surfactants, *Colloids Surfaces A Physicochem. Eng. Asp.* 324 (2008) 1–8. doi:10.1016/j.colsurfa.2008.03.020.
- [293] J.L. Dickson, B.P. Binks, K.P. Johnston, Stabilization of carbon dioxide-in-water emulsions with silica nanoparticles, *Langmuir*. 20 (2004) 7976–7983. doi:10.1021/la0488102.

- [294] Q. Xie, P. V. Brady, E. Pooryousefy, D. Zhou, Y. Liu, A. Saeedi, The low salinity effect at high temperatures, *Fuel*. 200 (2017) 419–426. doi:10.1016/j.fuel.2017.03.088.
- [295] Y. Zhou, X. Wu, X. Zhong, W. Sun, H. Pu, J.X. Zhao, Surfactant-Augmented Functional Silica Nanoparticle Based Nanofluid for Enhanced Oil Recovery at High Temperature and Salinity, *ACS Appl. Mater. Interfaces*. 11 (2019) 45763–45775. doi:10.1021/acsami.9b16960.
- [296] D. Weaire, The rheology of foam, *Curr. Opin. Colloid Interface Sci*. 13 (2008) 171–176. doi:10.1016/j.cocis.2007.11.004.
- [297] A. Rahim Risal, M.A. Manan, N. Yekeen, A. Mohamed Samin, N.B. Azli, Rheological properties of surface-modified nanoparticles-stabilized CO₂ foam, *J. Dispers. Sci. Technol*. 39 (2018) 1767–1779. doi:10.1080/01932691.2018.1462201.
- [298] M.G. Aarra, A. Skauge, J. Solbakken, P.A. Ormehaug, Properties of N₂- and CO₂-foams as a function of pressure, *J. Pet. Sci. Eng*. 116 (2014) 72–80. doi:10.1016/j.petrol.2014.02.017.
- [299] D. Wu, V. Mihali, A. Honciuc, PH-Responsive Pickering Foams Generated by Surfactant-Free Soft Hydrogel Particles, *Langmuir*. 35 (2019) 212–221. doi:10.1021/acs.langmuir.8b03342.
- [300] M.F. Fakoya, S.N. Shah, Emergence of nanotechnology in the oil and gas industry: Emphasis on the application of silica nanoparticles, *Petroleum*. 3 (2017) 391–405. doi:10.1016/j.petlm.2017.03.001.
- [301] J. Su, W. Dong, S. Zhou, M. Deng, Synthesis and Assessment of a CO₂-Switchable Foaming Agent Used in Drilling Fluids for Underbalanced Drilling, *J. Surfactants Deterg*. 21 (2018) 375–387. doi:10.1002/jsde.12029.
- [302] Z. Derikvand, M. Riazi, Experimental investigation of a novel foam formulation to

- improve foam quality, *J. Mol. Liq.* 224 (2016) 1311–1318.
doi:10.1016/j.molliq.2016.10.119.
- [303] E. Rio, W. Drenckhan, A. Salonen, D. Langevin, Unusually stable liquid foams, *Adv. Colloid Interface Sci.* 205 (2014) 74–86. doi:10.1016/j.cis.2013.10.023.
- [304] G. Zhao, C. Dai, Y. Zhang, A. Chen, Z. Yan, M. Zhao, Enhanced foam stability by adding comb polymer gel for in-depth profile control in high temperature reservoirs, *Colloids Surfaces A Physicochem. Eng. Asp.* 482 (2015) 115–124. doi:10.1016/j.colsurfa.2015.04.041.
- [305] W. Zhou, C. Xin, S. Chen, Q. Yu, K. Wang, Polymer-Enhanced Foam Flooding for Improving Heavy Oil Recovery in Thin Reservoirs, *Energy and Fuels.* 34 (2020) 4116–4128. doi:10.1021/acs.energyfuels.9b04298.
- [306] Y. Zeng, A. Muthuswamy, K. Ma, L. Wang, R. Farajzadeh, M. Puerto, S. Vincent-Bonnieu, A.A. Eftekhari, Y. Wang, C. Da, J.C. Joyce, S.L. Biswal, G.J. Hirasaki, Insights on Foam Transport from a Texture-Implicit Local-Equilibrium Model with an Improved Parameter Estimation Algorithm, *Ind. Eng. Chem. Res.* 55 (2016) 7819–7829. doi:10.1021/acs.iecr.6b01424.
- [307] K. Osei-Bonsu, P. Grassia, N. Shokri, Investigation of foam flow in a 3D printed porous medium in the presence of oil, *J. Colloid Interface Sci.* 490 (2017) 850–858. doi:10.1016/j.jcis.2016.12.015.
- [308] L.L. Schramm, J.J. Novosad, The destabilization of foams for improved oil recovery by crude oils: Effect of the nature of the oil, *J. Pet. Sci. Eng.* 7 (1992) 77–90. doi:10.1016/0920-4105(92)90010-X.
- [309] L.L. Schramm, J.J. Novosad, Micro-visualization of foam interactions with a crude oil, *Colloids and Surfaces.* 46 (1990) 21–43. doi:10.1016/0166-6622(90)80046-7.
- [310] A.J. Worthen, H.G. Bagaria, Y. Chen, S.L. Bryant, C. Huh, K.P. Johnston,

- Nanoparticle-stabilized carbon dioxide-in-water foams with fine texture, *J. Colloid Interface Sci.* 391 (2013) 142–151. doi:10.1016/j.jcis.2012.09.043.
- [311] R. Petkova, S. Tcholakova, N.D. Denkov, Foaming and foam stability for mixed polymer-surfactant solutions: Effects of surfactant type and polymer charge, *Langmuir*. 28 (2012) 4996–5009. doi:10.1021/la3003096.
- [312] L. Xu, M.D. Rad, A. Telmadarreie, C. Qian, C. Liu, S.L. Bryant, M. Dong, Synergy of surface-treated nanoparticle and anionic-nonionic surfactant on stabilization of natural gas foams, *Colloids Surfaces A Physicochem. Eng. Asp.* 550 (2018) 176–185. doi:10.1016/j.colsurfa.2018.04.046.
- [313] P. Wang, Q. You, L. Han, W. Deng, Y. Liu, J. Fang, M. Gao, C. Dai, Experimental Study on the Stabilization Mechanisms of CO₂ Foams by Hydrophilic Silica Nanoparticles, *Energy and Fuels*. 32 (2018) 3709–3715. doi:10.1021/acs.energyfuels.7b04125.
- [314] H. ShamsiJazeyi, R. Verduzco, G.J. Hirasaki, Reducing adsorption of anionic surfactant for enhanced oil recovery: Part I. Competitive adsorption mechanism, *Colloids Surfaces A Physicochem. Eng. Asp.* 453 (2014) 162–167. doi:10.1016/j.colsurfa.2013.10.042.
- [315] K.G. Uranta, S. Rezaei Gomari, P. Russell, F. Hamad, Application of polymer integration technique for enhancing polyacrylamide (PAM) performance in high temperature and high salinity reservoirs, *Heliyon*. 5 (2019). doi:10.1016/j.heliyon.2019.e02113.
- [316] M.M. Amro, A.-A.H. El-Sayed, E.S. Al-Homahdi, M.A. Al-Saddique, M.N. Al-Awad, Investigation of Polymer Adsorption on Rock Surface of Highly Saline Reservoirs, *Chem. Eng. Technol.* 25 (2002) 1005–1013. doi:10.1002/1521-4125(20021008)25:10<1005::AID-CEAT1005>3.0.CO;2-P.

- [317] S. Banerjee, Z.R. Abdulsattar, K. Agim, R.H. Lane, B. Hascakir, Mechanism of polymer adsorption on shale surfaces: Effect of polymer type and presence of monovalent and divalent salts, *Petroleum*. 3 (2017) 384–390. doi:10.1016/j.petlm.2017.04.002.
- [318] H. Jiang, Y. Sheng, T. Ngai, Pickering emulsions: Versatility of colloidal particles and recent applications, *Curr. Opin. Colloid Interface Sci.* 49 (2020) 1–15. doi:10.1016/j.cocis.2020.04.010.
- [319] K. Chrissafis, D. Bikiaris, Can nanoparticles really enhance thermal stability of polymers? Part I: An overview on thermal decomposition of addition polymers, *Thermochim. Acta.* 523 (2011) 1–24. doi:10.1016/j.tca.2011.06.010.
- [320] D. Bikiaris, Can nanoparticles really enhance thermal stability of polymers? Part II: An overview on thermal decomposition of polycondensation polymers, *Thermochim. Acta.* 523 (2011) 25–45. doi:10.1016/j.tca.2011.06.012.
- [321] N. Yekeen, M.A. Manan, A.K. Idris, E. Padmanabhan, R. Junin, A.M. Samin, A.O. Gbadamosi, I. Oguamah, A comprehensive review of experimental studies of nanoparticles-stabilized foam for enhanced oil recovery, *J. Pet. Sci. Eng.* 164 (2018) 43–74. doi:10.1016/j.petrol.2018.01.035.
- [322] A. Srivastava, W. Qiao, Y. Wu, X. Li, L. Bao, C. Liu, Effects of silica nanoparticles and polymers on foam stability with sodium dodecylbenzene sulfonate in water–liquid paraffin oil emulsions at high temperatures, *J. Mol. Liq.* 241 (2017) 1069–1078. doi:10.1016/j.molliq.2017.06.096.
- [323] S. Chen, H. Liu, Y. Zhu, W. Li, X. Yan, G. Wang, Y. Zhou, J. Zhang, Experimental and mathematical modeling investigation on the dynamic viscoelasticity behavior of free liquid films prepared by alpha olefin sulfonate, *J. Mol. Liq.* 251 (2018) 218–228. doi:10.1016/j.molliq.2017.12.076.

- [324] N. Yekeen, E. Padmanabhan, A.K. Idris, Synergistic effects of nanoparticles and surfactants on n-decane-water interfacial tension and bulk foam stability at high temperature, *J. Pet. Sci. Eng.* 179 (2019) 814–830. doi:10.1016/j.petrol.2019.04.109.
- [325] E. Dickinson, Structuring of colloidal particles at interfaces and the relationship to food emulsion and foam stability, *J. Colloid Interface Sci.* 449 (2015) 38–45. doi:10.1016/j.jcis.2014.09.080.
- [326] T.N. Hunter, R.J. Pugh, G. V. Franks, G.J. Jameson, The role of particles in stabilising foams and emulsions, *Adv. Colloid Interface Sci.* 137 (2008) 57–81. doi:10.1016/J.CIS.2007.07.007.
- [327] H. Zhou, C. Dai, Q. Zhang, Y. Li, W. Lv, R. Cheng, Y. Wu, M. Zhao, Interfacial rheology of novel functional silica nanoparticles adsorbed layers at oil-water interface and correlation with Pickering emulsion stability, *J. Mol. Liq.* 293 (2019) 111500. doi:10.1016/j.molliq.2019.111500.
- [328] S. Lam, K.P. Velikov, O.D. Velev, Pickering stabilization of foams and emulsions with particles of biological origin, *Curr. Opin. Colloid Interface Sci.* 19 (2014) 490–500. doi:10.1016/j.cocis.2014.07.003.
- [329] L. Jiang, S. Li, W. Yu, J. Wang, Q. Sun, Z. Li, Interfacial study on the interaction between hydrophobic nanoparticles and ionic surfactants, *Colloids Surfaces A Physicochem. Eng. Asp.* 488 (2016) 20–27. doi:10.1016/j.colsurfa.2015.10.007.
- [330] M.A. Ahmadi, S.R. Shadizadeh, Adsorption of novel nonionic surfactant and particles mixture in carbonates: Enhanced oil recovery implication, in: *Energy and Fuels*, American Chemical Society, 2012: pp. 4655–4663. doi:10.1021/ef300154h.
- [331] D.A. Espinoza, F.M. Caldelas, K.P. Johnston, S.L. Bryant, C. Huh, Nanoparticle-Stabilized Supercritical CO₂ Foams for Potential Mobility Control Applications, in: *SPE Improv. Oil Recover. Symp.*, Society of Petroleum Engineers, Tulsa,

- Oklahoma, USA, 2010. doi:10.2118/129925-MS.
- [332] A.E. Bayat, K. Rajaei, R. Junin, Assessing the effects of nanoparticle type and concentration on the stability of CO₂ foams and the performance in enhanced oil recovery, *Colloids Surfaces A Physicochem. Eng. Asp.* 511 (2016) 222–231. doi:10.1016/j.colsurfa.2016.09.083.
- [333] Q. Lin, K.H. Liu, Z.G. Cui, X.M. Pei, J.Z. Jiang, B.L. Song, pH-Responsive Pickering foams stabilized by silica nanoparticles in combination with trace amount of dodecyl dimethyl carboxyl betaine, *Colloids Surfaces A Physicochem. Eng. Asp.* 544 (2018) 44–52. doi:10.1016/j.colsurfa.2018.02.027.
- [334] W. Li, F. Wei, C. Xiong, J. Ouyang, L. Shao, M. Dai, P. Liu, D. Du, A Novel Supercritical CO₂ Foam System Stabilized With a Mixture of Zwitterionic Surfactant and Silica Nanoparticles for Enhanced Oil Recovery, *Front. Chem.* 7 (2019) 718. doi:10.3389/fchem.2019.00718.
- [335] C. Hübner, C. Fettkenhauer, K. Voges, D.C. Lupascu, Agglomeration-Free Preparation of Modified Silica Nanoparticles for Emulsion Polymerization - A Well Scalable Process, *Langmuir.* 34 (2018) 376–383. doi:10.1021/acs.langmuir.7b03753.
- [336] M.D. Morey, N.S. Deshpande, M. Barigou, Foam destabilization by mechanical and ultrasonic vibrations, *J. Colloid Interface Sci.* 219 (1999) 90–98. doi:10.1006/jcis.1999.6451.
- [337] N. Bagalkot, A.A. Hamouda, O.M. Isdahl, Dynamic interfacial tension measurement method using axisymmetric drop shape analysis, *MethodsX.* 5 (2018) 676–683. doi:10.1016/j.mex.2018.06.012.
- [338] H. Farhadi, S. Riahi, S. Ayatollahi, H. Ahmadi, Experimental study of nanoparticle-surfactant-stabilized CO₂ foam: Stability and mobility control, *Chem. Eng. Res. Des.*

- 111 (2016) 449–460. doi:10.1016/j.cherd.2016.05.024.
- [339] B. Vishal, P. Ghosh, Foaming in aqueous solutions of hexadecyltrimethylammonium bromide and silica nanoparticles: Measurement and analysis of rheological and interfacial properties, *J. Dispers. Sci. Technol.* 39 (2018) 62–70. doi:10.1080/01932691.2017.1295867.
- [340] A.J. Markworth, Comments on foam stability, Ostwald ripening, and grain growth, *J. Colloid Interface Sci.* 107 (1985) 569–571. doi:10.1016/0021-9797(85)90211-5.
- [341] S. Al-Anssari, M. Arif, S. Wang, A. Barifcani, M. Lebedev, S. Iglauer, Wettability of nano-treated calcite/CO₂/brine systems: Implication for enhanced CO₂ storage potential, *Int. J. Greenh. Gas Control.* 66 (2017) 97–105. doi:10.1016/j.ijggc.2017.09.008.
- [342] J.D. Berry, M.J. Neeson, R.R. Dagastine, D.Y.C. Chan, R.F. Tabor, Measurement of surface and interfacial tension using pendant drop tensiometry, *J. Colloid Interface Sci.* 454 (2015) 226–237. doi:10.1016/j.jcis.2015.05.012.
- [343] S. Al-Anssari, Z.U.A. Arain, A. Barifcani, A. Keshavarz, M. Ali, S. Iglauer, Influence of pressure and temperature on CO₂-nanofluid interfacial tension: Implication for enhanced oil recovery and carbon geosequestration, in: *Soc. Pet. Eng. - Abu Dhabi Int. Pet. Exhib. Conf. 2018, ADIPEC 2018, Society of Petroleum Engineers*, 2019. doi:10.2118/192964-ms.
- [344] S. Al-Anssari, S. Wang, A. Barifcani, S. Iglauer, Oil-water interfacial tensions of silica nanoparticle-surfactant formulations, *Tenside, Surfactants, Deterg.* 54 (2017) 334–341. doi:10.3139/113.110511.
- [345] B. Dollet, C. Raufaste, Rheology of aqueous foams, *Comptes Rendus Phys.* 15 (2014) 731–747. doi:10.1016/j.crhy.2014.09.008.
- [346] S. Marze, R.M. Guillermic, A. Saint-Jalmes, Oscillatory rheology of aqueous foams:

- Surfactant, liquid fraction, experimental protocol and aging effects, *Soft Matter*. 5 (2009) 1937–1946. doi:10.1039/b817543h.
- [347] Y. Bai, J. Zhao, D. Zhao, H. Zhang, Y. Fu, Pore structure and its control on reservoir quality in tight sandstones: a case study of the Chang 6 member of the Upper Triassic Yanchang Formation in the Jingbian oilfield in the Ordos Basin, China, *J. Pet. Explor. Prod. Technol.* (2020) 1–19. doi:10.1007/s13202-020-01042-9.
- [348] S. Sirivithayapakorn, A. Keller, Transport of colloids in saturated porous media: A pore-scale observation of the size exclusion effect and colloid acceleration, *Water Resour. Res.* 39 (2003). doi:10.1029/2002WR001583.

**RESEARCH PERFORMANCE EVALUATION COMMITTEE
(RPEC)**

1. Dr. Satish Kumar Sinha
Head of Department
Department of Petroleum Engineering & Geoengineering

2. Dr. Tushar Sharma (Supervisor)
Associate Professor and Chairman (DPGC)
Department of Petroleum Engineering & Geoengineering

3. Dr. Rakesh Kumar
Associate Professor
Department of Chemical Engineering and Biochemical Engineering

4. Dr. Shivanjali Sharma
Assistant Professor
Department of Petroleum Engineering and Geoengineering

PUBLICATION

Research Articles (in thesis)

- [1] **Chaturvedi KR**, Narukulla R, Trivedi J, Sharma T, Effect of Single-Step Silica Nanoparticle on Rheological Characterization of Surfactant Based CO₂ Foam for Effective Carbon Utilization in Subsurface Applications. Journal of Molecular Liquid, 2021, 116905 (IF=6.165)
- [2] **Chaturvedi KR**, Narukulla R, Amani M, Sharma T, Experimental Investigations to Evaluate Surfactant Role on Absorption Capacity of Nanofluid for CO₂ Utilization in Sustainable Crude Mobilization. Energy, 2021, 120321. (IF = 7.147)
- [3] **Chaturvedi KR**, Sharma T, In-Situ Formulation of Pickering CO₂ Foam for Enhanced Oil Recovery and Improved Carbon Storage in Sandstone Formation. Chemical Engineering Science, 2021, 235, 116484 (IF = 4.311)
- [4] **Chaturvedi KR**, Sharma T, Rheological Analysis and EOR Potential of Surfactant Treated Single-Step Silica Nanofluid at High Temperature and Salinity. Journal of Petroleum Science and Engineering, 2021, 196, 107704 (IF = 4.346)
- [5] **Chaturvedi KR**, Narukulla R, Sharma T. CO₂ Capturing Evaluation of Single-Step Silica Nanofluid through Rheological Investigation for Nanofluid Use in Carbon Utilization Applications. Journal of Molecular Liquids, 2020, 304, 112765. (IF = 6.165)
- [6] **Chaturvedi KR**, Trivedi J, Sharma T. Single-Step Synthesis of PAM based Silica Nanofluids for Improved CO₂ Flow and Reduced Formation Damage in Sandstone for Oilfield Applications. Energy, 2020, 197, 117276. (IF = 7.147)

Book Chapter

- [1] **Chaturvedi KR**, Sharma T, An Overview of the Application of Carbon Nanotubes for EOR and Carbon Sequestration in “Carbon Nanotubes for a Green Environment: Balancing the Risks and Rewards” edited by Kulkarni, Stoica and Haghi (Apple Academic Press)

International Conferences

- [1] **Chaturvedi KR**, Sharma T. Enhanced carbon capture & storage in depleted sandstone reservoirs using silica nanofluids, Matr. Today Proc. 2021, 46 (11), 5298-5303.
- [2] **Chaturvedi KR**, Sharma T, 2020. Re-imagining foam flooding: In-situ CO₂ foam flooding for improved oil recovery, International Conference on Energy and Environmental Technologies for Sustainable Development (Chem-Conflux), February 14-16th, Motilal Nehru National Institute of Technology, Allahabad, Prayagraj-211004, India.

CURRICULUM VITAE

Email (O): ppe17002@rgipt.ac.in

Mob: +918127819999

Krishna Raghav Chaturvedi

OBJECTIVE

To evolve into a competent professional by building upon my technical acumen, scientific temperament and organizational capabilities in a professional atmosphere and develop as a capable professional who is able to play an important role in improving the academic output and social development of my host institute.

ACADEMICS

Examination	Discipline	School/College	Board/ University	Year	C.P.I/%
Ph.D.	Petroleum Engineering	Rajiv Gandhi Institute of Petroleum Technology		Thesis submitted	8/10
Masters in Technology	Petroleum Engineering	Rajiv Gandhi Institute of Petroleum Technology		2017	8.84/10
Bachelors in Technology	Applied Petroleum Engineering (Upstream)	College of Engineering Technology	UPES, Dehradun	2014	70%
12 th	PCM	CMS GOMTI NAGAR	Indian School Certificate	2010	84%
10 th		CMS INDIRA NAGAR	Indian Council for School Certificate	2008	89%

HIGHLIGHTS OF PHD THESIS

Title: “Synthesis and Characterization of Single-step Silica Nanofluids for improved flow behavior and carbon utilization”

In this work, the synthesis and characterization of novel silica nanofluids, their rheological analysis, and the investigation of oil recovery using synthesized porous media and microfluidic unit was reported. The synthesized nanofluids resisted agglomeration for over 60 days, displayed high gas absorption and superior oil mobilization tendency.

CAREER HIGHLIGHTS

- Represented India as One of the 5 Finalists in Inaugural Shell Ideas360 competition held in Amsterdam, Netherlands on 14th May, 2014. The topic for the submission was “Fire in Ice”.
- Twice presented the “Appeal for a World Parliament” on behalf of 2 billion children and generations yet to be born in front of 120 Chief Justices of the World during the Chief Justices Conference Organized by CMS.

- Won Third Prize in Essay Writing Competition organized as Part of PETROTECH Youth Fest, 2016

AREAS OF RESEARCH

Carbon capture & storage, Microfluidics, Gas hydrates, rheology of oilfield suspensions, Enhanced oil recovery.

RESEARCH OUTPUT

Books (as editor)

1. Sharma T, Trivedi J, Chaturvedi KR, **Nanotechnology for CO₂ Utilization in Oilfield Applications**, Elsevier, (Author agreement signed: Manuscript under preparation)
2. Sharma T, Chaturvedi KR Ganat T, Ali I, **Advancements in Chemical Enhanced Oil Recovery**, CRC Taylor & Francis- Apple Academic Press, (Accepted for publication: First online August, 2021)

Patents

1. Sharma T, Chaturvedi KR, 2021, A system for hydrogen storage in heterogeneous formations, India, 202111037189, Filed (August 17, 2021).
2. Sharma T, Chaturvedi KR, 2021, A method for synthesizing alkali treated polymeric colloidal suspension of silica nanoparticles, India, 202111037165, Filed (August 17, 2021).

Journal publications

1. Singh A, **Chaturvedi KR**, Sharma T. Natural surfactant for sustainable carbon utilization in cleaner production of fossil fuels: Synthesis, characterization and application studies. *Journal of Environmental Chemical Engineering*, 2021, 9, 106231 (**IF= 5.909**)
2. **Chaturvedi KR**, Narukulla R, Sharma T, A comparative study of clay enriched polymer solutions for effective carbon storage and utilization (CSU) in saline reservoirs. *Colloid and Polymer Science*, 2021, 1-13 (**IF=1.931**)
3. Pandey A, Sinha ASK, **Chaturvedi KR**, Sharma T, Polysaccharide based Carbon Dioxide Foams and Their Characterization in Subsurface Saline Conditions for Effective Carbon Utilization and Geo-Storage Perspectives. *Energy*, 2021, 235, 121445 (**IF = 7.147**)
4. **Chaturvedi KR**, Narukulla R, Trivedi J, Sharma T, Effect of Single-Step Silica Nanoparticle on Rheological Characterization of Surfactant Based CO₂ Foam for Effective Carbon Utilization in Subsurface Applications. *Journal of Molecular Liquid*, 2021, 116905 (**IF=6.165**)
5. Kumar RK, Goswami R, **Chaturvedi KR**, Sharma T, Effect of Nanoparticle on Rheological Properties of Surfactant based Nanofluid for Effective Carbon Utilization: Capturing and Storage Prospects. *Environmental Science and Pollution Research*, 2021, 1-16 (**IF=4.223**)
6. **Chaturvedi KR**, Fogat M, Sharma T, Low Temperature Rheological Characterization of Single-Step Silica Nanofluids: An Additive in Refrigeration and Gas Hydrate Drilling Applications. *Journal of Petroleum Science and Engineering*, 2021, 196, 107704 (**IF = 4.346**)
7. **Chaturvedi KR**, Sinha ASK, Nair VC, Sharma T, Enhanced Carbon Dioxide Sequestration by Direct Injection of Flue Gas Doped with Hydrogen into Hydrate Reservoir: Possibility of Natural Gas Production. *Energy*, 2021, 120521. (**IF = 7.147**)
8. **Chaturvedi KR**, Narukulla R, Amani M, Sharma T, Experimental Investigations to Evaluate Surfactant Role on Absorption Capacity of Nanofluid for CO₂ Utilization in Sustainable Crude Mobilization. *Energy*, 2021, 120321. (**IF = 7.147**)

9. **Chaturvedi KR**, Sharma T, Investigating Dispersion Regimes for Effective Mass Transfer in Single-Step Silica Nanofluids for Improved CO₂ Utilization. *European Physical Journal Special Topics*, <https://doi.org/10.1140/epjs/s11734-021-00049-5> (**IF = 2.707**)
10. **Chaturvedi KR**, Sharma T, In-Situ Formulation of Pickering CO₂ Foam for Enhanced Oil Recovery and Improved Carbon Storage in Sandstone Formation. *Chemical Engineering Science*, 2021, 235, 116484 (**IF = 4.311**) *Selected as Journal Volume Cover Art.*
11. **Chaturvedi KR**, Kaleem W, Ravilla D, Jadhawar P, Sharma T, Impact of Low Salinity Water Injection on CO₂ Storage and Oil Recovery for Improved CO₂ Utilization. *Chemical Engineering Science*, 229, 116127 (**IF = 4.311**)
12. **Chaturvedi KR**, Sharma T, Rheological Analysis and EOR Potential of Surfactant Treated Single-Step Silica Nanofluid at High Temperature and Salinity. *Journal of Petroleum Science and Engineering*, 2021, 196, 107704 (**IF = 4.346**)
13. Kumar RS, **Chaturvedi KR**, Trivedi J, Igluer S, Sharma T, Impact of Anionic Surfactant on Stability, Viscoelastic Moduli, and Oil recovery of Silica Nanofluid in Saline Environment, *Journal of Petroleum Science and Engineering*, 2020, 195, 107634. (**IF = 4.346**)
14. **Chaturvedi KR**, Sharma T. Carbonated polymeric nanofluids for enhanced oil recovery from sandstone reservoir. *Journal of Petroleum Science and Engineering*, 2020, 194, 107499. (**IF = 4.346**)
15. **Chaturvedi KR**, Narukulla R, Sharma T. CO₂ Capturing Evaluation of Single-Step Silica Nanofluid through Rheological Investigation for Nanofluid Use in Carbon Utilization Applications. *Journal of Molecular Liquids*, 2020, 304, 112765. (**IF = 6.165**)
16. **Chaturvedi KR**, Trivedi J, Sharma T. Single-Step Synthesis of PAM based Silica Nanofluids for Improved CO₂ Flow and Reduced Formation Damage in Sandstone for Oilfield Applications. *Energy*, 2020, 197, 117276. (**IF = 7.147**)
17. **Chaturvedi KR**, Singh AK, Sharma T. Impact of Shale on Properties and Oil Recovery Potential of Sandstone Formation for Low Salinity Water (LSW) Flooding Applications. *Asia-Pacific Journal of Chemical Engineering*, e2352. (**IF = 1.447**)
18. **Chaturvedi KR**, Trivedi J, Sharma T. Evaluation of Polymer-Assisted Carbonated Water Injection in Sandstone Reservoir: Absorption Kinetics, Rheology, and Oil Recovery Results. *Energy & Fuels* 2019, 33, 65438-5451. (**IF = 3.605**)
19. **Chaturvedi KR**, Kumar R, Trivedi J, Sheng JJ, Sharma T. Stable silica nanofluids of an oilfield polymer for enhanced CO₂ absorption for oilfield applications. *Energy & Fuels*. 2018, 32, 12730-12741. (**IF = 3.605**)
20. Goswami R, **Chaturvedi KR**, Kumar RS, Chon BH, Sharma T. Effect of ionic strength on crude emulsification and EOR potential of micellar flood for oil recovery applications in high saline environment. *Journal of Petroleum Science and Engineering*, 2018, 170, 49-61. (**IF = 4.346**)

Book Chapters

1. Chaturvedi KR, Sharma T, *An Overview of the Application of Carbon Nanotubes for EOR and Carbon Sequestration* in “*Carbon Nanotubes for a Green Environment: Balancing the Risks and Rewards*” edited by Kulkarni, Stoica and Haghi (Apple Academic Press)

Conference presentations (Available online)

1. **Chaturvedi, KR**, Sharma, T., 2020. Enhanced carbon capture & storage in depleted sandstone reservoirs using silica nanofluids, Matr. Today Proc.
2. Kaspari, S., **Chaturvedi, KR**, Sihag, P., 2014. Perpetual Energy for future with Methane Gas Hydrates. SPE One Petro, IPTC-17708-MS.

NATIONAL EXAMS QUALIFIED

- Qualified **Graduate Aptitude Test in Engineering 2017** in Petroleum Engineering (Was ranked among top 20% percentile of all appearing students).
- Qualified **State Bank of India Probationary Officer 2017** (Was ranked among top 1% percentile of over 1.5 million applicants).

POSITIONS OF RESPONSIBILITY

- Member (Student Representative), Hostel Affairs Committee, RGIPT 2020-2021.
- Member (Student Representative), DPGC, Department of Petroleum Engineering, RGIPT 2017-2021.
- Member (Student Representative), Mess Monitoring Committee, RGIPT 2016-2019.
- Head, Organizing Committee, 3rd Research Scholars Symposium, RGIPT 2019.
- Deputy-head, Organizing Committee, 2nd Research Scholars Symposium, RGIPT 2018.
- Treasurer, Organizing Committee, 1st Research Scholars Symposium, RGIPT 2017.
- Student Head, Organizing Committee, APCEC International Conference, RGIPT 2017.
- Head of Logistics Committee, UPES 2nd National MUN 2013.

DELIVERED TALKS

- Delivered lecture on “Fundamentals of data gathering, analysis and advanced techniques” to 120 students of RGIPT Science & Technology Committee, 2018.
- Delivered invited talk on “Fundamentals of enhanced oil recovery” to 90 students of RGIPT SPE Student chapter, 2019.
- Delivered lecture on “How to ace group discussion” to 450 students of Mahendra classes, Indira Nagar, Lucknow.

EQUIPMENT SKILLS

HPHT Rheometer, Core Flooding Apparatus, Gas Lift System, Viscometers, Microfluidic unit, Dynamic Foam Analyzer, Ion Chromatography, Filter Press, Surface Tensiometer, Gas Chromatography, Gas hydrate synthesis cell, Particle Size Analyzer, CHNS, and Scanning electron microscope (SEM), Transmission electron microscope (TEM).

WORK EXPERIENCE

July, 2016- March, 2020 Lab Instructor, RGIPT

- Assisted faculty-in charges of Well Test Lab (Odd semester) and Reservoir Simulation lab (Even semester) in getting students of B.Tech. Petroleum engineering program acquainted with Industry relevant software.

Oct, 2014- July, 2015 Remote Operations Analyst, Mobilize

- Primary Job responsibility was to prepare KPI, NPT and ILT report for Bakken Shale Formation Drilling and the preparation of Well plans and directional drilling scorecards.
- Also, part of my responsibility is preparing daily operations summary for Morning Operations Meetings and monitoring for possible bad practices in hydro-fracking using the realtime ProdML based data feed.
- Also, involved with making data connections and monitoring real time drilling data coming in form of Wits/WitsML for possible alerts like Kicks, Mud Motor Stalls and Failures, Poor Weight Transfer etc.
- Prevented two Motor Stalls and one struck pipe situation.

May, 2013- June, 2013 Summer Intern, ONGC Ahmedabad Asset

Completed a Project on “Comparative Analysis of Artificial Lift Systems” which involved comparing the field performance of three methods of enhancing production i.e. the Sucker Rod Pump, the Gas Lift and the Electric Submersible Pump with the Jet Pumps and suggest the best production equipment considering not only technical but also logistical and fiscal criteria.

ACHIEVEMENTS IN CO-CURRICULAR ACTIVITIES

- Winner, “Strider Oil Business Challenge” organized by Petro First Solutions, November, 2012.
- Won the First Prize in a Model Making competition in Uurja 2010, the annual college fest.
- Won the Second Prize in an Infrastructure event organized by the Civil Department of UPES.
- Regional Finalist in various National Level Quizzes like Tata Crucible Biz Quiz 2013 Centre- Ghaziabad telecast on CNBC TV18 and Tata Crucible Biz Quiz 2012 Centre- Chandigarh telecast on CNBC TV18, on TCS IT Whiz 2009 Centre-Lucknow and on Bournvita Quiz Contest 2006 Centre-Lucknow.
- First Runner Up in UPES SPE Student Chapter organized “PETRA-QUIZ” 2011 and Tata Steel General Quiz “Geo-Synergy” at Cognizance 2012, IIT Roorkee, Winner of Quiz “NOESIS” organized by UPES SPE Student Chapter Year-2013, First Runner up in NOESIS 2014 and Twice Second Runner Up in UPES SPE Student Chapter organized quiz “NOESIS”, Years 2011& 2012.
- Secured Top Three Ranks in intra-college quizzes-REGIOMANIA 2011, CASETRACK 2011 and DE VICTORINA 2012, Atulya Bharat 2012 and in Inter School quizzes-Maggi Quiz 2001-2003, MACFAIR 2005, ODESSEY 2006 etc.
- Successfully organized the events, “Intellectual Battleground-2012” and “Crack Me-The UPES PETROTECH Chapter Open Quiz-2012” as the Event Head and the Event “Source Code” during UPES SPE Fest 2013

PERSONAL DETAILS

- Date of Birth (DD-MM-YYYY) : 05-10-1992
- Father’s Name: Mr. Prasanna Raghav
- Mother’s Name: Mrs.Reeta Raghav
- Marital status: Unmarried
- Nationality: Indian (Passport- L4457701)
- Permanent address: 15/221, INDIRA NAGAR, LUCKNOW-226016, INDIA.

References/contact details

1. **Dr. Tushar Sharma** (PhD Thesis Supervisor),
Assistant Professor, Dept. of Petroleum Engineering & Geoengineering,
Rajiv Gandhi Institute of Petroleum Technology, Jais, Amethi-229304,
India.
Ph. No. - +91 7080044156
Email Id- tsharma@rgipt.ac.in
2. **Prof. Japan Trivedi**,
Professor, Petroleum Engineering, Faculty of Engineering - Civil and
Environmental Engineering,
University of Alberta, Edmonton, Canada.
Ph. No. - +1 (780) 492-1247
Email Id- jtrivedi@ualberta.ca
3. **Prof. Stefan Iglauer**,
Professor & Director, Centre for Sustainable Energy and Resources,
School of Engineering, Edith Cowan University, Joondalup, Australia.
Ph. No. -+61 8 6304 5832
Email Id- s.iglauer@ecu.edu.au
4. **Dr. Mahmood Amani**,
Associate Professor, Petroleum Engineering Program,
Texas A&M University at Qatar, Qatar.
Ph. No. – +974 4423 0119
Email Id- mahmood.amani@tamu.edu

End
